UNIVERSITY OF DERBY

A NOVEL APPROACH TO THE CONTROL OF QUAD-ROTOR HELICOPTERS USING FUZZY-NEURAL NETWORKS

GWANGTIM TIMOTHY POYI

Doctor of Philosophy   **2014**

ABSTRACT

Quad-rotor helicopters are agile aircraft which are lifted and propelled by four rotors. Unlike traditional helicopters, they do not require a tail-rotor to control yaw, but can use four smaller fixed-pitch rotors. However, without an intelligent control system it is very difficult for a human to successfully fly and manoeuvre such a vehicle. Thus, most of recent research has focused on small unmanned aerial vehicles, such that advanced embedded control systems could be developed to control these aircrafts. Vehicles of this nature are very useful when it comes to situations that require unmanned operations, for instance performing tasks in dangerous and/or inaccessible environments that could put human lives at risk.

This research demonstrates a consistent way of developing a robust adaptive controller for quad-rotor helicopters, using fuzzy-neural networks; creating an intelligent system that is able to monitor and control the non-linear multi-variable flying states of the quad-rotor, enabling it to adapt to the changing environmental situations and learn from past missions.

Firstly, an analytical dynamic model of the quad-rotor helicopter was developed and simulated using Matlab/Simulink software, where the behaviour of the quad-rotor helicopter was assessed due to voltage excitation. Secondly, a 3-D model with the same parameter values as that of the analytical dynamic model was developed using Solidworks software. Computational Fluid Dynamics (CFD) was then used to simulate and analyse the effects of the external disturbance on the control and performance of the quad-rotor helicopter.

Verification and validation of the two models were carried out by comparing the simulation results with real flight experiment results. The need for more reliable and accurate simulation data led to the development of a neural network error compensation system, which was embedded in the simulation system to correct the minor discrepancies found between the simulation and experiment results.

Data obtained from the simulations were then used to train a fuzzy-neural system, made up of a hierarchy of controllers to control the attitude and position of the quad-rotor helicopter. The success of the project was measured against the quad-rotor's ability to adapt to wind speeds of different magnitudes and directions by re-arranging the speeds of the rotors to compensate for any disturbance. From the simulation results, the fuzzy-neural controller is sufficient to achieve attitude and position control of the quad-rotor helicopter in different weather conditions, paving way for future real time applications.

ACKNOWLEDGEMENTS

TABLE OF CONTENTS

LIST OF FIGURES

LIST OF TABLES

NOMENCLATURE

Symbol	Name	Unit
g	Acceleration due to gravity	ms^{-2}
ρ	Air density	Kgm^{-3}
$\dot{u}$, $\dot{v}$, $\dot{w}$	Components of acceleration with respect to the quad-rotor body frame in the x, y and z axes respectively.	ms^{-2}
p, q, r	Components of angular velocity with respect to the quad-rotor body frame in the x, y and z axes respectively.	$rads^{-1}$
F_x, F_y and F_z	Components of force with respect to the quad-rotor body frame	N
F_{Dx}, F_{Dy} and F_{Dz}	Components of the drag force in the three axes	N
F_{gx}, F_{gy} and F_{gz}	Components of the gravity force in the three axes	N
V_x, V_y, V_z	Components of velocity with respect to the earth frame.	ms^{-1}
$S(\omega^B) \times v^B$	Coriolis term	+
$\dot{R}_\Theta$	Derivative of the rotation matrix	-
D	Drag coefficient	-
C_{Dx}, C_{Dy}, C_{Dz}	Drag coefficients in each of the three axes	-
F_1, F_2, F_3 and F_4	Forces generated by rotors 1, 2, 3 and 4 respectively	N
F_g^B	Gravitational force with respect to the quad-rotor body frame	N
F_g^E	Gravitational force with respect to the earth frame	N
h_1, h_2, h_3, h_4 and h_c	Heights of quad-rotor motors and central hub respectively	m
l	Length of quad-rotor arm	m

τ_d	Load torque	Nm
m	Mass of the quad-rotor	Kg
m_1, m_2, m_3, m_4 and m_c	Masses of quad-rotor motors and central hub respectively	Kg
$\dot{\Omega}$	Motor angular acceleration	rads^{-2}
Ω	Motor angular velocity	rads^{-1}
i	Motor current	A
η	Motor efficiency	%
R	Motor resistance	Ohm
k_e	Motor speed constant	V.s.rad^{-1}
τ_m	Motor torque	Nm
k_q	Motor torque constant	Nm/A
f	Propeller figure of merit	-
R_p	Propeller radius	m
$\dot{\omega}^B$	Quad-rotor angular acceleration vector with respect to the body frame	rads^{-2}
$\ddot{\theta}^E$	Quad-rotor angular acceleration vector with respect to the earth frame	rads^{-2}
θ^E	Quad-rotor angular position vector with respect to the earth frame	rad
ω^B	Quad-rotor angular velocity vector with respect to the body frame	rads^{-1}
$\dot{\theta}^E$	Quad-rotor angular velocity vector with respect to the earth frame	rads^{-1}
F^E	Quad-rotor force vector with respect to the earth frame	N

$\xi[+]$	Quad-rotor generalised position vector	+
$\ddot{\Gamma}^E$	Quad-rotor linear acceleration vector with respect to the earth frame	ms^{-2}
$\dot{v}^B$	Quad-rotor linear acceleration vector with respect to the body frame	ms^{-2}
Γ^E	Quad-rotor linear position vector with respect to the earth frame	m
v^B	Quad-rotor linear velocity vector with respect to the body frame	ms^{-1}
v^E	Quad-rotor linear velocity with respect to the earth frame	ms^{-1}
x, y, z	Quad-rotor position coordinates	m
R_{Θ}	Quad-rotor rotation matrix	-
φ, θ, ψ	Quad-rotor tilt angles	rad
τ^E	Quad-rotor torque vector with respect to the earth frame	Nm
r_1, r_2, r_3, r_4 and r_c	Radii of quad-rotor motors and central hub respectively	m
τ_r, τ_p, and τ_y	Roll, pitch and yaw moments respectively	Nm
$R_x(\varphi)$	Rotation around the x-axis	-
$R_y(\theta)$	Rotation around the y-axis	-
$R_z(\psi)$	Rotation around the z-axis	-
I_{xx}	Rotational inertia along x-axis	Nms^{-2}
I_{yy}	Rotational inertia along y-axis	Nms^{-2}
I_{zz}	Rotational inertia along z-axis	Nms^{-2}
J_r	Rotor inertia	Kg.m^2

$S(\omega^B)$	Skew symmetric matrix	+
I	The inertia matrix of the quad-rotor with respect to the body frame	-
k_t	Thrust/torque constant	Ns^2
τ_i	Torque generated by each motor	Nm
F_B	Total force acting on the quad-rotor with respect to the body frame	N
J	Total motor moment of inertia	$Kg.m^2$
T_θ	Transfer matrix	-
u , v , w	Velocity components with respect to the quad-rotor body frame in the x, y and z axes respectively.	ms^{-1}
v_L	Voltage across the inductor L	V
v_R	Voltage across the resistor R	V
V	Voltage input to motors	V

INTRODUCTION

This chapter presents a general introduction to Unmanned Aerial Vehicles (UAVs). It starts by highlighting the major classes of UAVs and then goes on to a brief history of the miniature quad-rotor helicopter. It also gives an anatomy of the quad-rotor helicopter, describing its major components and basic concepts of aircraft flight as applied to quad-rotor helicopters. The extremely varying application domains of miniature quad-rotor helicopters are discussed, considering the fact that UAVs have proven their capabilities in executing operations that were considered too risky for manned aircraft.

1.0 Unmanned Aerial Vehicles (UAVs)

An Unmanned Aerial Vehicle (UAV) is an aircraft, which does not carry a human operator. It can be controlled remotely (from ground control stations or from another vehicle) or can fly independently, based on pre-programmed flight plans or some complex dynamic automation systems. There are a wide variety of UAV shapes, sizes and configurations, which are deployed predominantly for military and special operation applications, but also used in an increasing number of civil missions such as agriculture, policing, search and rescue, surveillance and fire fighting. UAVs are preferred for missions in places that are considered to be dangerous, dirty, dull and/or inaccessible for humans [1].

UAVs have been classified using different nomenclature, but most of them are either fixed-wing aircrafts or rotary-wing aircrafts (rotorcraft). While fixed-wing aircrafts fly because of the forward airspeed - using wings that generate lift, rotary-wing aircrafts rely on revolving rotor blades to keep them in flight. In powered fixed-wing aircrafts, thrust from a jet engine or a propeller is what moves the aircraft forward, whereas the blades of a rotary-wing aircraft revolve around a single mast called the rotor to generate lift and thrust, keeping it in flight.

Fixed-wing aircrafts have very simple mechanics, natural gliding capabilities and are able to carry greater payloads for longer distances on less power. However, when precision missions are requisite, rotorcrafts are the best choice because they can take off and land vertically within a very small area, are highly manoeuvrable (can fly forward, backward and laterally) and can hover on one spot. The limitations of a fixed-wing unmanned aircrafts (its inability to hover or fly at low speeds) as far as precision missions are concerned, have driven a number of researchers into considering the use of rotary-wing unmanned vehicles. So also, this research focuses on rotary-wing unmanned vehicles with particular emphasis on quad-rotor helicopters, because of their operational flexibility which surpasses their deficit of speed and endurance.

Rotary-wing vehicles have the advantages of vertical take-off and landing (VTOL) and high manoeuvrability, due to their ability to hover and to fly at low altitudes in all directions. These allow the vehicles to fly through tight spaces and small openings, eliminating the need for launching mechanisms like aircraft catapults and runways that are commonly used by fixed-wing UAVs, making them ideal for flight in built-up and crowded environments. Whereas this design has been widely chosen as platforms for flight control experiments,

because of their low cost and agile dynamics; they often suffer from complex mechanics, relatively small payload capacity (compared with their fixed-wing counterparts) and they consume a great deal of power to stay in flight, which drastically limits flight time [2].

There has been a dramatic increase in funding for UAV research in the last two decades. This has led to innovations in Artificial Intelligence, Automatic Control, Robotics, Communications and Sensor Technologies, which have positioned UAVs to become a major part of the aviation industry in the near future. From the current trend, it is expected that in the next decade, UAV research funding will more than double as there is a growing world demand for UAVs in the Intelligence, Surveillance, and Reconnaissance (ISR) sector [3].

1.1 The Miniature Quad-rotor Unmanned Aerial Vehicle

Early in the history of aircrafts, quad-rotor configurations were perceived as promising solutions to some of the persistent difficulties in vertical airlift, especially in the conventional helicopter design. This is because torque-induced control problems besides efficiency issues emanating from the small tail rotor blade, which does not actually generate any useful lift can be eliminated by counter-spinning individual or pairs of propellers on one vehicle.

There evolved some prototypes between 1920 and 1940, which were able to carry humans, however most of them suffered from poor performance at that time. The designs that came up later, exhibited poor stability augmentation and limited controllability, requiring the human pilot to do a lot of work to keep it aloft and land it safely [4].

The principles of Physics apply in the control of helicopters. When a propeller spins, a turning force called torque is produced by the engine (or motor) that spins it. The propeller wants to turn in one direction and the engine (or motor), the other direction; a very clear demonstration of Newton's law, which states that for every action, there is an equal and opposite reaction.

Another force caused by uneven thrust of the propellers at differing attitudes, is known as the P-factor. Conventional helicopters overcome these forces by using a tail rotor. As the main rotor blades are turning via the engine, the opposite force is trying to turn the helicopter's body in the opposite direction. The tail rotor has a variable pitch mechanism that simply pushes more air (or less as the case may be) and produces more linear thrust that offsets the effect of torque and "P factor". Without a tail rotor, a conventional helicopter's body would

spin out of control. To actually cause the helicopter's body to turn (or pirouette) the pilot either increases or decreases tail rotor pitch, depending upon which way the turn is to be initiated [5].

In the case of miniature quad-rotor helicopters, the same forces apply. The controller would normally be designed to match the front and back, left and right motor-rotor speeds to be identical. Interestingly, the miniature quad-rotor helicopter rotates the left and right motor-rotors in the opposite direction to the front and back motor-rotors. This, in effect neutralizes the torque and P-factor, allowing the quad-rotor to stay aloft without spinning out of control. Recently, quad-rotor helicopter designs have had miniaturized electronic devices and controls incorporated into the vehicles' system dynamics to increase stability and provide autonomous control of the helicopters. They can be flown indoors and outdoors, because of their small size and ease of manoeuvrability [6].

1.2 Anatomy of the Quad-rotor Helicopter

A quad-rotor helicopter has a symmetrically aligned cross-frame with four fixed-pitch rotors, one mounted at each end of the cross-frame. Being a rotary-wing aircraft, it has the ability to hover, take off, fly and land in small areas. It also has a simple control mechanism that does not require swash-plates and complex mechanical linkages for varying the pitch in the blades like that of a conventional helicopter. However, it is an unstable vehicle and can be very challenging to fly without modern embedded control systems. Control of vehicle motion is achieved by a variation in rotor speeds of individual or pairs of rotors to change the thrust and torque produced.

The major components of a quad-rotor UAV are described as follows:

1.2.1 Frame

The frame is a structure to which all the other essential bits and pieces are attached. There are pre-fabricated frames that can be bought off the shelf, or they could be designed to any specification. It has to be lightweight, strong and rigid. The frames are usually made of carbon composite materials or aluminium, making them cheap and easy to make or replace. At the end of each arm is a fixed motor mount and the electronics are housed in a flat bay area around the center of the cross-frame as shown in figure 1-1. Provisions can be made

underneath the frame for a payload such a camera or a robotic arm, depending on the mission to be accomplished by the quad-rotor.

Figure 1-1: Quad-rotor helicopter frame

1.2.2 Landing Gear

Quad-rotors could have different types of landing gears. However, the most important thing that has to be considered is the contribution that the landing gear will make to the overall weight of the quad-rotor helicopter. It should be as light as possible, but strong enough to withstand any forceful landing as shown in figure 1-2.
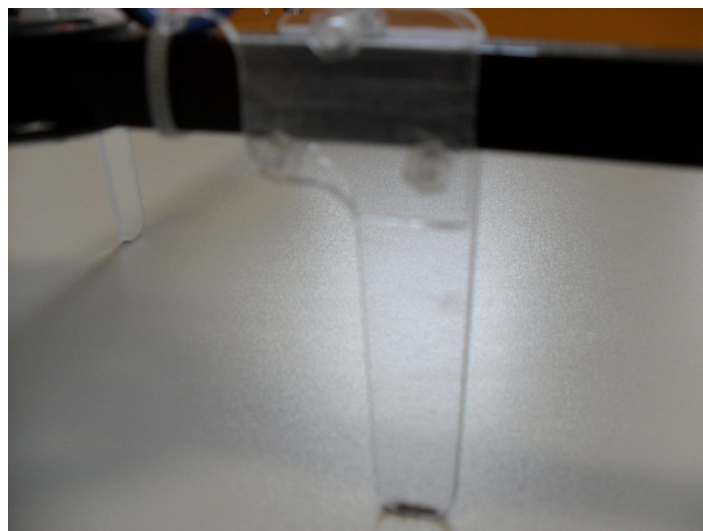
Figure 1-2: Quad-rotor landing gear

1.2.3 Motors and Propellers

The Quad Rotor's actuation mechanisms are relatively simple as shown in figure 1-3. The Quad Rotor uses four brushless motors to power the propellers. Brushless Motors generate more power, have greater efficiency, are more reliable, produce less noise and a longer lifetime than brushed motors. However, they are obtained at a higher cost. Each of the four brushless motors is independently controlled by an electronic speed controller (ESC). An ESC takes input from a logic board and sends varying pulses to the motor to make it spin at different rates.

The propellers are used to provide the thrust for lifting and maneuvering the quad-rotor and each is directly attached to a brushless motor. The size of the propeller is important as it directly affects power consumption and lift generation.
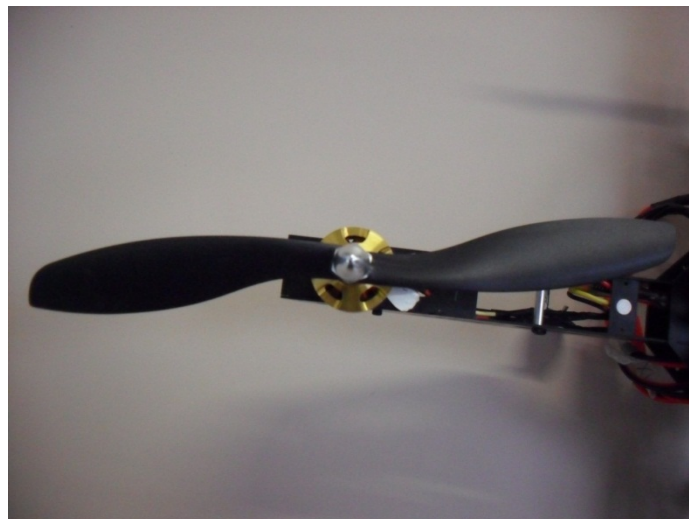
Figure 1-3: Propeller mounted on a brushless DC motor

The motors and propellers are configured such that two of them spin clockwise and other two spin counter-clockwise. This arrangement brings about a balance of forces and moments, giving some stability to the quad-rotor helicopter.

1.2.4 Battery

Quad-rotor helicopters are known for high energy consumption as a major drawback. They are normally fitted with lightweight rechargeable batteries that have the capacity to power the motors and other electronics through the desired flight endurance period. Most quad-rotor helicopter manufacturers use Lithium-ion Polymer (LiPoly) batteries as shown in figure 1-4.

Figure 1-4: Battery

1.2.5 Sensors

Quad-rotors are equipped with flight sensors, including – accelerometers, gyroscopes, sonars, barometric pressure sensors and GPS receivers as shown in figure 1-5. Sensors are very important as they can help any robotic device in understanding its environment by estimating the state of the robot. Data obtained from sensors can tell if the vehicle is going to flip over when it tilts one more degree; if it is flying horizontally or if it is nose-diving, if there are other vehicles or objects within range.

All of these sensors are continually sending their outputs to an on-board flight computer. These signals are then analysed, processed and adjustments made to keep the helicopter aloft.
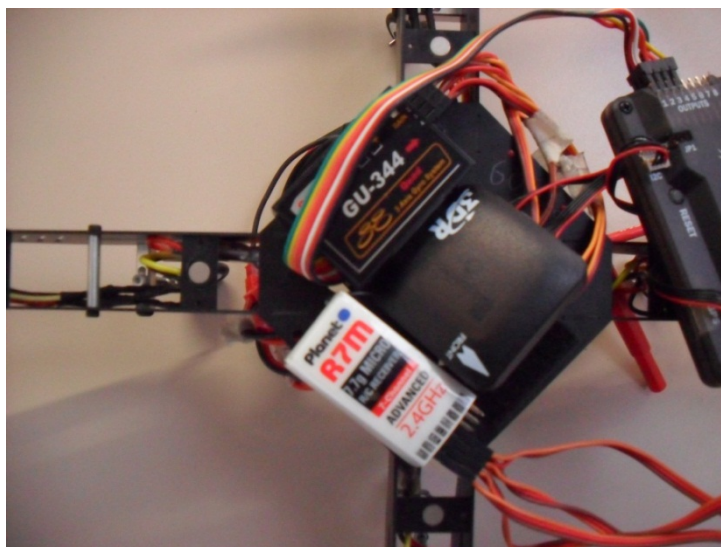
Figure 1-5: Inertial measurement unit

a) Accelerometer

An accelerometer is an electromechanical device that measures forces due to acceleration. These forces may be static – like the gravitational pull or they could be dynamic – as a result of movements or vibrations.

The angle of tilt of the vehicle with respect to the earth can be determined by measuring the amount of static acceleration due to the gravitational pull. Furthermore, analysis of the movement of the device can be done by sensing the amount of dynamic acceleration.

b) Gyroscope

A gyroscope is a device for measuring or maintaining orientation of the vehicle, based on the principle of conservation of angular momentum. It measures angular velocity by detecting Coriolis acceleration and is typically used for measuring the rate of rotation of the vehicle. Conventional aircrafts would normally use about a dozen gyroscopes in everything from its compass to its autopilot.

An arrangement of three sensitive accelerometers and two gyroscopes, with their axes lined up at right angles on the quad-rotor helicopter structure articulates accurately where the vehicle is heading. It also tells how its motion is changing in all three directions.

c) Sonar

A sonar sensor is a device that is designed to use sound propagation to detect obstacles in the robot's environment. It creates a pulse of sound and then listens for reflections of the pulse. To measure the distance from the transmitter to an object, the time broadcast of a pulse to reception is measured and converted into a range by knowing the speed of sound.

d) Barometric pressure sensor

A barometric pressure sensor usually acts as a transducer and generates an electrical signal as a function of the pressure imposed. It is often used for monitoring and control in numerous applications. To sustain its altitude, a quad-rotor helicopter requires such a transducer.

e) GPS receiver

This sensor uses the Global Positioning System, a satellite-based navigation system that sends and receives radio signals. It provides information about current location in different weather conditions in an unobstructed line of sight to four or more GPS satellites. The accuracy of the GPS signal may vary from a few meters to a hundred meters, depending on its configuration.

1.2.6 Flight Control Board

The flight control board is a critical element of the quad-rotor helicopter, as it essentially acts as the brains of the vehicle. It houses the sensors (accelerometers, gyroscopes and barometric pressure sensor) as shown in figure 1-6.

Since quad-rotors don't glide like the fixed-wing aircrafts, the only thing that keeps them aloft is the precise control of the motors and propellers. The flight control board uses the sensors to keep track of the vehicle's position and orientation by monitoring how the quad-rotor flies in relation to its environment and the commands given to it.
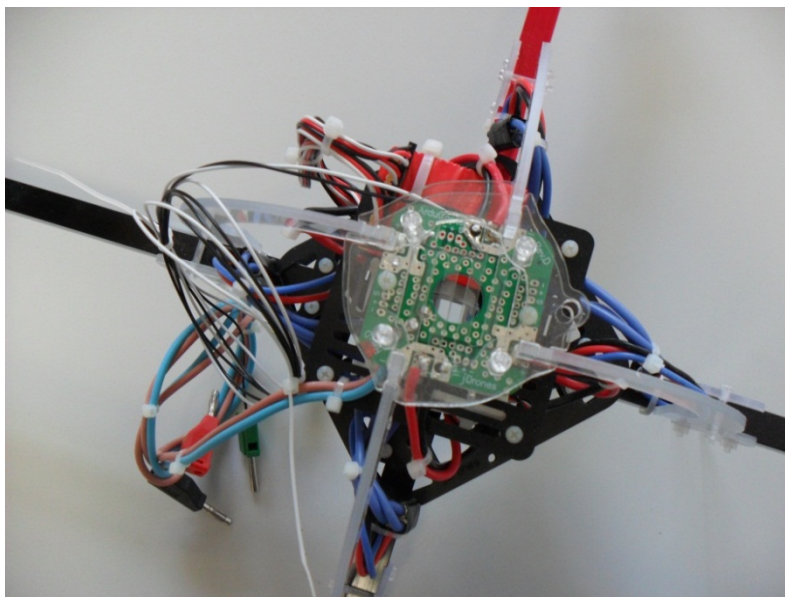
Figure 1-6: Flight control board

1.2.7 Transmitter and Receiver

These are the parts that send and receive signals between the quad-rotor and the remote control or ground station. The transmitters and receivers (pictured in figure 1-7) are also very important in communication between vehicles when a swarm of quad-rotors are working together cooperatively.

There is a wide range of receiver and transmitter combination; however, most quad-rotor helicopters use the traditional remote controls and radio frequency technology.

Figure 1-7: Transmitter-receiver

The figure 1-8 below shows a miniature quad-rotor UAV in outdoor flight. Its frame, lift-generating propellers, electric motors, landing gear and payload (in this case a camera) are clearly visible in the picture. The camera payload suggests that the mission is mainly to capture images, whether still photos or videos. It is able to save information to a small storage device attached to and at the same time send back images to the remote control or a ground station as it flies around.

CONTENT REMOVED FOR COPYRIGHT REASONS

Figure 1-8: Quad-rotor helicopter [7]

1.3 Basic concepts of the quad-rotor helicopter

The quad-rotor helicopter is very well modelled with its four rotors in a cross configuration style. Two of the motors (front-1 and rear-3) rotate counter-clockwise, while the other two (left-2 and right-4) rotate clockwise. In this configuration, the helicopter does not spin on its vertical axis since the rotational inertia is cancelled out, completely eliminating the need for a tail rotor which is used to stabilize the conventional helicopter. When the pair that's spinning in one direction is faster than the other pair, the helicopter will spin on its vertical axis, thereby leading to a change of heading or control of the helicopter's direction of movement.

Angular accelerations about the pitch and roll axes can be caused separately without affecting the yaw axis. Each pair of blades rotating in the same direction controls one axis, either roll or pitch, and increasing thrust for one rotor while decreasing thrust for the other will maintain the torque balance needed for yaw stability and induce a net torque about the roll or pitch axes. This way, fixed rotor blades can be made to manoeuvre the quad-rotor vehicle in all dimensions. Translational acceleration is achieved by maintaining a non-zero pitch or roll angle.

The figure 1-9 below shows a simplified quad-rotor helicopter structure in hover state, with the red circle defining the front of the vehicle.
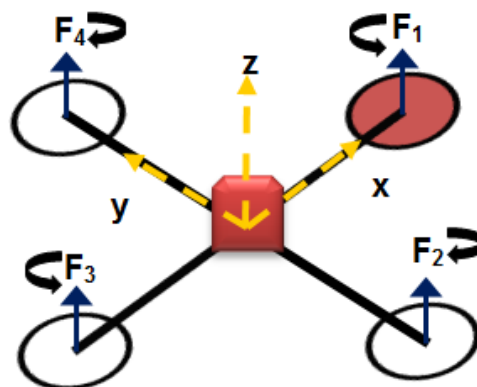
Figure 1-9: Simplified quad-rotor helicopter structure

Hovering is the term used to describe a situation when a helicopter maintains a constant position at a selected point in the air. At this point, it can be said that the forces of lift and weight have reached a state of equilibrium. Generally, helicopters can climb or descend by upsetting the vertical balance of forces acting on them.

In figure 1-9 above, all the propellers rotate at the same (hovering) speed to generate a collective lift force that offsets the weight of the quad-rotor helicopter (which equals its mass multiplied by acceleration due to gravity acting at the centre of the cross frame of the vehicle). Consequently, the quad-rotor neither climbs nor descends, it does not stall, roll, pitch or yaw and therefore there is no horizontal movement in any direction. It stays at a fixed point in the air and does not move from its position because there is a balance in all the forces and torques that are acting on the vehicle.

Despite its six degrees of freedom (DOF), the quad-rotor helicopter is equipped with only four propellers. Therefore it is not possible to reach a desired set-point for all the DOF, but four at a maximum. Nevertheless, because of its structure, it is possible to choose the four best variables that can be controlled and to decouple them, thereby making the controller formulation a lot easier. The four quad-rotor targets are related to four basic control actions, which allow the vehicle to reach a certain altitude and attitude. These control actions are described as follows:

1.3.1 Throttle

This control action is realized by simultaneously increasing (or decreasing) all propeller speeds by identical amounts as shown in figure 1-10. In consequence, the quad-rotor helicopter is raised or lowered to a certain altitude, because of the collective vertical force generated by the four propellers with respect to the body-fixed frame. It is expected that if the helicopter is in horizontal position, the vertical direction of the inertial frame and that of the body-fixed frame should coincide. Otherwise the provided thrust generates accelerations in both vertical and horizontal directions in the inertial frame.
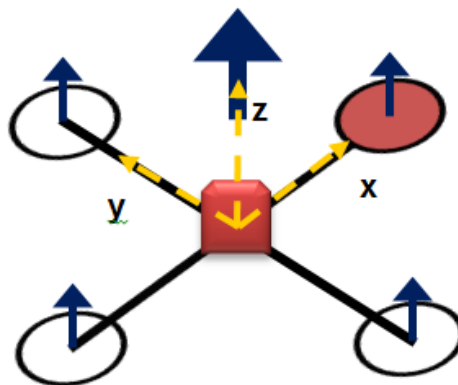
Figure 1-10: Throttle command response

1.3.2 Roll

The roll command is provided by simultaneously increasing (or decreasing) the left propeller speed and decreasing (or increasing) the right propeller speed, while keeping the front and rear propellers spinning at the same speed. With one rotor spinning faster than the rotor on the opposite side, more lift will be generated on the side of the faster spinning rotor, thereby tilting the helicopter to the opposite side. This is because of the torque created by the changes in lift forces with respect to the quad-rotor body x-axis and that creates a roll angle, φ, as shown in figure 1-11.

When the helicopter is tilted, the air is deflected slightly sideways instead of directly downwards, and the helicopter will move in the direction of its tilt. The total vertical thrust is maintained as in hovering, thus this command leads only to a roll angular acceleration.
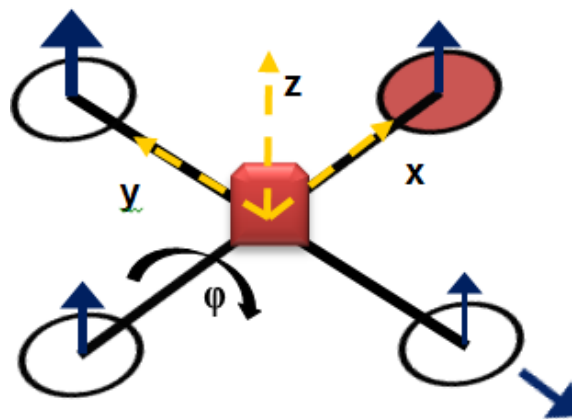
Figure 1-11: Roll command response

1.3.3 Pitch

The pitch and roll commands are very similar. It is provided by simultaneously increasing (or decreasing) the rear propeller speed and decreasing (or increasing) the front propeller speed, while keeping the left and right propellers spinning at the same speed. Since more lift is generated on the side of the faster spinning rotor, the helicopter will tilt towards the side of the slower spinning rotor. This is because of the torque created by the changes in lift forces with respect to the quad-rotor body y-axis and that creates a pitch angle, θ (known as a nose-up or nose-down in a conventional aircraft), as shown in figure 1-12.

When the helicopter is tilted, the air is deflected slightly sideways instead of directly downwards, and the helicopter will move in the direction of its tilt. Again, the total vertical

thrust is maintained as in hovering, thus this command leads only to a pitch angular acceleration.
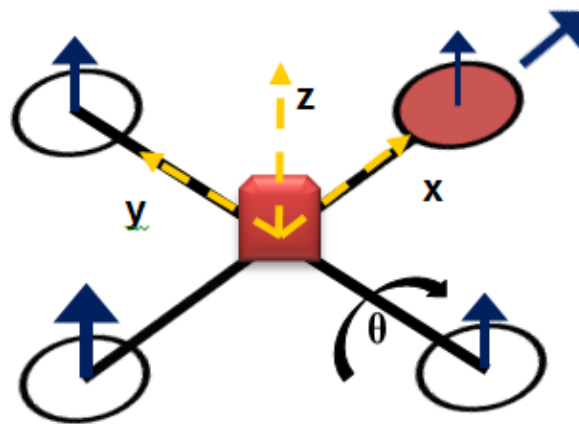
Figure 1-12: Pitch command response

1.3.4 Yaw

This command, which simulates the rudder on a conventional aircraft is provided by simultaneously increasing (or decreasing) the front-rear propellers' speed and decreasing (or increasing) that of the left-right duo. This creates a torque imbalance with respect to the quad-rotor body z-axis, which makes the quad-rotor helicopter to pirouette about that axis, creating an angle, ψ, in response to whichever direction the command is given as shown in figure 1-13.

In this case, there is no translational motion since the helicopter does not tilt in any direction and all the air is deflected directly downwards. As observed in roll and pitch movements, the total vertical thrust is still maintained as in hovering; hence this command leads only to a change of heading.
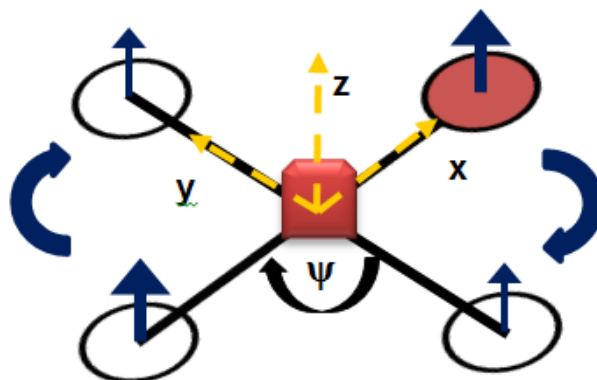
Figure 1-13: Yaw command response

1.4 Applications of Miniature Quad-rotor Helicopters

Modern society is no longer tolerant to the losses of human lives. Regardless of whether these losses emanate from a war or a hazardous accident; the mind-set of the global citizen cannot simply accept death in such a technically advanced world. The aviation industry, since inception has witnessed the loss of human lives as a result of accidents; and however much of funding and devotion the industry commits in order to provide safety will not prevent such mishaps from happening. It is very improbable, even in the future that such mishaps will be completely eradicated, since factors such as human error and dangerous flight situations are beyond human control.

The removal of the pilot from the cockpit gives UAVs a great advantage over manned aircraft, such that at no time during flight are human lives at stake. This advantage gives them the ability to carry out operations, which their manned counterparts find very tasking and dangerous to do. Some of the many examples of missions that could be classified as unsafe for manned aircrafts are – surveillance over nuclear reactors, surveillance over hazardous chemicals, fire patrol, volcano patrol, hurricane observations and rescue missions over adverse weather conditions [8].

The unsuitability of manned aircraft in undertaking these types of missions has repeatedly occurred throughout history. There have been situations where survivors from sea accidents were drowned, just because the aerial rescue operation conducted by manned aircraft was delayed in tracking them due to bad weather, which the pilots had to contend with. In the past, UAVs have been given the chance to test their capabilities in executing operations that were considered too risky for manned aircrafts. A good example is the Aerosonde UAV, which was flown around the tropical cyclone Typhoon in the western coast of Australia in 1998. The mission was a great success as it turned out to be the very first time when meteorologists were able to take readings from an aerial platform so close to the cyclone [9].

Miniature quad-rotor helicopters have extremely varying application domains that cover many indoor and outdoor applications including:

1.4.1 Border Patrol

Miniature quad-rotor helicopters have been engaged in aerial surveillance and monitoring of borders, ground based objects. With intelligent computer control and minimal human supervision, individual or multiple autonomous quad-rotors are able to patrol borders. The

use of a swarm of quad-rotors would permit continuous aerial surveillance, with new vehicles launched to take over from those in need of a battery recharge or ones that may have been damaged in the process [10].

Many countries and organizations are making efforts in wildlife conservation to protect rare and endangered animals like the one-horned rhino from poachers by using such UAVs to patrol the borders of the vast parks as shown in figure 1-14. This is made possible because multiple and distributed quad-rotor platforms working together can create the potential for a dynamic wireless routing layer, where the increased throughput and extended range of a mesh network becomes very beneficial.

CONTENT REMOVED FOR COPYRIGHT REASONS

Figure 1-14: An image from a UAV on border patrol [11]

1.4.2 Disaster Management/ Search and Rescue

There have been a large number of natural and man-made disasters throughout the world. Some of them are due to earthquakes, weather conditions or human acts of terrorism (e.g. the World Trade Centre Twin Tower attacks – 2001, Hurricane Katrina – 2005, the Haiti earthquake – 2010, the Japanese earthquake and tsunami – 2011, the Nairobi mall siege – 2013 among others). In such situations, disaster management or search and rescue teams have to swing into action to contain a situation or to find and save the victims as shown in figure 1-15.

<div style="border: 1px solid black; text-align: center; padding: 150px 0;">

CONTENT REMOVED FOR COPYRIGHT REASONS

</div>

Figure 1-15: UAV for search and rescue in the coastlines [12]

Reducing detection time is very critical to disaster management operations, because the rescue teams would have little or no time before a situation gets out of control. In fact, they would typically have about 48 hours to rescue victims before their chances of survival decrease dramatically. It is hard to analyze disasters or to locate human beings or objects buried under piles of rubble or floating on water, especially in difficult weather conditions. Sniffer dogs have proved to be very helpful in search and rescue operations; however, the dogs always find it difficult in climbing across much of the debris and the dust-laden air tends to weaken the dogs' intense sense of smell. Robots may be the most effective solution for such time constrained and dangerous disaster management or rescue missions, because they use sensors that can be more effective in such conditions [13].

Like the sniffer dogs, ground-moving robots also have difficulty navigating some terrains because of the many impediments in such scenarios. Flying robots like the miniature quad-rotor helicopters are able to help in assessing disasters situations, find victims trapped in buildings or under piles of rubble, and provide first-responders with information about a site, very quickly and accurately as shown in figure 1-16. UAVs are able to perform well for days successively devoid of becoming stressed in dangerous gasses, at night, in collapsed buildings, over water and in other dire situations, asking only for a 90-second battery swap a few times in return.

Figure 1-16: UAV for search and rescue in disaster situations in the Philippines [14]

1.4.3 Wild fire detection

UAVs equipped with advanced infrared sensors can perform surveillance and fire detection missions over forests (where access by foot or ground vehicles is difficult or impossible) and alert the fire brigade on time. Wildfires differ from other fires by their extensive sizes, the speed at which they can spread, their potential to change direction unexpectedly, and their ability to jump gaps such as roads, rivers and fire breaks. In many parts of the world, they pose a great risk to life and infrastructure as they can have negative ecological effects and cause extensive damage to human lives and property [15].

Early detection is a key factor to wildfire fighting. Strategies of wildfire prevention, detection and suppression have varied over the years – including public hotlines, fire lookout towers and ground patrols. However, the accuracy of these methods, which largely depend on human observations have their limitations such as operator fatigue, time of the day, time of the year and geographic location. As captured in figure 1-17, aerial monitoring through the use of quad-rotor helicopters can provide a wider view and give more accurate information about the location of the outbreak of the fire as well as many other factors, which could aid the spread of the fire – such as wind speed, temperature and humidity [16].

CONTENT REMOVED FOR COPYRIGHT REASONS

Figure 1-17: Fire monitoring using a UAV (left) and a thermal infrared scanner (right) [16, 11]

1.4.4 Photography

The field of aerial imagery has seen the largest use of miniature quad-rotor helicopters. Such vehicles have within very short periods of time helped photographers create 3-dimensional models of many locations instead of the normal flat maps. Having on-board cameras gives the users the option of streaming live videos to the ground when the helicopter is aloft. Several establishments have also used this for real estate photography and property inspection as shown in figure 1-18. Others take advantage of the quad-rotor's closed-circuit television capabilities and ability to provide an eye in the sky to the action below.

CONTENT REMOVED FOR COPYRIGHT REASONS

Figure 1-18: Remote controlled helicopters fitted with cameras fly above Sydney [17]

1.4.5 Military and Law enforcement

UAVs can take on the role of manned police helicopters in a more cost effective way as they can quietly hover when stalking or collecting status data of an object of interest and beam back information or images to the military and law enforcement agencies as shown in figure 1-19. Their small size enables them to penetrate an enemy's radar defences because of their decreased radar, acoustical and infrared signatures. This prevents them from being easily detected by the enemy. Even if they are detected and shot down, no human life would be lost as the operator would not be on-board like that of a manned aircraft [8].

These vehicles could serve as mobile communication links between military commands where or when satellite or radio communication installations are unavailable. They could also be configured and deployed as a swarm of vehicles to form a co-operative structure, forming a dynamic communication network that reconfigures itself based on needs or circumstances leading to constant communication coverage of the combat area. A real time view of the combat area will be very helpful to commanders in making quick and tactical real time decisions that could lead to victory.

CONTENT REMOVED FOR COPYRIGHT REASONS

Figure 1-19: UAVs assist the law enforcement agencies with tracking and aerial photography [11]

1.4.6 Research

Any kind of research (environmental, atmospheric, archaeological, pollution and many more) can be carried out by UAVs equipped with the appropriate payloads. Miniature quad-rotor helicopters are popular devices that are used by universities and research establishments in

testing and assessing innovative concepts and designs in a number of diverse fields as shown in figure 1-20.

They are relatively cheap to acquire, available in a range of shapes, sizes and configurations, with their simple mechanical design meaning not much of maintenance is required. Due to the multi-disciplinary nature of quad-rotors, researchers from a number of fields need to align their skills and efforts to make momentous improvements to the way quad-rotors perform. Such research projects are characteristically partnerships between aerospace engineering, control engineering, mechanical engineering, electrical engineering, artificial intelligence and computer science experts.

Major world-class research laboratories currently working on advanced control techniques and applications for quad-rotors are MIT's Aerospace Controls Lab, ETH's Flying Machine Arena, University of Essex Robot Arena, STARMAC at Stanford University and GRASP Lab at University of Pennsylvania [18].

CONTENT REMOVED FOR COPYRIGHT REASONS

Figure 1-20: Flight demo at University of Derby (left) and the autonomous squadron from KMel Robotics (right) [19]

1.4.7 Agricultural and Industrial applications

When it comes to agricultural and industrial applications, quad-rotors have proved to be very useful. Such applications can be crops spraying, nuclear factory surveillance, surveillance of pipelines and many more.

Farmers are already using miniature quad-rotors to monitor their crops in the field. An overhead picture of a farm taken at regular intervals can give information needed to adjust the

use of chemicals, water and other farm materials on the plants, thereby saving money and the environment [20].

CONTENT REMOVED FOR COPYRIGHT REASONS

Figure 1-21: A quad-rotor helicopter working alongside heavy farm equipment [21]

Quad-rotor UAVs can be used to perform geophysical surveys and energy companies use them to monitor the integrity of electric pylons, gas pipelines and related installations. For above-ground pipelines, this monitoring activity could be performed using cameras mounted on one or more quad-rotor UAVs as shown in figure 1-22.

CONTENT REMOVED FOR COPYRIGHT REASONS

Figure 1-22: A quad-rotor helicopter used to monitor industrial installations [22]

1.5 Chapter Summary

Over the past two decades, the research community has taken particular interest in UAVs because of the emergence of a large number of potential civil and military applications. Currently, many research establishments are working to produce remotely piloted UAVs that are capable of air to air combat, aerial refueling, combat search and rescue with facial recognition, resupply to agents on the ground and many more.

The possibilities of the use of such vehicles are endless, because in future, they will be able to perform an increasingly sophisticated array of missions apart from what they are capable of doing today. However, such vehicles will never fully replace humans because of the costs involved in developing systems as complicated as humans and technical risks that would follow the implementation of such systems.

STATE OF THE ART AND KEY RESEARCH REVIEWS

This chapter provides a review of literature, which is relevant to the study and which critically appraises the works of others. It goes on to outline the state of the art principles of control and simulation techniques as applied in this research, giving examples of their general applications in problem solving and specifically stating their applications relating to flight control – namely Computational Fluid Dynamics (CFD), Artificial Neural Networks (ANNs) and Fuzzy logic (FL). It also provides the background for the research with details of the project aim and objectives; gives a justification for the choice of control technique and highlights the contributions of this work.

2.0 Previous works on the quad-rotor helicopter

UAVs have continued to capture enormous commercial potential by attracting the attention of many people including laymen, potential appliers, vehicle professionals and researchers. Research and development in this field has gained increasing significance, due to the emergence of a large number of potential civil applications. Several structures and configurations have been developed to allow 3-D movements. For example, there are blimps, fixed-wing planes, single rotor helicopters, bird-like prototypes, quad-rotors, etc. Each of them best suited for certain types of missions, considering their advantages and drawbacks.

A plethora of research groups are using the quad-rotor design as a test bed for a swarm of projects. Some of the common uses are in developing advanced control systems, improved autonomous control, sensor arrays and surveillance equipment. To effectively control the quad-rotor helicopter, two major motion problems have to be carefully analysed and solved. First, it should be able to hover stably and second, it should be able to keep up with the planned path and speed, despite any disturbance.

With the rapid advancement in electronics leading to the availability of miniaturized motion sensors, high power to weight ratio batteries and high speed DC motors, there have been many different approaches to the control of quad-rotors; none of which may either be completely right or wrong, because the solutions to these problems are not straight forward. Some are obviously more suited than others in some situations, but any working alternative can be defended.

The numerous amount of published work using quad-rotor design is suggestive of the variety of topics involved. While the bulk of the published work deals with control systems and sensor arrays, some papers have dwelt on developing accurate aerodynamic models, improving the system design and developing point-to-point real time communication between multiple quad-rotor vehicles. The hobbyist community has not been left behind as it has documented a great deal of work with regards to developing very cheap home built (possibly DIY) quad-rotors for personal use.

There have been a number of attempts to build quad-rotors, by and large though; the dynamics for all the different models remain unchanged [23]. There are a few exceptions, however, such as Dodd in [24] made provision for the rotors to be tilted to achieve translational motion without necessarily rotating the vehicle. Researchers use the quad-rotor

helicopter as an excellent test-bed for advanced control techniques due to the simplicity of their construction and maintenance, their ability to hover and also to take-off and land vertically and also the fact that control of the vehicle is achieved only by varying the speed of the 4 rotors.

A notable group that has contributed to quad-rotor literature is Castillo et al [25], whose work has looked into back-stepping with nested saturations, for real-time control of the quad-rotor. This non-linear control technique has constraints placed on the amplitudes of the inputs; it then operates to meet these constraints. It seemed to perform well in the presence of disturbances. In [26], the same group compared the nested saturation approach with classical PD control, where the benefits of the nested saturations algorithms are shown to be an improved handling of disturbances.

Bouabdallah [27], developed PID controllers for orientation stabilization and modern LQ control are compared, despite realizing that the later one yielded average results due to assumptions made during modelling that could have introduced errors into the control strategy. The main advantage of this technique is that the optimal input signal turns out to be obtainable from full state feedback (by solving the Ricatti equation). On the other hand the analytical solution to the Ricatti equation is difficult and takes time to compute. The OS4 Project was started at the Swiss Federal Institute of Technology in 2003 with an aim to develop devices for searching and monitoring hostile indoor environments. It resulted in the development of a control law based on classical control and also modern control methodology.

Over the years, the Australian National University has carried out meticulous studies on quad-rotors. The X4-flyer Mark II, which weighs about 2kg and measures up to 70cm in length with rotors of 11inch diameter, was designed and fabricated [23]. They incorporated a discrete-time PID control law to their model, including the very fast blade flapping dynamics. The closed loop behaviour turned out to be poor at higher speeds, approaching an unstable behaviour and that was attributed to high-frequency noise from the rotors interfering with the accelerometer readings.

The Robotics Laboratory of Versailles [28, 29, 30] has also considered sliding mode control, back stepping and dynamic feedback for stabilization and simple trajectory tracking. Here, the dynamic feedback control was implemented on quad-rotor test beds to transform the closed loop part of the system into a linear, controllable and decoupled subsystem but was

seen to be insufficient to cope with significant external disturbances, the sliding mode controller proved to be better in simulation.

Tayebi and McGilvary in [31, 32] undertook a thorough study on control techniques for attitude stabilization of a quad-rotor. They used quaternion for attitude representation, Lyapunov stability criterion and a PD2 feedback structure, with which a model-independent PD controller was compared. Both configurations achieved stability and disturbance rejection. Their experimental results start a deviation from the trend within the papers reviewed that seems to suggest that traditional linear controllers are not sufficient for stabilization of the quad-rotor.

Other examples of trajectory following controllers include [33], where H_∞ is considered. This control technique, using a two degree of freedom architecture has the ability to cope with modelling inaccuracies. The results through simulation show good tracking as well as good disturbance rejection. In [34], Driessen and Robin proposed a two phase controller in which the first phase considers attitude and the second phase position and the yaw angle. Using differential flatness, global convergence of the tracking error to zero is proven assuming positive thrust.

There are considerably fewer trajectory generation papers for the quad-rotor. In [35] output space trajectory generation is considered using differential flatness. Here, they only consider straight line trajectories using a simple parameterization and is, therefore, not considering optimality and is assuming feasibility of the straight line.

The fluctuation and/or unavailability of GPS signals inside buildings or in certain areas with high rise buildings or mountains creates a situation where the papers reviewed so far are usually based on simulation results with a number also including results from a 2 degree of freedom experimental rig. There are a number of alternatives for solving this problem. In [36] the test-bed at Massachusetts Institute of Technology (MIT) is described. Consisting of VICON cameras and a number of quad-rotors with visual markers, this system provides accurate attitude and position feedback to a ground station; however, the system is certainly not cheap and does not offer a commercial solution.

At Stanford University a multiple vehicle test-bed is used for comparison of design control techniques [37]. This test-bed with a capacity for up to 8 vehicles [38] is only operational outdoors however as it relies on GPS. A cheaper solution which has been considered by a

number of institutions is that of visual feedback. In [39] and [40] two cameras are used for POSE (Position and Orientation) estimation, one camera is on-board the vehicle and the second is a ground based pan tilt camera. This set up is used to compare nonlinear control techniques. However this is not a complete solution as noted in [39] 'A helicopter cannot be fully autonomous if it depends on an external camera.' In [41] a single on-board camera system is proposed which tracks a moving ground vehicle. In [42] a circular trajectory is followed, using a positional estimate, obtained through an on-board camera, viewing a square target on the ground.

In [43] an adaptive neural network control to stabilize a quad-rotor helicopter against modelling error and wind disturbance was proposed. It was compared with both dead zone and e-modification adaptive techniques, but also stops at a simulation without implementation on the real hardware. The results of the simulation show an improvement in achieving a desired attitude and reduction of weight drift.

In [44], the group tried to augment a conventional PD controller conceived mainly for hovering, with an adaptive element using a real-time tuning single hidden layer neural network in an inner-outer loop combined architecture to account for model inversion error cancellation, issued in the feedback linearization process. Simulation results show a good performance of the augmented controller in tracking manoeuvres.

In [45] the quad-rotor's linearized equations of motion were used to develop control laws for way point tracking paths. The performance of the laws with uncertainties such as wind and saturation were analysed and results showed that the laws do not perform well when there is an uncertainty. In [46], system modelling and control algorithm development was done, with a comparison of PID controllers developed. A simulator and a real platform were developed to test the results.

AI-Younes and Jarrah [47] introduced a backstepping fuzzy Logic controller (BFL) and backstepping least mean square controller (BLMS) as new approaches to control the attitude stabilization of a quad-rotor. A recursive Lyapunov function was used bring about stability around a fixed set-point using backstepping control algorithm. The BFL controller utilizes the advantage of fuzzy logic to schedule the backstepping controller parameters. It showed improved performance compared with that achieved by backstepping controller alone. A comparison between Backstepping, BFL and BLMS controllers showed that the BLMS

controller suffered from a slow time response while having reduced control effort when compared with the BFL controller.

Abeywardena [48] used a fuzzy logic design to try to stabilize and control the quad rotor. The controller was controller was then used to achieve stable hovering of the quad-rotor, amidst velocity disturbances. The simulation results show good results at stable hover.

Dierks [49] introduced a framework for leader-follower formation control for multiple quad-rotor UAVs, based on spherical coordinates. The control objective for the follower UAV is to track its leader at a desired- separation, angle of incidence, and a bearing by using an auxiliary velocity control. Then, a neural network (NN) control law for the dynamical system was introduced to learn the complete dynamics of the UAV including unmodelled dynamics like aerodynamic friction. Results show some stability achieved in the entire formation using Lyapunov theory.

Raffo [50] used dynamic motion equations obtained by Lagrange-Euler formalism in a hierarchical control structure consisting of a model predictive controller (MPC) to track the reference trajectory together with a non-linear H_∞ controller to stabilize the rational movements. The trajectory was maintained by performing an on-line trajectory re-optimization during the flight to obtain the optimal path in terms of cost. This makes it adapt to the constantly changing environment. In both controllers, the integral of the position error was considered and a null steady-state error was achieved when sustained disturbances acted on the system.

Theerasak [51] worked on a control methodology for a UAV with quad-rotor mechanism. A conventional PID controller and self-tuning PID based on fuzzy logic were compared and analyzed. The performance results of the two controllers when applied to a quad-rotor UAV show that both controllers are acceptable in the case of no variation in load.

Again, Pounds [6] used tuned plant dynamics with an on-board embedded attitude controller to stabilize flight, independent linear SISO controllers were designed to regulate flyer attitude and performance of the system was demonstrated in indoor and outdoor flight.

Dierks [52] proposed a nonlinear controller for a quad-rotor UAV, using neural networks (NNs) and output feedback. The NN is introduced to learn the complete dynamics of the UAV online and an NN observer is introduced to estimate the translational and angular

velocities of the UAV, and an output feedback control law is developed. Simulations show that the proposed controller outperforms a conventional linear controller.

In 2008, He [53] developed a motion planning algorithm for a quad-rotor helicopter flying autonomously without GPS using the Belief Roadmap (BRM) Algorithm to plan the vehicle trajectory that incorporates sensing. The helicopter was able to navigate an indoor environment with a laser range-finder. Cowling [1] achieved trajectory following using a number of linear control techniques, with the LQR being unable to adapt to environmental changes. A test of Model-based predictive control (MBPC), was found to guarantee constraint satisfaction at every time step, but was also found to be time consuming and therefore a combined controller was proposed using MBPC and LQR.

Balas [54] described the use of PID and LQR methods to control the position and the yaw angle of a quad-rotor helicopter using a full non-linear Simulink model, starting with the most mathematical approach and moving towards the most physically feasible approach. Results show that the quad-rotor was satisfactorily able to track the given input trajectory.

Lee [55] in 2010 developed a nonlinear tracking controller on the special Euclidean group SE (3) with desirable closed loop properties that are almost global and went on to illustrate the versatility of the controller in simulations. Markus [56] presented an algorithm that calculates the flight trajectories for quad-rotors, with a demonstration of the trajectory generation and tracking performance at the ETH Zurich Flying Machine Arena test-bed. It was observed that the unmodelled aerodynamic effects caused trajectory deviations when the helicopter was decelerating from high speeds – with an emphasis on the need for improving the performance and correcting for aerodynamic effects.

Stingu [57] in 2011, focused on quad-rotor control and heterogenous multi-vehicle cooperation. In this work, reinforcement learning algorithms were used to design suboptimal controllers for a class of complex systems that can be conceptually split in local loops with simpler dynamics and relatively weak coupling to the rest of the system.

In 2012, Mellinger [58] described an approach to modelling and control of a single quad-rotor, with methods that worked well for near hover flight and also controls for large roll or pitch angles. The thesis also extended the developed control methods to systems with multiple quad-rotors attached to the same rigid body, enabling the vehicles to work together and then went on to develop trajectory generation methods for the vehicles.

Javier [59] attempted to prove the viability of using a quad-rotor helicopter as a measurement instrument of wind profiles within large offshore wind farms. The project analyzed the idea of wind profile characterization by relating the attitude of a quad-rotor to local wind profile.

In 2013, Kushleyev [60] described a prototype of an autonomous micro quad-rotor with on-board attitude estimation and control that operates with an external localization system. The paper went on to discuss the aerodynamics of vertical flight and the contributions of ground effect to the vehicle performance. It also presented architecture and algorithms to coordinate a swarm of micro quad-rotors.

Abdolhosseini [61] developed a model predictive control algorithm to control a quad-rotor helicopter. A model reduction technique was developed to reduce the burden of calculations in the application of the controller into an airborne platform.

In 2014, Alexis [62] developed a model predictive control strategy for the trajectory tracking of a quad-rotor helicopter. The dynamics of the quad-rotor were modelled using a hybrid systems approach, and specifically, a set of piecewise affine (PWA) systems around different operating points of the translational and rotational motions. Simulations show efficiency of the controller in trajectory tracking and aerodynamic disturbance attenuation.

A number of other works will be referred to in this thesis as found applicable to the chapters.

2.1 The basics concepts of Computational Fluid Dynamics (CFD)

Computational Fluid Dynamics (CFD) is a branch of fluid mechanics that uses numerical methods and computer algorithms to solve and analyze problems that involve fluid flows. This design tool has been developed over the past few decades and will continually be developed as the understanding of the physical and chemical phenomena underlying CFD theory improves. In CFD, computers are used to execute the calculations required to simulate the interaction of fluids (liquids and gases) with surfaces defined by boundary conditions. Using computers with high-speed processors offers better solutions in analyzing and solving fluid flow problems. The goals of CFD are to be able to accurately predict fluid flow, heat transfer and chemical reactions in complex systems, which involve one or all of these phenomena [63].

Presently, CFD is increasingly being employed by many industries either to reduce manufacturing design cycles or to provide an insight into existing technologies so that they

may be analysed and improved to provide solutions to many problems. Examples of such industries include medical, aerospace, power generation, process industries, automotive, chemical engineering and construction as shown in figure 2-1.

CONTENT REMOVED FOR COPYRIGHT REASONS

Figure 2-1: CFD application in automotive simulation (left) and blood flow in the human body (right) [64, 65]

As a design tool, CFD presently sits behind experimental analysis due to the fact that it does not produce absolute results. The reason for this is that the numerical methods, which govern the solutions in a CFD problem, rely on several modelling assumptions that may not have been validated to a satisfactory level. However, [64, 66] state that CFD presently offers itself as a powerful design tool and even more so in the future because:

a) Dangerous or expensive trial and error experiments can be simulated and design parameters observed prior to any physical prototype being constructed;

b) Computers are becoming even more powerful and less expensive, thus allowing larger CFD simulations to be performed, or more detailed simulations of present CFD problems;

c) The numerical schemes and physical models that are the building blocks of CFD are continually improving.

d) If a CFD model can be established yielding accurate results on one particular design, then the model can be used as a tool of prediction for that design under many different operating conditions.

2.1.1 Applications of Computational Fluid Dynamics (CFD) in Aircraft Control

Recent technology has led to aircrafts (especially military jets) that often manoeuvre in extreme conditions of the flight envelope, characterized by vortical flows and great shock effects - conditions which can cause flight dynamics and aero elastic instabilities [67]. Evidently, the linearized unsteady aerodynamic models no longer work at these conditions because the approximations cannot effectively cater for the ever-changing flow conditions. Presently, computational fluid dynamics (CFD) solutions are considered as the state of the art in modelling unsteady nonlinear flow physics [68] and such solutions provide timely, enhanced understanding and prediction of the aerodynamic characteristics of aircrafts as shown in figure 2-2.

It is well known that unsteady aerodynamic forces and moments not only depend on the instantaneous states but also on all of the states at times before the current state [69]. Unfortunately, this makes the solution of the aircraft equations of motion an infinite-dimensional problem, where the current states depend on the evolution of previous states at infinitely many points in time [70]. In [71-73], it is shown that technological advances have made it possible to solve this problem by developing a full-order model, based on direct solution of discretized Reynolds-averaged Navier–Stokes (RANS) equations coupled with the dynamic equations governing the aircraft motion.

It was thought that an alternative approach to creating the full-order model is to develop a reduced order model (ROM) that seeks to approximate CFD results by extracting information from a limited number of full-order simulations as described in [74, 75]. These ROM techniques have been used extensively for flutter prediction, limit cycle oscillation, and gust-response modelling as seen in [76], but their applications to aircraft stability and control are still new [77].

CONTENT REMOVED FOR COPYRIGHT REASONS

Figure 2-2: CFD application in simulation of vortices around aircrafts [77]

Details of the CFD process, which has to do with airflow and turbulence simulations as applied to this research, are presented in chapter 5 of this thesis.

2.2 The basic concepts of Artificial Neural Networks

An artificial neural network is a computational structure inspired by the study of biological neural processing. There are many different types of neural networks, from relatively simple to very complex, just as there are many theories on how biological neural processing works. It is a powerful data modelling tool that is able to capture and represent complex input/output relationships [78]. The motivation for the development of neural network technology stemmed from the desire to develop an artificial system that could perform "intelligent" tasks similar to those performed by the human brain. Neural networks resemble the human brain in the following ways:

a) A neural network acquires knowledge through learning.
b) A neural network's knowledge is stored within inter-neuron connection strengths known as synaptic weights.

The human brain is known to contain about 100 billion nerve cells, or neurons. On the average, each neuron is connected to other neurons through about 10,000 synapses, though the actual figures may vary greatly from one neuro-anatomy to the other. The human brain's network of neurons forms an enormous parallel information processing system. This contrasts

with conventional computers, in which a single processor executes a single series of instructions. Against this, consider the time taken for each elementary operation, where neurons typically operate at a maximum rate of about 100 Hz, while a conventional computer CPU carries out several hundred million machine level operations per second. Despite being built with very 'slow hardware'; the human brain has quite remarkable capabilities [79].

The true power and advantage of neural networks lies in their ability to represent both linear and non-linear relationships and in their ability to learn these relationships directly from the data being modelled. Traditional linear models are simply inadequate when it comes to modelling data that contains non-linear characteristics.

ANNs being non-programmed adaptive information processing systems can autonomously develop operational capabilities in response to an information environment. They learn from experience and are able to generalize from previous examples. They can also modify their behaviour in response to the situations they are faced with, and are ideal in cases where the required mapping algorithm is not known and tolerance to faulty input information is required. ANNs offer certain advantages over conventional electronic processing techniques. These advantages are the generalization capability, parallelism, distributed memory, redundancy, and learning [80].

Figure 2-3 shows a simple artificial neural network model, normally referred to as an MLP (Multi-Layer Perceptron).
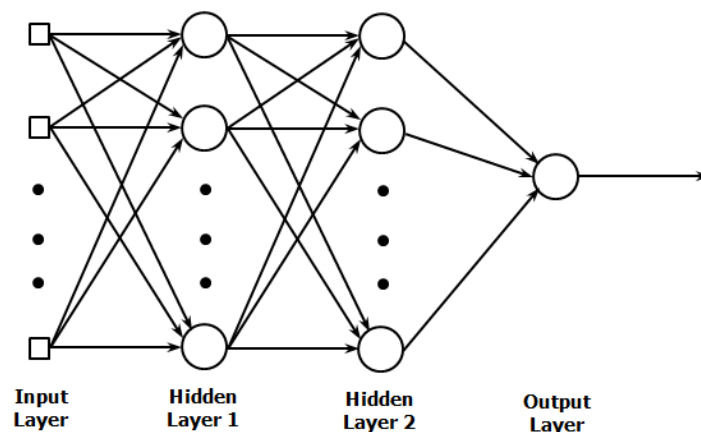
Figure 2-3: Artificial neural network model

Despite ANNs' attempts to bring computers closer to the human brain's capabilities by imitating certain aspects of its information processing in a highly simplified way, the performance of the best ANN is trivial when compared with even the simplest biological

system. Artificial Neural Networks are not universal solutions to all problems; they are just an excellent alternative mathematical device for rapidly processing information and data.

ANNs are being applied to a wide variety of automation problems including adaptive control, optimization, medical diagnosis, decision making, as well as information and signal processing, including speech processing. They have proven to be very suitable for processing sensor data, in particular, feature extraction and automated recognition of signals and multi-dimensional objects. Pattern recognition has, however, emerged as a major application because the network structure is suited to tasks that biological systems perform well, and pattern recognition is a good example where biological systems out-perform traditional rule-based artificial intelligence approaches.

2.2.1 Applications of Artificial Neural Networks in Aircraft Control

Intelligent flight control systems are the next generation of flight control systems, designed to provide increased safety for the crew and passengers of aircraft as well as to optimize the aircraft performance. In the past few decades, major advances have been made in the area of adaptive control of linear time-invariant plants with unknown parameters. The choice of the controller structure is normally based on well-established results in the theory of linear systems, while stable adaptive laws which assure the global stability of the overall system are derived based on properties of the system to be controlled. Artificial Neural Network based control schemes have attracted much attention because of their powerful ability to approximate continuous nonlinear functions as depicted in figure 2-4.

Neural control strategies can be broadly classified into off-line and on-line schemes based on how the parameters of the network are tuned. When the neural controller operates in an on-line mode, it has no a priori knowledge of the dynamics of the system to be controlled and the network parameters are updated while the input – output data is received. In the off-line control, the network's parameters are determined from the unknown training pairs and then those parameters are fixed for control purposes [81]. A neural controller with on-line learning capabilities can adapt to changes in the dynamics of any system and hence is an ideal choice for controlling highly nonlinear systems with high degrees of uncertainty [82]. The control engineering community has continually explored the use of biologically inspired techniques to solve difficult optimization and control problems [83].

The performance of aircraft systems is highly dependent on the capabilities of the guidance, navigation and control systems. This demands the need for reliable adaptive control systems.

It is not in doubt that developing flight control systems for today's aerospace vehicles is complex and time consuming. While the theory is understood, its application could be lengthened because of the need to align the skills and efforts of different disciplines in science and engineering to achieve a successful system design.
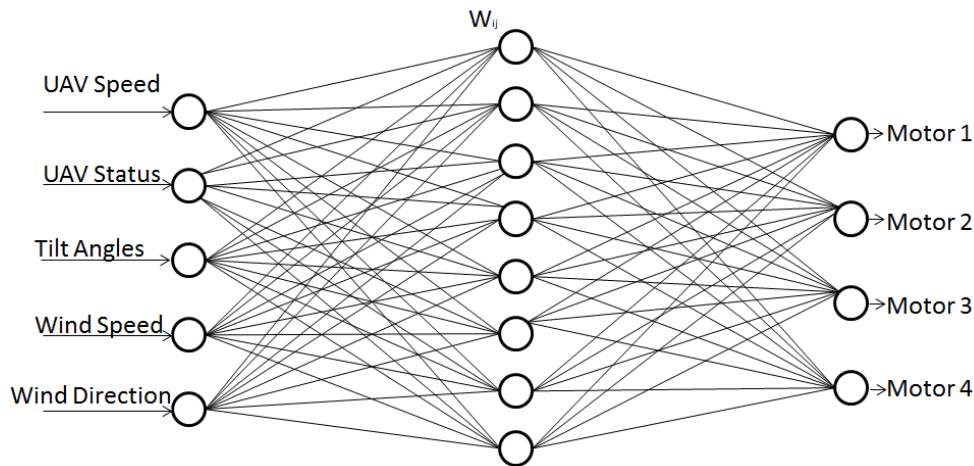
Figure 2-4: Artificial neural network model for UAV control

Details of the neural network system, which has to do with Control simulations as applied to this research, are presented in chapter 7.

2.3 The basics concepts of Fuzzy Logic

Fuzzy logic is a problem-solving system that provides an approximate but effective means of describing the behaviour of systems that are too complex, vague, imprecise or not easily analysed mathematically. Logic generally deals with true or false, but a proposition can be true on one occasion and false on another – like "Apple is a red fruit". A green apple makes that proposition false. On the other hand, a red apple makes it true. If a proposition is true, it has a truth value of 1; if it is false, its truth value is 0. These are the only possible truth values when using the normal Boolean logic.

Propositions can be combined to produce other propositions, by means of logical operations. Statements are said to be crisp when they are made with certainty. However, some statements cannot be made with such certainty because of surrounding circumstances, which may not be easily defined or predicted. This type of situations is what fuzzy logic was developed to

model. Fuzzy logic deals with propositions that can be true to a certain degree – somewhere between 0 and 1 [84].

Fuzzy logic was first developed in the mid-1960s when Zadeh argued that efforts to automate various types of activities from assembling hardware to medical diagnosis have been hampered by the gap between the way human beings reason and the way computers are programmed. In this case, graded statements rather than ones that are strictly true or false, yes or no are used. It attempts to incorporate the "rule of thumb" approach generally used by human beings for decision making. Thus, fuzzy logic provides an approximate but effective way of describing the behaviour of systems that are not easy to describe accurately.

Fuzzy logic controllers, for example, are extensions of the common expert systems that use production rules like "if x and y then z". With fuzzy controllers, however, linguistic variables like "hot" and "very hot" might be integrated into a conventional expert system. The result is that fuzzy logic can be used in controllers that are capable of making intelligent decisions in unpredictable and rapidly changing problem situations. Fuzzy logic's approach to problem-solving mimics how a human being would make decisions, only much faster [69]. Figure 2-5 shows a typical fuzzy logic system.
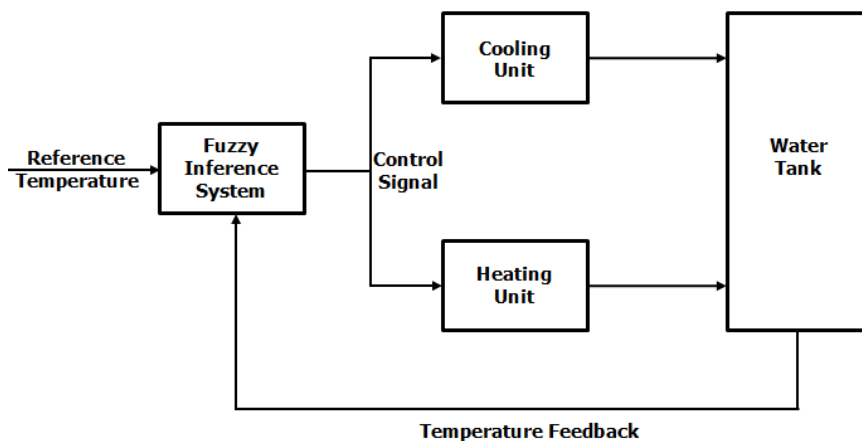
Figure 2-5: A simple fuzzy logic application

This control technique has been successfully applied in a number of applications: computer vision, decision making, and system design including ANN training. The most extensive use of fuzzy logic is in the area of control, where examples include controllers for cement kilns, braking systems, elevators, washing machines, hot water heaters, air-conditioners, video cameras, rice cookers, and photocopiers.

Fuzzy logic was considered a better method for sorting and handling data, but has proven to be an outstanding choice for many control system applications since it mimics human control logic. It can be built into anything from small, hand-held products to large computerized process control systems. It uses an imprecise but very descriptive language to deal with input data more like a human operator. It is very robust and often works when first implemented with little or no tuning.

2.3.1 Applications of Fuzzy Logic in Aircraft Control

The use of fuzzy logic in flight control is increasing rapidly. In [85], an investigation on autonomous flight control system for an atmospheric re-entry vehicle to cover the re-entry flight regions characterized by different actuator configurations was carried out. Simulation results showed very little tracking errors and performance within the acceptable range referred to as optimal. In [86] a flight simulator was used to assess a fuzzy logic based autopilot, whose rule set was developed from interviewing a pilot with great wealth of experience and flight hours, stating what control actions he would have taken in different flight conditions. This controller was found capable of keeping the aircraft along the glide path during final approach and landing.

Flight tests and simulations were carried out in [87] to demonstrate the ability of fuzzy logic in providing the required control for UAVs used for different civil and military mission as shown in figure 2-6.
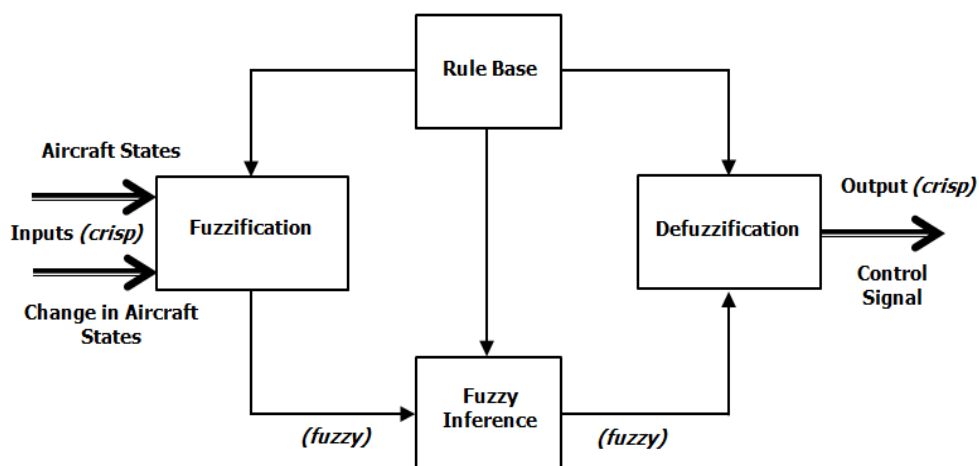
Figure 2-6: Fuzzy logic application in aircraft control

Details of the Fuzzy logic system, which have to do with control simulations as applied to this research, are presented in chapter 7 of this thesis.

2.4 Aim and Objectives of the research project

Helicopters are generally known to be dynamically unstable vehicles; hence the need to achieve stability using suitable control methods. The changing helicopter parameters and complex weather conditions make the vehicle unstable, although the unstable dynamics are good for providing it with the required agility.

This implies that the flight status of the quad-rotor must be continually monitored and controlled, as the ever-changing weather conditions (mainly the wind speed and direction) make them susceptible to even modest changes in environmental conditions. Without a robust adaptive controller, the quad-rotor is very likely to be slowed down in its operation or blown off the planned path, thereby leading to a failed, delayed or aborted mission or even the loss of the helicopter itself.

This research aims to demonstrate a consistent way to develop a novel robust adaptive controller for GPS-independent quad-rotor helicopters, using Fuzzy-Neural Networks. The controller is used to monitor and control the non-linear, multi-variable flying states of the quad-rotor helicopter; keeping it in the planned flight path and the desired flight speed through a series of complex weather conditions.

To complete the research project, the following objectives had to be achieved:

a) Development of a faithful analytical mathematical representation of the quad-rotor helicopter.
b) Investigation and evaluation of a Fuzzy-Neural network model for the quad-rotor helicopter flight controller.
c) Development of an innovative PC based controller for intelligent quad-rotor flight monitoring and control.

2.5 Choosing a Control Technique

The review of key literature for quad-rotor helicopter control techniques shows that some control techniques are better at solving particular problems than others. It also shows that using a combination of control techniques gives a better approach to achieving both stable

hover and precise direct motion, when it comes to rejecting or recovering from a disturbance. This is because in using a combination of control techniques, the strengths of one technique can be used as a compensation for the weakness of the other. The two control techniques chosen for this research are neural networks and fuzzy logic. A combination of the two would be a fuzzy-neural technique. This is expected to give the quad-rotor helicopter some form of human reasoning (from fuzzy logic) and the ability to learn (from neural networks).

2.5.1 Capabilities of Fuzzy- Neural Systems

Fuzzy systems can utilize approximate reasoning and are recommended for very complex processes, where simple mathematical models are difficult to derive. That is a major advantage of fuzzy logic, because the designer does not need to know everything about the system. It defines operations for modifying sets and allows elements to partially belong to the set, which offers a lot more flexibility. The reason for the popularity of fuzzy logic lies in the application of fuzzy sets, which give much greater flexibility than a regular set of numbers.

Neural networks on the other hand, have the ability to learn the system dynamics through training, which enables the system to adjust its weights in order to achieve better results. They do not require critical decision-making in their algorithms.

A combination of fuzzy logic and neural networks can alleviate the problems associated with each of these technologies. Neural network technology can be used to learn system behaviour based on system input-output data. This learned knowledge can then be used to generate fuzzy logic rules and membership functions, significantly reducing the development time. This provides a more cost effective solution as fuzzy implementation is typically a less expensive alternative than neural networks for embedded control applications.

This combination also helps solve the neural network's "Black Box" problem discussed earlier. Expressing the weights of the neural network using fuzzy rules helps provide greater insights into the neural networks, thus leading to a design of better neural networks.

Neural Fuzzy Systems can generate fuzzy logic rules and membership functions for complex systems for which a conventional fuzzy approach may fail. For such systems, conventional fuzzy logic approach uses complex hierarchical rules to keep their number low so that it remains within the limits of human capabilities.

2.6 Contributions of this work

The contributions of this work lie in the following:

a) **Analytical dynamic modelling** – design and analysis of control systems are usually started by carefully considering mathematical models of physical systems. An adequate dynamic system modelling of the quad-rotor helicopter involves a faithful mathematical representation of the whole system, normally described by differential equations. The equations of motion of quad-rotors have been modelled and simulated using Matlab/Simulink software. The model made it possible to define and predict the positions that the helicopter will reach at any point in time, by varying the speeds of the four motors. The model referred to in this contribution can be calibrated and linearized for use on any quad-rotor helicopter.

b) **CFD simulation and analysis** – a 3-D Solidworks model was developed with the same parameter values as that of the analytical dynamic model developed in Matlab/Simulink. Computational Fluid Dynamics (CFD) was then used to simulate and analyse the effects of the external environment/disturbances on the flow patterns of the quad-rotor helicopter within a given computational domain. After validation with actual flight experiment data, the model was found suitable for future analysis and prediction of the behaviour of the quad-rotor helicopter in an outdoor environment.

c) **Error compensation using artificial neural networks** – In an effort to generate more accurate simulation results so as to improve the performance and control of the quad-rotor helicopter, especially in the rejection of and recovery from a disturbance; a compensation system, which adopted a post correction technique, was developed to correct the error in the two models. The system, having being trained with data obtained from actual flight experiments at University of Essex, computed the compensation values of the two simulation models. The output of the system was used to train the quad-rotor fuzzy-neural controller.

d) **Development of a novel adaptive controller** – this research demonstrates a consistent way to develop a robust adaptive controller for quad-rotor helicopters, using Artificial Neural Networks and Fuzzy logic. Data obtained from simulations were used to train a fuzzy-neural system, creating controls which enable the quad-rotor helicopter to adapt to ever-changing environmental situations and learn from past missions.

2.7 Thesis layout

In order to achieve the research aim and objectives, this thesis has been tailored to nine distinct, but logically linked chapters.

Chapter 1 introduces unmanned aerial vehicles, giving a background, describing the major components of the quad-rotor helicopter, its basic concepts and applications.

Chapter 2 reviews relevant literature, outlines the principles and applications of key control and simulation techniques used in this research – namely Computational Fluid Dynamics (CFD), Artificial Neural Networks (ANNs) and Fuzzy logic. It also provides the background for the research with details of the project aim, objectives and gives a justification for the choice of control technique.

In chapter 3, the analytical dynamic model was developed using the Newton-Euler Formalism and considering the force-moment balance. This led to a set of equations of motion and the actuator dynamics equation, which were considered a faithful mathematical representation of the quad-rotor helicopter.

Chapter 4 shows an implementation of the analytical dynamic model using block libraries in Matlab/Simulink. Calibration and preliminary calculations were then carried out to ensure that the model performs as expected and to determine the operating point parameters. Simulations were run to investigate the open loop flight dynamics.

In chapter 5, a 3-D CAD model was designed with the same parameter values as that of the analytical dynamic model simulated in chapter 4. This model corroborated the analytical dynamic model as the responses of the two models were found to be very similar. Computational Fluid Dynamics (CFD) was then used to simulate and analyse the effects of wind flow patterns on the performance and control of the quad-rotor helicopter.

Chapter 6 affords details of the verification, validation and equipment used to acquire real flight test data in order to determine the credibility of the two models designed in chapters 4 and 5. Results of simulations performed with the two models were compared with results from real flight experiments performed at University of Essex Robot Arena. An artificial neural network function approximation tool, which was trained with the real flight experiment data was used to correct the errors found in the two models.

Chapter 7 demonstrates the design a novel robust adaptive fuzzy-neural controller for quad-rotor helicopters. Data obtained from simulations of the models developed in chapters 4, 5 and 6 were used to train the fuzzy-neural system.

In chapter 8, the fuzzy-neural controller was then integrated into a simulation system to show how the quad-rotor helicopter adapts to its changing environmental situations. The quad-rotor experienced winds of differing magnitudes and the results show how the controller compensates for the errors in the position and speed of the vehicle.

In conclusion, chapter 9 delivers the research summary, conclusions and recommendations for future studies.

2.8 Chapter Summary

Miniature helicopters have turned out to be a popular device used in the research of unmanned aerial vehicles (UAVs) due to their simple yet unique design. Regardless of their simplicity in the hardware design, the vehicles remain intrinsically unstable. Many different approaches to the control and stabilization of quad-rotor helicopters have been proposed, none of which may either be completely right or wrong, because the solutions to these problems are not straight forward. Some are obviously more suited than others, depending on the situation.

The review of key literature shows that using a combination of control techniques gives better results, because the strengths of one technique can be used as a compensation for the weakness of the other. The two control techniques chosen for this research are neural networks and fuzzy logic. A combination of the two would be a fuzzy-neural technique, which gives the quad-rotor helicopter some form of human reasoning (from fuzzy logic) and the ability to learn (from neural networks).

Figure 2-4 below shows a layout of the research project.
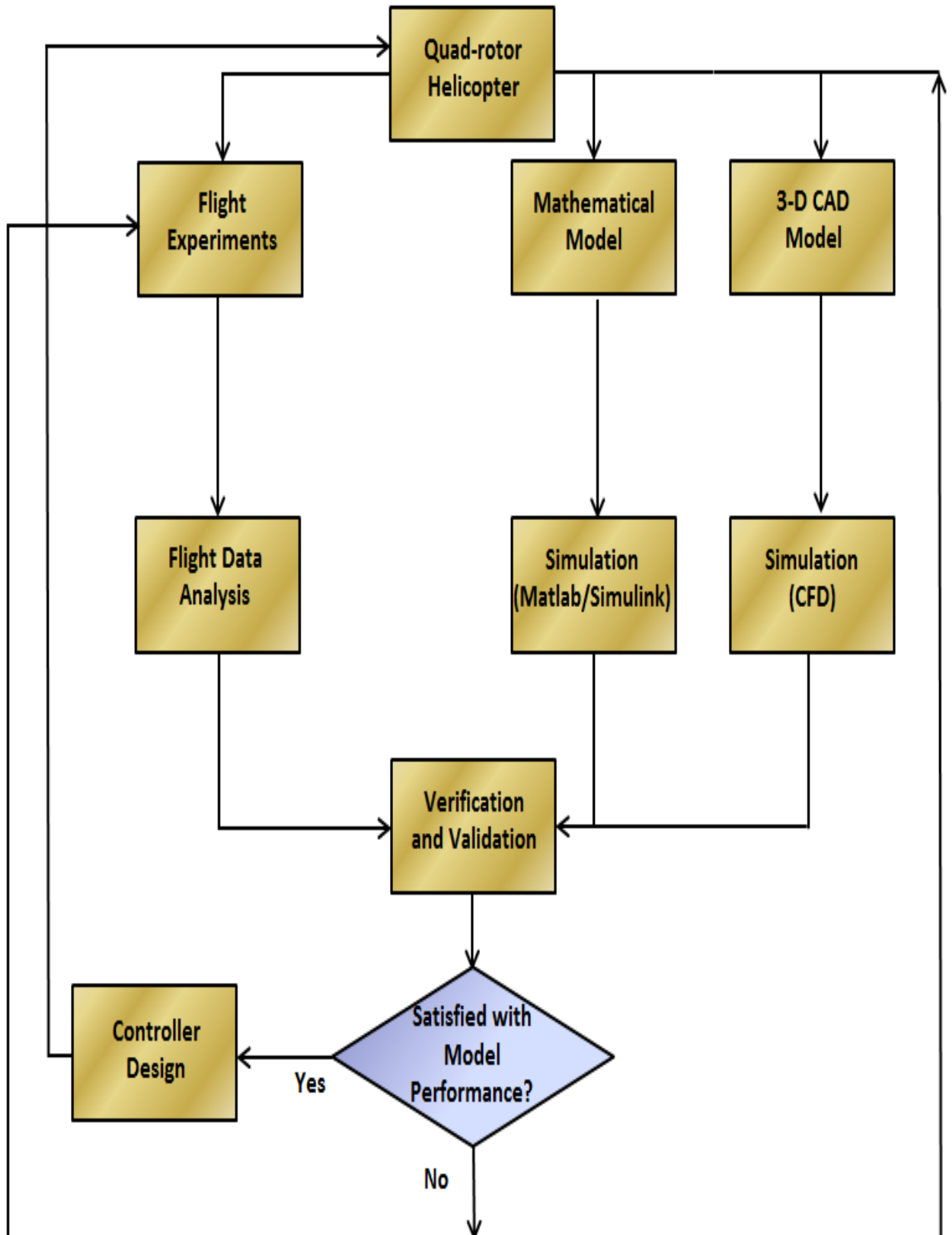
Figure 2-7: Overall Project Framework

ANALYTICAL DYNAMIC MODEL OF THE QUAD-ROTOR

This chapter presents the development of an analytical dynamic model of the quad-rotor helicopter using the Newton-Euler Formalism. The force-moment balance is considered, leading to a set of differential equations of motion, out of which three compute the angular accelerations of roll, pitch and yaw; and another three compute the linear accelerations in the x, y and z directions. The actuator (brushless DC motor) dynamics are also considered to establish its own equation. The set of equations in this case is considered a faithful mathematical representation of the quad-rotor helicopter.

3.0 The Newton-Euler model

Control systems exist in many fields of engineering so that components of a control system may be electrical, mechanical and hydraulic or any other kind of device as is the case with the quad-rotor helicopter. If a system has to be designed to perform in a specific way, there is need to develop descriptions of how the outputs of the individual components, which make up the system will respond to changes in their inputs. This is known as mathematical modelling and can be done either from the basic laws of physics or from processing the input and output signals, in which case it is known as identification. Examples of physical modelling include deriving differential equations for electrical circuits involving resistance, inductance and capacitance and for combinations of masses, springs and dampers in mechanical systems. Mathematical models of any device will always be approximate, even if non-linear effects and time variations are also included by using more general non-linear or time varying differential equations. Thus, it is always important when using mathematical models, to have an appreciation of the conditions under which they are valid and to what accuracy [88].

The dynamic behaviour of the quad-rotor is usually described by differential equations. Such equations can be linearized using the first order Taylor series and the Laplace transform transfer function can be used to simplify the method of solution and reduce computation time [89]. However, the linearized models do not work well at some extreme conditions because the approximations cannot effectively cater for the ever-changing flow conditions around the helicopter. Therefore, the non-linear model was used throughout this thesis, since the aim is to monitor and control the helicopter through a series of complex weather conditions.

A good model should use theory usually applied for helicopters. Having four rotors in close proximity complicates the problem even further, because there are interactions between the wakes produced by the rotors and the fuselage, and also between individual rotors. Being that the propellers are made of plastic, they are quite flexible and present flapping at translational speeds. They cannot be modelled precisely as propellers and require models similar to helicopter rotors. Except for hover, the expression for the rotor wash induced velocities cannot be obtained in closed-form, creating difficulties when the model is used to design certain types of controllers.

The general motion of a rigid body in space is a combination of translational and rotational motions, therefore the complete dynamics of a helicopter, taking into account aero-elastic

effects, flexibility of the wings, internal dynamics of the actuators and the whole set of changing variables are quite complex and to a certain degree unmanageable for the purposes of control. Therefore, it is remarkable to consider a simplified model of a quad-rotor helicopter formed by a minimum number of states and inputs, but retaining the main features that must be considered when designing laws that control large sized helicopters.

In this section, the dynamics of a quad-rotor helicopter are modelled using the Newton-Euler formalism. This can further be divided into the following sub-sections:

*Throughout this section, these notations have been adopted: c = cos, s = sin, t = tan.

3.0.1 Coordinate Frames

A coordinate system uses one or more numbers, or coordinates to uniquely determine the position of a point or other geometric element on a manifold such as Euclidean space. The order of the coordinates is significant and they are identified by their position in an ordered tuple. The use of such a system allows problems in geometry to be translated into problems about numbers and vice versa.

As a starting point, there are two coordinate systems to be clearly defined:

1. The earth inertial frame (E-frame) - The E-frame (O_E, X_E, Y_E, Z_E) is chosen as the inertial right-hand reference. X_E points toward the North, Y_E points toward the West, Z_E points upwards respect to the earth and O_E is the axis origin. This frame is used to define the linear position Γ^E [m] and the angular position θ^E [rad] of the quad-rotor.
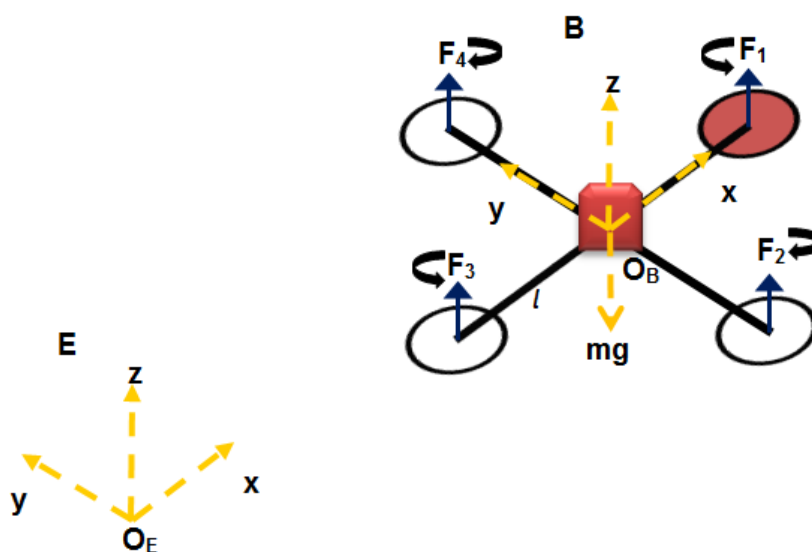
Figure 3-1: The quad-rotor axes definition

2. The body-fixed frame of the vehicle (B-frame) - The B-frame (O_B, X_B, Y_B, Z_B) is attached to the quad-rotor body. X_B points toward the quad-rotor front, Y_B points toward the quad-rotor left, Z_B points upwards and O_B is the axis origin. O_B is chosen to coincide with the centre of mass of the quad-rotor helicopter.

These two coordinates are related through three successive rotations:

Roll: Rotation of φ around the x-axis;

Pitch: Rotation of θ around the y-axis;

Yaw: Rotation of ψ around the z-axis.

The linear velocity v^B [m/s], the angular velocity $ω^B$ [rad/s], the forces F^B [N] and the torques τ^B [N m] are defined in this frame. It is relatively easier to formulate differential equations that describe motion in the body-fixed frame of a vehicle, rather than the earth inertial frame because the inertia matrix is time-invariant and the advantage of body symmetry of the quad-rotor helicopter can be taken to simplify the equations. It was also thought that measurements taken on-board are easily converted to body-fixed frame and the control forces are almost always given in body-fixed frame [46, 90].

3.0.2 Quad-rotor Modelling Assumptions

A model is a representation of a real physical system and the results of the computation of any model are only approximations of the actual results that would be observed in real world conditions, which are mostly very difficult to simulate. Models intentionally simplify reality, in order to make it tractable. What is important is a good understanding of how the model simplifies reality. Good modelling assumptions make work easier and don't adversely affect the simulations results, but bad assumptions produce results that diverge wildly from reality.

It was very necessary for the following reasonable assumptions to be made concerning the modelling of the quad-rotor helicopter:

1. The origin of the body-fixed frame O_B coincides with the centre of mass (COM) of the body of the vehicle. Otherwise, another point (COM) should have considered and that would have significantly complicated the body equations.
2. The axes of the B-frame coincide with the body principal axes of inertia. In this case the inertia matrix *I* is diagonal and, once again, the body equations become easier to work with.

3. The acceleration of gravity is constant and perpendicular to the surface of the Earth.

4. The quad-rotor body as well as the propellers will be treated as a rigid body.

5. Being an indoor experiment setup, the helicopter is assumed to fly at low speeds, the air friction is very low and can be ignored, gyroscopic effects and the aerodynamic torques can be cancelled.

3.0.3 Quad-rotor Helicopter State Variable definition

The state or set of system variables describe the status of a particular system at any time instant. Since the primary concern is how system behaviour changes with time, the most useful state variables are often the rate-of-change variables within any system or combinations of these variables and their derivatives. For example - in a mechanical system, the interest is more on the position and/or velocity (rate-of change of position) of a given component which moves due to an input force. In defining a state variable model, the inputs, outputs and state variables for the given system are clearly stated. The whole representation is referred to as a state-space system, which is simply a working region where system descriptions are represented by states and the rules for the space include rules for operations on these states.
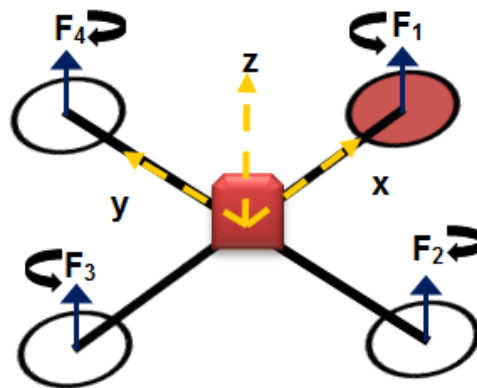
Figure 3-2: Quad-rotor Configuration Scheme

Let the linear position of the quad-rotor helicopter be a vector Γ^E. It is normally determined by the coordinates (x, y, z) of the vector between the origin of the quad-rotor body frame (B-frame) and the origin of the earth frame (E-frame) with respect to the E-frame as shown in the equation (3-1) below.

$$\Gamma^E = x\vec{i} + y\vec{j} + z\vec{k} = \begin{bmatrix} x \\ y \\ z \end{bmatrix} \qquad (3\text{-}1)$$

Let the attitude (or angular position) of the quad-rotor helicopter be another vector Θ^E. This is defined by the orientation of the B-frame with respect to the E-frame. It is given by three consecutive rotations (φ, θ, ψ) about the main axes. These rotations take the E-frame into the B-frame.

$$\Theta^E = \begin{bmatrix} \varphi \\ \theta \\ \psi \end{bmatrix} \qquad (3\text{-}2)$$

Let ξ [+] be the generalised position vector, which is made up of the quad-rotor linear Γ^E [m] and angular Θ^E [rad] position vectors with respect to the E-frame as shown in the equation (3-3) below.

$$\xi = \begin{bmatrix} \Gamma^E \\ \Theta^E \end{bmatrix} = \begin{bmatrix} x \\ y \\ z \\ \varphi \\ \theta \\ \psi \end{bmatrix} \qquad (3\text{-}3)$$

Let v^B and ω^B be the quad-rotor linear and angular velocity vectors respectively. The compositions of the linear and angular velocity vectors are:

$$v^B = u\vec{i} + v\vec{j} + w\vec{k} = \begin{bmatrix} u \\ v \\ w \end{bmatrix} \qquad (3\text{-}4)$$

And

$$\omega^B = p\vec{i} + q\vec{j} + r\vec{k} = \begin{bmatrix} p \\ q \\ r \end{bmatrix} \qquad (3\text{-}5)$$

Similarly, let v [+] be composed of the quad-rotor linear and angular velocity vectors with respect to the B-frame as shown in the equation below.

$$v = \begin{bmatrix} v^B \\ \omega^B \end{bmatrix} = \begin{bmatrix} u \\ v \\ w \\ p \\ q \\ r \end{bmatrix} \tag{3-6}$$

From equations (3-3) and (3-6), we see that it is possible to combine linear and angular quantities to give a full representation of a body in space.

3.0.4 Direction Cosine Matrix

The direction cosine matrix is so called because its elements can be determined from the dot products that involve the direction cosines between corresponding axes of the new and old coordinate systems. To transform the vectors from the E-frame to the B-frame, a direction cosine matrix is required. The rotation of one Cartesian coordinate system with respect to another can always be described by three successive rotations, and the angles of rotation are called the Euler angles. These angles are specified in diverse ways in different fields of Science. In this thesis, the rotations are performed by rotating first around x-axis, then around y axis and finally around the z axis as found in [27, 91]. The matrix is given by:

$$R_\Theta = R(\varphi, \theta, \psi) = R_x(\varphi) * R_y(\theta) * R_z(\psi) \tag{3-7}$$

The basic (gimbal-like) rotation matrices rotate vectors about the x, y, or z axes, in three dimensions and are described separately as:

$R_x(\varphi)$, rotation around the x-axis.

$R_y(\theta)$, rotation around the y-axis.

$R_z(\psi)$, rotation around the z-axis.

They are represented by:
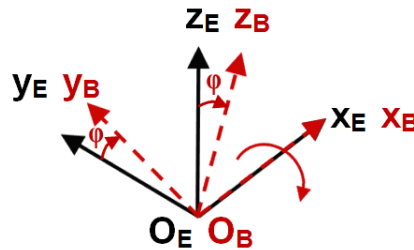
Figure 3-3: Rotation around the X axis of the angle φ (roll)

$$R_x(\varphi) = \begin{bmatrix} 1 & 0 & 0 \\ 0 & c\varphi & -s\varphi \\ 0 & s\varphi & c\varphi \end{bmatrix}$$
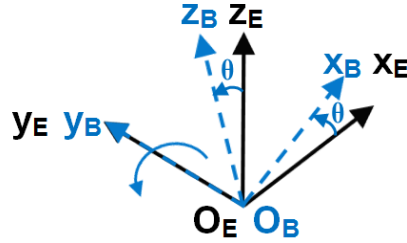
Figure 3-4: Rotation around the Y axis of the angle θ (pitch)

$$R_y(\theta) = \begin{bmatrix} c\theta & 0 & s\theta \\ 0 & 1 & 0 \\ -s\theta & 0 & c\theta \end{bmatrix}$$
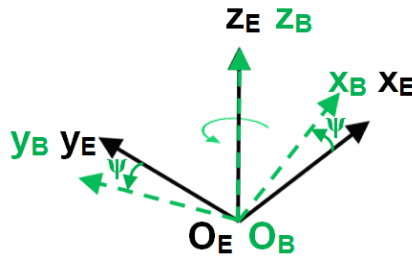
Figure 3-5: Rotation around the Z axis of the angle ψ (yaw)

$$R_z(\psi) = \begin{bmatrix} c\psi & -s\psi & 0 \\ s\psi & c\psi & 0 \\ 0 & 0 & 1 \end{bmatrix}$$

With the tilt angles $\varphi, \theta \in \left(-\dfrac{\pi}{2}, \dfrac{\pi}{2} \right) \psi \in (-\pi, \pi)$

The complete rotation matrix is the product of the three basic rotation matrices:

$$R_\Theta = R(\varphi, \theta, \psi) = R_x(\varphi) * R_y(\theta) * R_z(\psi)$$

This gives the following matrix:

$$R_\Theta = \begin{bmatrix} c\theta c\psi & c\psi s\theta s\varphi - s\psi c\varphi & s\varphi s\psi + c\varphi c\psi s\theta \\ s\psi c\theta & c\psi c\varphi + s\psi s\theta s\varphi & s\psi s\theta c\varphi - c\psi s\varphi \\ -s\theta & c\theta s\varphi & c\varphi c\theta \end{bmatrix} \quad (3\text{-}8)$$

3.0.5 Quad-rotor Kinematics

Kinematics describes the motion of points, objects and system of bodies without considering the causes of motion. The study of kinematics is usually referred to as the geometry of motion. To describe motion, kinematics studies the trajectories of points, lines and other geometric objects and their differential properties such as velocity and acceleration.

Having defined the transformation matrices, we can now find the velocity of the vehicle in the inertial frame instead of the Body coordinate frame.

The rotation matrix R_θ is involved in the relationship between the linear velocity v^B [m/s] in the body-fixed frame and the linear velocity v^E [m/s] in the earth frame as shown below.

$$v^E = \dot{\Gamma}^E = \begin{bmatrix} \dot{x} \\ \dot{y} \\ \dot{z} \end{bmatrix} = R_\Theta v^B = R_\Theta \begin{bmatrix} u \\ v \\ w \end{bmatrix} = \begin{bmatrix} c\theta c\psi & c\psi s\theta s\varphi - s\psi c\varphi & s\varphi s\psi + c\varphi c\psi s\theta \\ s\psi c\theta & c\psi c\varphi + s\psi s\theta s\varphi & s\psi s\theta c\varphi - c\psi s\varphi \\ -s\theta & c\theta s\varphi & c\varphi c\theta \end{bmatrix} \begin{bmatrix} u \\ v \\ w \end{bmatrix} \quad (3\text{-}9)$$

$$v^E = \begin{bmatrix} (c\theta c\psi)u + (c\psi s\theta s\varphi - s\psi c\varphi)v + (s\varphi s\psi + c\varphi c\psi s\theta)w \\ (s\psi c\theta)u + (c\psi c\varphi + s\psi s\theta s\varphi)v + (s\psi s\theta c\varphi - c\psi s\varphi)w \\ (-s\theta)u + (c\theta s\varphi)v + (c\varphi c\theta)w \end{bmatrix} \quad (3\text{-}10)$$

The relationship between the angular velocity $\dot{\Theta}^E$ in the earth frame and the angular velocity in the body-fixed frame is given by

$$\dot{\Theta}^E = T_\Theta \omega^B \quad (3\text{-}11)$$

The transfer matrix T_θ can be found by resolving the Euler angle rates $\dot{\Theta}^E$ into the body fixed frame as shown in equation (3-12) below.

$$\begin{bmatrix} p \\ q \\ r \end{bmatrix} = \begin{bmatrix} \dot{\varphi} \\ 0 \\ 0 \end{bmatrix} + R_x(\varphi)^{-1} \begin{bmatrix} 0 \\ \dot{\theta} \\ 0 \end{bmatrix} + R_x(\varphi)^{-1} R_y(\theta)^{-1} \begin{bmatrix} 0 \\ 0 \\ \dot{\psi} \end{bmatrix} = T_\theta^{-1} \begin{bmatrix} \dot{\varphi} \\ \dot{\theta} \\ \dot{\psi} \end{bmatrix} \quad (3\text{-}12)$$

$$T_\theta = \begin{bmatrix} 1 & s\varphi t\theta & c\varphi t\theta \\ 0 & c\varphi & -s\varphi \\ 0 & s\varphi/c\theta & c\varphi/c\theta \end{bmatrix} \quad (3\text{-}13)$$

3.0.6 Quad-rotor Dynamics

Dynamics is concerned with the study of forces and torques together with their effects on motion, as opposed to kinematics, which studies the motion but does not refer to its causes. The study of dynamics is based mostly on the fundamental physical laws defined by Isaac Newton.

The study of dynamics could be linear or rotational. Linear dynamics pertains to objects moving in a line and involves quantities such as force, mass/inertia, displacement, velocity, acceleration and momentum. On the other hand, rotational dynamics pertains to objects that are rotating or moving in a curved path and involves quantities such as torque, moment of inertia/rotational inertia, angular displacement, angular velocity, angular acceleration and angular momentum.

Since it is known from Euler's first axiom of Newton's second law of motion, that the applied force in the E-frame is the product of the vehicle's mass and its acceleration, i.e.

$$Force = mass \times acceleration = ma$$

It can be deduced that

$$F^E = m(\frac{dv}{dt}) = m(\frac{d^2\Gamma^E}{dt^2}) \tag{3-14}$$

From equation (3-9), $\dfrac{d^2\Gamma^E}{dt^2}$ is given by

$$\frac{d^2\Gamma^E}{dt^2} = \ddot{\Gamma}^E = \begin{bmatrix} \ddot{x} \\ \ddot{y} \\ \ddot{z} \end{bmatrix} \tag{3-15}$$

This leads to

$$F^E = m\ddot{\Gamma}^E \tag{3-16}$$

And

$$F^E = \begin{bmatrix} F_x \\ F_y \\ F_z \end{bmatrix} = m\ddot{\Gamma}^E = m\frac{d}{dt}\dot{\Gamma}^E = m\frac{d}{dt}v^E = m\frac{d}{dt}\begin{bmatrix} \dot{x} \\ \dot{y} \\ \dot{z} \end{bmatrix} = m\begin{bmatrix} \ddot{x} \\ \ddot{y} \\ \ddot{z} \end{bmatrix} \tag{3-17}$$

Where F^E has components in x, y and z. Multiplying both sides by the direction cosine matrix in equation (3-8) gives the following

55

$$F^E R_\Theta = F^B = R_\Theta m \frac{d}{dt} \dot{\Gamma}^E = R_\Theta m \frac{d}{dt} v^E = R_\Theta m \frac{d}{dt} \begin{bmatrix} \dot{x} \\ \dot{y} \\ \dot{z} \end{bmatrix} = R_\Theta m \begin{bmatrix} \ddot{x} \\ \ddot{y} \\ \ddot{z} \end{bmatrix} \quad (3\text{-}18)$$

$$F^B = m R_\Theta \frac{d}{dt} \dot{\Gamma}^E \quad (3\text{-}19)$$

Going further:

$$F^B = m R_\Theta \frac{d}{dt} (R_\Theta v^B) = m R_\Theta (R_\Theta \dot{v}^B + \dot{R}_\Theta v^B) = m(R_\Theta R_\Theta \dot{v}^B + R_\Theta \dot{R}_\Theta v^B)$$

$$F^B = m(\dot{v}^B + R_\Theta \dot{R}_\Theta v^B) = m(\dot{v}^B + R_\Theta [R_\Theta S(\omega^B)] \times v^B)$$

$$F^B = m(\dot{v}^B + S(\omega^B) \times v^B) \quad (3\text{-}20)$$

Where m [kg] is the mass of the quad-rotor helicopter, $\ddot{\Gamma}^E$ [m/s^2] is the quad-rotor helicopter linear acceleration vector with respect to the E-frame, F^E [N] is the quad-rotor helicopter forces vector with respect to the E-frame, $\dot{v}^B$ [m/s^2] is the quad-rotor helicopter linear acceleration vector with respect to the B-frame, $\dot{R}_\Theta$ is the derivative of the rotation matrix and the symbol $\times$ denotes a vector product.

Since $R_\Theta = T_\Theta S(\omega^B)$, where $S(\omega^B)$ is a skew symmetric matrix. The Coriolis term $S(\omega^B) \times v^B$ is expressed as:

$$S(\omega^B) \times v^B) = \omega^B \times v^B = \begin{bmatrix} qw - rv \\ ru - pw \\ pv - qu \end{bmatrix} \quad (3\text{-}21)$$

Obtaining the differential of equation (3-4) [$\dot{v}^B$ from v^B] and substituting in equation (3-20), together with equation (3-21), gives the following

$$F^B = m(\begin{bmatrix} \dot{u} \\ \dot{v} \\ \dot{w} \end{bmatrix} + \begin{bmatrix} qw - rv \\ ru - pw \\ pv - qu \end{bmatrix}) \quad (3\text{-}22)$$

Substituting the column vector for F^B and dividing both sides by m

$$\frac{1}{m}\begin{bmatrix} F_x \\ F_y \\ F_z \end{bmatrix} = \begin{bmatrix} \dot{u} \\ \dot{v} \\ \dot{w} \end{bmatrix} + \begin{bmatrix} qw - rv \\ ru - pw \\ pv - qu \end{bmatrix} \tag{3-23}$$

On re-arranging the terms,

$$\begin{bmatrix} \dot{u} \\ \dot{v} \\ \dot{w} \end{bmatrix} = \frac{1}{m}\begin{bmatrix} F_x \\ F_y \\ F_z \end{bmatrix} - \begin{bmatrix} qw - rv \\ ru - pw \\ pv - qu \end{bmatrix} \tag{3-24}$$

Where F_x, F_y and F_z are the components of force in the body coordinate frame, while u, v, w and $\dot{u}$, $\dot{v}$, $\dot{w}$ are the velocity and the acceleration components in the B-frame. p, q, r are defined as the components of angular velocity in the B-frame in the x, y and z axes respectively.

Next is the derivation of the angular components of the body motion from the Euler's second axiom of Newton's second law.

$$\tau^E = I\frac{d^2\Theta^E}{dt^2} \tag{3-25}$$

$$\tau^E = \frac{d}{dt}(T_\Theta I \omega^B) \tag{3-26}$$

$$\tau^E = \dot{T}_\Theta I \omega^B + T_\Theta \dot{I} \omega^B + T_\Theta I \dot{\omega}^B = T_\Theta(\omega^B \times I\omega^B) + T_\Theta I \dot{\omega}^B \tag{3-27}$$

$$T_\Theta \tau^B = T_\Theta[T_\Theta(\omega^B \times I\omega^B)] + T_\Theta[T_\Theta I \dot{\omega}^B] \tag{3-28}$$

$$T_\Theta \tau^B = \begin{bmatrix} \tau_r \\ \tau_p \\ \tau_y \end{bmatrix} = I\dot{\omega}^B + [\omega^B \times (I\omega^B)] \tag{3-29}$$

Where I [N m s^2] is the inertia matrix of the quad-rotor helicopter in the B-frame, $\frac{d^2\Theta^E}{dt^2}$ [rad/s^2] is the quad-rotor angular acceleration vector with respect to the E-frame, $\dot{\omega}^B$ [rad/s^2] is the quad-rotor angular acceleration vector with respect to the B-frame, τ^E [N m] is the quad-rotor torque vector with respect to the E-frame. τ_r, τ_p, and τ_y define the roll, pitch and yaw moments respectively.

$$I = \begin{bmatrix} I_{xx} & I_{xy} & I_{xz} \\ I_{yx} & I_{yy} & I_{yz} \\ I_{zx} & I_{zy} & I_{zz} \end{bmatrix} = \begin{bmatrix} I_{xx} & 0 & 0 \\ 0 & I_{yy} & 0 \\ 0 & 0 & I_{zz} \end{bmatrix} \tag{3-30}$$

($I_{xy} = I_{xz} = I_{yx} = I_{yz} = I_{zx} = I_{zy} = 0$, since the quad-rotor helicopter is assumed to be symmetric in nature)

From equation (3-29), the angular acceleration is given by the equation

$$\dot{\omega}^B = I^{-1}[T_\Theta \tau^B - [\omega^B \times (I\omega^B)]] \tag{3-31}$$

Also from equation (3-30), we can find the inverse of the inertia matrix, which is given as

$$I^{-1} = \begin{bmatrix} \dfrac{1}{I_{xx}} & 0 & 0 \\ 0 & \dfrac{1}{I_{yy}} & 0 \\ 0 & 0 & \dfrac{1}{I_{zz}} \end{bmatrix} \tag{3-32}$$

From equation (3-5), differentiating the angular velocity gives

$$\dot{\omega}^B = \begin{bmatrix} \dot{p} \\ \dot{q} \\ \dot{r} \end{bmatrix} \tag{3-33}$$

Substituting and simplifying in equation (3-31),

$$\dot{\omega}^B = \begin{bmatrix} \dot{p} \\ \dot{q} \\ \dot{r} \end{bmatrix} = I^{-1}[T_\Theta \tau^B - [\begin{bmatrix} p \\ q \\ r \end{bmatrix} \times [\begin{bmatrix} I_{xx} & 0 & 0 \\ 0 & I_{yy} & 0 \\ 0 & 0 & I_{zz} \end{bmatrix} \begin{bmatrix} p \\ q \\ r \end{bmatrix}]]]$$

$$\dot{\omega}^B = \begin{bmatrix} \dot{p} \\ \dot{q} \\ \dot{r} \end{bmatrix} = I^{-1}[T_\Theta \tau^B - [\begin{bmatrix} p \\ q \\ r \end{bmatrix} \times \begin{bmatrix} pI_{xx} - qI_{xy} - rI_{xz} \\ -pI_{yx} + qI_{yy} - rI_{yz} \\ -pI_{zx} - qI_{zy} + rI_{zz} \end{bmatrix}] = I^{-1}[T_\Theta \tau^B - [\begin{bmatrix} p \\ q \\ r \end{bmatrix} \times \begin{bmatrix} pI_{xx} \\ qI_{yy} \\ rI_{zz} \end{bmatrix}]$$

$$\dot{\omega}^B = \begin{bmatrix} \dot{p} \\ \dot{q} \\ \dot{r} \end{bmatrix} = I^{-1}[T_\Theta \tau^B - [\begin{bmatrix} p \\ q \\ r \end{bmatrix} \times \begin{bmatrix} pI_{xx} \\ qI_{yy} \\ rI_{zz} \end{bmatrix}] = I^{-1}[T_\Theta \tau^B - \begin{bmatrix} qrI_{zz} - rqI_{yy} \\ rpI_{xx} - prI_{zz} \\ pqI_{yy} - qpI_{xx} \end{bmatrix}]$$

$$
\dot{\omega}^B = \begin{bmatrix} \dot{p} \\ \dot{q} \\ \dot{r} \end{bmatrix} = I^{-1}\left[\begin{bmatrix} \tau_r \\ \tau_p \\ \tau_y \end{bmatrix} - \begin{bmatrix} qrI_{zz} - rqI_{yy} \\ rpI_{xx} - prI_{zz} \\ pqI_{yy} - qpI_{xx} \end{bmatrix} \right]
$$

From equation (3-32), substitution can be made for I^{-1}

$$
\dot{\omega}^B = \begin{bmatrix} \dot{p} \\ \dot{q} \\ \dot{r} \end{bmatrix} = \begin{bmatrix} \dfrac{1}{I_{xx}} & 0 & 0 \\ 0 & \dfrac{1}{I_{yy}} & 0 \\ 0 & 0 & \dfrac{1}{I_{zz}} \end{bmatrix}\left[\begin{bmatrix} \tau_r \\ \tau_p \\ \tau_y \end{bmatrix} - \begin{bmatrix} qrI_{zz} - rqI_{yy} \\ rpI_{xx} - prI_{zz} \\ pqI_{yy} - qpI_{xx} \end{bmatrix} \right]
$$

Simplifying further,

$$
\begin{bmatrix} \dot{p} \\ \dot{q} \\ \dot{r} \end{bmatrix} = \begin{bmatrix} \dfrac{\tau_r}{I_{xx}} \\ \dfrac{\tau_p}{I_{yy}} \\ \dfrac{\tau_y}{I_{zz}} \end{bmatrix} - \begin{bmatrix} (I_{zz} - I_{yy})\dfrac{qr}{I_{xx}} \\ (I_{xx} - I_{zz})\dfrac{pr}{I_{yy}} \\ (I_{yy} - I_{xx})\dfrac{pq}{I_{zz}} \end{bmatrix} \tag{3-34}
$$

3.0.7 Quad-rotor Aerodynamic Forces

There would normally be four forces acting on any helicopter in flight. These forces are lift, thrust, weight and drag. A very good distribution of these forces while the helicopter is aloft ensures movement in the intended direction.

3.0.7.1 Lift and Thrust forces

A fluid flowing past the surface of a body exerts a force on it. Lift is the component of this force that is perpendicular to the relative fluid flow. This force is generated by the spinning rotor to keep the helicopter in the air.

Thrust is also generated by the rotation of the rotor blades. This is the force that propels the helicopter through the air. For the quad-rotor helicopter, thrust can be forward, backward, sideward and vertical.

The quad-rotor helicopter's motion (vertical and horizontal) is affected by actions of the four propellers. The resultant of lift and thrust determines the direction of movement of the helicopter.

$$F_T = \begin{bmatrix} 0 \\ 0 \\ F_1 + F_2 + F_3 + F_4 \end{bmatrix} = \begin{bmatrix} F_x \\ F_y \\ F_z \end{bmatrix} \qquad (3\text{-}35)$$

Where F_1, F_2, F_3, F_4 are the forces generated by rotors 1, 2, 3 and 4 respectively. As shown in equation (3-35), there are components of the collective force generated by the four rotors. When the quad-rotor is moving vertically (up or down), the collective force is channelled towards balancing its weight, therefore the horizontal components are 0 – implying that the thrust is 0. As stated earlier, the resultant of the lift and thrust determines the direction of movement. A tilt about the x or y axis will create a thrust in a particular direction, leading to a component of the force in that direction. Since the helicopter is still in the air, it would definitely need to overcome its weight by maintaining the total lift force.

3.0.7.2 Weight

This is the force that opposes lift and it is caused by the downward pull of gravity. Gravitational pull, F_g^E is the major force acting on the quad-rotor helicopter in the E-frame. This force acts along negative z-axis (downwards) and is a result of the product of the total mass of the quad-rotor helicopter and the acceleration due to gravity as shown in equation (3-36) below:

$$F_g^E = \begin{bmatrix} 0 \\ 0 \\ mg \end{bmatrix} \qquad (3\text{-}36)$$

Using the direction cosine matrix, we can have equation (3-36) to a force acting in the B-frame as

$$F_g^B = R_\Theta F_g^E = R_\Theta \begin{bmatrix} 0 \\ 0 \\ mg \end{bmatrix} = \begin{bmatrix} -mg\sin\theta \\ mg\sin\varphi\cos\theta \\ mg\cos\varphi\cos\theta \end{bmatrix} = \begin{bmatrix} F_{gx} \\ F_{gy} \\ F_{gz} \end{bmatrix} \qquad (3\text{-}37)$$

Where F_g^B is the gravitational force in the B-frame and F_{gx}, F_{gy}, F_{gz} are the components of the gravity force in the x, y, and z directions, respectively.

3.0.7.3 Drag Force

Drag is the force that opposes the motion of an aircraft through the air. It is primarily a function of airspeed, directly opposing lift and thrust. It is normally computed as a product of the coefficient of drag and the square of the velocity in each of the three axes.

$$
F_D^E = \begin{bmatrix} \dfrac{1}{2} C_{Dx} A_c \rho (V_x^E)^2 \\ \dfrac{1}{2} C_{Dy} A_c \rho (V_y^E)^2 \\ \dfrac{1}{2} C_{Dz} A_c \rho (V_z^E)^2 \end{bmatrix} \tag{3-38}
$$

Where A is the cross-sectional area, ρ the air density; V_x, V_y, V_z are the E-frame components of velocity. C_{Dx}, C_{Dy}, C_{Dz} are the drag coefficients in each of the three axes. The transformation matrix can also be used in this case to get the B-frame components of the drag force.

$$
F_D^B = R_\Theta F_D^E = \begin{bmatrix} \dfrac{1}{2} C_{Dx} A_c \rho \, \dot{x}^2 \\ \dfrac{1}{2} C_{Dy} A_c \rho \, \dot{y}^2 \\ \dfrac{1}{2} C_{Dz} A_c \rho \, \dot{z}^2 \end{bmatrix} = \begin{bmatrix} F_{Dx} \\ F_{Dy} \\ F_{Dz} \end{bmatrix} \tag{3-39}
$$

The quad-rotor helicopter operates at airspeeds low enough for us to assume that the drag force is very little and therefore can be ignored as confirmed in [90].

3.0.7.4 Collective Force acting on the Quad-rotor

The total force is the sum of the lift/thrust, weight and drag forces:

$$
F_B = \begin{bmatrix} F_x \\ F_y \\ F_z \end{bmatrix} = \begin{bmatrix} F_{gx} \\ F_{gy} \\ F_{gz} \end{bmatrix} + \begin{bmatrix} F_{Dx} \\ F_{Dy} \\ F_{Dz} \end{bmatrix} + \begin{bmatrix} F_{Tx} \\ F_{Ty} \\ F_{Tz} \end{bmatrix} \tag{3-40}
$$

$$
F_B = \begin{bmatrix} F_x \\ F_y \\ F_z \end{bmatrix} = \begin{bmatrix} -mg\sin\theta \\ mg\sin\varphi\cos\theta \\ mg\cos\varphi\cos\theta \end{bmatrix} + \begin{bmatrix} \dfrac{1}{2} C_{Dx} A_c \rho \, \dot{x}^2 \\ \dfrac{1}{2} C_{Dy} A_c \rho \, \dot{y}^2 \\ \dfrac{1}{2} C_{Dz} A_c \rho \, \dot{z}^2 \end{bmatrix} + \begin{bmatrix} 0 \\ 0 \\ F_1 + F_2 + F_3 + F_4 \end{bmatrix}
$$

$$\begin{bmatrix} F_x \\ F_y \\ F_z \end{bmatrix} = \begin{bmatrix} -mg\sin\theta + \dfrac{1}{2}C_{Dx}A_c\rho\,\dot{x}^2 \\[2mm] mg\sin\varphi\cos\theta + \dfrac{1}{2}C_{Dy}A_c\rho\,\dot{y}^2 \\[2mm] mg\cos\varphi\cos\theta + \dfrac{1}{2}C_{Dz}A_c\rho\,\dot{z}^2 + (F_1 + F_2 + F_3 + F_4) \end{bmatrix} \qquad (3\text{-}41)$$

3.0.8 Quad-rotor Moments (Torques)

The moment or torque of a force about a turning point is the product of the force and the perpendicular distance to the force from the turning point. For an object to be in equilibrium, the sum of clockwise and anticlockwise moments about a turning point must be equal to 0. This is the exact principle the quad-rotor helicopter uses to remain stable as it flies around with its two pairs of counter-rotating blades.

If τ_i is the torque generated by each motor, the rolling moment τ_r is produced by changing the speeds of the right and left motors.

$$\tau_r = \tau_2 - \tau_4 = F_2 l - F_4 l = l(F_2 - F_4) \qquad (3\text{-}42)$$

Similarly the pitching moment τ_p (torque) is produced by changing the speeds of the front and rear motors.

$$\tau_p = \tau_1 - \tau_3 = F_1 l - F_3 l = l(F_1 - F_3) \qquad (3\text{-}43)$$

Considering Newton's third law of motion, which states that for every action there is an equal and opposite reaction; the drag of the propellers produces a yawing moment on the quad-rotor helicopter. Consequently, the total yawing moment is obtained from all the rotor speeds and is given by

$$\tau_y = \sum \tau_m = \tau_{m1} - \tau_{m2} + \tau_{m3} - \tau_{m4} = (F_1 - F_2 + F_3 - F_4)d \qquad (3\text{-}44)$$

3.0.9 Quad-rotor Moments of Inertia

A moment of inertia is the mass property of a rigid body that defines the torque needed for a desired change in angular velocity about an axis of rotation. This moment depends on the shape of the body, amount and distribution of its mass and may differ around one axis of rotation and another.

3.0.9.1 Moment of Inertia about the x-axis

In deriving the moment of inertia around the x-axis, the central hub and all the motors of the quad-rotor helicopter are assumed to be cylindrical in shape.
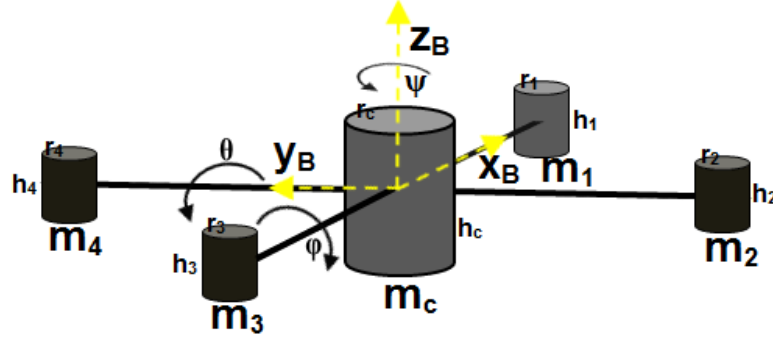
Figure 3-6: Quad-rotor moments of inertia

Let the following parameters be used as masses of motors and central hub m_1, m_3, m_c; radii r_1, r_3, r_c and height h_1, h_3, h_c, respectively. Here, only the rolling motion is considered. Firstly, the moment of inertia about the x-axis would be due to the motion of the main body and the front and rear motors about x-axis. Secondly, the moment of inertia would be due to the motion of the left and right motors about the x-axis.

$$I_{xx} = I_{2,4} + I_1 + I_3 + I_c \qquad (3\text{-}45)$$

The moment of inertia of a cylinder about an axis perpendicular to its body, as specified in [94], thus the moment of inertia due to main body and the two motors are given by:

$$I_{c,x} = \frac{m_c r_c^2}{4} + \frac{m_c h_c^2}{12} \qquad (3\text{-}46)$$

$$I_{1,x} = \frac{m_1 r_1^2}{4} + \frac{m_1 h_1^2}{12} \qquad (3\text{-}47)$$

$$I_{3,x} = \frac{m_3 r_3^2}{4} + \frac{m_3 h_3^2}{12} \qquad (3\text{-}48)$$

The moment of inertia of two identical spheres connected together by a horizontal arm, rotating about a vertical axis, which is passing through the centre of the arm and is perpendicular to it, according to [92, 93] can be approximated to be

$$I_{2-4,x} = 2m_r l^2 \qquad (3\text{-}49)$$

Since the motors are assumed to be identical:

$$m_1 = m_2 = m_3 = m_4 = m_r, \ r_1 = r_2 = r_3 = r_4 = r, \text{and } h_1 = h_2 = h_3 = h_4 = h_r$$

63

Finally, the total inertia about the x-axis is found by substituting equations (3-46), (3-47), (3-48) and (3-49) in equation (3-45)

$$I_{xx} = \frac{m_c r_c^2}{4} + \frac{m_c h_c^2}{12} + \frac{m_1 r_1^2}{4} + \frac{m_1 h_1^2}{12} + \frac{m_3 r_3^2}{4} + \frac{m_3 h_3^2}{12} + 2m_r l^2$$

$$I_{xx} = \frac{m_c r_c^2}{4} + \frac{m_c h_c^2}{12} + \frac{m_r r_r^2}{2} + \frac{m_r h_r^2}{6} + 2m_r l^2 \tag{3-50}$$

3.0.9.2 Moment of Inertia about the y-axis

In the same way, the moment of inertia about the y-axis can be found because of the earlier assumption that the quad-rotor helicopter structure is symmetrical and the motors are identical. Going through the process that was done in finding the moment of inertia about the x-axis gives

$$I_{yy} = \frac{m_c r_c^2}{4} + \frac{m_c h_c^2}{12} + \frac{m_r r_r^2}{2} + \frac{m_r h_r^2}{6} + 2m_r l^2 \tag{3-51}$$

3.0.9.3 Moment of Inertia about the z-axis

The moment of inertia about the z-axis will be due to the motion of the main body and also due to the motion of all the motors [92, 93]. The moment of inertia due to the main body can be found to be:

$$I_{c,z} = \frac{m_c r_c^2}{2} \tag{3-52}$$

The moment of inertia due to all the motors can be approximated to be:

$$I_{1-2-3-4,z} = 4m_r l^2 \tag{3-53}$$

Therefore, the total inertia about z-axis is the sum of the two:

$$I_{zz} = \frac{m_c r_c^2}{2} + 4m_r l^2 \tag{3-54}$$

3.0.10 Equations of Motion

Putting together the equations (3-24) and (3-41) gives:

$$\begin{bmatrix} \dot{u} \\ \dot{v} \\ \dot{w} \end{bmatrix} = \frac{1}{m} \begin{bmatrix} -mg\sin\theta + \frac{1}{2}C_{Dx}A_c\rho\dot{x}^2 \\ mg\sin\varphi\cos\theta + \frac{1}{2}C_{Dy}A_c\rho\dot{y}^2 \\ mg\cos\varphi\cos\theta + \frac{1}{2}C_{Dz}A_c\rho\dot{z}^2 + (F_1 + F_2 + F_3 + F_4) \end{bmatrix} - \begin{bmatrix} qw - rv \\ ru - pw \\ pv - qu \end{bmatrix}$$

$$
\begin{bmatrix} \dot{u} \\ \dot{v} \\ \dot{w} \end{bmatrix} = \begin{bmatrix} -g\sin\theta + \dfrac{1}{2m}C_{Dx}A_c\rho\,\dot{x}^2 + (rv - qw) \\ g\sin\varphi\cos\theta + \dfrac{1}{2m}C_{Dy}A_c\rho\,\dot{y}^2 + (pw - ru) \\ g\cos\varphi\cos\theta + \dfrac{1}{2m}C_{Dz}A_c\rho\,\dot{z}^2 + \dfrac{1}{m}(F_1 + F_2 + F_3 + F_4) + (qu - pv) \end{bmatrix}
\tag{3-55}
$$

$$
\begin{bmatrix} \dot{u} \\ \dot{v} \\ \dot{w} \end{bmatrix} = \begin{bmatrix} -g\sin\theta + (rv - qw) \\ g\sin\varphi\cos\theta + (pw - ru) \\ g\cos\varphi\cos\theta + \dfrac{1}{m}(F_1 + F_2 + F_3 + F_4) + (qu - pv) \end{bmatrix}
\tag{3-56}
$$

In the same way combining equations (3-18) and (3-41), gives:

$$
F^B = \begin{bmatrix} F_x \\ F_y \\ F_z \end{bmatrix} = mR_\Theta \frac{d}{dt}\dot{\Gamma}^E = mR_\Theta \begin{bmatrix} \ddot{x} \\ \ddot{y} \\ \ddot{z} \end{bmatrix}
$$

The terms can be re-arranged to give

$$
\begin{bmatrix} \ddot{x} \\ \ddot{y} \\ \ddot{z} \end{bmatrix} = \frac{1}{m}R_\Theta^{-1}\begin{bmatrix} F_x \\ F_y \\ F_z \end{bmatrix}
$$

Since it is known from equation (3-41) that

$$
\begin{bmatrix} F_x \\ F_y \\ F_z \end{bmatrix} = \begin{bmatrix} -mg\sin\theta \\ mg\sin\varphi\cos\theta \\ mg\cos\varphi\cos\theta \end{bmatrix} + \begin{bmatrix} \dfrac{1}{2}C_{Dx}A_c\rho\,\dot{x}^2 \\ \dfrac{1}{2}C_{Dy}A_c\rho\,\dot{y}^2 \\ \dfrac{1}{2}C_{Dz}A_c\rho\,\dot{z}^2 \end{bmatrix} + \begin{bmatrix} 0 \\ 0 \\ F_1 + F_2 + F_3 + F_4 \end{bmatrix}
$$

Substitutions can be made and the equation simplified further, remembering that the matrix representing the drag forces can be reduced to 0 as stated earlier.

$$
\begin{bmatrix} \ddot{x} \\ \ddot{y} \\ \ddot{z} \end{bmatrix} = \frac{1}{m}R_\Theta^{-1}[\begin{bmatrix} -mg\sin\theta \\ mg\sin\varphi\cos\theta \\ mg\cos\varphi\cos\theta \end{bmatrix} + \begin{bmatrix} 0 \\ 0 \\ F_1 + F_2 + F_3 + F_4 \end{bmatrix}]
$$

On simplifying, it ends up as follows

$$\begin{bmatrix} \ddot{x} \\ \ddot{y} \\ \ddot{z} \end{bmatrix} = \begin{bmatrix} \dfrac{1}{m}(F_1 + F_2 + F_3 + F_4)(\sin\varphi\sin\psi + \cos\varphi\cos\psi\sin\theta) \\ \dfrac{1}{m}(F_1 + F_2 + F_3 + F_4)(\sin\psi\sin\theta\cos\varphi - \cos\psi\sin\varphi) \\ \dfrac{1}{m}(F_1 + F_2 + F_3 + F_4)(\cos\varphi\cos\theta) \end{bmatrix} \qquad (3\text{-}57)$$

The next section describes the actuator model, where relationships between voltage, angular velocity of propeller and thrust were found, leading to a modification of equation (3-57) and a derivation of the angular acceleration equations to form the quad-rotor analytical dynamic model. The final equations of motion are listed at the end of section 3.2.

3.1 Actuator Dynamics (DC-motor)

The DC-motor is an actuator which converts electrical energy into mechanical energy (and vice versa). It is composed of two interactive electromagnetic circuits. The first one (called rotor) is free to rotate around the second one (called stator) which is fixed instead. In the rotor, several groups of copper windings are connected in series and are externally accessible thanks to a device called commutator. In the stator, two or more permanent magnets impose a magnetic field which affects the rotor. By applying a DC-current flow into the windings, the rotor turns because of the force generated by the electrical and magnetic interaction. Thanks to the rotor and the commutator geometries, the motor keeps turning while supplied by a DC-voltage on its terminals.

The DC-motor has a well-known model which binds electrical and mechanical quantities. This model is composed of the series of a resistor R [Ω], an inductor L [H] and a voltage generator e [V]. The resistor represents the Joule loss due to the current flow into the copper conductor. Its value depends on geometric and material characteristics such as wire resistivity, length and section. The inductor behaviour derives from the shape of the motor wires which are winded in the middle of the rotor. Lastly, the generator e (called also BEMF) supplies a voltage proportional to the motor speed. The model is represented in the figure 3-7 below.
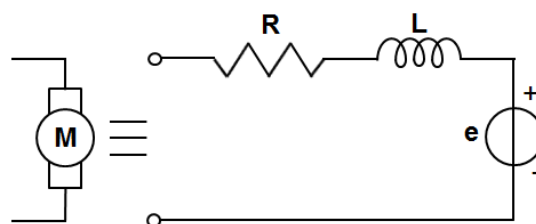
Figure 3-7: Schematic of a DC Motor

The circuit of the DC-motor is controlled by a real voltage generator v [V], which gives the control input. In theory, another resistor should be added in series of the voltage generator representing the driver losses. However, in a good project, the generator losses are kept low therefore it is possible to neglect them in the model. The basic electrical circuit is shown figure 3-8 below.
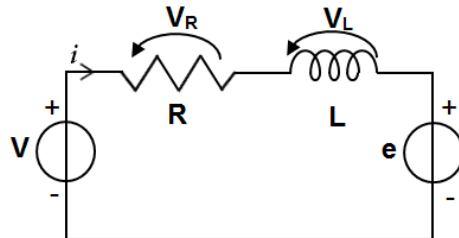
Figure 3-8: DC Motor circuit

By applying Kirchhoff's voltage law, it follows that.

$$v = v_R + v_L + e \tag{3-58}$$

Where v_R [V] is the voltage across the resistor R and v_L [V] is the voltage across the inductor L. The equation above can be rewritten as in the next equation.

$$v = Ri + L\frac{\partial i}{\partial t} + k_e \Omega \tag{3-59}$$

Where i [A] is the motor current, K_e [Vs/rad] is called the motor constant and Ω [rad/s] is the motor angular speed. The first addend has been changed using the Ohm's law $v_R = Ri$, while the second one using the inductor differential equation $v_L = L\frac{\partial i}{\partial t}$. The last member of the equation shows that mechanics and electrics are correlated.

The contribution of the inductor part is important to determine the characteristic of the DC-motor driver. However it is often neglected in the mechanics computation because of the reasons that follow:

a) A greater percentage of the motors used in robotics show very small inductance because of design optimization.

b) The response time of the electrical part is always much faster than the mechanical part, hence the speed of the overall system will be determined by the slowest contribution.

c) It is much easier to solve a first order differential equation rather than a second order one.

For the reasons mentioned above, the inductor effect was neglected in this thesis. Therefore the equation above can be simplified according to the one below.

$$v = Ri + k_e \Omega$$

The dynamics of the motor is described by the following equation.

$$J \dot{\Omega} = \tau_m - \tau_d \qquad (3\text{-}60)$$

Where J [Nms^2] is the total motor moment of inertia, $\dot{\Omega}$ [rad/s^2] is the motor angular acceleration, τ_m [Nm] is the motor torque and τ_d [Nm] is the load torque. When the motor torque τ_m and the load torque τ_d are not the same, then there is an acceleration (or deceleration) of the motor angular speed Ω. This variation of speed depends also on the total motor moment of inertia J : the smaller the value of J , the higher the acceleration. Figure 3-9 below is a sketch of the simplified mechanic structure.
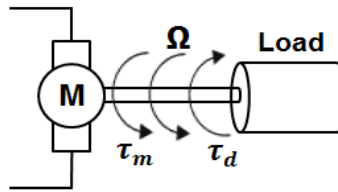
Figure 3-9: Simplified DC motor system

The motor torque τ_m is proportional to the electrical current i through k_q [Nm/A]: $\tau_m = k_q\, i$. Hence it can be written as

$$J \dot{\Omega} = k_q i - \tau_d$$

A differential equation in Ω can be easily derived:

$$J \dot{\Omega} = -\frac{k_e k_q}{R} \Omega - \tau_d + \frac{k_q}{R} v \qquad (3\text{-}61)$$

It must be pointed out that the two constants k_e and k_q have the almost the same value even though the units of measurement differ. This mismatch comes from the electric P_E [W] and mechanic P_M [Nm/s] power balance [4].

$$P_E = P_M \quad \left| \begin{array}{l} P_E = ei = k_e i \Omega \\ P_M = \tau_m \Omega = k_q i \Omega \end{array} \right. \Rightarrow k_e \approx k_q \qquad (3\text{-}62)$$

3.1.1 Voltage and Angular Velocity of Propeller

Since the voltage inputs (V) to motors affect the rotational speed (Ω) of propellers.

$$V - e = iR$$

From equation (3-60), the dynamics of the motor is described by the following equation

$$\tau_m - \tau_d = J\dot{\Omega}$$

The above equation states that when the motor torque τ_m and the drag torque τ_d are not equal there is an acceleration (or deceleration). This variation of speed depends also on the rotor inertia J. The smaller the value of J, the higher the acceleration. The back electromotive-force voltage being proportional to the motor speed gives

$$e = K_e\Omega$$

Also, the motor torque is known to be proportional to field current

$$\tau_m = k_q i$$

On substituting, it gives rise to

$$V = \tau_d \frac{R}{k_q} + \frac{RJ\dot{\Omega}}{k_q} + k_e\Omega \qquad (3\text{-}63)$$

The drag torque is also known to be proportional to the square of propeller's speed, leading to

$$\tau_d = D\Omega^2 \qquad (3\text{-}64)$$

The relationship between angular velocity and voltage can then be obtained as

$$V = \frac{RD\Omega^2}{k_q} + \frac{RJ\dot{\Omega}}{k_q} + k_e\Omega \qquad (3\text{-}65)$$

3.1.2 Voltage and Thrust

The voltage is the input of the quad-rotor plant. Thrust force (F_T) is produced by each rotor through the torque applied by brushless DC motor. As stated earlier, the motor torque is proportional to field current

$$\tau_m = k_q i$$

Making i the subject of the formula, gives

$$\frac{\tau_m}{k_q} = i \qquad (3\text{-}66)$$

The electrical power is calculated by using Joule's law.

$$P = IV = \frac{\tau_m}{k_q} V \tag{3-67}$$

The mechanical power output of the motor's efficiency is given by

$$P_m = \eta P = \eta \frac{\tau_m}{k_q} V \tag{3-68}$$

The Figure of merit f of the propeller is defined as the ratio of the induced power P_h to the power put into the propeller P_m.

$$f = \frac{P_h}{P_m} \tag{3-69}$$

Re-arranging and substituting for P_m from equation (3-68), gives

$$P_h = \eta f \frac{\tau_m}{k_q} V \tag{3-70}$$

The ideal power is the thrust force times the speed it is applied at. At hover P_h is

$$P_h = F v_h$$

$$\eta f \frac{\tau_m}{k_q} V = F v_h \tag{3-71}$$

Using the momentum theory,

$$v_h = \sqrt{\frac{F}{2 \rho A}}$$

Substituting for v_h in equation (3-70), gives

$$\eta f \frac{\tau_m}{k_q} V = F \sqrt{\frac{F}{2 \rho A}} \tag{3-72}$$

The torque is proportional to the thrust with constant ratio k_t depending on the geometry of the blade.

70

$$\tau_m = k_t F$$

Substituting for τ_m in equation (3-72), gives

$$\eta f \frac{k_t F}{k_q} V = F \sqrt{\frac{F}{2\rho A}}$$

The relationship between thrust and voltage input is then established as:

$$F = 2\rho A \left[\frac{f\eta k_t}{k_q} \right]^2 V^2 \tag{3-73}$$

3.1.3 Rolling Moment

As shown in equation (3-42), the rolling moment caused by the roll actuators action can be defined as:

$$\tau_r = l(F_2 - F_4)$$

And $\tau_r = I_{xx} \ddot{\varphi}$, therefore

$$I_{xx} \ddot{\varphi} = l(F_2 - F_4) \tag{3-74}$$

From equation (3-73), the thrust force is defined as $F = 2\rho A \left[\dfrac{f\eta k_t}{k_q} \right]^2 V^2$

Substituting in equation (3-74), gives

$$I_{xx} \ddot{\varphi} = l(2\rho A \left[\frac{f\eta k_t}{k_q} \right]^2 V_2^2) - (2\rho A \left[\frac{f\eta k_t}{k_q} \right]^2 V_4^2)$$

Simplifying further, leads to the final equation for roll angular acceleration, which is as follows

$$\ddot{\varphi} = \frac{2\rho A l}{I_{xx}} \left[\frac{f\eta k_t}{k_q} \right]^2 (V_2^2 - V_4^2) \tag{3-75}$$

3.1.4 Pitching Moment

From equation (3-43), the pitching moment caused by the pitch actuators action can be defined as:

$$\tau_p = l(F_3 - F_1)$$

And $\tau_p = I_{yy} \ddot{\theta}$, therefore

$$I_{yy} \ddot{\theta} = l(F_2 - F_4) \tag{3-76}$$

Substituting for the thrust force from equation (3-73), gives

$$I_{yy} \ddot{\theta} = l(2\rho A \left[\frac{f\eta k_t}{k_q} \right]^2 V_3^2) - (2\rho A \left[\frac{f\eta k_t}{k_q} \right]^2 V_1^2)$$

Simplifying further, leads to the final equation for pitch angular acceleration, which is as follows

$$\ddot{\theta} = \frac{2\rho A l}{I_{yy}} \left[\frac{f\eta k_t}{k_q} \right]^2 (V_3^2 - V_1^2) \tag{3-77}$$

3.1.5 Yawing Moment

The yaw moment is caused by a counter-torque imbalance. From equation (3-44), the torque about the z-axis is generally defined as:

$$\tau_y = \sum \tau_m = \tau_{m1} - \tau_{m2} + \tau_{m3} - \tau_{m4} = (F_1 - F_2 + F_3 - F_4)d$$

Each motor supplies machine torque τ_m which is balanced by the drag torque so the net torque on propeller is:

$$\tau_m - \tau_d = J\dot{\Omega}$$

Making τ_m the subject, gives

$$\tau_m = J\dot{\Omega} + \tau_d \tag{3-78}$$

The yaw torque along the z-axis is given by:

$$\tau_y = I_{zz}\ddot{\psi} = \tau_{m1} + \tau_{m3} - \tau_{m2} - \tau_{m4} \tag{3-79}$$

Substituting equation (3-78) in equation (3-79), gives

$$I_{zz}\ddot{\psi} = J\dot{\Omega}_1 + \tau_{d1} + J\dot{\Omega}_3 + \tau_{d3} - J\dot{\Omega}_2 - \tau_{d2} - J\dot{\Omega}_4 - \tau_{d4} \tag{3-80}$$

Re-arranging the equation (3-80), leads to

$$I_{zz}\ddot{\psi} = J(\dot{\Omega}_1 + \dot{\Omega}_3 - \dot{\Omega}_2 - \dot{\Omega}_4) + (\tau_{d1} + \tau_{d3} - \tau_{d2} - \tau_{d4}) \tag{3-81}$$

Since it is assumed in equation (3-64) that the drag torque is proportional to the square of propeller's speed - $\tau_d = D\Omega^2$; substituting in equation (3-81) leads to

$$I_{zz}\ddot{\psi} = J(\dot{\Omega}_1 + \dot{\Omega}_3 - \dot{\Omega}_2 - \dot{\Omega}_4) + D(\Omega_1{}^2 + \Omega_3{}^2 - \Omega_2{}^2 - \Omega_4{}^2)$$

Simplifying further, gives the final equation for yaw angular acceleration as follows

$$\ddot{\psi} = \frac{J}{I_{zz}}(\dot{\Omega}_1 + \dot{\Omega}_3 - \dot{\Omega}_2 - \dot{\Omega}_4) + \frac{D}{I_{zz}}(\Omega_1{}^2 + \Omega_3{}^2 - \Omega_2{}^2 - \Omega_4{}^2) \tag{3-82}$$

3.1.6 Acceleration along the x-axis

From equation (3-57), the acceleration along the x-axis, caused by actuators action is defined as:

$$\ddot{x} = \frac{1}{m}(F_1 + F_2 + F_3 + F_4)(\cos\varphi\sin\theta\cos\psi + \sin\varphi\sin\psi) \tag{3-83}$$

Substituting equation (3-73), which defines the thrust force and simplifying further, gives the final equation for linear acceleration in the x-direction as follows

$$\ddot{x} = \frac{2\rho A}{m}\left[\frac{f\eta k_t}{k_q}\right]^2 (V_1{}^2 + V_2{}^2 + V_3{}^2 + V_4{}^2)(\cos\varphi\sin\theta\cos\psi + \sin\varphi\sin\psi) \tag{3-84}$$

3.1.7 Acceleration along the y-axis

Similar to that of the x-axis, it was shown in equation (3-57) that actuators action produces the following acceleration, which acts along the y-axis:

$$\ddot{y} = \frac{1}{m}(F_1 + F_2 + F_3 + F_4)(\sin\psi \sin\theta \cos\varphi - \cos\psi \sin\varphi) \tag{3-85}$$

Substituting equation (3-73), which defines the thrust force and simplifying further, gives the final equation for linear acceleration in the y-direction as follows

$$\ddot{y} = \frac{2\rho A}{m}\left[\frac{f\eta k_t}{k_q}\right]^2 \left(V_1^2 + V_2^2 + V_3^2 + V_4^2\right)(\sin\psi \sin\theta \cos\varphi - \cos\psi \sin\varphi) \tag{3-86}$$

3.1.8 Acceleration along z-axis

A lift force perpendicular to the plane of the propellers is generated by the spin of the four propellers. This implies that when the roll and pitch angles are zero, the force in totality acts along the z-axis. On the contrary, when one of the two angles is non-zero, only a component of the total forces $F\cos\theta\cos\varphi$ acts along z-axis, while the other component(s) act in the x or y directions to propel the quad-rotor helicopter in a particular direction. The weight of the helicopter always acts along the negative z-axis; therefore this component of force has to cancel it out in order to lift the vehicle into the air. As shown in equation (3-57), the acceleration along the z-axis as a result of the action of the actuators is given as

$$\ddot{z} = \frac{1}{m}(F_1 + F_2 + F_3 + F_4)\cos\theta \cos\varphi \tag{3-87}$$

But the weight has to be taken into account,

$$- mg$$

The net force at the centre of mass of the vehicle is then given by

$$F = m\ddot{z} = (F_1 + F_2 + F_3 + F_4)\cos\theta \cos\varphi - mg \tag{3-88}$$

Where m is the net mass of the quad-rotor helicopter. Since equation (3-73) has it that

$$F = 2\rho A\left[\frac{f\eta K_t}{K_q}\right]^2 V^2$$

Substituting in equation (3-88) and simplifying further, gives the final equation for linear acceleration in the z-direction as follows

$$\ddot{z} = \frac{2\rho A}{m}\left[\frac{f\eta k_t}{k_q}\right]^2 \left(V_1^2 + V_2^2 + V_3^2 + V_4^2\right)(\cos\theta \cos\varphi) - g \tag{3-89}$$

3.2 Chapter Summary

Design and analysis of any control system is usually started by carefully considering a mathematical model of the physical system. The model is very important because it gives a description of how the system responds to the inputs given to it. An adequate dynamic system modelling of the quad-rotor helicopter involves a faithful mathematical representation of the whole system, usually described by differential equations.

Equations (3-65), (3-75), (3-77), (3-82), (3-84), (3-86) and (3-89) make up the analytical dynamic model of the quad-rotor helicopter that has been used throughout this thesis. These are summarized in equation (3-90) below.

$$
\begin{bmatrix} \dot{V} \\ \ddot{\varphi} \\ \ddot{\theta} \\ \ddot{\psi} \\ \ddot{x} \\ \ddot{y} \\ \ddot{z} \end{bmatrix} = \begin{bmatrix} \dfrac{RD\Omega^2}{k_q} + \dfrac{RJ\dot{\Omega}}{k_q} + k_e\Omega \\[2mm] \dfrac{2\rho Al}{I_{xx}} \left[\dfrac{f\eta k_t}{k_q} \right]^2 (V_2{}^2 - V_4{}^2) \\[2mm] \dfrac{2\rho Al}{I_{yy}} \left[\dfrac{f\eta k_t}{k_q} \right]^2 (V_3{}^2 - V_1{}^2) \\[2mm] \dfrac{J}{I_{zz}}(\dot{\Omega}_1 + \dot{\Omega}_3 - \dot{\Omega}_2 - \dot{\Omega}_4) + \dfrac{D}{I_{zz}}(\Omega_1{}^2 + \Omega_3{}^2 - \Omega_2{}^2 - \Omega_4{}^2) \\[2mm] \dfrac{2\rho A}{m} \left[\dfrac{f\eta k_t}{k_q} \right]^2 \left(V_1{}^2 + V_2{}^2 + V_3{}^2 + V_4{}^2 \right)(\cos\varphi\sin\theta\cos\psi + \sin\varphi\sin\psi) \\[2mm] \dfrac{2\rho A}{m} \left[\dfrac{f\eta k_t}{k_q} \right]^2 \left(V_1{}^2 + V_2{}^2 + V_3{}^2 + V_4{}^2 \right)(\sin\psi\sin\theta\cos\varphi - \cos\psi\sin\varphi) \\[2mm] \dfrac{2\rho A}{m} \left[\dfrac{f\eta k_t}{k_q} \right]^2 \left(V_1{}^2 + V_2{}^2 + V_3{}^2 + V_4{}^2 \right)(\cos\theta\cos\varphi) - g \end{bmatrix}
$$

(3-90)

SIMULATION OF THE QUAD-ROTOR ANALYTICAL DYNAMIC MODEL IN MATLAB/SIMULINK

This chapter shows an implementation of the quad-rotor non-linear analytical dynamic model using block libraries in Matlab/Simulink R2013a software. Calibration of the model and preliminary calculations are then carried out to ensure that the model performs as expected and to determine the operating point parameters. Simulations are run to investigate the open loop flight dynamics.

4.0 Matlab/Simulink Software

Simulating the analytical dynamic model of the quad-rotor helicopter is necessary when designing a controller as it reduces potential risks, design errors, cost and saves time. The systems have to be simulated and tested rigorously to get a high degree of precision. This also ensures a good understanding of the helicopter's responses to its rotor speed changes and enables realistic constraints to be included in the development of a suitable controller.

Matlab is a high-level technical computing language and interactive environment for algorithm development, data visualization, data analysis and numeric computation [94]. As real-world systems have to respond to both continuous and instantaneous changes, Matlab is an invaluable tool because of its features that support such and it is widely used in engineering and science. It is very easy to understand and has many features of a programming language or a simple calculator. Matlab's code optimization enhances quick performance of matrix operations and errors are easily detected and fixed since it is an interpreted language. Its foremost flaw is that it sometimes turns out to be slow.

Simulink is an extension of Matlab, which provides an atmosphere for multi-domain simulation and model-based design for dynamic and embedded systems. It provides an interactive graphical environment and a customizable set of block libraries which allow for design, simulation, implementation, and testing of a variety of time-varying systems. Prior to the development of simulation systems, scientists and engineers had to write computer codes (programs) to represent the mathematical models of dynamic systems in a suitable programming language. In Simulink, the computer codes are the block diagrams and the use of these blocks removes the risks of a user's error in writing the computer codes or the risk that the computer program may not precisely implement the block diagram. The potential productivity improvement and cost savings realized from the block diagram approach to programming is dramatic.

Matlab and Simulink are products of the MathWorks. These two outstanding software packages for scientific and engineering computations are used in many research and educational establishments, in the aerospace, telecommunications and automotive industries; for environmental applications and many more. Matlab and Simulink enable researchers to solve many advanced numerical problems rapidly and efficiently [94]. The Matlab and Simulink environments are incorporated into one entity, and thus it is easy to analyse,

simulate, and review models in either environment at any point in time. Figure 4-1 shows the open loop simulation system.
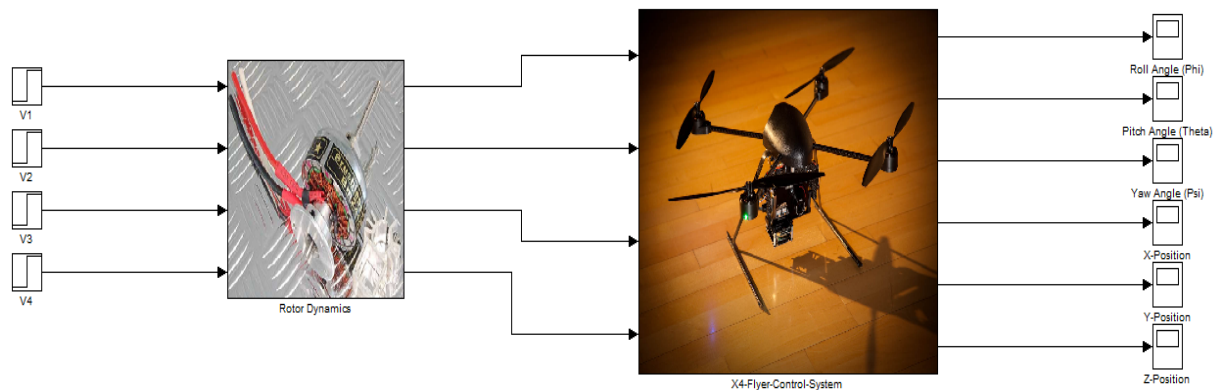
Figure 4-1: Open loop simulation system

4.1 Model Implementation in Matlab/Simulink

The model of the whole system is composed of several interconnected blocks. The dynamics represent the physics of the quad-rotor and provide the position, velocity and acceleration of both linear and angular quantities. The inputs, labelled V_1, V_2, V_3 and V_4 are the voltages, which serve as motor control inputs for the brushless DC motors. The outputs can be selected at will from the variables available, some of which are $x, y, z, u, v, w, \varphi, \theta, \psi, p, q, r$.

Matlab/Simulink allows for fast development of new control algorithms, therefore new ideas can be easily integrated and tested immediately. The Matlab/Simulink model allows for commands to be sent to the quad-rotor and its sensor data to be received by the model.

4.1.1 Summary of equations of motion

The set of differential equations that resulted from chapter 3, using the force-moment balance of the quad-rotor helicopter have been modelled and simulated using Matlab/Simulink software. The equations are as listed below:

1. Actuator (electric motor):

$$V = \frac{JR\dot{\Omega}}{k_q} + k_e\Omega + \frac{RD\Omega^2}{k_q} \tag{4-1}$$

2. Angular accelerations:

$$\text{Pitch - } \ddot{\theta} = \frac{2l\rho A}{I_{xx}}\left[\frac{f\eta k_t}{k_q}\right]^2\left(V_3^2 - V_1^2\right) \tag{4-2}$$

$$\text{Roll - } \ddot{\varphi} = \frac{2l\rho A}{I_{yy}}\left[\frac{f\eta k_t}{k_q}\right]^2\left(V_2{}^2 - V_4{}^2\right)$$ (4-3)

$$\text{Yaw - } \ddot{\psi} = \frac{J}{I_{zz}}\left(\dot{\Omega}_1 + \dot{\Omega}_3 - \dot{\Omega}_2 - \dot{\Omega}_4\right) + \frac{D}{I_{zz}}\left(\Omega_1^2 + \Omega_3^2 - \Omega_2^2 - \Omega_4^2\right)$$ (4-4)

3. Linear accelerations:

$$\text{X-direction - } \ddot{x} = \frac{2\rho A}{m}\left[\frac{f\eta k_t}{k_q}\right]^2\left(V_1{}^2 + V_2{}^2 + V_3{}^2 + V_4{}^2\right)\left(\cos\varphi\sin\theta\cos\psi + \sin\varphi\sin\psi\right)$$ (4-5)

$$\text{Y-direction - } \ddot{y} = \frac{2\rho A}{m}\left[\frac{f\eta k_t}{k_q}\right]^2\left(V_1{}^2 + V_2{}^2 + V_3{}^2 + V_4{}^2\right)\left(\sin\psi\sin\theta\cos\varphi - \cos\psi\sin\varphi\right)$$ (4-6)

$$\text{Z-direction - } \ddot{z} = \frac{2\rho A}{m}\left[\frac{f\eta k_t}{k_q}\right]^2\left(V_1{}^2 + V_2{}^2 + V_3{}^2 + V_4{}^2\right)\left(\cos\theta\cos\varphi\right) - g$$ (4-7)

The open loop simulation system has a total of 10 sub-systems, with four of them simulating the actuator dynamics (the actuator subsystem – being that the quad-rotor has four electric motors), three of them simulating the angular accelerations (pitch, roll and yaw subsystems) and the last three simulating the linear accelerations (x-motion, y-motion and z-motion subsystems). The outputs of the actuator sub-systems are the angular velocities of the propellers (rad/s). These serve as inputs to the yaw subsystem, which computes the yaw angular acceleration. The other subsystems labelled roll, pitch, x-motion, y-motion and z-motion are also fed with the same motor speed control inputs.

Details of individual subsystems are discussed next and the interconnection of the subsystems is presented in appendix A.

4.1.2 Actuator Subsystem

This subsystem as shown in figure 4-2 is based on the differential equation obtained from the electric motor dynamics represented by equation (4-1). Each of the terms of the equation is represented by a hardware block and all the values of the parameters can be obtained from the physical model of the quad-rotor or they may be found as a result of mechanical design process.

$$V = \frac{JR\dot{\Omega}}{k_q} + k_e\Omega + \frac{RD\Omega^2}{k_q}$$
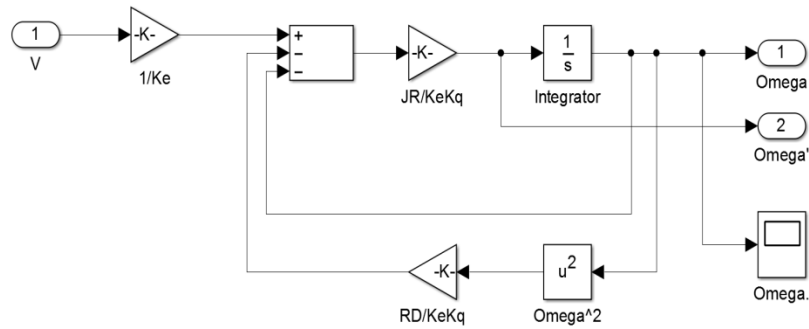
Figure 4-2: The Actuator (Electric Motor) Subsystem

4.1.3 Roll Subsystem

The inputs here are motor voltage control inputs for the left and right motors as shown in figure 4-3. It computes the roll angular acceleration as output. The roll angular velocity is obtained from the direct integral of the roll angular acceleration. Likewise, the roll angular displacement is a direct integral of the roll angular velocity. The angular displacements are used in computing the translational motions.

$$\ddot{\varphi} = \frac{2l\rho A}{I_{yy}} \left[\frac{f\eta k_t}{k_q} \right]^2 \left(V_2{}^2 - V_4{}^2 \right) \qquad [\text{Where } Q = \frac{2l\rho A}{I_{yy}} \left[\frac{f\eta k_t}{k_q} \right]^2]$$
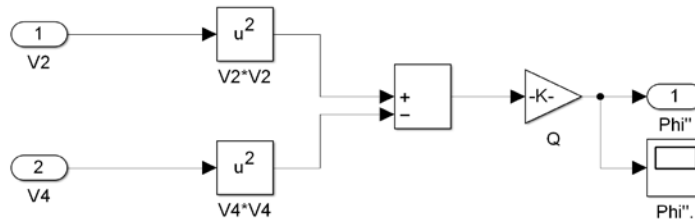
Figure 4-3: The Roll Subsystem

4.1.4 Pitch Subsystem

Very similar to the roll subsystem, the pitch subsystem also has inputs as motor voltage control inputs for the front and rear motors as shown in figure 4-4. It computes the pitch angular acceleration as output. The pitch angular velocity is obtained from the direct integral of the pitch angular acceleration. Similarly, the pitch angular displacement is a direct integral of the pitch angular velocity. All the angular displacements are needed to compute the linear accelerations.

$$\ddot{\theta} = \frac{2l\rho A}{I_{xx}} \left[\frac{f\eta k_t}{k_q} \right]^2 \left(V_3^2 - V_1^2 \right) \qquad [\text{Where } W = \frac{2l\rho A}{I_{yy}} \left[\frac{f\eta k_t}{k_q} \right]^2]$$
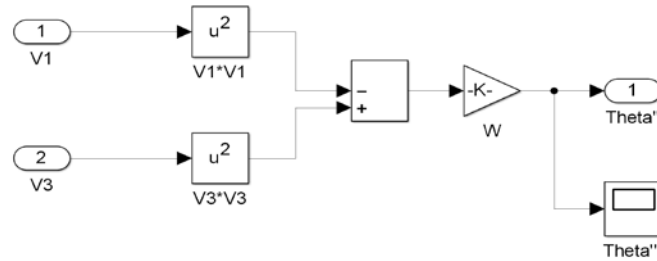
Figure 4-4: The Pitch Subsystem

4.1.5 Yaw Subsystem

The yaw subsystem has its inputs as the four motor speeds, which are used in the equation to compute the yaw angular acceleration as shown in figure 4-5. The yaw angular velocity is obtained from the direct integral of the yaw angular acceleration. Similarly, the yaw angular displacement is a direct integral of the yaw angular velocity. As stated earlier, the angular displacements are very important because they define the attitude of the helicopter and are needed to compute the linear accelerations in the subsystems that follow.

$$\ddot{\psi} = \frac{J}{I_{zz}} \left(\dot{\Omega}_1 + \dot{\Omega}_3 - \dot{\Omega}_2 - \dot{\Omega}_4 \right) + \frac{D}{I_{zz}} \left(\Omega_1^2 + \Omega_3^2 - \Omega_2^2 - \Omega_4^2 \right)$$
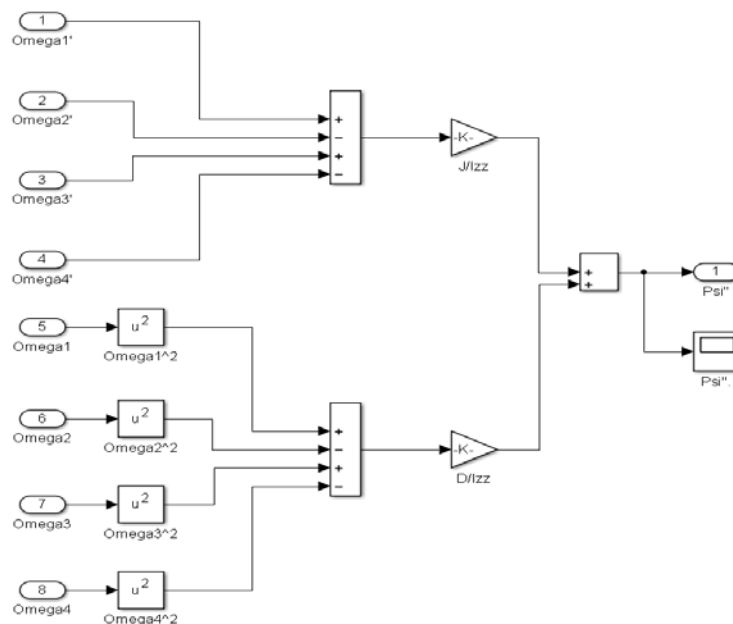
Figure 4-5: The Yaw Subsystem

4.1.6 X-Motion Subsystem

The x-motion subsystem is based on the differential equation for motion along the x-axis. The input signals to the subsystem are the speed control inputs of motors and the roll, pitch and yaw angular displacements as shown in figure 4-6. It computes the acceleration along the x-axis. The linear velocity is obtained by directly integrating the linear acceleration. The position of the helicopter on the x-axis is also obtained by integrating the linear velocity.

$$\ddot{x} = \frac{2\rho A}{m}\left[\frac{f\eta k_t}{k_q}\right]^2 \left(V_1^2 + V_2^2 + V_3^2 + V_4^2\right)\left(\cos\varphi\sin\theta\cos\psi + \sin\varphi\sin\psi\right) \qquad \text{[Where } X = \frac{2\rho A}{m}\left[\frac{f\eta k_t}{k_q}\right]^2 \text{]}$$
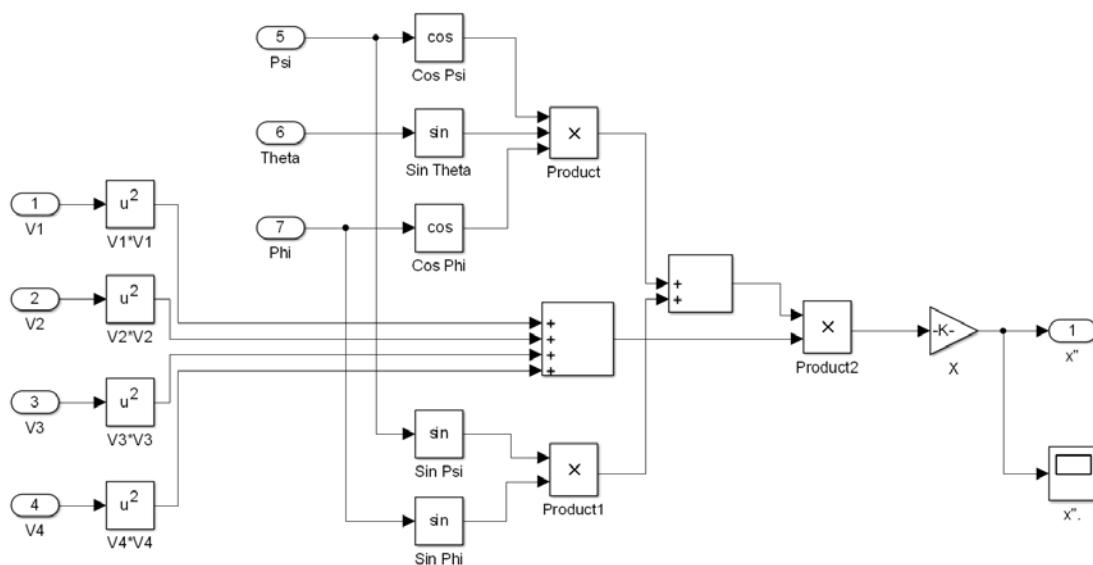
Figure 4-6: X-Motion Subsystem

4.1.7 Y-Motion Subsystem

The y-motion subsystem is based on the differential equation for motion along the y-axis. The input signals to the subsystem are the speed control inputs of motors and the roll, pitch and yaw angular displacements as shown in figure 4-7. It computes the acceleration along the y-axis. The linear velocity is obtained by directly integrating the linear acceleration. The position of the helicopter on the y-axis is also obtained by integrating the linear velocity.

$$\ddot{y} = \frac{2\rho A}{m}\left[\frac{f\eta k_t}{k_q}\right]^2 \left(V_1^2 + V_2^2 + V_3^2 + V_4^2\right)\left(\sin\psi\sin\theta\cos\varphi - \cos\psi\sin\varphi\right) \qquad \text{[Where } Y = \frac{2\rho A}{m}\left[\frac{f\eta k_t}{k_q}\right]^2 \text{]}$$
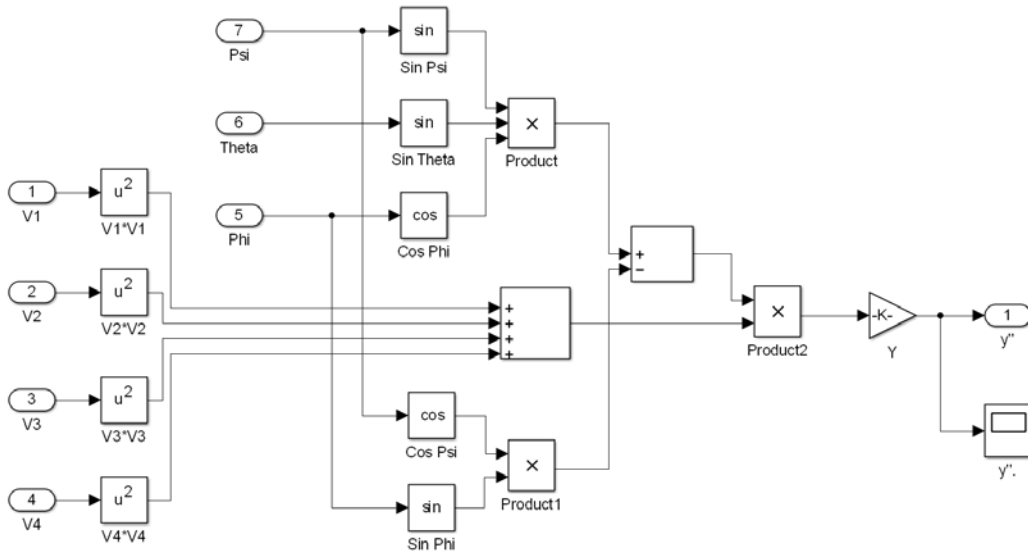
Figure 4-7: Y-Motion Subsystem

4.1.8 Z-Motion Subsystem

The z-motion subsystem is a direct implementation of the equation for vertical acceleration in Simulink. The input signals to the subsystem are the speed control inputs of motors and the roll and pitch angular displacements as depicted in figure 4-8. It computes the acceleration along z-axis. The linear velocity is obtained directly from the integral of the linear acceleration and the position of the helicopter on the z-axis is obtained by integrating the linear velocity.

$$\ddot{z} = \frac{2\rho A}{m}\left[\frac{f\eta k_t}{k_q}\right]^2 \left(V_1^2 + V_2^2 + V_3^2 + V_4^2\right)(\cos\theta\cos\varphi) - g \qquad [\text{Where } Z = \frac{2\rho A}{m}\left[\frac{f\eta k_t}{k_q}\right]^2]$$
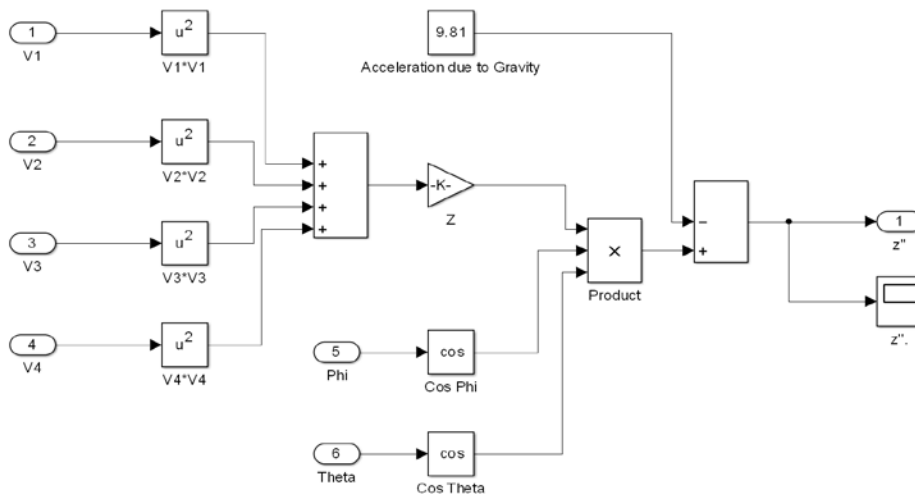
Figure 4-8: The z-motion Subsystem

4.2 Running the Simulation

In the Matlab/Simulink environment, a model can be simulated at any time by clicking the run button on the model editor displaying the model. However, before starting the simulation, it is important to specify various simulation options, such as the start and stop time (in this case chosen to be 4 seconds), the type of solver used to solve the model at each simulation step time (in this case a variable-step solver was used). It is also very important to carry out some preliminary calculations before starting the simulation; otherwise the simulation results may not make any meaning. After defining a model configuration set and doing the preliminary calculations, the simulation is ready to run. It runs from the specified start time to the specified stop time and the results can be viewed and analysed in the Simulink displays or the Matlab workspace. For this chapter, the model will be run in an open loop with no controller in use.

A test run of simulations without properly defining the configuration settings or doing the preliminary calculations would give results similar to the graph displayed in figure 4-9 below.
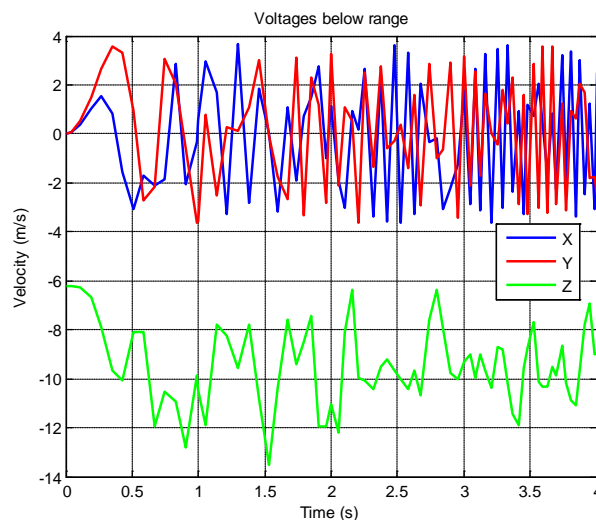
Figure 4-9: Simulation results without proper configuration and calibration of the model

In the figure 4-9 above, all the voltage inputs to the motors were below the operating voltage.

4.2.1 Calibration and Preliminary Calculations

Generally, models will not be very useful unless they are calibrated. Calibration is the process of assigning values or adjusting a model or system to meet certain specifications. Through

calibration and preliminary calculations, adjustments made ensure that a model or system performs as expected.

In the quad-rotor analytical dynamic model developed in chapter 3, the parameters used were not assigned any values. Therefore the model subsystems that were built in this chapter are incomplete, until realistic or practical values of all the constants used in the equations are substituted. The model can be calibrated for use with data obtained from any quad-rotor helicopter experiment.

4.2.1.1 Calibration of the quad-rotor helicopter model

The table 4-1 below contains the set of realistic values of various parameters taken from practical systems and will be used during the simulation of Quad-rotor plant.

Table 4-1: Main parameters of the quad-rotor helicopter [27, 46]

Symbol	Parameter name	Value	Unit
m	total mass of quad-rotor helicopter	0.65	kg
l	Length of quad-rotor arm	0.19	m
I_{xx}	rotational inertia along x-axis	0.0075	$kg.m^2$
I_{yy}	rotational inertia along y-axis	0.0075	$kg.m^2$
I_{zz}	rotational inertia along z-axis	0.013	$kg.m^2$
R_p	propeller radius	0.16	m
f	propeller figure of merit	0.5	
J_r	rotor inertia	6.0e-5	$kg.m^2$
R	motor resistance	0.6	ohms
k_e	motor speed constant	0.0015	$volts.s.rad^{-1}$
k_q	motor torque constant	0.0056	N.m/A
η	motor efficiency	0.75	%
k_t	torque constant	0.01	Ns^2
g	acceleration due to gravity	9.81	m/s^2
D	drag coefficient	7.50e-7	
ρ	air density	1.1	$kg.m^3$

4.2.1.2 Calculation of operating point voltage and motor speed

An operating point has been chosen, in this case when the quad-rotor is hovering. This implies that the vehicle's x-y body plane is parallel to the x-y earth plane equivalent to a situation when the vehicle's roll, pitch and yaw angles together with their first and second derivates (i.e. the angular velocities and accelerations) are all equal to zero. Also, there is no movement in the x-, y- or z- directions, meaning that the linear velocities and accelerations are all equal to zero. The operating point input voltage that corresponds to achieving the situation described above can be calculated from the quad-rotor system equation 4-7, which relates the voltage and the vertical acceleration. Here, all operating points are represented with subscript 'h'.

$$\ddot{z} = \frac{2\rho A}{m} \left[\frac{f\eta k_t}{k_q} \right]^2 \left(V_1^2 + V_2^2 + V_3^2 + V_4^2 \right)(\cos\theta\cos\varphi) - g$$

With

$$\begin{vmatrix} \theta = \varphi = \psi = \dot{\theta} = \dot{\varphi} = \dot{\psi} = \ddot{\theta} = \ddot{\varphi} = \ddot{\psi} = 0 \\ \Omega = \Omega_h \\ \dot{\Omega} = \ddot{\Omega} = 0 \\ \dot{x} = \ddot{x} = \dot{y} = \ddot{y} = \dot{z} = \ddot{z} = 0 \end{vmatrix}$$

(4-8)

Substituting the values of all the constants from the calibration table 4-1 and the conditions listed in equation 4-8 above, the following is obtained

$$0 = \left(\frac{2 \times 1.1 \times 0.08042}{0.65} \right) \left(\frac{0.5 \times 0.75 \times 0.01}{0.0056} \right)^2 \left(V_1^2 + V_2^2 + V_3^2 + V_4^2 \right)(\cos 0\cos 0) - 9.81$$

$$0 = (0.27219)(0.44842) \left(V_1^2 + V_2^2 + V_3^2 + V_4^2 \right) - 9.81$$

$$0 = 0.12206 \times \left(V_1^2 + V_2^2 + V_3^2 + V_4^2 \right) - 9.81$$

Here, it is assumed that all the motors behave in exactly the same way and the design of the helicopter is symmetric; hence their voltage inputs at operating point are thought to be equal.

$$V_h = V_1 = V_2 = V_3 = V_4$$

(4-9)

$$0 = 0.12206 \times \left(4V_h^2 \right) - 9.81$$

$$V_h = \sqrt{20.09333}$$

$$V_h = 4.48 Volts \tag{4-10}$$

Equation 4-10 gives the operating point voltage input for the motors of the quad-rotor helicopter. For this voltage, we can find the speed with which the motors spin at the operating point by substituting using the equation 4-1, which describes the relationship between the motor speed and voltage input.

$$V = \frac{JR\dot{\Omega}}{k_q} + k_e\Omega + \frac{RD\Omega^2}{k_q}$$

At the operating point voltage V_h, let the motor speed be Ω_h

$$V_h = \left(\frac{0.00006 \times 0.6}{0.0056}\right)\dot{\Omega} + 0.0015\Omega + \left(\frac{0.60 \times 0.00000075}{0.0056}\right)\Omega^2$$

$$4.48 = 0.00643\dot{\Omega} + 0.0015\Omega + 0.0000804\Omega^2$$

$$\dot{\Omega} = 696.73406 - 0.23328\Omega - 0.01250\Omega^2$$

Since the motor speeds remain constant at hover, $\dot{\Omega}=0$ and on substituting we have the following quadratic equation

$$696.73406 - 0.23328\Omega - 0.01250\Omega^2 = 0 \tag{4-11}$$

Using the almighty formula for solving quadratic equations,

$$x = \frac{-b \pm \sqrt{b^2 - 4ac}}{2a}$$

$$\Omega_h = \frac{-(-0.23328) \pm \sqrt{(-0.23328)^2 - [4 \times (-0.01250) \times 696.73406]}}{2 \times (-0.01250)}$$

$$\Omega_h = \frac{0.23328 \pm \sqrt{34.89112}}{-0.025}$$

$$\Omega_h = \frac{0.23328 + \sqrt{34.89112}}{-0.025} \text{ Or } \Omega_h = \frac{0.23328 - \sqrt{34.89112}}{-0.025}$$

$$\Omega_h = -245.61 rad / s \text{ Or } \Omega_h = 226.94 rad / s$$

By discarding the negative root of the quadratic equation, the speed at operating voltage is

$$\Omega_h = 226.94 rad / s \qquad (4\text{-}12)$$

Figure 4-10 shows a graph of the motor speed versus time for the operating point voltage of 4.48 volts, confirming that the electric motor rises quickly to the operating point speed of 226.94 rad/s and remains there provided there is no voltage change.
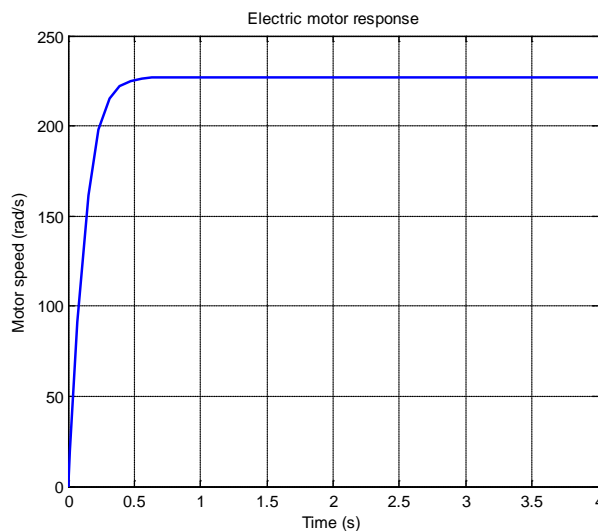
Figure 4-10: Electric motor response to operating voltage step input

The motor voltage for each of the motors has to be at least the value of the operating point voltage (4.48volts) to offset the weight of the helicopter. This leads to the helicopter just lifting off the ground and hovering at a certain height. Outside that, the simulation results are not valid as the motors may spin, but not have any effect on the helicopter model because they do not generate enough lift to move it. Therefore, the operating point voltage serves as the minimum voltage to be applied throughout this simulation process and the motors require very little changes in voltages for control of the quad-rotor helicopter, because of its inherent sensitivity to changes in rotor speeds.

4.2.2 Hover

In the hover mode, it is assumed that the helicopter is at a height, far enough from the ground such as to avoid the ground effect [a condition of improved performance encountered when operating near (within 1/2 rotor diameter) of the ground. It is due to the interference of the surface with the airflow pattern of the rotor system, and it is more pronounced the nearer the ground is approached]. Here, all the propellers rotate at the same (hovering) speed to generate a collective lift force that offsets the weight of the quad-rotor helicopter. As a consequence, the quad-rotor neither climbs nor descends, it does not stall, roll, pitch or yaw and therefore there is no horizontal movement in any direction. It stays at a fixed point in the air and does not move from its position because there is a balance in all the forces and torques that are acting on the vehicle. All simulations performed in this chapter were done while trying to maintain a height of 0.92m as shown in figure 4-11 below.
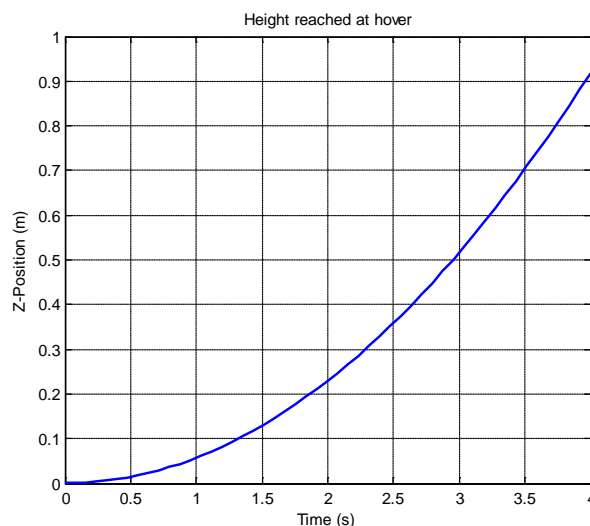
Figure 4-11: Height reached at hover

As explained in the basic concepts of the quad-rotor helicopter (chapter 1), there are four basic control actions, which allow the quad-rotor helicopter to reach a certain altitude and attitude. Simulations have been run for each of the four basic control actions and results displayed with analysis of the quad-rotor behaviour according to each of the commands.

4.2.3 Throttle (Vertical Motion)

This control action is realized by simultaneously increasing (or decreasing) all propeller speeds by identical amounts. This implies that from an initial hover state, if the same amount of voltage is added to the four motors simultaneously, the quad-rotor helicopter will heave

(move vertically upwards), because of the collective vertical force generated by the four propellers.

Fig 4-12 shows the height attained by the quad-rotor helicopter when an input of 4.6 volts is given to each of the motors.
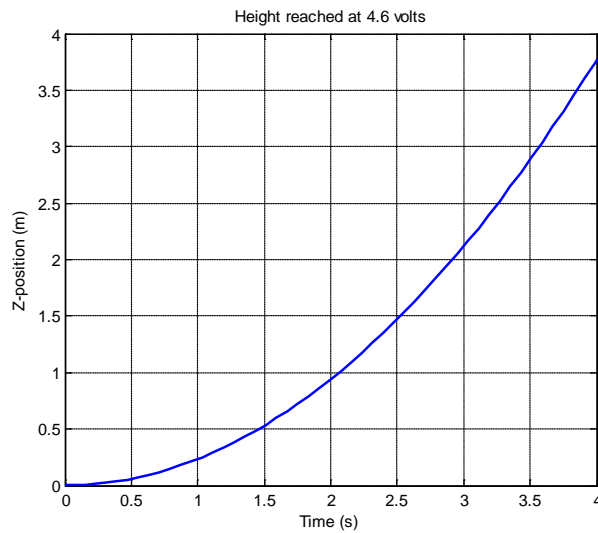
Figure 4-12: Height reached when each motor is given an input of 4.6volts

It is seen to reach a height of about 3.75m. This clearly shows that for very little voltage changes, the motion of the quad-rotor helicopter is affected.

From the fig 4-13 below, it can be clearly seen that the upward velocity quickly increases and then stops at a certain value because the voltage remains constant at that point.
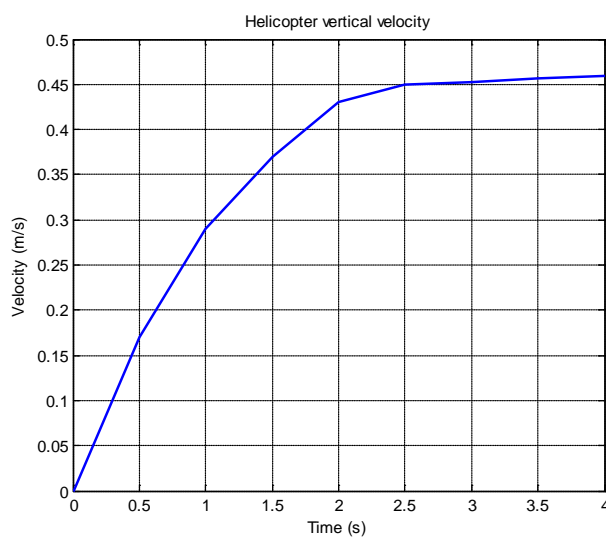
Figure 4-13: Upward velocity of quad-rotor helicopter

Therefore the simultaneous increase to a certain value of the voltages in the four motors by the same amount means that the collective vertical thrust generated by the four rotors becomes greater than the weight of the helicopter and so the vehicle starts a vertical climb. However, with an increase in the vertical speed, the thrust coefficient decreases, and so will the collective vertical thrust, hence the total thrust equates the weight of the helicopter again – defining a new point of equilibrium. Having reached that point of equilibrium, the helicopter climbs at a steady speed, implying a zero upward acceleration, as also confirmed in [2]. Figure 4-14 shows the total thrust generated at different motor speeds.
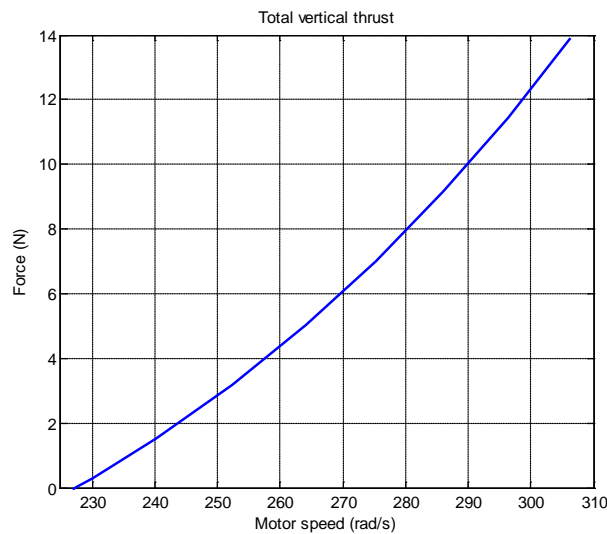
Figure 4-14: Total thrust generated at different motor speeds

The dependence of the collective vertical thrust on the vertical speed is also applicable to situations when the helicopter is descending, but this time the collective vertical thrust increases. Therefore, if the voltages are simultaneously decreased to a certain value by the same amount, the helicopter will descend at increasing speeds until a limit value is reached.

It is worthy of note that, since z-axis points upwards, a negative velocity or acceleration, simply means that the quad-rotor helicopter is descending, and a negative altitude means that it is below the starting level.

4.2.4 Roll

The roll command is provided by simultaneously increasing (or decreasing) the left propeller speed and decreasing (or increasing) the right propeller speed, while keeping the front and rear propellers spinning at the same speed. With one rotor spinning faster than the rotor on the opposite side, more lift will be generated on the side of the faster spinning rotor, therefore

the helicopter will tilt at a certain angle as shown in figure 4-15. This is because of the torque created by the changes in lift forces with respect to the quad-rotor body x-axis.
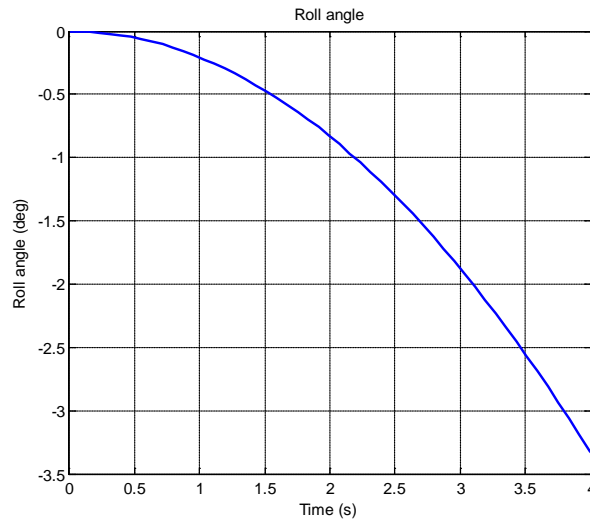
Figure 4-15: Roll angle

While the front and rear motors were given a voltage supply of 4.5200 volts each (keeping each of them at a speed of 227.9938 rad/s), the left motor had a voltage input of 4.5198 volts (spinning at a speed of 227.9889 rad/s) and the right motor had an input of 4.5202 volts (spinning at a speed of 227.9990 rad/s). The result as seen in the figure 4-15 is an angle of -3.33 degrees. It is worthy of note that the – (minus) sign in the angle shows only the direction of tilt and movement of the quad-rotor helicopter and does not in any way affect the magnitude of the angle.

Figure 4-16 shows the position reached by the helicopter as a result of the roll angle created.
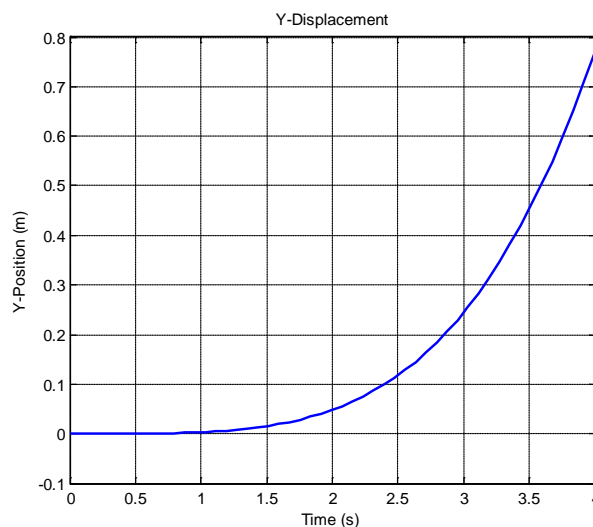
Figure 4-16: Y-displacement as a result of roll angle

The simulation shows the quad-rotor helicopter has been displaced by about 0.77m in the y-direction. This is because the helicopter accelerates in its direction of tilt, depending on the magnitude of the tilt angle created and the length of time it is tilted at that angle.

In the figure 4-17 below, the simulation shows the components of forces acting on the quad-rotor helicopter as a result of the roll angle of -3.33 degrees created by the little voltage differences in the motors.
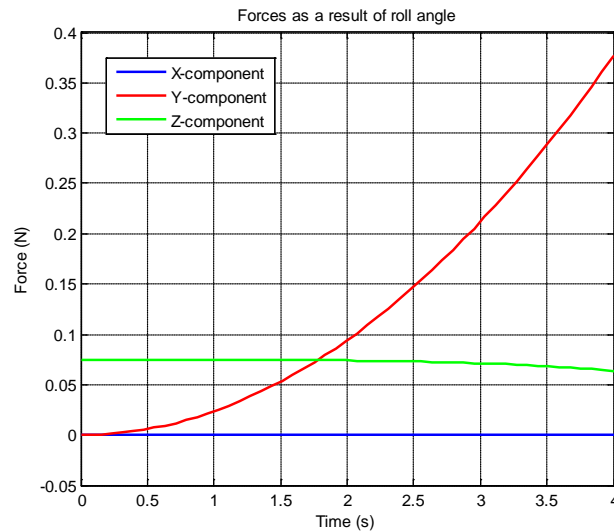
Figure 4-17: Components of forces as a result of the rolling moment

As expected, the y-component (red line) of the force increases with the roll angle, while the x-component (blue line) remains at its lowest of 0. Against the expectation that the helicopter should maintain its total vertical thrust, it is seen that the z-component (green line) of the force decreases slightly – implying that there is a little drop in the helicopter altitude as it moves in the y-direction. This one of the tasks the fuzzy-neural controller developed in chapter 7 is expected to compensate for.

Figure 4-18 describes the movement of the helicopter in the 3 directions.
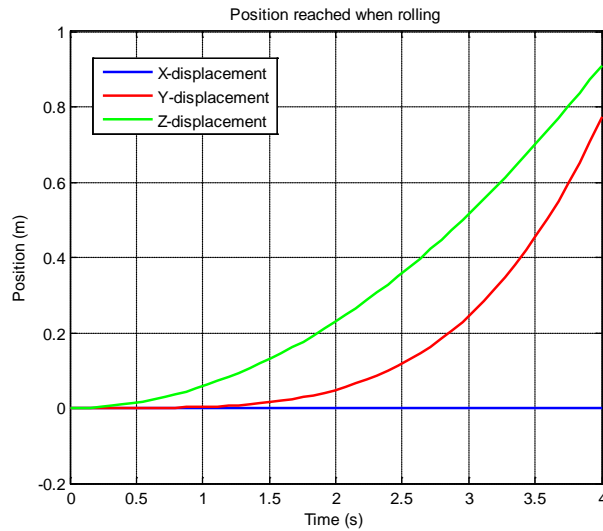
Figure 4-18: Position reached when rolling

The graph in figure 4-11 shows the helicopter reaching a height of about 0.92m when all the input voltages are 4.52 volts. Conversely figure 4-18 shows the quad-rotor helicopter dropping to a height of 0.91m while moving to a position of about 0.77m in the y-direction, corroborating the fact that a little bit of the total vertical thrust was lost during this movement, despite the simultaneous increase (decrease) of the speeds of the left-right motor pair. This could be as a result of some modelling assumptions, which the fuzzy-neural controller is expected to deal with.

The figure 4-17 shows the components of forces acting on the quad-rotor helicopter as a result of a particular roll angle (-3.33 degrees), where the y-component of the force increased with the roll angle and the z-component decreased slightly. The graph in fig 4-19 shows simulations carried out for different roll angles. While the y-component increased as the roll angle got larger, the z-component continued to decrease – meaning that helicopter continued to loose altitude with greater roll angles. The x-component (not shown in the graph) appeared to be 0 or close to 0 for all the angles – implying that there was no movement in the x-direction.
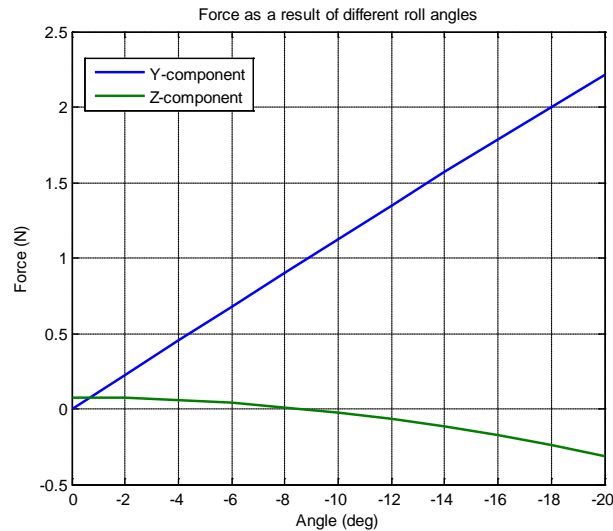
Figure 4-19: Forces acting on the helicopter as a result of different roll angles

The coupling between attitude and altitude control makes this control command more complex than the throttle command as the quad-rotor helicopter is expected to maintain the total thrust when rolling left or right. To prevent yawing, the total reaction torque has to be kept equal to zero at all times. This was found to impose a constraint on the amount of thrust that can be increased in one rotor relative to the other, implying that it is not mandatory for the speeds of the left and right propellers to be increased (or decreased) by exactly the same amount – even if the electric motors behave in exactly the same way.

It has been found that there is a lot of difficulty in maintaining a very good balance of forces and torques while adjusting the thrusts of the individual or pairs of rotors, since these torques will also depend on some rotor modelling parameters like the rotor pitch rate, etc. For the sake of these simulations, some of those effects have been ignored.

4.2.5 Pitch

The pitch and roll commands are very similar due to the assumed axial symmetry of the quad-rotor helicopter. It is provided by simultaneously increasing (or decreasing) the rear propeller speed and decreasing (or increasing) the front propeller speed, while keeping the left and right propellers spinning at the same speed. With one rotor spinning faster than the rotor on the opposite side, more lift will be generated on the side of the faster spinning rotor, therefore the helicopter will tilt. This is because of the torque created by the changes in lift forces with respect to the quad-rotor body y-axis and that creates a pitch angle (known as a nose-up or nose-down in a conventional aircraft).

When the helicopter is tilted, the air is deflected slightly sideways instead of directly downwards, and the helicopter will move in the direction of its tilt. Again, the total vertical thrust is maintained as in hovering, thus this command leads only to a pitch angular acceleration.

The same explanation that was given for roll holds for pitch. Again there is the coupling between attitude and altitude control, which makes this control command more complex than the throttle command, just like that of roll. The quad-rotor helicopter is still expected to remain at the same altitude by maintaining the total thrust when pitching up or down. To demonstrate the similarity in the behaviour of the roll and pitch angles, a different set of voltages was chosen to give a slightly different pitch angle of 1.67 degrees as against the - 3.33 degrees used for roll.

In figure 4-20, while the left and right motors were given a voltage supply of 4.5200 volts each (keeping each of them at a speed of 227.9938 rad/s), the front motor had a voltage input of 4.5199 volts (spinning at a speed of 227.9912 rad/s) and the rear motor had an input of 4.5201 volts (spinning at a speed of 227.9964 rad/s). The result as seen in figure 4-20 is an angle of 1.67 degrees.
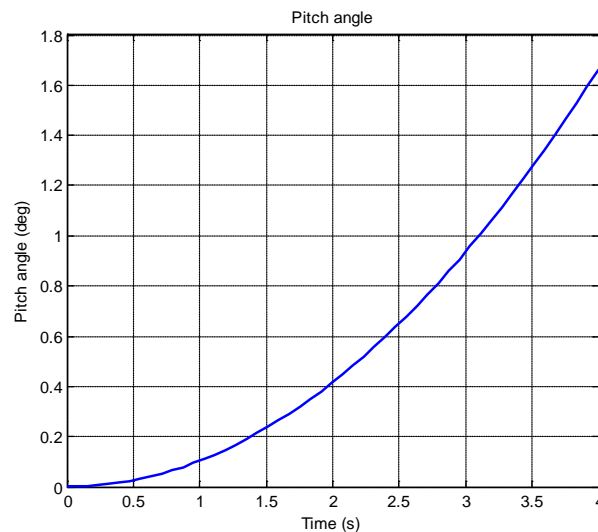
Figure 4-20: Pitch angle

In figure 4-21, the simulation shows the quad-rotor helicopter moving to a position of about 0.39 m in the x-direction. As explained in the section for roll, the helicopter always moves in its direction of tilt, depending on the magnitude of the tilt angle created and the length of time it is kept tilted at that angle.
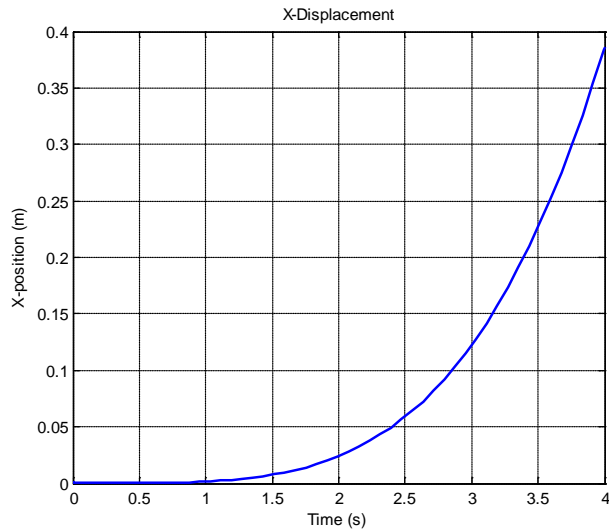
**Figure 4-21: X-displacement as a result of pitch angle**

In figure 4-22, the graph shows the components of forces acting on the quad-rotor helicopter as a result of the pitch angle of 1.67 degrees. As seen in the roll angle simulation, the x-component (blue line) of the force increases with the pitch angle, while the y-component (red line) remains at its lowest of 0. Again it is clearly seen that the helicopter does not maintain its total vertical thrust as the z-component (green line) of the force decreases slightly with a movement in the x-direction as a result of the pitch angle.
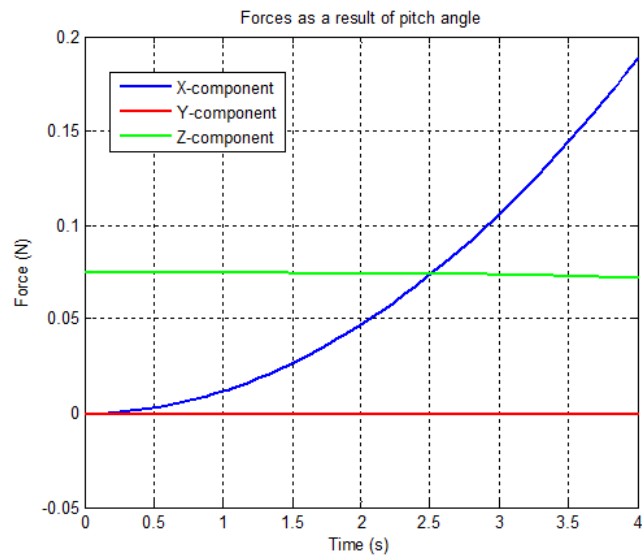
Figure 4-22: Components of forces as a result of the pitching moment

Comparing again with the graph in figure 4-11, which shows the helicopter reaching a height of 0.92m when all the input voltages are 4.52 volts, it is seen in figure 4-23 that the quad-rotor helicopter drops to a height of 0.917m while moving to a position of about 0.39 m in the

97

y-direction, confirming the fact that a little bit of the total vertical thrust was lost during this movement, despite the simultaneous increase (decrease) of the speeds of the front-rear motor pair.
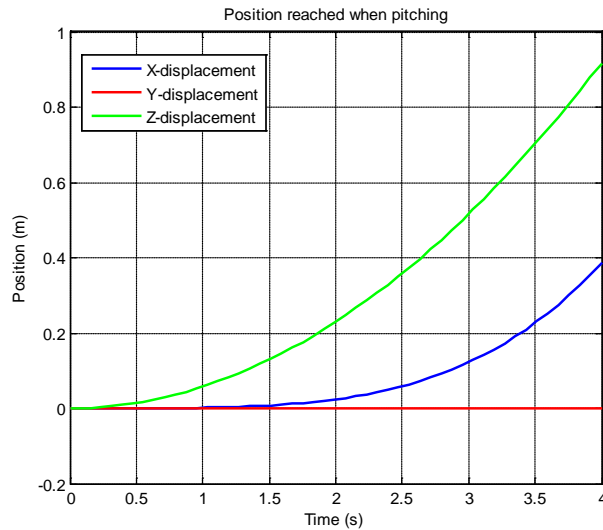
Figure 4-23: Position reached when pitching

In figure 4-22, we see the components of forces acting on the quad-rotor helicopter as a result of a pitch angle of 1.67 degrees. The x-component of the force increased with the pitch angle (just like the y-component did with the roll angle in fig 4-17) and the z-component decreased slightly. The graph in figure 4-24 shows simulations carried out for different pitch angles. While the x-component increased as the pitch angle got larger, the z-component continued to decrease – meaning that helicopter continued to loose altitude with greater pitch angles.
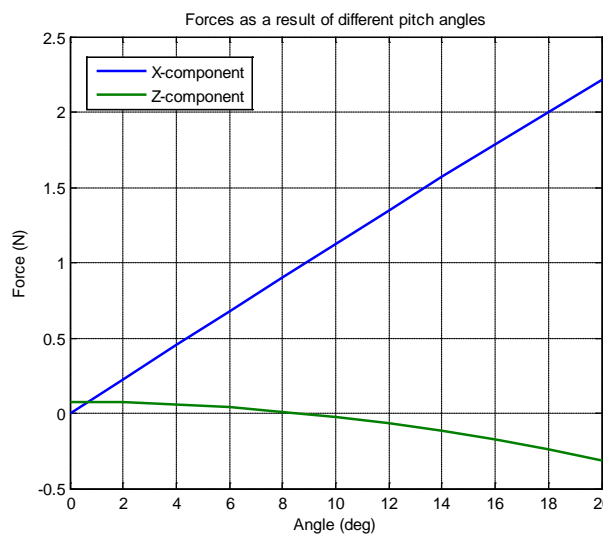
Figure 4-24: Forces acting on the helicopter as a result of different pitch angles

4.2.6 Yaw

This command simulates the rudder on a conventional fixed wing aircraft. It is realized by simultaneously increasing (or decreasing) the front-rear propellers' speed and decreasing (or increasing) that of the left-right duo. As a result, there is a torque imbalance with respect to the quad-rotor body z-axis and this makes the quad-rotor helicopter to pirouette about the same axis in response to whichever direction the command is given.

While the left and right motors were given a voltage supply of 4.5150 volts each (keeping each of them at a speed of 227.8627 rad/s), the front and rear motors each had a voltage input of 4.525 volts (keeping each of them spinning at a speed of 228.1248 rad/s). The torque imbalance results in a yaw angle of about 6.72 degrees as shown in figure 4-25.
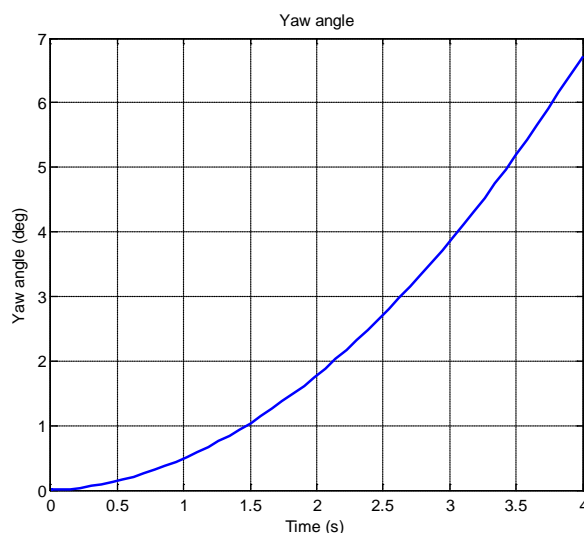
Figure 4-25: Yaw angle

In the figure 4-26, the simulation shows the quad-rotor helicopter climbing to a height of about 0.922m. This is as a result of a slight increase in the total vertical thrust occasioned by spinning the front-rear motor pair a little faster than the left-right duo, which created the torque imbalance on the helicopter. No horizontal movement was recorded because the pitch and roll angles remained very close to 0 and could not cause any acceleration in the x or y directions.
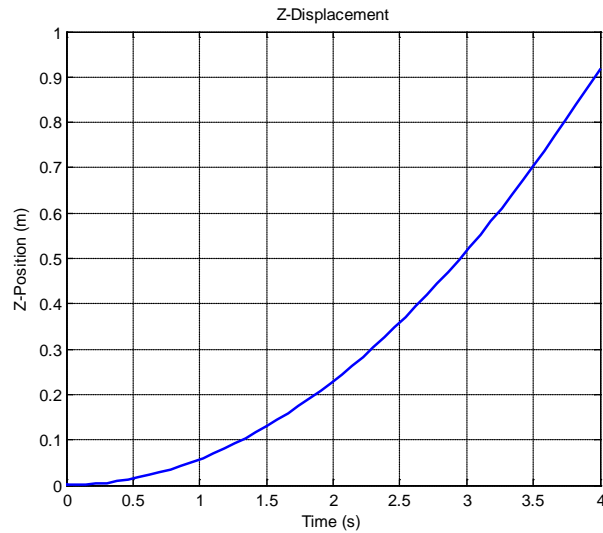
Figure 4-26: Z-displacement

In the figure 4-27, the graph shows the components of forces acting on the quad-rotor helicopter as a result of the yaw angle of 6.72 degrees. While the z-component (green line) of the force increased slightly, the x and y components remained very close to 0 – implying the helicopter only moved vertically upwards while changing heading by 6.72 degrees.
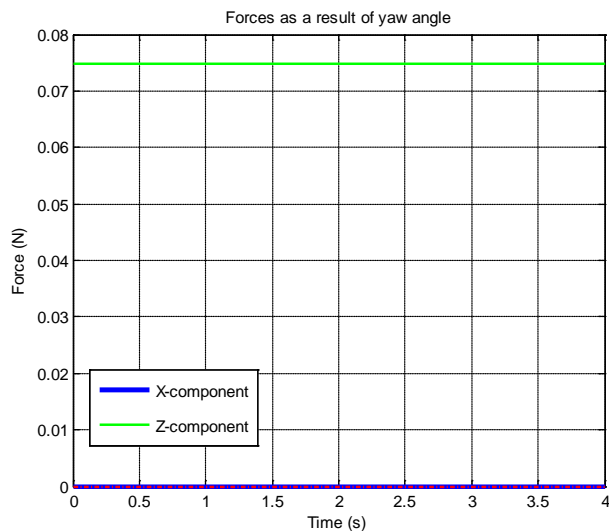
Figure 4-27: Components of forces as a result of the yawing moment

On comparing with the graph in figure 4-11, which shows the helicopter reaching a height of 0.92m when all the input voltages are 4.52 volts, it is seen in figure 4-28 that the quad-rotor helicopter climbs to a height of 0.922m while yawing 6.72 degrees, confirming the fact that there was a little increase in the total vertical thrust.
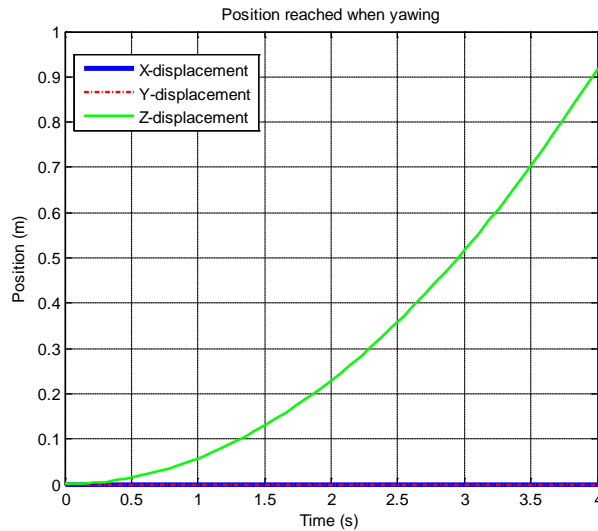
Figure 4-28: Position reached when yawing

Figure 4-29, shows a slight but steady rise in the z-component of the force as the yaw angle increases. Having to increase the speed of one pair while keeping the other pair constant is responsible for this slight increase in the total vertical thrust.
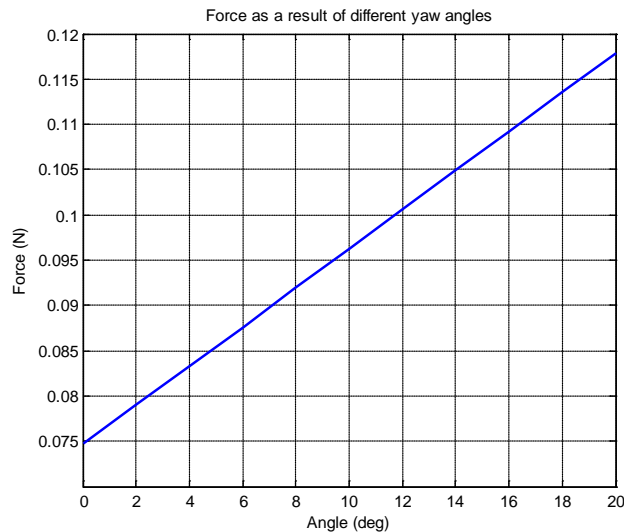
Figure 4-29: Forces acting on the helicopter as a result of different yaw angles

This control is a little easier to achieve, because the inertia of the quad-rotor around the z-axis is approximately double those of the x- and y- axes. Furthermore, there is no obvious cross-coupling between the yaw and altitude controls. There is no translational motion since the helicopter does not tilt in any direction and since the total vertical thrust is expected to be maintained as in the hover state, there has to be a constraint on the amount of torque that can be increased in a pair of rotors relative to the other. Normally, the rotor speed changes required to achieve such control are very small, so it can be assumed that to maintain the total

thrust, the increase and decrease of the speeds of the motor pairs are done by the same amounts.

4.3 Chapter Summary

The developed analytical model has been simulated in Matlab/Simulink software and the dynamic behaviour of the quad-rotor assessed due to voltage changes. The main purpose of this chapter was to analyse the results produced by the Simulink model, given different voltage inputs. Previously known flight behaviours were confirmed, possible control problems were identified and new flight behaviours were noted, preparatory to the design of the controller.

Inevitably some effects have not been included in the model, and these effects could modify the results that have been obtained here. The model can further be calibrated and linearized for use on any quad-rotor helicopter, depending on the nature of the flight control problem. Please see appendix F for more details on linearization.

QUAD-ROTOR 3-D CAD MODEL AND COMPUTATIONAL FLUID DYNAMICS (CFD) SIMULATION

This chapter presents details of CFD simulation and analysis of the quad-rotor helicopter. It starts by showing how SolidWorks 2013 software is used to develop a 3-D CAD model of the quad-rotor helicopter, with the same parameter values as that of the analytical dynamic model developed in chapter 3 and simulated in chapter 4 of this thesis. Computational Fluid Dynamics (CFD) as a computer based mathematical modelling tool is then used to simulate and analyse the effects of wind flow patterns on the performance and control of the quad-rotor helicopter.

5.0 Quad-rotor Helicopter CFD

Computational Fluid Dynamics (CFD) as a computer based mathematical modelling tool can be considered as the combination of theory and experimentation in fluid flows. It is now generally accepted and extensively used as a valid engineering tool in industry.

CFD computations are founded upon the fundamental governing equations of fluid dynamics – the conservation of mass, momentum and energy. These equations combine to form the Navier-Stokes equations, which are known to be a set of partial differential equations that cannot be solved analytically except in a limited number of cases. Nevertheless, approximate solutions can be obtained using discretisation methods that approximate the partial differential equations by a set of algebraic equations. The most frequently used are the finite volume method, the finite element method and the finite difference method. The resulting algebraic equations relate to small sub-volumes within the flow, at a finite number of discrete locations.

Any air-breathing propulsion system, be it a pure jet, an engine-propeller combination, an engine-rotor combination, or a motor-rotor combination (like the quad-rotor helicopter), derives its net thrust by adding momentum to a volume of air [95]. Therefore, the production of thrust in helicopters is based solely on the action of the propeller. As the propeller rotates, it causes the air around it to accelerate from one side to the other, which results in the development of thrust in the opposite direction of the flow.

The rotor blades of the quad-rotor helicopter are responsible for three basic functions:
1. The generation of a vertical lifting force (thrust) in opposition to the aircraft weight.
2. The generation of a horizontal propulsive force for forward flight and sideways flight.
3. A means of generating forces and moments to control the attitude and altitude of the helicopter.

The aerodynamics of the helicopter is one of the most challenging problems facing aerodynamicists, but with the rapid increase in computational power and storage in recent times, CFD simulation has turned out to be a realistic way of predicting the air flow around the rotor blade. This certainly makes way for accurate prediction and understanding of the aerodynamics of the entire quad-rotor helicopter [96].

The physics which governs fluids is relatively simple; the laws of motion and thermodynamics with a little bit of chemistry. However, the solutions are very complex and

this makes analytical methods (pen and paper) largely unusable for industrial applications. A common engineering approach to such complex dilemmas is to replace the problem with a number of smaller less complex problems [97].

As the quad-rotor helicopter flies around, the fluid in which it is submerged (in this case air) must move out of its way. The manner in which the air flows around it depends on its shape as the flow could be smooth but more likely will contain vortices, shockwaves and other disturbances as shown in figure 5-1.
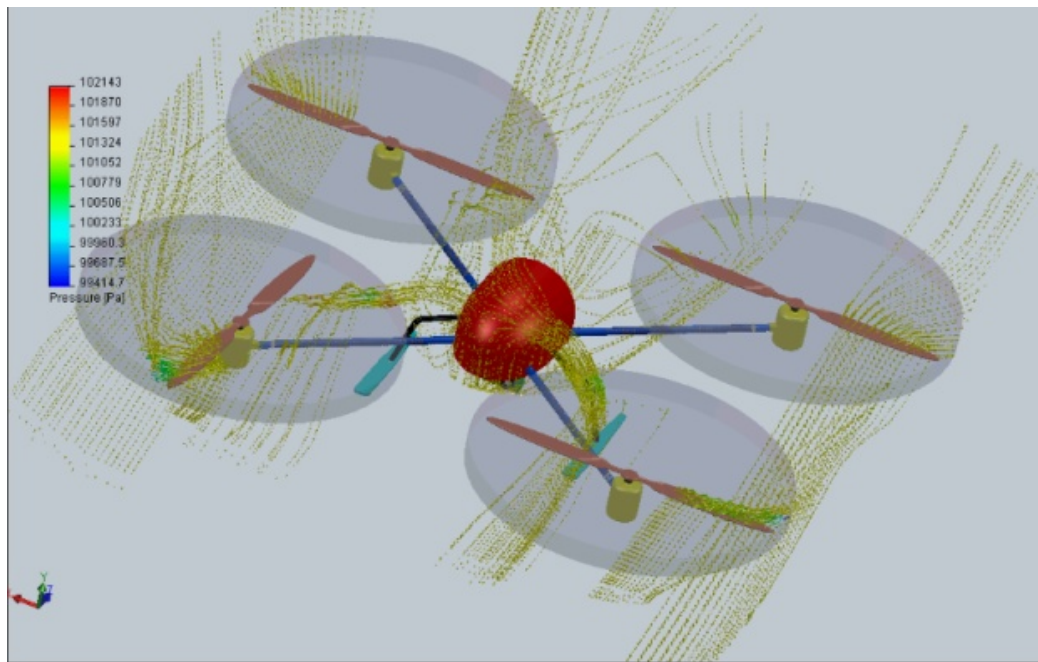
Figure 5-1: Air flows around the quad-rotor helicopter in a CFD simulation

To model the behaviour of the fluid (air) the volume is split into many small sub-volumes, called a mesh (or grid). A mesh can be simply the same sub-volume repeated throughout the space or, more usually, it can be moulded around the helicopter CAD model as shown in figure 5-2. Splitting the volume into sub-volumes is elegant in theory but hard in practice. The art is to create a mesh with exactly the right sub-volumes – if the sub-volumes are too big then the solution will have errors, if the volumes are too small then the calculation will take too long.
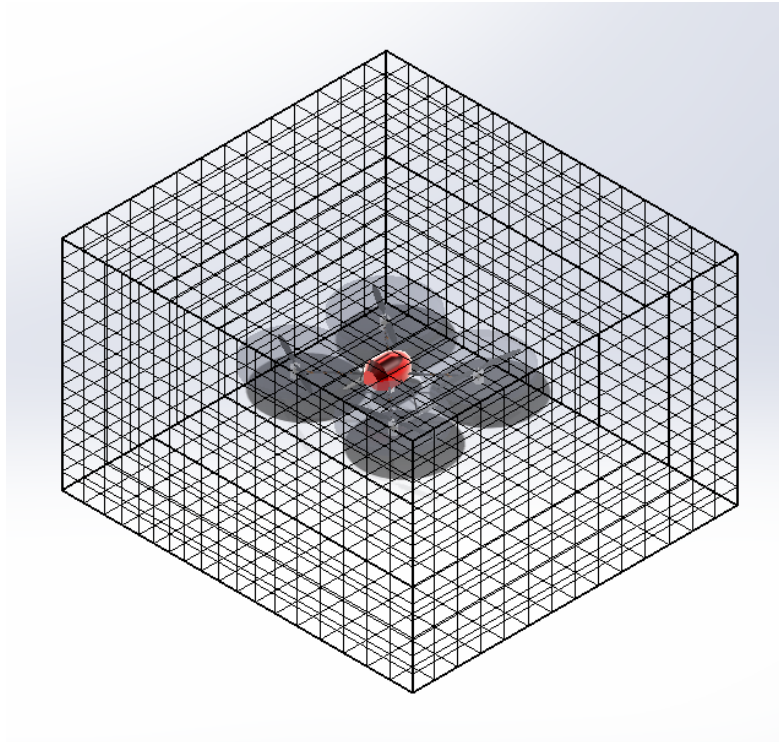
Figure 5-2: CFD mesh diagram

The airflow is analysed by starting from an initial flow, which can be either a guess at the solution or a specific initial condition. Using this initial flow the conservation equations are used to predict the flow a short time later. A new prediction is then made from the newly calculated flow. In this way the evolution of the airflow can be solved. In some situations (mostly when flying indoors or even outdoors without a disturbance), flows around the rotor blades of the helicopter are steady. For these steady flows, the process is repeated until the solution doesn't change from one time to the next, i.e. a convergence. The opposite of this is when the flows around the rotor blades are unsteady. For these uneven flows, the solution never settles down and CFD aims to track how the flow changes with time [63].

This explanation of using the conservation equations as a flow solver is a simplification; there are other more complex solvers. However, these methods produce similar outputs and, more importantly, CFD systems look the same to a user regardless of the solution technique.
Having obtained a flow solution, the user is presented with the flow at every point in the mesh. This is a vast amount of data and not very useful on its own. The last phase of the CFD process is to extract from these data the information that the user actually wants, in this case the velocities, accelerations and forces acting on the quad-rotor helicopter.

The flowchart in figure 5-3 shows the three major stages involved in using CFD to simulate a quad-rotor helicopter.
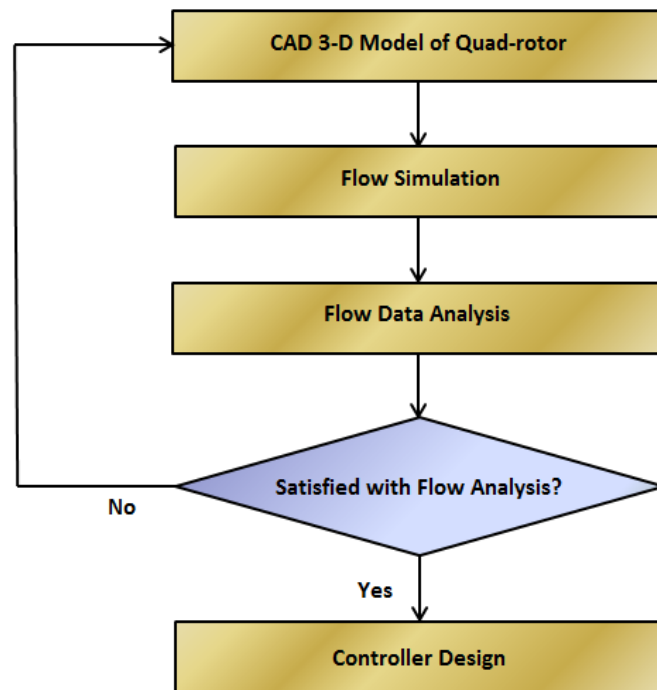
Figure 5-3: CFD process flow

a) Computer Aided Design (CAD) – using software to build a model of the quad-rotor helicopter and to represent it in the flow domain. It entails the following:
   ▪ Approximation of the geometry – the geometry of the quad-rotor needs to be approximated by a geometric CAD type model. More accurate results are obtained from a model geometry that more closely represents the actual geometry.
   ▪ Creation of the numerical grid within the geometrical model – to identify the discrete, finite locations at which the variables are to be calculated, the geometry is divided into a finite number of cells that make up the numerical grid. Before doing this, it is necessary to identify the physical flow phenomena expected (turbulence, compressible flow, shocks, multiphase flow, mixing, etc.) so that the grid generated is suitable to capture these phenomena.
   ▪ Selection of models and modelling parameters – once the geometry and grid have been established, the mathematical models and parameters for those phenomena are then selected and boundary conditions defined throughout the computational domain.

b) CFD Flow Solver – obtaining a flow solution by running a flow-solver to simulate the quad-rotor helicopter's fluid environment using the grid for flow conditions specified by the researcher. It involves:

- Calculation of the variable values – discretisation yields a large number of algebraic equations (one set for each cell). These equations are then generally solved using an iterative method, starting with a first guess value for all variables and completing a computational cycle. Error or residual values are computed from the discretised equations and the calculations repeated many times, reducing the residual values, until a sufficiently converged solution is judged to have been reached.

- Determination of a sufficiently converged solution – the final stage in the solution process is to determine when the solution has reached a sufficient level of convergence. When the sum of the residual values around the system becomes sufficiently small, the calculations are stopped and the solution is considered converged. A further check is that additional iterations produce negligible changes in the variable values.

c) Data Analysis, Presentation and Verification – analysing the flow data from the results of the flow-solver and modifying the model until a design satisfaction is achieved. It involves:

- Post Processing – once a converged solution has been calculated, the results can be presented as numerical values or pictures, such as velocity vectors and contours of constant values (e.g. pressure or velocity).

- Solution Verification and Validation – once the solution process is complete, each solution should be verified and validated. If this cannot be completed successfully, re-simulation may be required, with different assumptions and / or improvements to the grid, models and boundary conditions used.

5.1 Quad-rotor 3-D CAD Model

Building such a model commonly begins with a 2-D draft of the helicopter parts. The draft comprises of geometry such as points, lines, arcs, conics and etc. Measurements are then added to the draft to outline the size and positions of the geometry. The relationships between the parts such as their intersections at tangents, their being perpendicular or parallel or concentric are normally used to define attributes. With its parametric nature, SolidWorks allows the measurements and relations to drive the geometry. The measurements in the draft

can be organized individually, or by relationships to other parameters inside or outside of the draft [98]. Table 5-1 shows the quad-rotor helicopter parts designed using SolidWorks.

Table 5-1: Quad-rotor UAV CAD parts

Part	Description	Quantity	Mass (g)
	BLDC motor	4	40 x 4 = 160.00
	Arm	4	35 x 4 = 140.00
	Propeller	4	12.60 x 4 = 50.40
	Central Hub (with all electronics and battery)	1	253.30
	Landing gear	2	15.20 x 2 = 30.40
	Payload (camera)	1	15.90
Total weight			650.00

Having carefully designed the different components based on the same parameter values as that of the analytical dynamic Matlab/Simulink model in chapter 4, they were assembled to form the quad-rotor helicopter model shown in figure 5-4 below, with details given in appendix B of this thesis.

Figure 5-4: SolidWorks 3-D model of the quad-rotor helicopter

5.2 CFD Flow Solver

The flow-solver used in this research work is SolidWorks Flow Simulation 2013. Flow Simulation is a fluid flow and heat transfer analysis software fully integrated into SolidWorks. It simulates the quad-rotor helicopter's 3-D prototype in its working fluid environment, thereby giving predictions of the effects of the fluid flow on the helicopter prototype and the helicopter's effects on the fluid flow around it.

The outstanding feature of Flow Simulation is its intuitively clear and comfortable interface including a pre-processor for defining the type of analysis, specifying data and boundary conditions for the calculation (with an Engineering Database on substance properties); co-processor for monitoring and controlling the computation process and checking the convergence where necessary; postprocessor for visualizing the results obtained [99].
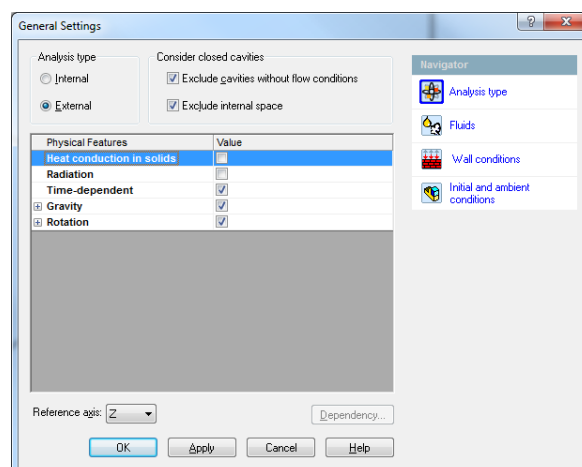
Figure 5-5: Flow-solver dialogue box

The main objective of conducting the CFD simulation in this research is to simulate the effects of the external environment on the flow patterns of the quad-rotor helicopter within a computational domain.

The computational domain is a rectangular parallelepiped for both the 3D analysis and 2D analysis. Its boundaries are parallel to the Global Coordinate System planes as shown in figure 5-6. Sometimes overlooked, the computational domain is one of the many important factors that influence the validity and accuracy of CFD simulation results. The use of different computational domains has turned out varied results, even for the same set of rotor speeds. Therefore, the choice of computational domain could significantly affect the results of such simulations.
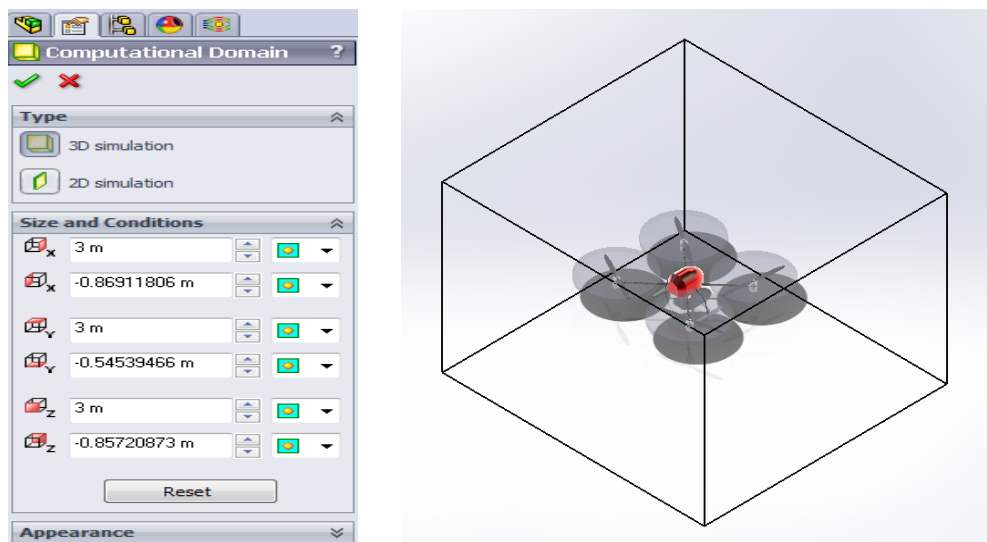
Figure 5-6: Computational domain of CFD simulation

In many cases, the advantage of working on a rectangular computational domain, with a uniform rectangular grid, compensatory to the more complicated form of the equation being used. The problem is finding the coordinate transformation, which maps the physical domain into the needed computational domain, such that the uniform rectangular grid in the computational domain corresponds to a non-uniform curvilinear grid in the physical domain [100].

Due to specified conditions, the characteristics of the fluid flow may have large variations in some regions in the physical space. In these regions, a refinement of the grid should be very useful, as it yields increased accuracy, without a supplementary computing effort.

Figure 5-7 shows the distribution of air around the rotors of the quad-rotor helicopter as they spin and add momentum to the volume of air they are immersed in. The lift force would normally rise perpendicularly to the air stream caused by Bernoulli Effect. This causes a lower pressure on top of the rotor blade, compared with the pressure at the bottom. The curvature on the top of the blade leads to a higher stream velocity than at the bottom and hence a lower pressure [101].
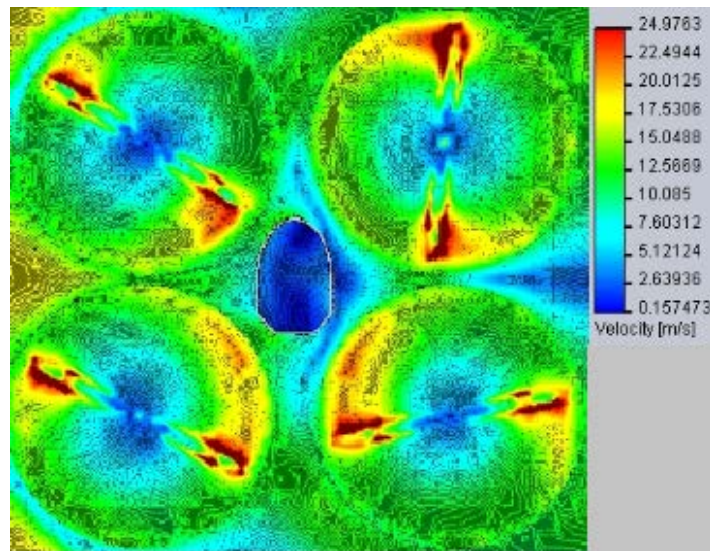
Figure 5-7: Air distribution around the rotors during simulation

A close observation shows that near the ends of the rotating blades, there is some turbulence and the airflow tends to move upwards. Interactions between the wakes produced by the rotors and the fuselage, and also between individual rotors can also be observed. The cumulative air flow tends to go upwards, compensating the lift force.

5.3 Analysis of CFD results

In the analytical dynamic Matlab/Simulink model in chapter 4, voltage applied to the DC-motor model results in angular acceleration; the same sets of angular accelerations obtained from the Matlab/Simulink model were used in the flow simulation in this chapter, as shown in figure 5-8. The accelerations and forces produced as a result of each of the four basic commands of throttle, roll pitch and yaw were recorded and analysed for situations with and without wind disturbance. In the windy situations, the quad-rotor helicopter was exposed to wind speeds of different magnitudes and directions.
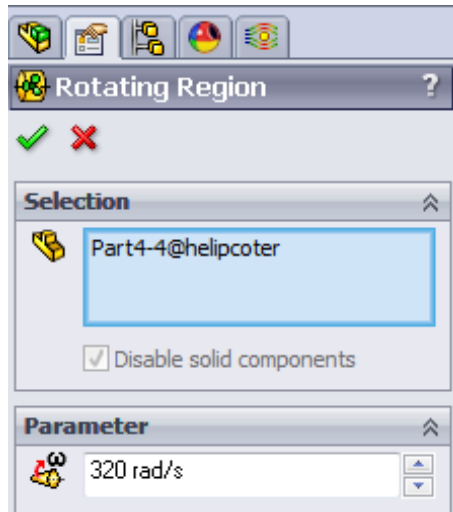
Figure 5-8: Flow-simulation dialogue box for changing rotor speeds

5.3.1 Results of CFD simulation in a no wind situation

The no wind CFD simulations were carried out to determine the response of the 3-D CAD model when there is no disturbance and to check if the results obtained are close to those recorded from the analytical dynamic Matlab/Simulink model built in chapter 4 of this thesis, since the two models were developed using the same parameter values. In this situation, flows around the rotor blades of the helicopter were assumed to be steady and the rotors working under the same conditions, because the winds speeds in the three directions (x, y and z) were kept at 0m/s as shown in figure 5-9.
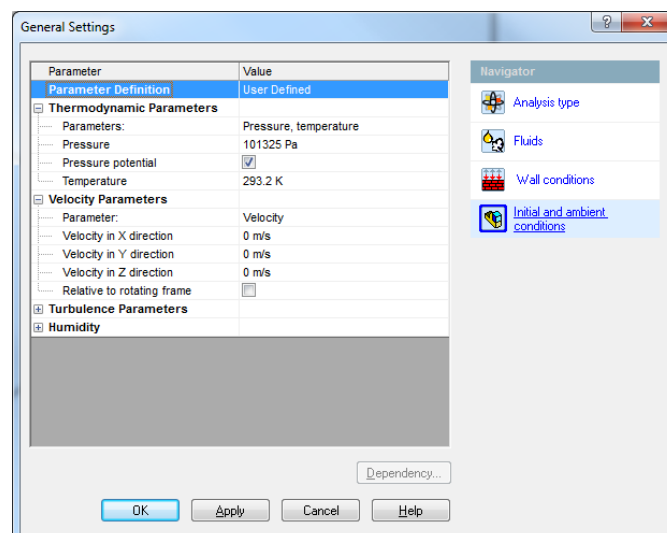
Figure 5-9: Flow-simulation dialogue box showing all wind speeds at 0m/s

A comparison of the results obtained from the analytical dynamic Matlab/Simulink model, the 3-D Solidworks model and real flight experiment data is done in chapter 6 of this thesis, where a compensation architecture is also developed.

5.3.1.1 Throttle

As explained in chapter 1, spinning the four rotors at the same speed would either increase or decrease the altitude of the helicopter, thereby generating a collective vertical force from the four propellers. The upward velocity of the quad-rotor helicopter and the collective lift force at different rotor speeds from the flow simulation are represented in figures 5-10 and 5-11 below.
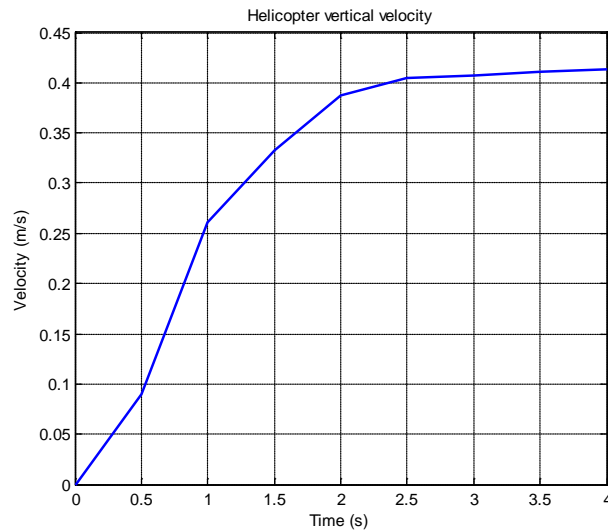
Figure 5-10: Upward velocity of quad-rotor helicopter

Again the figure shows the upward velocity rising and then stops at about 0.41m/s because the motor speeds remain constant.

It can be seen from figure 5-11 that as noted in the Matlab/Simulink model, the collective vertical thrust increases as the motor speeds increase.
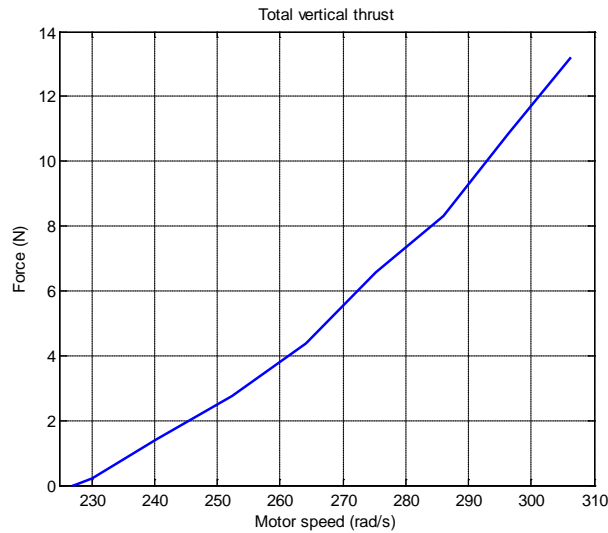
Figure 5-11: Total thrust generated at different motor speeds

5.3.1.2 Roll

As stated earlier, differential thrust between the left and right rotors provides the roll torque. The total vertical thrust is expected to be maintained as in hovering. The forces produced at different tilt angles are shown in figure 5-12 below.
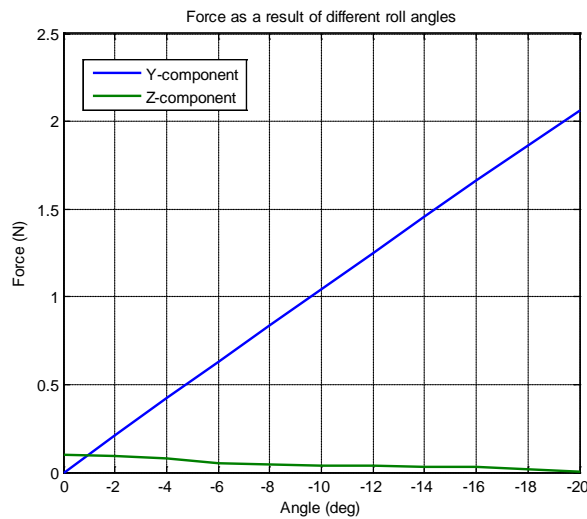
Figure 5-12: Forces acting on the helicopter as a result of different roll angles

While the front and rear motors were kept spinning at a speed of 227.9938 rad/s, the left motor was spinning at a speed of 227.9889 rad/s and the right motor was spinning at a speed of 227.9990 rad/s. This is the same set of motor speeds that created a roll angle of -3.33 degrees in the Matlab/Simulink model (figure 4-14 of chapter 4).

In the figure 5-13, the CFD simulation shows a very similar behaviour with the Matlab/Simulink model. The components of forces acting on the quad-rotor helicopter were not exactly the same for the two models; they were a little bit lower but not too far apart. As expected, the y-component (red line) of the force increases, while the z-component (green line) of the force decreased slightly, the CFD simulation seemed better at maintaining the total vertical thrust of the helicopter.
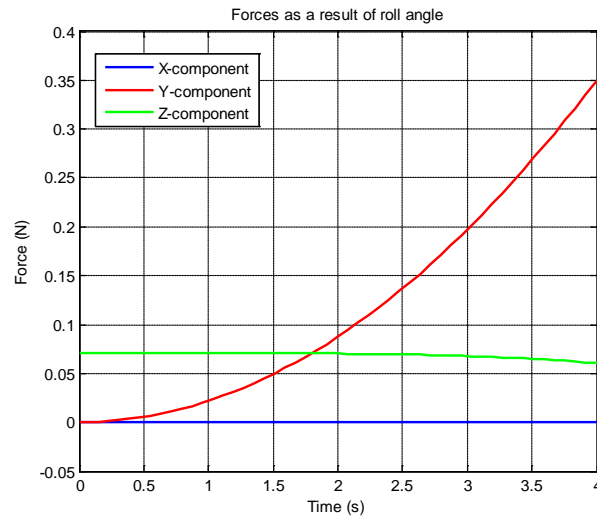
Figure 5-13: Components of forces as a result of the roll moment

Despite the minor discrepancies in the magnitude of forces acting on the vehicle in the two models, the results obtained show that the two models are very similar, having being built using the same parameters.

5.3.1.3 Pitch

The differential thrust between the front and rear rotors provides the pitch torque. The total vertical thrust is expected to be maintained as in hovering. The forces produced at different tilt angles are shown in figure 5-14 below.
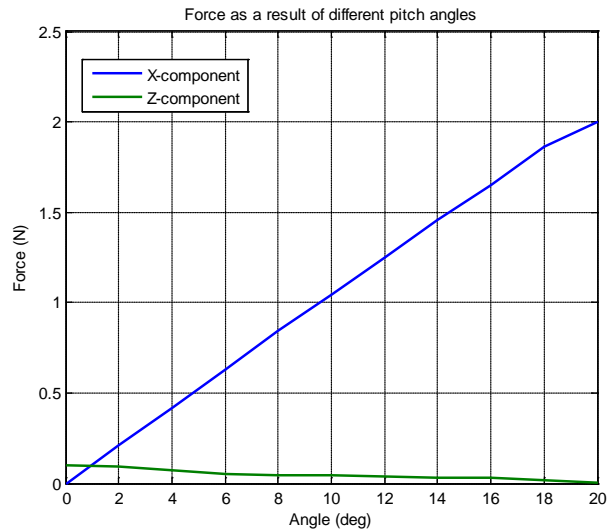
Figure 5-14: Forces acting on the helicopter as a result of different pitch angles

In the figure 5-15 below, the graph shows the components of forces acting on the quad-rotor helicopter as a result of the same motor speeds that produced a pitch angle of 1.67 degrees in the Matlab/Simulink model in figure 4-20 of chapter 4.

In this case, the left and right motors were spun at a speed of 227.9938 rad/s each, the front motor was spun at a speed of 227.9912 rad/s and the rear motor at a speed of 227.9964 rad/s.
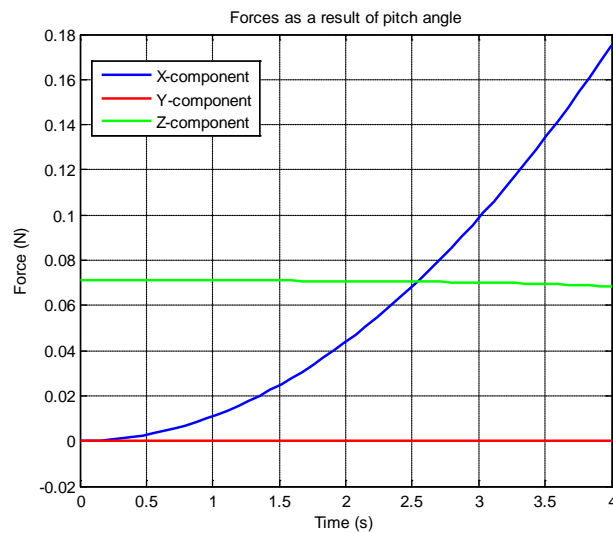
Figure 5-15: Components of forces as a result of the pitching moment

5.3.1.4 Yaw

Differential torque between the pairs of counter-rotating rotors provides the yaw torque. The torque imbalance with respect to the z-axis makes the quad-rotor turn about the same axis. In

the figure 5-16 below, while the left-right duo was spun at 227.8627 rad/s, the front-rear pair was spun at 228.1248 rad/s, just like the set of motor speeds that created a torque imbalance that resulted in a yaw angle of 6.72 degrees in the Matlab/Simulink model in chapter 4 (figure 4-24).
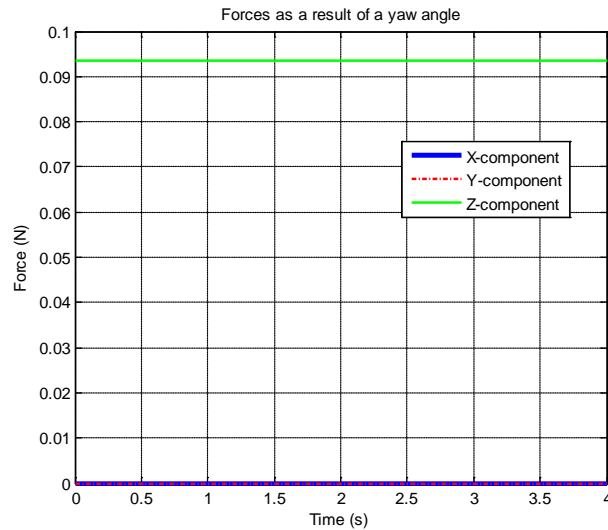
Figure 5-16: Components of forces as a result of the yawing moment

It is observed here that z-component of force is greater than the one produced in figure 4-24 of chapter 4, against the expectation that it should be a little bit lower as observed in the roll and pitch tests.
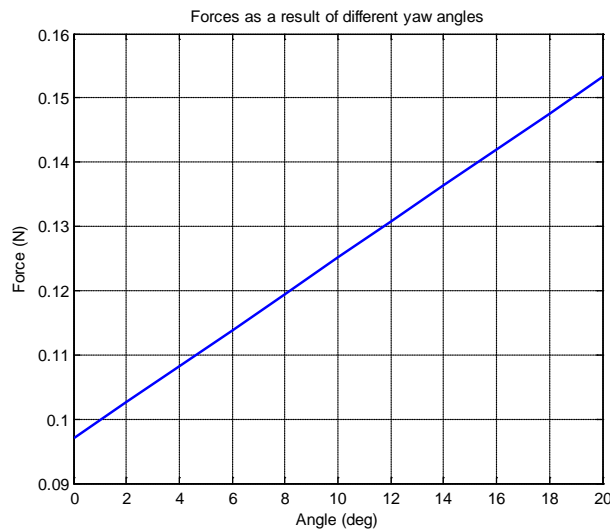
Figure 5-17: Forces acting on the helicopter as a result of different yaw angles

An observation of the no wind CFD simulation results shows very little discrepancies with those of the analytical dynamic Matlab/Simulink model in chapter 4, suggesting a general agreement of the two models.

There are discrepancies because the computational fluid dynamics simulation considers some of factors/conditions (such as drag and some modelling assumptions) ignored in the Matlab/Simulink model, thereby providing a situation closer to actual flight experiments. Despite the general agreement, the need for a verification and validation of the two models with data obtained from real flight experiments as carried out in chapter 6 cannot be extravagant.

5.3.2 Results of CFD simulation in windy situations

Wind speed and direction play important roles in flying any aircraft. The wind that flows opposite to the flight path of the quad-rotor helicopter (headwind) slams the front of the quad-rotor and slows it down, while a flow from the back (tailwind) forces the quad-rotor in the direction of flight, increasing its speed. There could also be crosswinds that blow from the sides, across the flight path and they are equally dangerous to the quad-rotor. These conditions can lead to loss of control, deviation from the planned path or even a crash; depending on the magnitude of the winds.

In this simulation, the quad-rotor helicopter experiences unsteady flows around its rotor blades, with winds speeds of different magnitudes ranging from 0-15m/s in the three directions (x, y and z) at different times as shown in the dialogue box in figure 5-18. The flow data obtained here were very useful in the design and training of the controller in chapter 7, since the quad-rotor is expected to fly through a series of complex weather conditions.
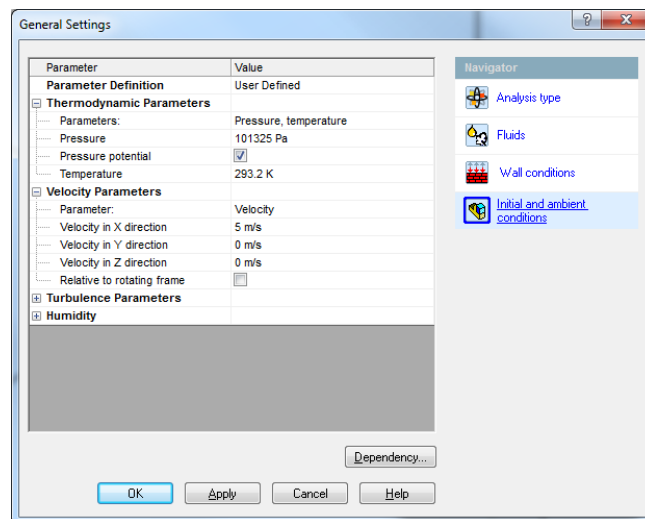
Figure 5-18: Dialogue box showing how the different wind speeds were set

In this situation, the rotors of the helicopter are working under different conditions, because of the varying wind speeds and the non-uniformity of the flow of air around them. This is expected to create some extra aerodynamic moments over the airframe.

For the control system to ensure that it keeps to the planned path in the presence of a disturbance, a quad-rotor tilt angle must be created to compensate the drag force with a horizontal component of the collective thrust force generated by the rotors, with stronger winds requiring larger tilt angles.

With SolidWorks Flow Simulation, it is very easy to calculate fluid forces and understand the impact of air flows on the performance and control of the quad-rotor helicopter as shown in figures 5-19 below and 5-20.
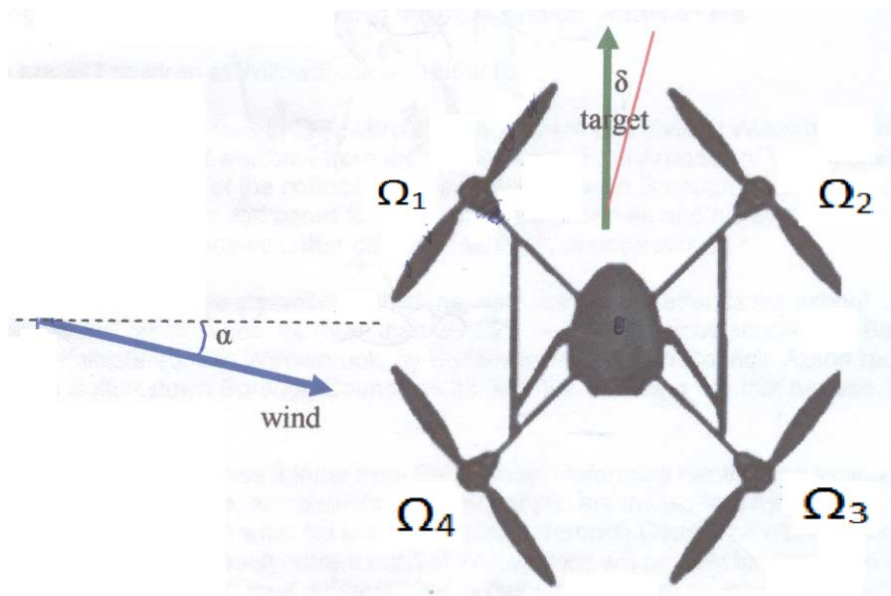
Figure 5-19: Calculating the effect of wind disturbance on the quad-rotor helicopter

Based on the results obtained from the flow-solver, the effects of the vertical and horizontal wind flows on the quad-rotor helicopter are summarised and discussed next.
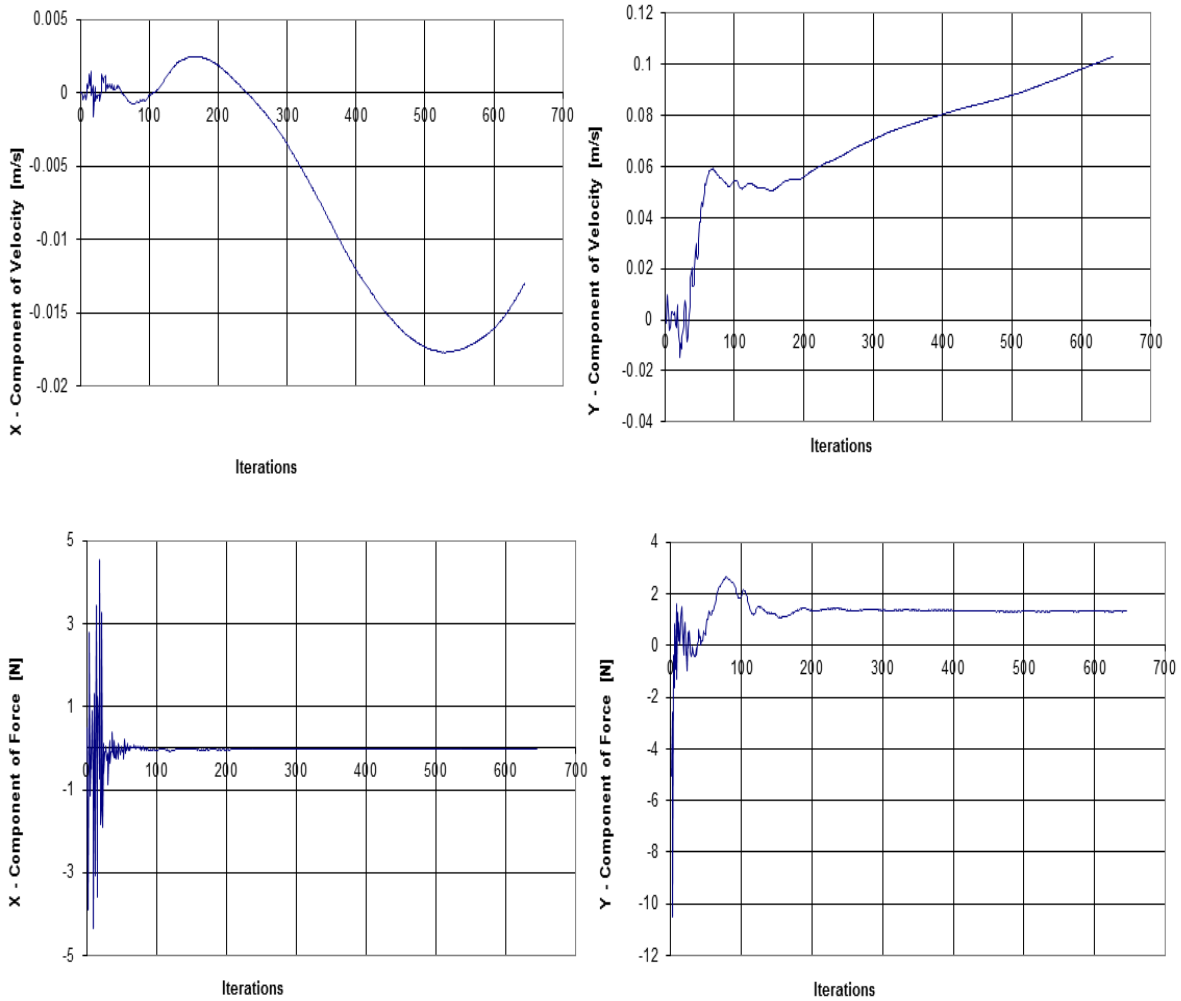
Figure 5-20: Impact of air flows on the performance of the quad-rotor helicopter

5.3.2.1 Vertical Wind Flow

As the helicopter flies, it is normal to have airflows above and below it; the wind flow in the z-direction could slam the helicopter from above or below and these would have different effects on the vehicle. In these simulations, the quad-rotor helicopter is allowed to experience both situations at different times and the results discussed.

At hover state, winds blowing at different speeds from the top of the helicopter will pass through the rotors from above and tend to decrease the thrust generated by the individual rotors, thereby causing a loss in the collective vertical thrust. This will force the quad-rotor to descend, unless the speed of the wind is reduced. With approximately the same wind speed (though with non-uniform flow) and higher angular velocities of the four rotors, the quad-rotor is able to oppose the force exerted on it by the wind and maintain its altitude, but as the

force exerted by the wind overcomes the collective thrust generated by the rotors, the helicopter is always forced to descend.

The curves in figure 5-21 show a continuous reduction in the collective vertical thrust as the wind speed increases without a corresponding change in the motor speeds.

Since the air flow and distribution is not uniform, there is a possibility that the quad-rotor will either pitch or roll and move horizontally, even when a vertical movement is expected.
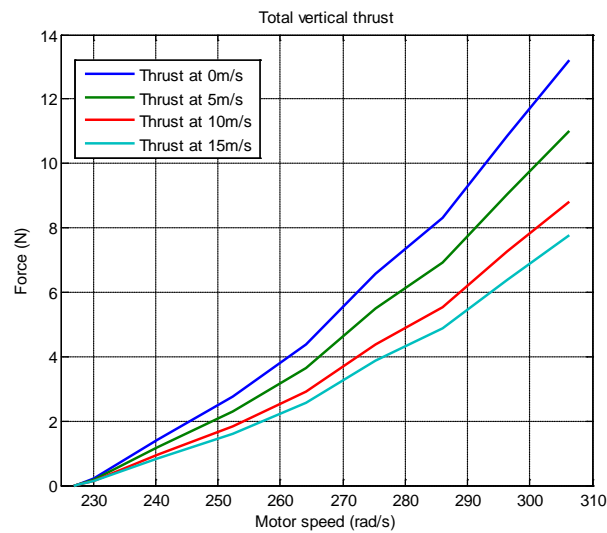
Figure 5-21: Total vertical thrust in downward flow of wind

The exact opposite would happen if the wind blew from below the helicopter as shown in figure 5-22 below. The air will pass through the rotor blades from below and tend to increase the collective vertical thrust generated by the rotors, leading to the quad-rotor ascending to a certain height, only to stabilize when the wind or rotor speeds are reduced.
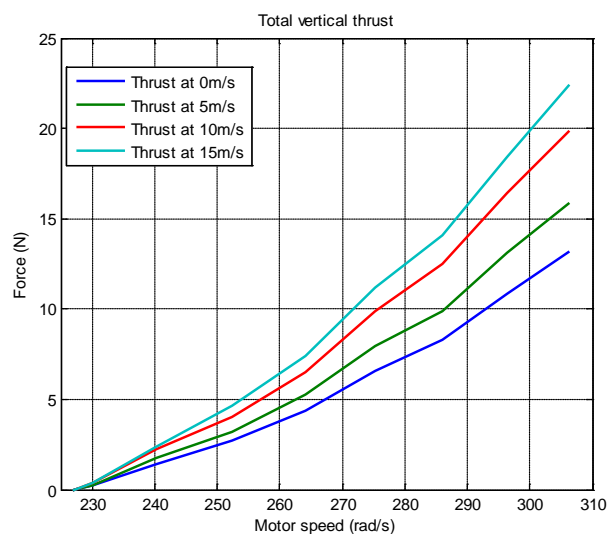
Figure 5-22: Total vertical thrust in upward flow of wind

5.3.2.2 Horizontal Wind Flow

The horizontal wind velocity normally has a crosswind component and a headwind/tailwind component, which affect its speed relative to the ground. When the quad-rotor helicopter experiences such a flow of wind around it, there certainly will be unwanted moments in addition to other possible effects that act due to the fact that the flight conditions are much more unstable. The quad-rotor helicopter is likely to depart from the state of equilibrium in flight, leading to a possible loss of control.

In these simulations, the quad-rotor helicopter was exposed to headwinds, tailwinds and crosswinds of different magnitudes as depicted in figure 5-23.
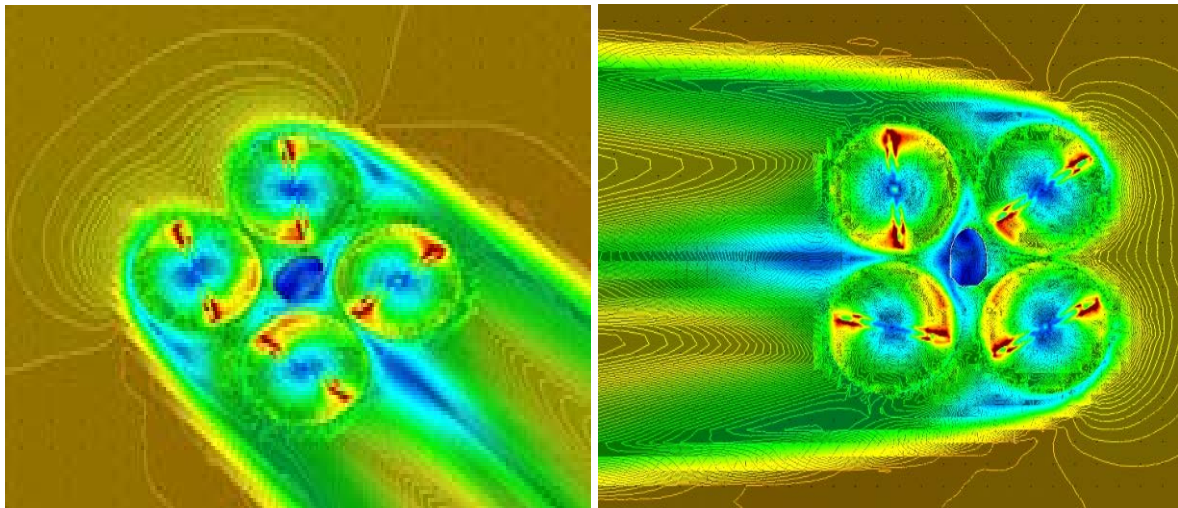
Figure 5-23: Quad-rotor experiencing cross winds in simulation

a) Headwind

In a headwind situation, the effect of the wind slamming the front of the quad-rotor helicopter is seen from the curves in figures 5-24. The combined effect of the headwind and the helicopter's speed and forces always produces a resultant speed or force that is lower than the one the helicopter had before it encountered the wind. There could also be a change in direction of flight as suggested by the y-component (red line), depending on the direction and magnitude of the wind.
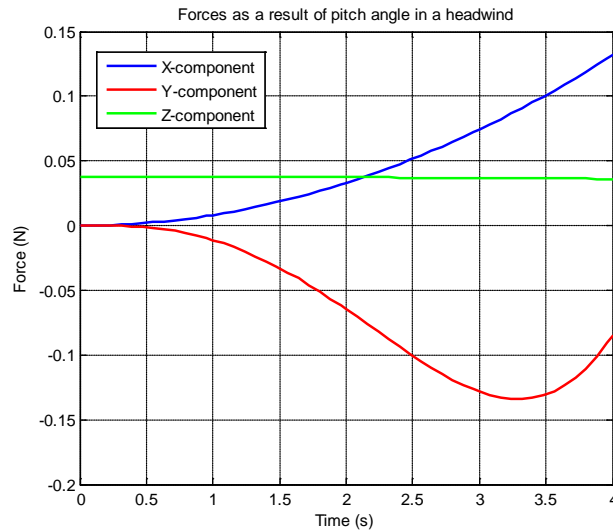
Figure 5-24: Forces acting on the helicopter in a headwind

Stronger winds have a greater reduction effect on the quad-rotor's speed and forces as depicted in figure 5-25. Also notice that as the winds get stronger (red and light blue lines at 10m/s and 15m/s respectively), the quad-rotor seems to pitch violently as it struggles to stay in flight.
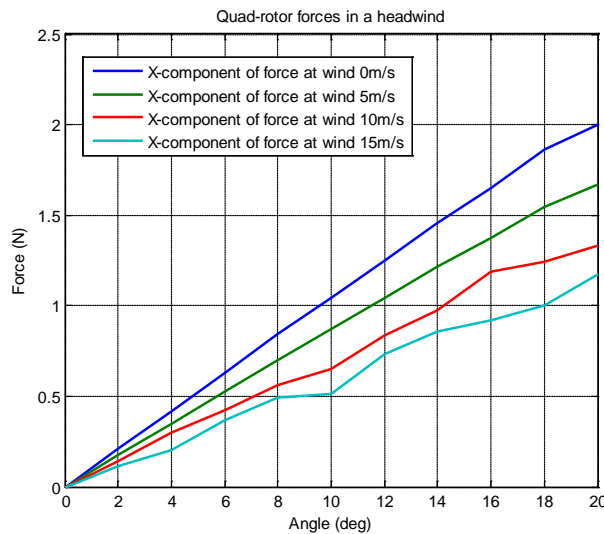
Figure 5-25: Forces acting on the helicopter in a headwind at different tilt angles

b) Tailwind

Naturally, a tailwind is expected to increase the quad-rotor speed and forces in the direction of flight as shown in figure 5-26 below. The effect of a tailwind on the forces acting on the quad-rotor helicopter may not be the exact opposite of the curves in figure 5-25 above as the effects of a headwind cannot be overcome by a tailwind of the same magnitude. Figure 5-26 shows increasing components of the x and y forces (blue and red lines) from 1-3 seconds of the simulation, while the z-component experiences a little decrease. However, after 3 seconds

the y-component (red line) begins to decrease because of the fact that a tailwind would have a greater effect on the pitch angle/moments of the quad-rotor helicopter and also the non-uniform flow around it.
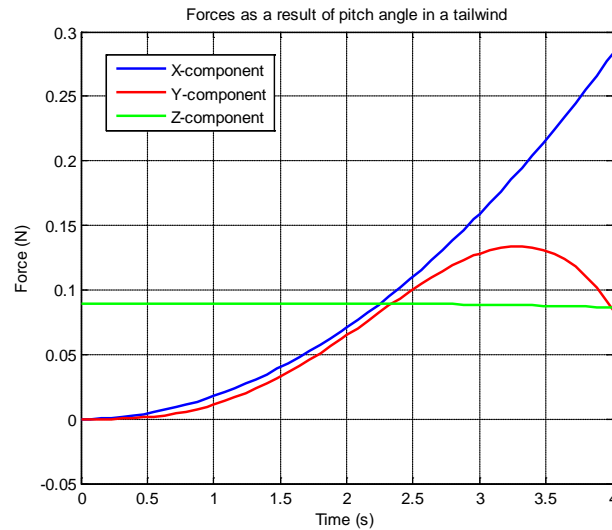
Figure 5-26: Quad-rotor forces in a tailwind

c) Crosswind

A crosswind would normally create an in-plane force that acts on the vehicle and tends to create a moment that makes the quad-rotor helicopter tilt. The instant the quad-rotor starts to tilt, it accelerates in its direction of tilt. However, too much of a tilt would make the quad-rotor to start loosing equilibrium, thereby leading to a possible oscillation and loss of control of the whole vehicle. Only a timely and accurate re-arrangement of the motor speeds can maintain that equilibrium and keep it in the planned path.

As shown in figure 5-27 below, the wind blows in the direction of tilt of the helicopter. The y-component (red line) of force increases with the crosswind, but since the flow is non-uniform, there is a fluctuation in the x-component (blue line) of force, while the z-component (green line) decreases. This clearly suggests instability in the vehicle because of the disturbance.
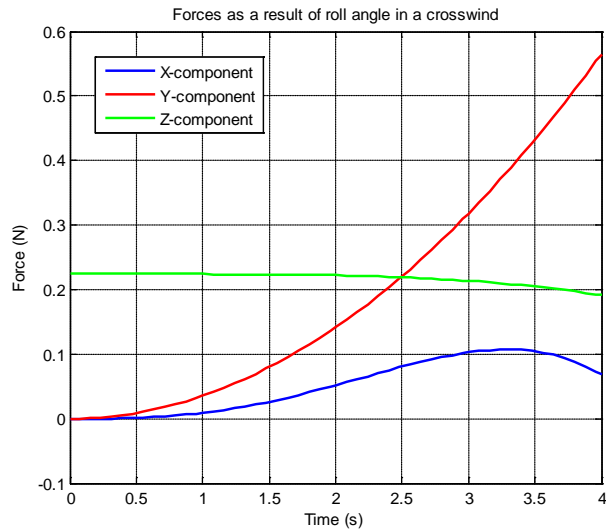
Figure 5-27: Quad-rotor forces in a crosswind blowing in the direction of tilt of the helicopter

When the wind blows against the direction of tilt of the helicopter as shown in figure 5-28 below, the forces generally decrease. Notably, the x-component (blue line) of force reduces to the negative, implying that the helicopter moved in the negative x-direction. Such simulations would have been much easier if the winds hit the quad-rotor helicopter directly in front, at the back or from the sides. However, the curves clearly indicate the result of an uneven distribution of the force of the wind on the quad-rotor, making the problem of control even more complex.
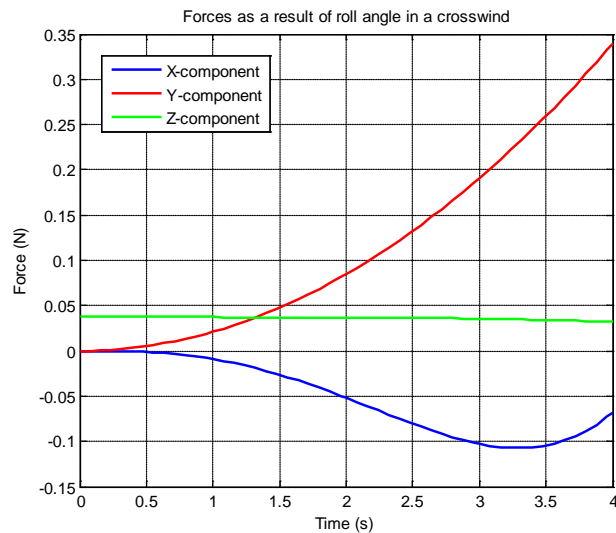
Figure 5-28: Quad-rotor forces in a crosswind blowing against the direction of tilt of the helicopter

Figure 5-29 shows the major forces acting on the quad-rotor in a crosswind. An increase in the wind speed records an increase in the force if the wind is blowing in the direction of movement of the helicopter. Note that from 10m/s (red line), the force curve begins to

oscillate, suggesting that the helicopter could be loosing equilibrium and possibly veering off the planned path. A further increase in the wind speed could even see the quad-rotor helicopter flip upside down and crash, if there is no adjustment made to the rotor speeds in good time. The direction of movement or behaviour of the quad-rotor helicopter can be difficult to predict if the wind is allowed to blow it off course.
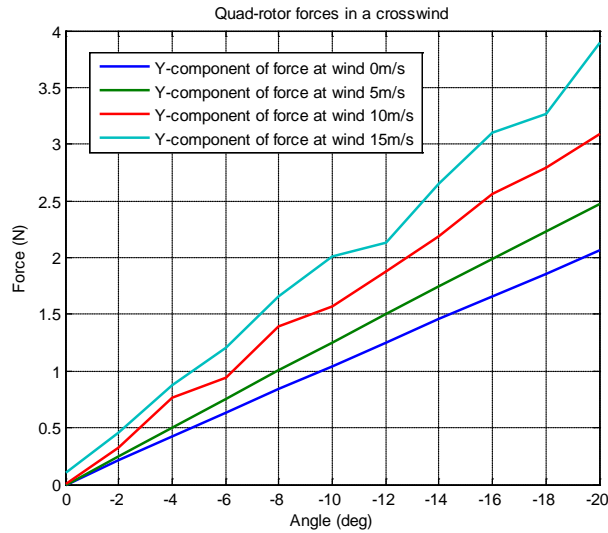
Figure 5-29: Forces acting on the helicopter in a crosswind at different angles of tilt

5.4 Chapter Summary

CFD studies provide meaningful insight into the impact of fluid flow, enabling Engineers to address problems early, reduce the need for costly prototypes, and eliminate rework.

A 3-D Solidworks model was also developed with the same parameter values as that of the model developed in Matlab/Simulink. CFD was used to simulate and analyse the effects of the external environment/disturbances on the flow patterns of the quad-rotor helicopter within a given computational domain.

The helicopter stability and control analysis requires a very large number of CFD simulations to determine appropriate forcing parameters within the expected range of motion. Typically, the time accurate CFD simulations start from a steady state solution and are iterated in pseudo time within each physical time step using a dual-time stepping scheme.

This chapter investigated the use of a 3-D Solidworks model that significantly reduced the CFD simulation time required to create a full aerodynamics database, making it possible to accurately model the quad-rotor static and dynamic characteristics from a limited number of time-accurate CFD simulations, preparatory to the development of a robust adaptive controller for the helicopter.

VALIDATION OF MODELS WITH FLIGHT EXPERIMENT DATA

This chapter affords details of the verification, validation and equipment used to acquire real flight test data in order to determine the credibility of the two models developed in chapters 4 and 5 of this thesis. Results of simulations performed with the two models are compared with results from real flight experiments performed at University of Essex Robot Arena. An artificial neural network function approximation tool, is trained with real flight experiment data and used to correct the errors found in the two models.

6.0 Verification and Validation

There has been an increasing demand for dependable predictions of complex processes encompassing, where possible, accurate predictions of full behaviours of non-linear dynamic systems. This requirement is driven by the need for scientifically informed assessments in support of very important judgements that affect humanity, including fault-tolerant and safety critical systems, global warming, national security, health and transport.

Three possible methods are normally used for the prediction and analysis of the behaviours of such systems: conducting experiments (real flight situations in the case of the quad-rotor helicopter), theoretical analysis and computational or simulation methods. Results of experiments are most reliable, but could be expensive and difficult to obtain. Theoretical analysis has its confines, because equations that describe the system could be complex and probably be solved for very simple known cases. The most viable method is to carry out computer-based simulations to produce quantitative, predictive information about such complex systems, just as has been done in chapters 4 and 5 of this thesis.

Generally, simulation models are inexact imitations of real-world systems and they never accurately imitate the real-world system. Due to this fact, inaccuracies can pose very high risks. It is therefore vital that simulation results have a high level of confidence. Verification and validation of the simulation models using data obtained from actual experiments must be done with the ultimate goal of producing an accurate and credible model as depicted in the flowchart in figure 6-1 below.
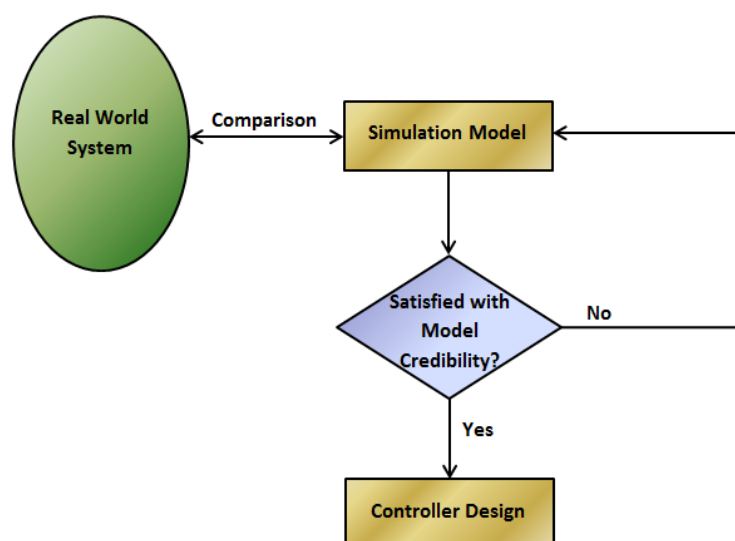
Figure 6-1: Verification and validation process flow

In this chapter, results of simulations performed with the analytical Matlab/Simulink model of the quad-rotor helicopter built in chapter 4 and those obtained using CFD on a 3-D Solidworks model of the same helicopter in chapter 5 are compared with results of real flight experiments performed at University of Essex Robot Arena. This ensures that any modelling and simulation errors discovered are fixed. This also helps in deciding whether the simulation models and results are realistic enough to be used for the quad-rotor fuzzy-neural controller development.

6.1 Flight Experiments with the Quad-rotor helicopter

Quad-rotor flight experiments were conducted at the University of Essex to verify and validate the two models developed in this thesis. The Essex Robotic Arena is an advanced mobile robot research facility featuring a 100 square metre powered floor and real-time 3-D VICON motion tracking system. It also boasts of a data logging system, which allows the automatic logging of robot behaviour for subsequent analysis.

6.1.1 Experimental Set-up in the Robot Arena

The hardware set-up used for flight experiments as described in [102] is depicted in figure 6-2 below and explained in subsections that follow.
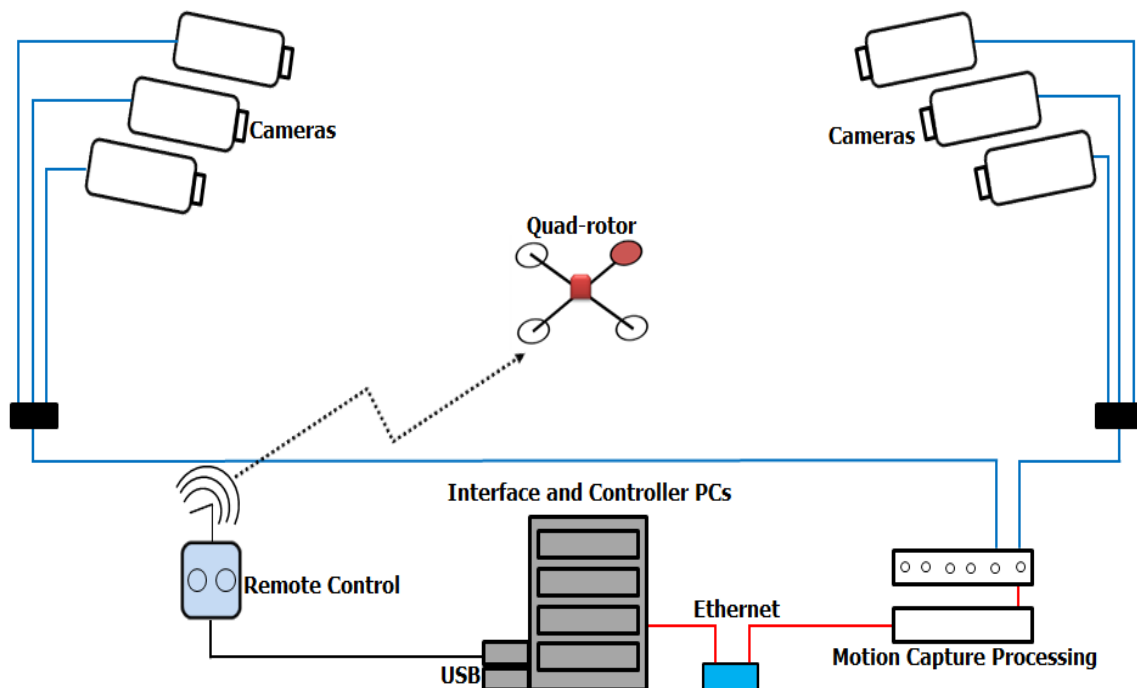
Figure 6-2: Hardware set-up for flight experiments

a) Interface and Controller Computers

This is needed in the setup to run the algorithms for the behaviours and the controls. The Workstation software takes information captured by the VICON hardware and combines it with calibration data and a set of other parameters to create 3-D positions for each marker in the capture volume. The positions are calculated frame-by-frame and combined to create a complete set of trajectories of the markers positions throughout the time span of the experiment. This would then open a USB port on the computer and send the required control values to the USB to Serial Converter based on the information obtained from the VICON video system.

b) USB to Serial Converter

This receives the control values from the computer and converts them to serial communications protocol format. It then transmits the control values over a wired link to the remote control's port.

c) Hi-Tec Remote Control.

The remote control has a trainer port that allows a connected trainee remote control fly the quad-rotor helicopter through it. By flicking the training switch to training mode, the trainee can fly the helicopter through the master remote control. If however the trainee loses control, the trainer can release the training switch to disconnect the trainee remote control and then take over flying the helicopter. The commands received from the USB to Serial Converter are then sent wirelessly to the helicopter.

d) The Quad-rotor Helicopter.

The quad-rotor helicopter is equipped with an IMU (Inertial Measurement Unit) sensor to measure its angular velocity, and affixed with passive optical markers that are tracked by the VICON system. The VICON motion tracking system feeds position in space of the quad-rotor helicopter into the lab's computer-driven navigation system.

There is a wireless transmission of the control commands from a hi-Tec remote control to the helicopter, which responds to them accordingly. The commands received from the hi-Tec Remote Control are throttle, yaw, roll and pitch commands, which would normally vary the speeds of the motors to achieve the desired control.

e) VICON motion tracking system.

It is normal to calculate the position of mobile robots using the GPS technology, however this is not possible in GPS denied environments (like in clustered area or inside a building). This gives rise to the use of systems such as motion tracking, artificial vision or the use of locator signals.

Motion tracking is the process in which movements of a particular object (or group of objects) are recorded and translated into a digital model. There are so many applications of motion tracking in the military, the entertainment industry, the medical industry, sports, research industry and many more.

The VICON motion tracking system is a state-of-the-art infrared marker-tracking system that offers millimetre resolution of 3D spatial displacements. Such optical tracking systems use special visual markers on the performer and a number of high-speed cameras (running at 30-1000 frames per second) to determine the 3D location of the markers. The markers could be passive – usually made of objects such as retro-reflective spheres or active – usually LED lights, with only one marker illuminated at a time to help the system keep track of the movements. This obtains the orientation and position information of the quad-rotor helicopter and sends it through the Ethernet to the computer.

6.1.2 Comparison of results

As stated in the introduction to this chapter, simulations invariably involve theory, experimental data and numerical modelling, all with their attendant errors. It is thus expected to ask if the simulations are believable and if the results are accurate and reliable. In this section, a comparison is made between the simulated results and data obtained from real flight experiments.

Thanks to the data logging system in the Robot Arena, which makes the automatic logging of robot behaviour very easy for subsequent analysis - flight experiment data can be pulled up and used at any time. The measured control input was sent through the two models, and the outputs were compared with those measured from the quad-rotor helicopter.

The tilt angles of the helicopter and that of the simulations from the two models, together with their corresponding accelerations and forces produced in different directions were assessed.

Figure 6-3 shows flight data plot of the quad-rotor helicopter as captured by the VICON motion systems.
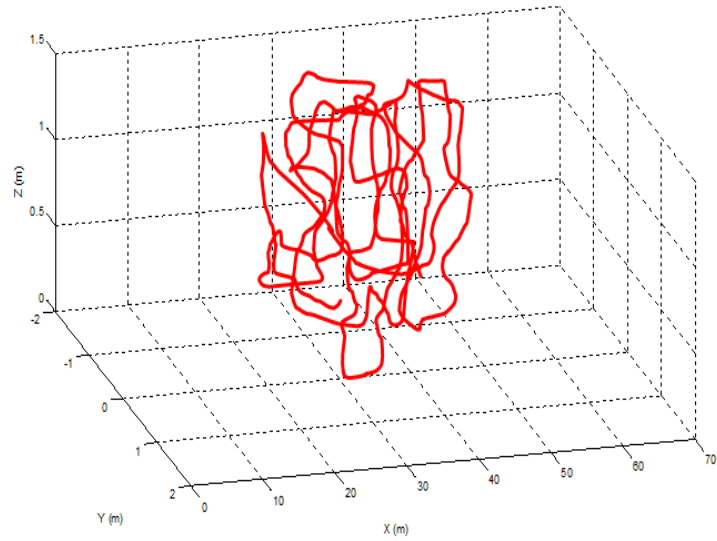
Figure 6-3: Quad-rotor flight data plot from the VICON data logging system

Several flight experiments were performed, out of which the best input/output relations were selected. This section shows the comparison of simulation and experiment results. Data sets obtained from flight experiments (a sample of which is shown appendix D) were used in the simulation models and the responses were analysed.

a) Throttle test

Spinning the four rotors at the same speed would generate a collective vertical force from the four propellers, thereby increasing or decreasing the altitude of the quad-rotor helicopter. The collective vertical thrust at different rotor speeds from the actual flight experiment is compared with those obtained from the two models.
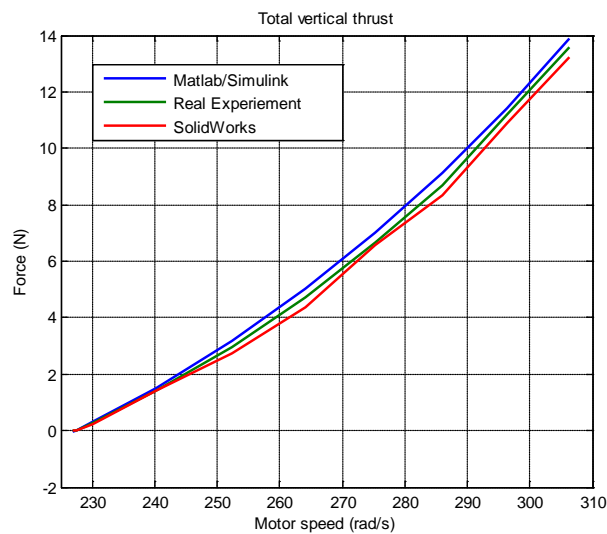
Figure 6-4: Comparison of results in throttle test

It is quite clear from the graph that the curves are very similar, despite the difference in the magnitude of the forces as the rotor speeds increase. The Matlab/Simulink model produced the highest values of the three curves, while that of the Solidworks was the lowest with the real flight experiments finding a narrow space in between the two curves.

According to the curves in figure 6-4, the largest error of about 0.4N in the Matlab/Simulink model is recorded at speed 286rad/s, while the smallest of 0.017N is observed at speed 227.5rad/s. In the case of the Solidworks model, the largest error of about 0.36N is recorded at speed 306.3rad/s and the lowest of 0.032N is found at 240.3rad/s.

The effect of a force of 0.4N could be quite significant when it comes to the perfomance and control of a vehicle of this nature, considering its very light weight and very high sensitivity to rotor speed changes.

b) Roll and Pitch tests

Differential thrust between opposite rotors provides roll and pitch torques. The torques are created with respect to the x or y axes, making the quad-rotor to tilt about that axis. However, the total vertical thrust should be maintained as in hovering. The angles and forces produced at different tilt angles are compared in figures 6-5 and 6-6 below.
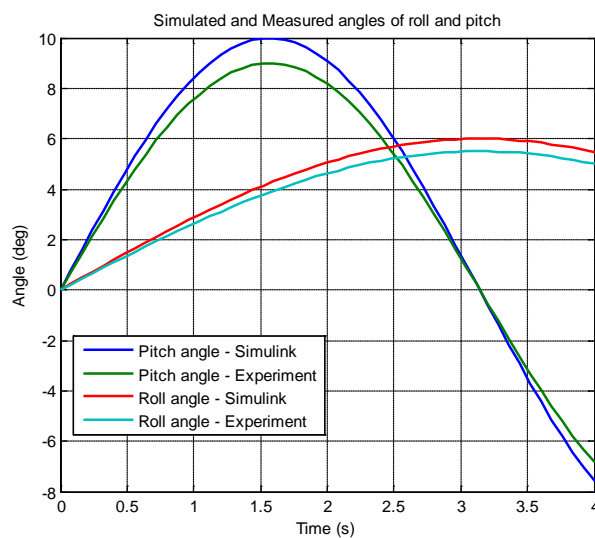
Figure 6-5: Comparison of simulated and measured roll and pitch angles

At most times, it is assumed that because of the symmetric nature of the quad-rotor, the behaviour of the vehicle with regards to roll and pitch angles would be the same. As observed from the curves in figures 6-5, the results are not exactly the same. It is clear that the

symmetry of the quad-rotor helicopter only holds in ideal situations, which are very rare to come by.
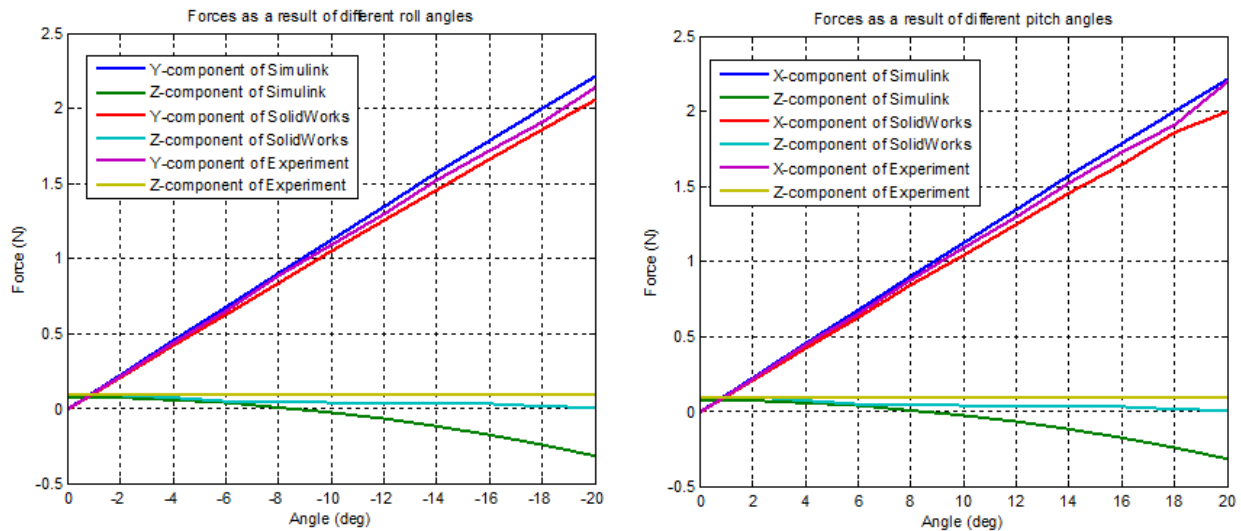
Figure 6-6: Comparison of simulated and measured forces in roll and pitch tests

The components of forces are compared here and seen to be very similar again, but with differences in their magnitudes. It was also observed from figure 6-6 that there was a loss of about 0.3N in the collective vertical thrust, which led to a loss in altitude in the Matlab/Simulink model, signifying that the total vertical thrust was not maintained as expected, because of the absence of a controller that would stabilise it when the thrust vector is tilted as a result of the pitch angle.

c) Yaw test

Differential thrust between the two pairs of counter-rotating rotors provides the yaw torque. The torque imbalance with respect to the z axis makes the quad-rotor turn about the same axis. Normally, it is expected that the total vertical thrust is still maintained as in hovering. Again very similar results are obtained for the yaw command, showing very comparable angles and a near constant vertical thrust in figures 6-7 and 6-8 respectively.
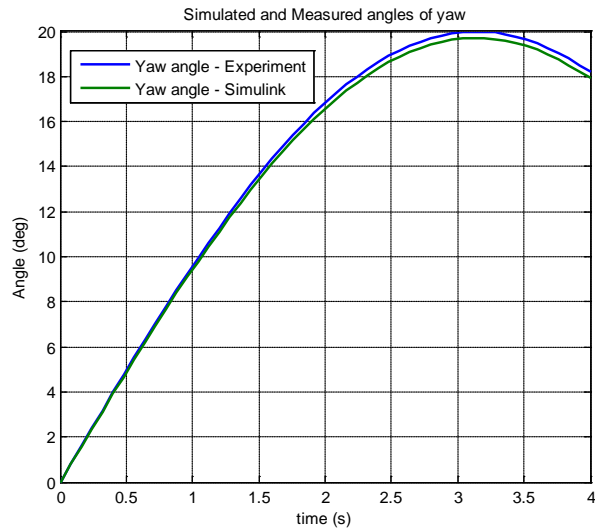
Figure 6-7: Comparison of simulated and measured yaw angles

While the differences between the simulated and measured angles are not far apart, the performance and control of the quad-rotor helicopter could still be hampered when it comes to missions that require very high precision manouveres, especially when the vehicle encounters a disturbance or an obstacle or even when a swarm of quad-rotors are working together in close proximity.
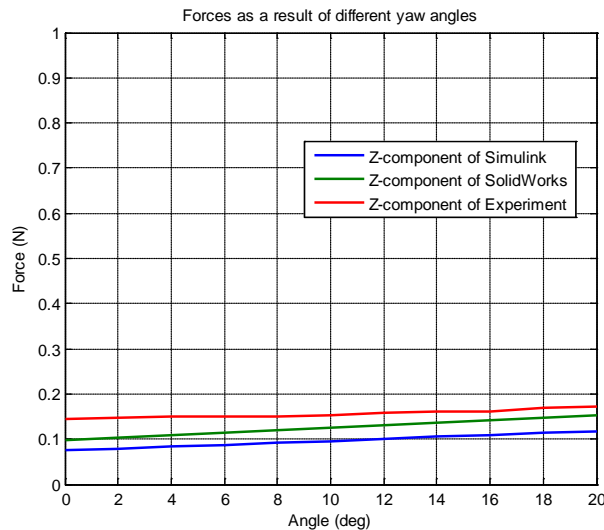
Figure 6-8: Comparison of simulated and measured forces as a result of different yaw angles

While the total vertical thrusts in the two models increased gradually as the yaw angle increased, that of the real flight experiment looked more stable. This goes on to emphsize the need for a good controller for the models.

From the results obtained in the two models, the behaviour of the quad-rotor helicopter in simulation resembles its behaviour in actual flight; thereby corroborating the fact that the two models developed in chapters 3, 4 and 5 are good (though not perfect) representations of the dynamics of the actual helicopter. However, the neural network error compensation promises more reliable and accurate results.

6.2 Error Compensation using Artificial Neural Networks

Artificial neural networks are used in many important engineering and scientific applications, some of which are signal enhancement, noise cancellation, pattern classification, system identification, prediction, error compensation and control.

Neural networks provide a reliable tool for the fast solution of repetitive nonlinear curve fitting problems. In fitting a curve, a neural network is trained using a set of inputs in order to produce an associated set of target outputs. Once the neural network has fit the data, it forms a generalization of the input-output relationship and can be used to generate outputs for inputs it was not trained on [103].

The neural network design and training was done in the Matlab/Simulink environment and data obtained from actual flight experiments were used for off-line training of the network. Neural network training in the Matlab/Simulink environment is normally done using one of the built-in functions incorporated in its Neural Network Toolbox.

The problem at hand is that of function approximation and the whole idea is to diminish the error between the simulation results and the actual flight experiments to the barest minimum.

6.2.1 Compensation Architecture

The compensation system used here adopts a post correction technique. It takes its inputs from the two models (Matlab/Simulink and Solidworks) developed in chapters 4 and 5 respectively as shown in figure 6-9 below. The system, having been trained with data obtained from actual flight experiments, computes the compensation value of the two simulation models. The output of the system is the data used to train the quad-rotor fuzzy-neural controller.
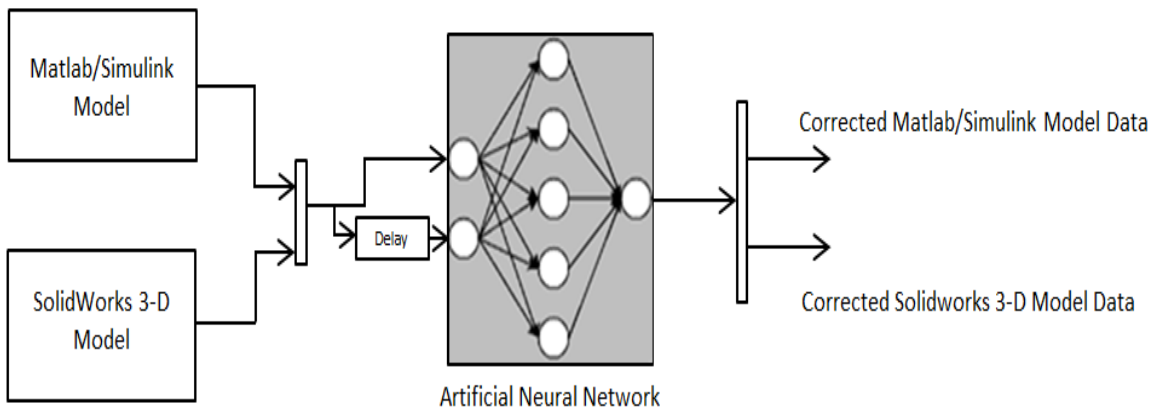
Figure 6-9: Artificial neural network correction system

The neural network architecture is made up of layers of nodes (input, hidden and output) which are the processing units. The input nodes receive directly the output data from the two models, the hidden nodes process the data while the output node gives out the corrected value. The output of the nodes is given by:

$$s_j = F(\sum_i w_{ij}o_i + b) \tag{6-1}$$

Where F is the activation function, o_i is the output from the ith node of the *k-1* layer, w_{ij} is the weight and b the bias.

A simple neural network with two input neurons, 30 neurons in the hidden layer with a log-sigmoid activation function, and a single output neuron was used for the compensation as shown in figure 6-9. Computation of the compensation values was done by calculating the feed-forward action of the network.

Table 6-1 shows a small sample of the errors before the neural network compensation was done.

Table 6-1: Compensation of Total Vertical Thrust

Motor speed (rad/s)	Total Vertical Thrust Real Experiment (N)	Total Vertical Thrust Matlab/Simulink (N)	Total Vertical Thrust CFD (N)	Error Matlab/Simulink	Error CFD
226.9	0	-0.0395	0	0.0395	0
227.5	0.0001	0.0175	0.0126	-0.0174	-0.0125
230.1	0.2900	0.3063	0.2205	-0.0163	0.0695
240.3	1.4350	1.5250	1.4030	-0.0900	0.0320
252.4	2.9670	3.1910	2.7440	-0.2240	0.2230
264.1	4.7100	5.0160	4.3640	-0.3060	0.3460
275.2	6.6750	6.9990	6.5790	-0.3240	0.0960
286.0	8.6780	9.1410	8.3190	-0.4630	0.3590
296.3	11.2030	11.4400	10.8730	-0.2370	0.3300
306.3	13.5700	13.9000	13.2145	-0.3300	0.3555

The simulation results from the two models were passed through the compensation system and some of the results obtained were plotted in comparison with the actual flight experiments as shown in figure 6-10. These were used to determine the effectiveness of the compensation system.
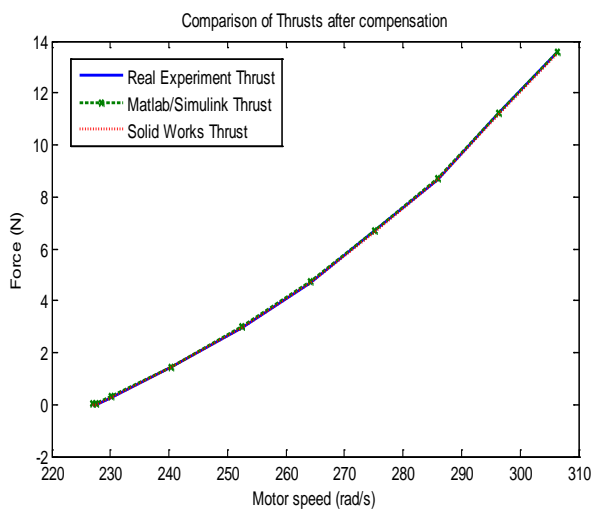
(a) **Vertical Thrust**
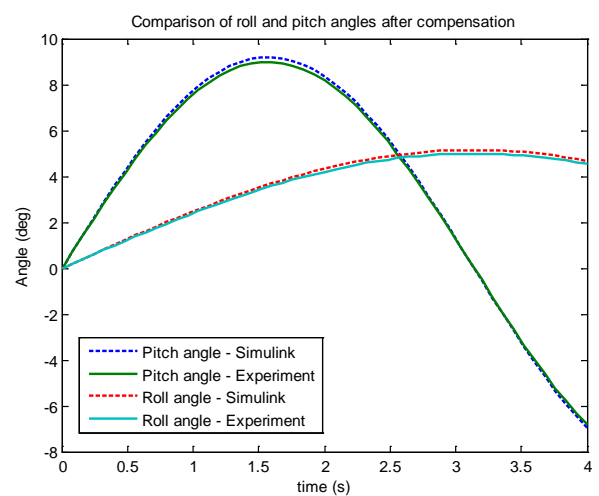
(b) **Roll and Pitch angles**
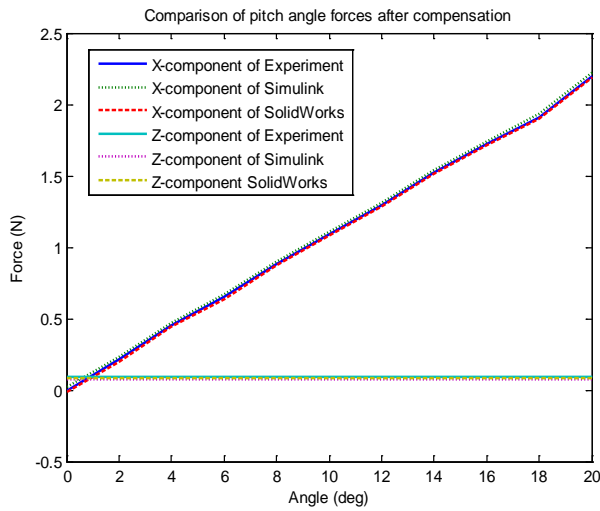
(c) Forces as a result of pitch angles
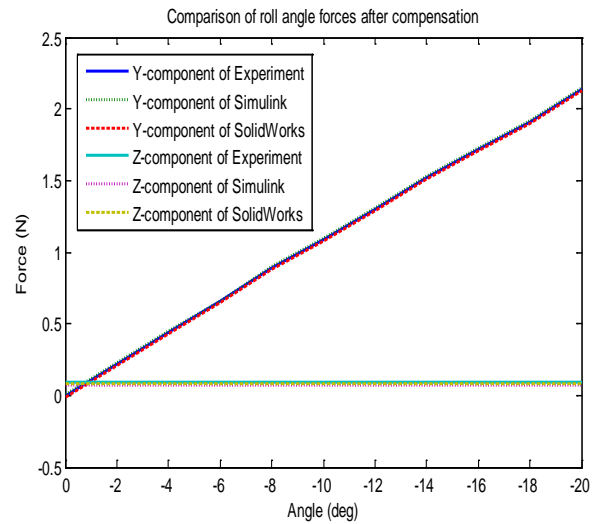
(d) Forces as a result of roll angles
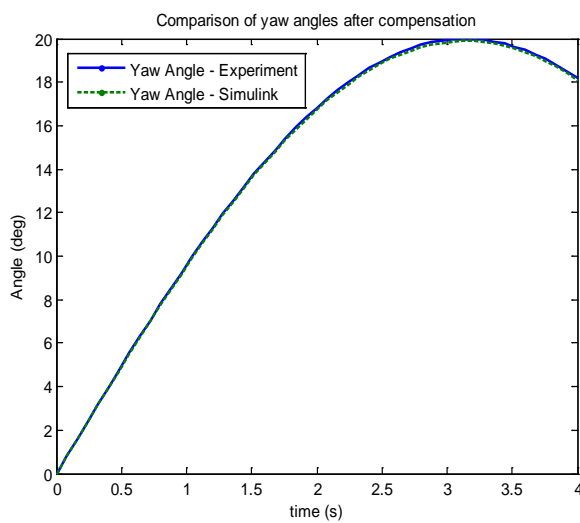
(e) Yaw angles
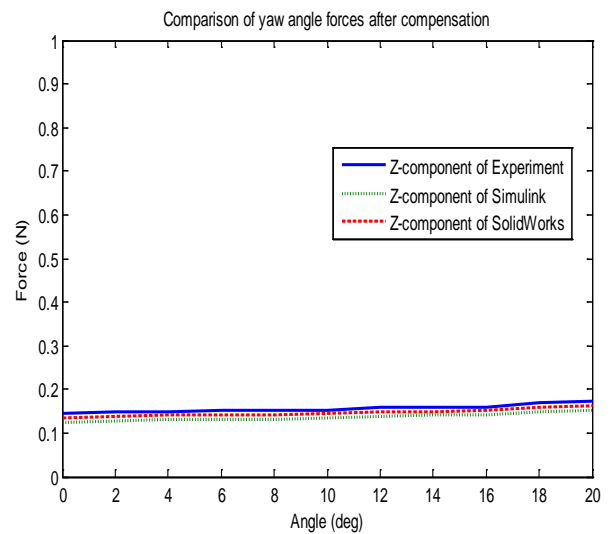
(f) Forces as a result of yaw angles

Figure 6-10: Results of Neural Network Compensation

Figure 6-10 shows that the neural network error compensation system was able to correct for the modelling and simulation errors with all the curves almost super-imposing on one another. The overall maximum average error was reduced from 0.11936 N to 0.01879 N – 15.74% of the uncompensated error.

6.3 Chapter Summary

Computations performed with an analytical model of the quad-rotor built in Matlab/Simulink and those obtained using CFD (Computational Fluid Dynamics) on a 3-D Solidworks model of the same helicopter have been compared with experiment data gathered from actual flight experiments at Essex University. In [98], a general agreement between numerical and experimental results was judged satisfactory and found to be good enough to validate the use

of the CFD simulation results for future wind flow analysis and prediction of the helicopter movements. It was also thought that more reliable and accurate simulation results would improve the performance and control design of the quad-rotor helicopter, especially in the rejection of and recovery from a disturbance [103]. This is because of the helicopter's inherent sensitivity to rotor speed changes and disturbances like wind gusts.The use of function approximation in this chapter clearly shows that a neural network is a viable technology for computing compensation values for the quad-rotor modelling and simulation errors.

INTELLIGENT CONTROLLER DESIGN

This chapter presents the development of a robust adaptive fuzzy-neural controller for quad-rotor helicopters. Data obtained from simulations of the models developed in chapters 4, 5 and 6 of this thesis are used to train a fuzzy-neural system, made up of a hierarchy of controllers to control the attitude and position of the quad-rotor helicopter.

7.0 Aircraft Navigation in the Wind

Aircrafts moving though still air generally move in the direction they are pointed. However the wind will always alter the course and speed of the craft relative to the ground depending on the wind direction and speed.

The relatively low weight and cruising speed of quad-rotor helicopters make them susceptible, particularly in strong winds. Consequently the computation of the effect of wind on aircraft movement relative to the ground is a major part of UAV flight planning and navigation.

The problem is one of trigonometry; the vector triangle involving wind speed and direction, air speed and heading, ground speed and track must be solved. Figure 7-1 illustrates the problem. The triangle is geometrically laid out with the known quantities (e.g., wind speed and direction forms one vector, the desired track determines the orientation of the second side and the desired air speed forms the magnitude of the third) [95].

1. The wind vector represents the motion of the air mass over the ground. It is defined by wind direction and wind speed.
2. The heading vector represents the motion of the aircraft through the air mass. It is defined by heading angle and air speed.
3. The ground vector represents the motion of the aircraft over the ground. It is defined by ground track and ground speed. The ground vector is the resultant of algebraically adding the air vector and the wind vector.
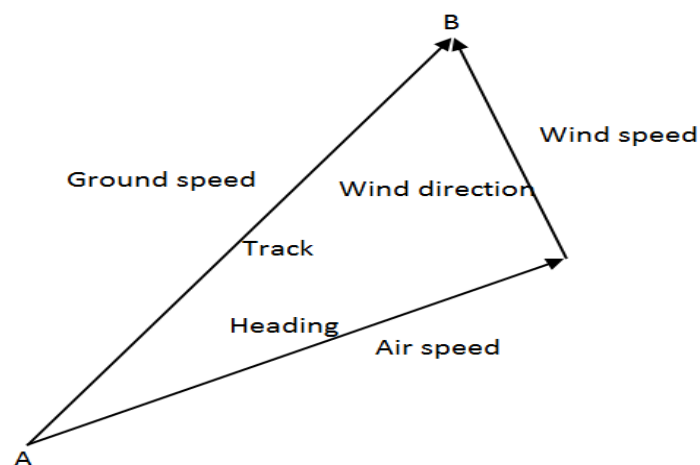
Figure 7-1: Navigation vector relationship

In this case, the speeds or distances covered can be used, because they are directly proportional. Under constant input conditions, a flight for any length of time would cover a distance proportional to the speed of the helicopter; therefore the wind triangle would have exactly the same shape, whichever variable is used.

The ends of the wind speed vector determine two points of the triangle; the intersection of an arc, whose radius represents the air speed magnitude, with the straight line defining the desired track is the third point. Thus the helicopter heading required to maintain track and groundspeed along that track are determined.

$$v_e = u + u_w \qquad (7\text{-}1)$$

Where v_e is the inertial velocity vector made up of the ground speed and track; u is air speed vector made up of heading and air speed and u_w is the wind vector made up of the wind speed and direction.

The motion of the helicopter in turbulence is akin to that of a ship on a rough sea or an automobile on a rough road. It is subjected to buffeting by random external forces, so that the attitude angles and trajectory vary randomly with time. These changes cause corresponding changes in forces and moments felt by the helicopter, resulting in structural forces and moments and vehicle motions [104].

7.1 Neural Network Model

As stated in chapter 2, artificial neural networks are among the newest control technologies in this day and age. The field of work is interdisciplinary, with lots of applications in everyday life. Just like its biological predecessor, an artificial neural network is an adaptive system - meaning that parameters change during its operations and are deployed to solve problems as they develop.

Neural networks are developed using a logical step-by-step process, which optimizes a criterion commonly known as the learning rule. The training data are important for these networks, as they convey the information that is necessary for determining the optimal operating point. Furthermore, the non-linear characteristics associated with neural networks make them very flexible processing systems [80].

Once an input is presented to the neural network, and a corresponding target response is set at the output, an error is composed from the difference of the target response and the real system output. The error information is then fed back to the system which makes all adjustments to their parameters using the learning rule. This process is repeated until the desired output is acceptable.

In the neural network design process, there must be the choice of a network topology, a trigger or performance function, a learning rule and the criteria for stopping the training phase. As there is no hard and fast rule in determining the size and parameters of the network, the Engineer is left with quite a difficult task at hand. Several adjustments have to be made in order to arrive at the best possible network performance.

7.1.1 Mathematical Model of a Neural Network

The synapses of a biological neuron are modelled as weights (usually numbers) of the artificial neural network – ensuring interconnection of the neural network and giving the strength of the connection. A negative value of the weight suggests an inhibitory connection, while a positive value designates excitatory connection. Secondly, the activities of the cell body in the biological neuron are represented by all the inputs, which are summed altogether and modified by the weights. Finally, an activation function controls the amplitude of the output. Mathematically, this process is described in the figure 7-2 below.
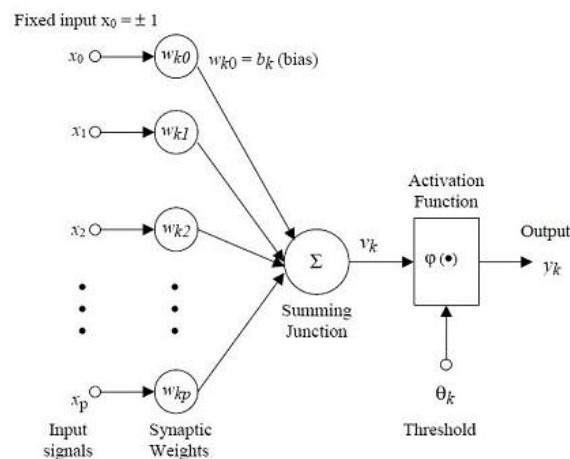
Figure 7-2: The mathematical model of a neural network

From this model the interval activity of the neuron can be shown to be:

$$v_k = \sum_{j=1}^{p} w_{kj} x_j$$

The output of the neuron y_k, would therefore be the outcome of some activation function on the value of v_k.

7.1.2.1 Activation Functions

The activation function serves the purpose of a squashing function, such that the output of a neuron is between specified values (typically 0 and 1, or -1 and 1) as shown in figure 7-3 below. In general, there are three types of activation functions.

First, there is the Threshold Function which takes on a value of 0 if the summed input is less than a certain threshold value (v), and the value 1 if the summed input is greater than or equal to the threshold value.

$$\varphi(v) = \begin{cases} 1 & if v \geq 0 \\ 0 & if v < 0 \end{cases}$$

Secondly, there is the Piecewise-Linear function. This function again can take on the values of 0 or 1, but can also take on values between that depending on the amplification factor in a certain region of linear operation.

$$\varphi(v) = \begin{cases} 1 & v \geq \dfrac{1}{2} \\ v & -\dfrac{1}{2} > v > \dfrac{1}{2} \\ 0 & v \leq -\dfrac{1}{2} \end{cases}$$

Thirdly, there is the sigmoid function. This function can range between 0 and 1, but it is also sometimes useful to use the -1 to 1 range. An example of the sigmoid function is the hyperbolic tangent function.

$$\varphi(v) = \tanh(\frac{v}{2}) = \frac{1 - \exp(-v)}{1 + \exp(-v)}$$
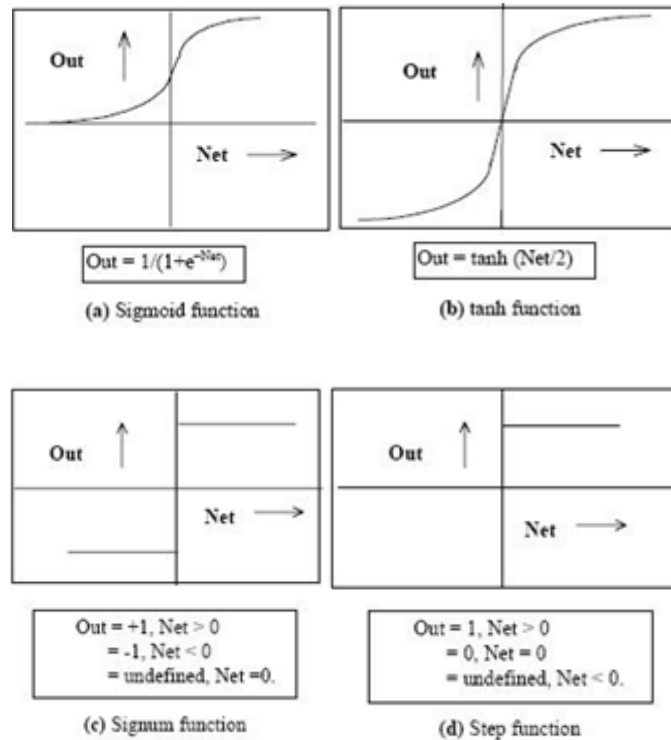
Figure 7-3: Neural Network activation functions

7.1.2.2 Neural Network Topology

The focus here is on the pattern of connections between the units and the propagation of data. The main distinction that can be made is between:

- Feed-forward neural networks, where the data flow from input to output units is strictly feed-forward. The data processing can extend over multiple (layers of) units, but no feedback connections are present. In other words, there are no connections extending from outputs of units to inputs of units in the same layer or other layers.

- Recurrent neural networks that do contain feedback connections. Contrary to feed-forward networks, the dynamical properties of the network are important. In some cases, the activation values of the units undergo a relaxation process such that the neural network will evolve to a stable state in which these activations do not change anymore. In other applications, the changes of the activation values of the output neurons are significant, such that the dynamical behaviour constitutes the output of the neural network [84].

7.1.2.3 Neural Network Training

A neural network has to be configured such that the application of a set of inputs produces (either 'direct' or via a relaxation process) the desired set of outputs. There are numerous methods of setting the strengths of the connections. One way is to set the weights explicitly, using a priori knowledge. Another way is to train the neural network by feeding it teaching patterns and letting it change its weights according to a specified learning rule.

Training and learning functions are mathematical procedures used to automatically adjust the network's weights and biases as shown in figure 7-4 below. The training function dictates a global algorithm that affects all the weights and biases of a given network. The learning function can be applied to individual weights and biases within a network.
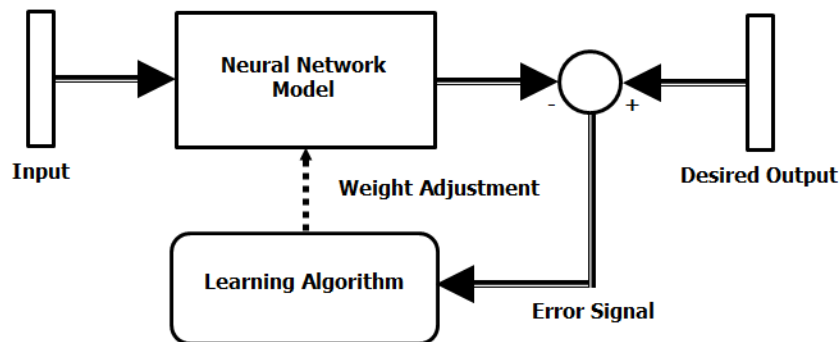
Figure 7-4: Neural Network training

Learning situations can be categorised into the following:

1. Supervised learning or Associative learning in which the network is trained by providing it with input and matching output patterns. These input-output pairs can be provided by an external teacher, or by the system which contains the neural network (self-supervised).

2. Unsupervised learning or Self-organisation in which an (output) unit is trained to respond to clusters of pattern within the input. In this paradigm the system is supposed to discover statistically salient features of the input population. Unlike the supervised learning paradigm, there is no a priori set of categories into which the patterns are to be classified; rather the system must develop its own representation of the input stimuli.

3. Reinforcement Learning. This type of learning may be considered as an intermediate form of the above two types of learning. Here the learning machine does some action on the environment and gets a feedback response from the environment. The learning system grades its action good (rewarding) or bad (punishable) based on the environmental

response and accordingly adjusts its parameters. Generally, parameter adjustment is continued until an equilibrium state occurs, following which there will be no more changes in its parameters. The self-organizing neural learning may be categorized under this type of learning.

7.2 Fuzzy Set Theory used in the Neural Network Model

The notion of fuzzy logic is very similar to human reasoning and inference process. Unlike classical control strategy, which is point-to-point control, fuzzy logic control is a range-to-point or range-to-range control. The output of a fuzzy controller is derived from fuzzifications of both inputs and outputs using the associated membership functions. A crisp input will be converted to the different members of the associated membership functions based on its value. From this point of view, the output of a fuzzy logic controller is based on its memberships of the different membership functions, which can be considered as a range of inputs [105].

The idea is to map an input space to an output space, and the principal mechanism for doing this is a list of if-then statements referred to as rules. All rules are evaluated in parallel, not really minding the order in which they come. These rules refer to the variables and adjectives that describe those variables. For a system that interprets rules as is the case with fuzzy logic, it is very important to define the terms to be used and the adjectives that describe them right from the beginning. Figure 7-5 shows a good description of a section of the fuzzy system.
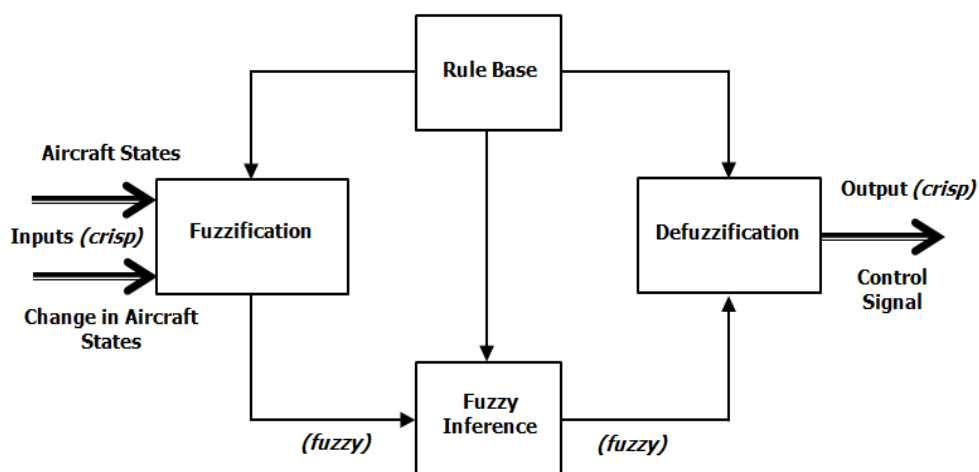
Figure 7-5: Fuzzy inference system for quad-rotor control

Fuzzy inference interprets the values in the input vector and, based on some set of rules, assigns values to the output vector.

Fuzzy logic begins with the theory of a fuzzy set. A fuzzy set is one without crisp, clearly defined boundaries. It could be made up of components with only a partial degree of membership.

Any statement can be fuzzy. The major advantage that fuzzy reasoning offers is the ability to reply to a yes-no question with a not-quite-yes-or-no answer. Human beings do such things many times a day, but it is a rather new 'knowledge' for computers and machines. Reasoning in fuzzy logic is just a matter of generalizing the familiar true-false, on-off, yes-no (Boolean) logic. If the numerical value of 1 is given to true and 0 given to false, fuzzy logic also permits in-between values like 0.3, 0.675 and many more.

7.2.1 Membership Functions

A *membership function* (MF) is a curve that defines how each point in the input space is mapped to a membership value (or degree of membership) between 0 and 1 as shown in figure 7-6 below. The input space is sometimes referred to as the *universe of discourse*.

The only condition a membership function must really satisfy is that it must vary between 0 and 1. The function itself can be an arbitrary curve whose shape can be defined as any suitable function from the point of view of simplicity, convenience, speed, and efficiency.

It is known that a classical set might be expressed as

$$A = \{x \mid x > 6\}$$

A fuzzy set is an extension of a classical set. If X is the universe of discourse and its elements are denoted by *x*, then a fuzzy set A in X is defined as a set of ordered pairs.

$$A = \{x, \mu_A(x) \mid x \in X\}$$

$\mu_A(x)$ is called the membership function (or MF) of *x* in A. The membership function maps each element of X to a membership value between 0 and 1.

The basic membership functions are:
▪ piece-wise linear functions

- the Gaussian distribution function

- the sigmoid curve

- quadratic and cubic polynomial curves
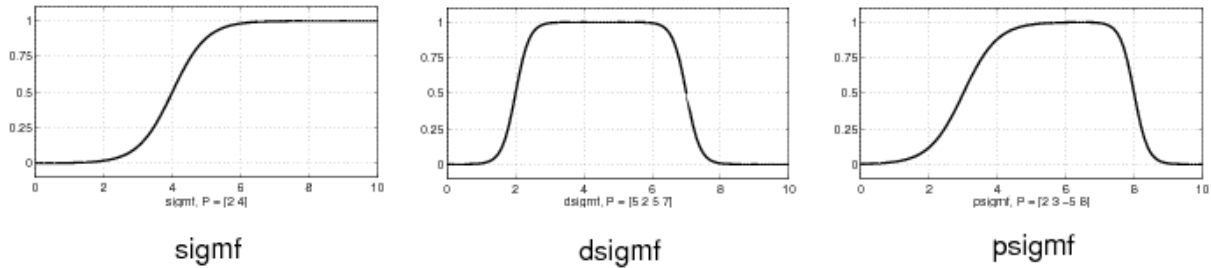
Figure 7-6: Fuzzy logic membership functions [105]

The most important thing to realize about fuzzy logical reasoning is the fact that it is a superset of the standard Boolean logic. In other words, if you keep the fuzzy values at their extremes of 1 (completely true) or 0 (completely false), standard logical operations will hold.

7.2.2 If-Then Rules

Fuzzy sets and fuzzy operators are the subjects and verbs of fuzzy logic. The if-then rule statements are used to formulate the conditional statements that comprise fuzzy logic. The general form of a single fuzzy if-then rule is:

if *x* is *A* then *y* is *B*

Where *A* and *B* are linguistic values defined by fuzzy sets on the ranges X and Y, respectively. The if-part of the rule "*x* is *A*" is called the *antecedent* or premise, while the then-part of the rule "*y* is *B*" is called the *consequent* or conclusion.

The interpretation of an if-then rule involves the following:

1. Fuzzify inputs: Resolve all fuzzy statements in the antecedent to a degree of membership between 0 and 1. If there is only one part to the antecedent, then this is the degree of support for the rule.

2. Apply fuzzy operator to multiple part antecedents: If there are multiple parts to the antecedent, apply fuzzy logic operators and resolve the antecedent to a single number between 0 and 1. This is the degree of support for the rule.

3. Apply implication method: Use the degree of support for the entire rule to shape the output fuzzy set. The consequent of a fuzzy rule assigns an entire fuzzy set to the output. This fuzzy set is represented by a membership function that is chosen to indicate the qualities of the consequent. If the antecedent is only partially true, (i.e., is assigned a value less than 1), then the output fuzzy set is truncated according to the implication method.

7.3 Fuzzy-Neural Model for the Quad-rotor Helicopter

Neural networks and fuzzy logic have shown great capabilities in solving many problems, but have not yet been able to solve the really complex problems that their biological counterparts can (e.g., vision). It is useful to fuse neural networks and fuzzy systems to offset the demerits of one technique by the merits of another technique.

Hybrid fuzzy-neural systems are homogeneous and usually resemble neural networks. In this case, the fuzzy system is construed as special kind of neural network. The advantage of such a system is its architecture, which sees both systems fully fused as one entity and its ability to learn online and offline as shown in figure 7-7.
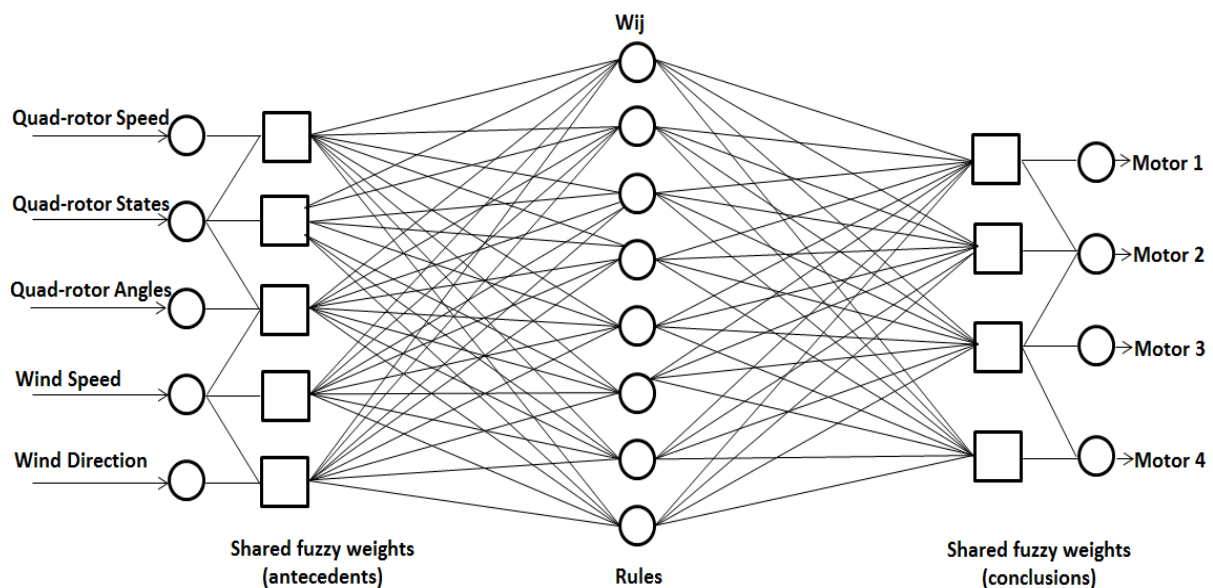
Figure 7-7: Hybrid FNN Model for Quad-rotor Control

As shown in figure 7-7 above, the rule base of a fuzzy system is interpreted as a neural network. The fuzzy sets can be regarded as weights whereas the input and output variables and the rules are modelled as neurons. Neurons can be included or deleted in the learning step. Finally, the neurons of the network represent the fuzzy knowledge base. Obviously, the

capabilities of both systems (as highlighted in section 2.5.1 of chapter 2 of this thesis) are thus exhibited.

As stated in the previous section, membership functions that express the linguistic terms of the inference rules must be defined in order to start building a fuzzy controller. The optimization of these functions in terms of generalizing the data is very important to any fuzzy systems, a solution which the neural networks can provide.

When the shapes of the membership functions are chosen, the neural network can then optimize the parameters using the gradient descent algorithm. This implies that in addition to providing details of the membership function shapes, there must be data to be used for training – which was obtained from the models built in chapters 4 and 5 and validated in chapter 6 of this thesis.

7.4 Controller design

Having established a satisfactory model of the quad-rotor system dynamics, based on the validation with real flight experiment data, it is of great significance to show how a controller is developed using fuzzy-neural networks as the chosen control technique. The structure in figure 7-8, gives a description of the entire control system.

Flying a quad-rotor helicopter is a challenging task because of its inherent sensitivity to rotor speed changes. It is even more difficult in the presence of a disturbance like wind. Data obtained from the validated models in chapter 6 of this thesis have been used to train the fuzzy-neural network system.

The controller implements these gained controls in the form of a command to the quad-rotor system. The plant responds to the changes in the control variables, and then sensors detect actual motion or state of the vehicle. The error between the desired input and the actual measured input from the sensor is fed back into the controller where it adjusts the command to attain the desired results as shown in figure 7-9.
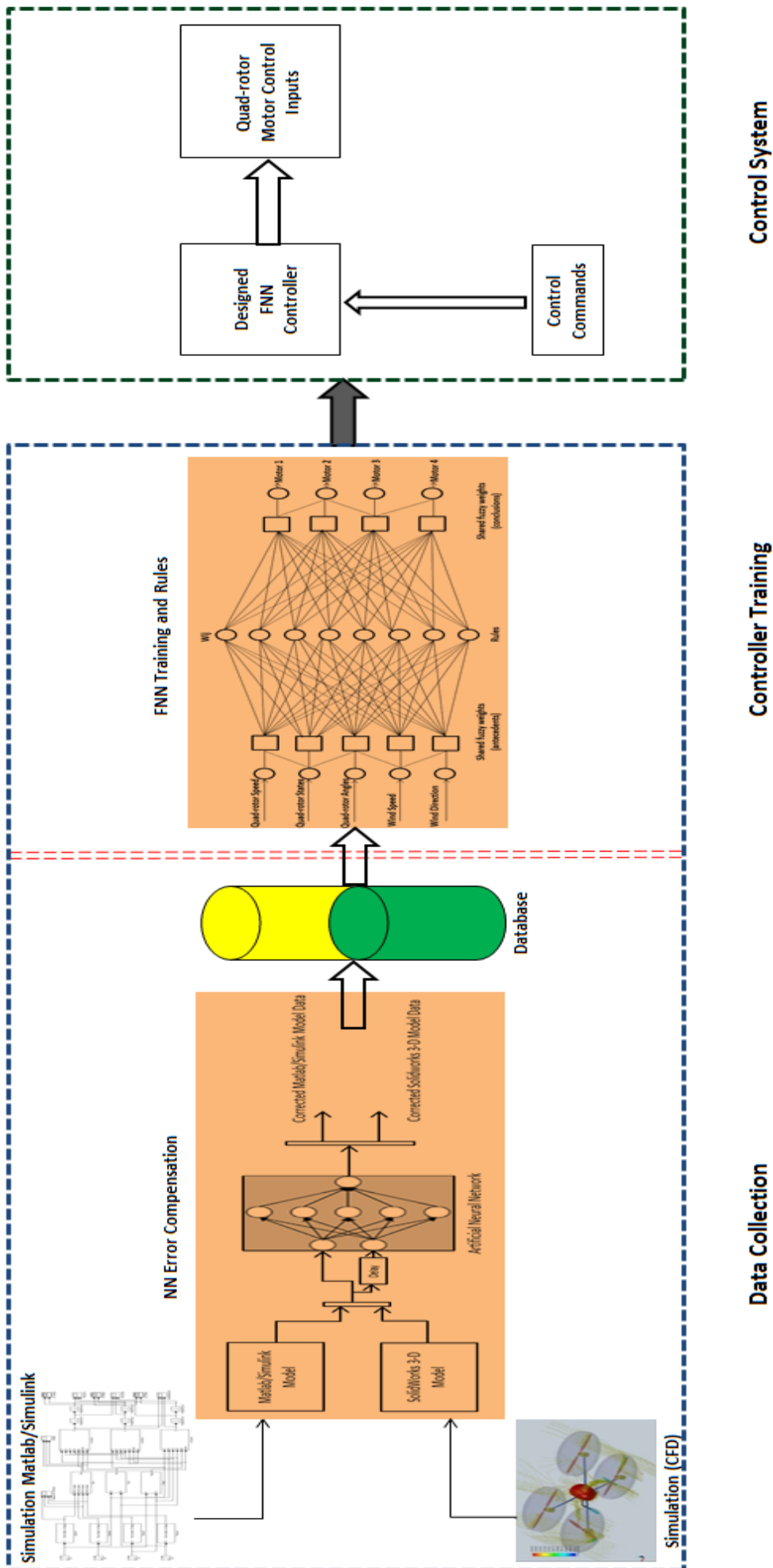
Figure 7-8: Hybrid FNN Control System for Quad-rotor Helicopters

154

A hierarchy of controllers was developed for the quad-rotor instead of having a single controller, for more effective management of the states of the helicopter as shown in figure 7-9 below. Training the initial single controller was quite a difficult task because of the nature of data and the sensitivity of the quad-rotor helicopter to little changes in the speeds of it motors.
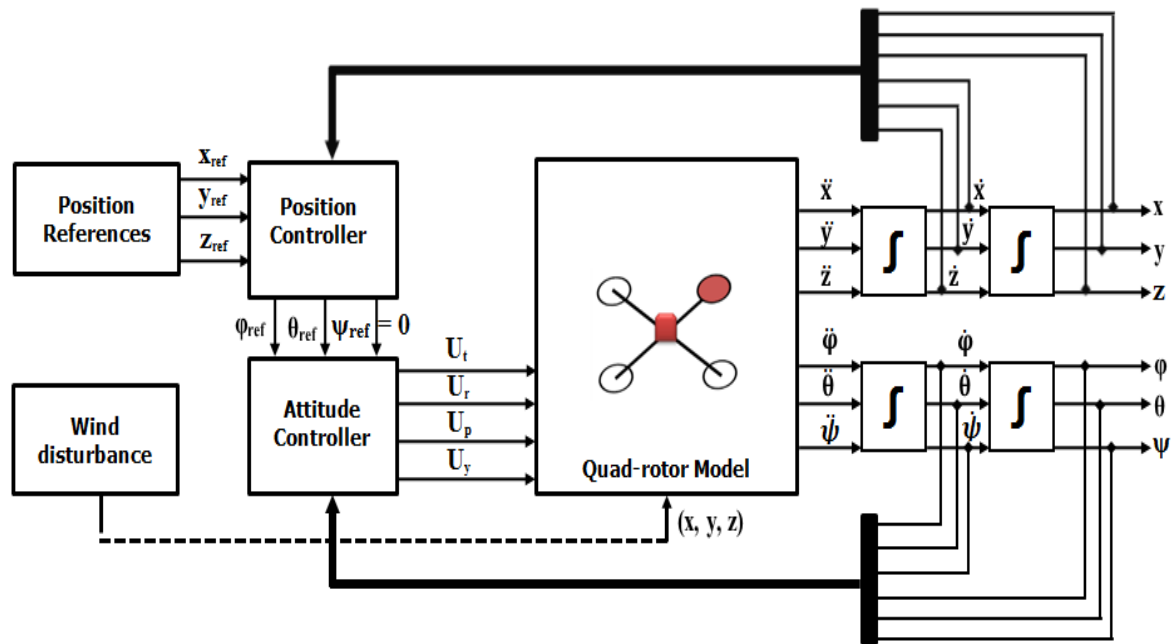
Figure 7-9: Controller framework

At the top of the hierarchy is the position controller, which directs the movement of the quad-rotor by providing the lower level controller (the attitude controller) with the desired roll, pitch, and yaw angles in addition to the helicopter's velocity. The attitude controller is comprised of four lower level controllers that autonomously direct the rotor speed changes, using voltage inputs to control the four attitude variables of throttle, roll, pitch and yaw as shown in figure 7-10 below.
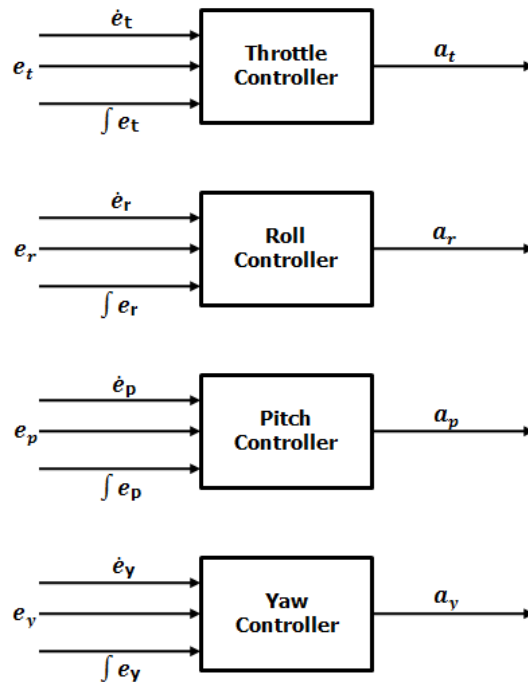
Figure 7-10: Block diagram of attitude controllers

Weight adjustment is a very important aspect of the controller, which the fuzzy system is employed to do in this case. A set of weight adjustment (if-then) rules were determined and integrated into the fuzzy-neural system that was used to adjust the weights of the neural network system. This weight adjustment mechanism takes as inputs the error, e and error rate, $\dot{e}$; and makes use of the fuzzy rules to modify the weights on-line, as shown in table 7-1.

The following fuzzy values were chosen to describe the language variables of e and $\dot{e}$:

BN - Big Negative, MN - Medium Negative, SN - Small Negative, ZO - Zero, SP - Small Positive, MP - Medium Positive, BP - Big Positive.

Values were also chosen for the outputs:

VVS - Very Very Small, VS - Very Small, S - Small, M - Medium, B - Big, VB - Very Big, VVB - Very Very Big.

Identical membership functions made up of the triangular and Gaussian members were chosen for all the inputs and outputs as shown in figure 7-11. The error e and error rate, $\dot{e}$ are calculated and normalized to the intervals $(-1, +1)$ and $(-3, +3)$, respectively.
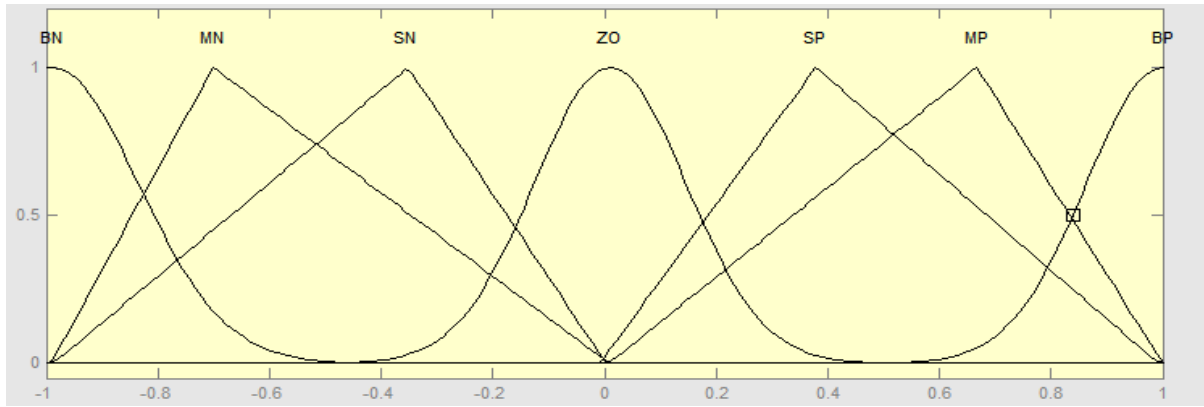
Figure 7-11: Membership functions for inputs and outputs

The rule base is also very important to any fuzzy system. As easy as it sometimes feels, translating experience from an expert into such fuzzy rules; it gets more complicated and confusing as the rules required to define the actions of the controller become too many [106].

Table 7-1: Fuzzy rule matrix for neural network weight adjustment

$\dot{e}$ / e	BN	MN	SN	ZO	SP	MP	BP
BN	M	S	VS	VVS	VS	S	M
MN	B	M	S	VS	S	M	B
SN	VB	B	M	S	M	B	VB
ZO	VVB	VB	B	M	B	VB	VVB
SP	VB	B	M	S	M	B	VB
MP	B	M	S	VS	S	M	B
BP	M	S	VS	VVS	VS	S	M

An example of the rules interpretation is given below:

From the second column and last row, if the error is BN (i.e. a Big Negative value) and the error rate is BP (i.e. a Big Positive value) then the adjustment should be M (i.e. a Medium value).

Since a dynamical system cannot understand such a value as a control input, there must be a conversion, back to numbers that can serve as the control input – a process called defuzzification, which practically the conclusion from the shared fuzzy weight as shown in figure 7-7.

7.4.1 Attitude Controller

Flight in the desired direction and the general stabilization of the quad-rotor helicopter are directed by this controller. Based on the commands from the position controller and information received from sensors, it re-arranges the speeds of the rotors by changing the voltage supply as described in figure 7-12. The action of this controller ensures that the vehicle flies along the commanded path and at the desired speed.
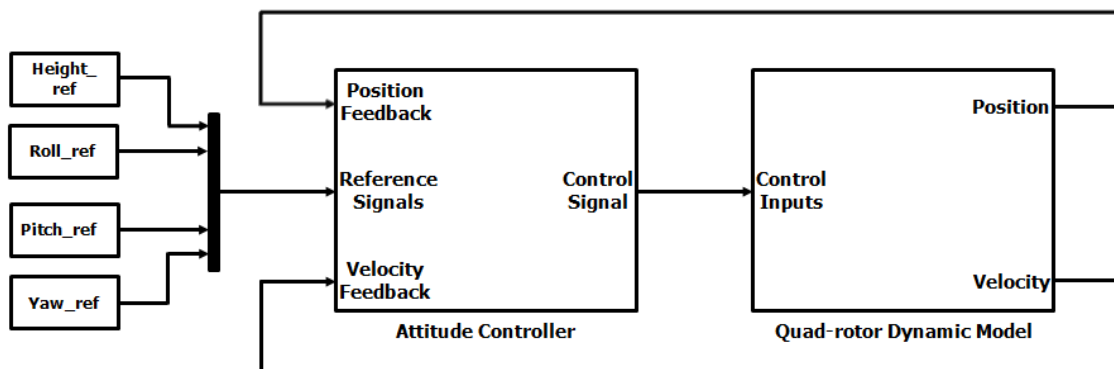
Figure 7-12: Attitude controller framework

The position controller sends information about the desired attitude and the sensors provide information about the current state of the quad-rotor helicopter in flight. A communication with the ground station also gives the quad-rotor helicopter good information with regards to the changing wind speeds when GPS signals are not available.

Collating all the information would give the controller a good understanding of what adjustments are expected since the error between the desired and actual variables, together with the derivatives and integrals of those errors are known. The controller now knows about the absolute error and the rate of change of it, therefore it is able to compute the desired rotor voltages for all four rotors, accordingly.

The four independent controllers that make up the attitude controller (equation 7-2) regulate against any disturbance the upward velocity, together with the roll, pitch, and yaw angles using the appropriate input combinations. These four attitude parameters use the following combination:

$$\begin{cases} V_1 = a_t + a_r + a_y \\ V_2 = a_t - a_p - a_y \\ V_3 = a_t - a_r + a_y \\ V_4 = a_t + a_p - a_y \end{cases} \qquad (7\text{-}2)$$

Where V_i is the voltage input of each motor, a_t, a_r, a_p and a_y are the modifications made to control the upward velocity, roll, pitch and yaw angles.

Data generated for throttle, roll, pitch and yaw were used in the training of each of the controllers independently. This resulted in very quick learning of their separate actions on the quad-rotor helicopter. After the training, the four simple controllers were arranged as shown in figure 7-10. This gave rise to a single attitude controller that produces the desired rotor speeds from the twelve inputs fed to the attitude controller as shown in figure 7-13.
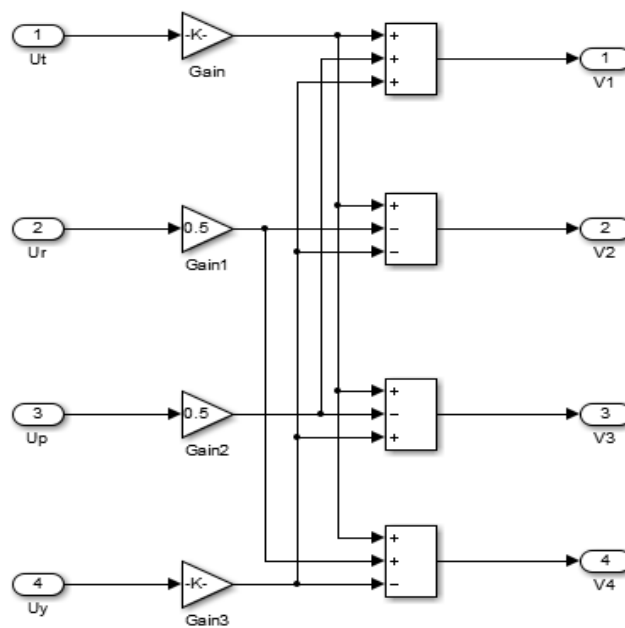
Figure 7-13: The attitude controller voltage combination

7.4.1.1 Attitude Controller Training

Iterative training is conducted to minimize the mean square error (MSE) using the hybrid optimization method (a combination of least squares and back propagation gradient descent method). The reason for training is to obtain the most suitable and optimized values of the weights for closest prediction through iterations. The training process is iterative and can be stopped either when total training error reaches a bottom threshold or when training error ceases to decrease any further. There is flexibility for varying number of neurons in the

159

hidden layers to optimize error. Starting from a small number of neurons, the number can be gradually increased or decreased until an accepted training error is achieved [107].

Before training the fuzzy-neural system (off-line), the data set was divided into training, test and validation sets. The training set was used to tune the fuzzy-neural model, while the test set was used to determine when the training should be terminated, so as to prevent over-fitting. The validation set was used to check the performance of the network.

A convenient start point of stable hover at a height of about 1m was chosen. A fuzzy-neural controller was trained with data obtained for each of the Euler angles. During the training, each of the controllers was given a set of data points that were expected to cover the range of motion: $-\frac{\pi}{4}, \frac{\pi}{4}$ for the roll and pitch controllers, since a little tilt would lead to acceleration in the direction of tilt. The yaw controller had a range of $-\pi, \pi$, since the quad-rotor is able to change heading without much effects on the stability of the vehicle.

Training was carried out with at least 8000 data samples generated from the neural network compensation model developed in chapter 6 of this thesis. Since at some point the rotor speeds would need to be increased and at other points they would need to be reduced, depending on the desired attitude variable, a hyperbolic tangent was used as the activation function to give activated nodes values between -1 and 1.

Although the angles can be controlled independently of each other, the thrust adjustment will differ between the roll and pitch angles of the quad-rotor helicopter. Increasing the throttle adjustment when all the tilt angles of the quad-rotor are zero, will only increase the upward velocity; but when the craft is tilted at a certain angle, an adjustment of the same amount will give a different result . The quad-rotor will move vertically as well as horizontally because of the component of force as a result of the tilt angle.

Each time a neural network is trained, can result in a different solution due to different initial weight and bias values and different divisions of data into training, validation, and test sets. As a result, different neural networks trained on the same problem can give different outputs for the same input. To ensure that a neural network of good accuracy has been found, the controllers were retrained several times.

A number of different configurations of the controllers were evaluated to correct such a situation, making use of a wide range of roll and pitch values to be used in the evaluations. When all four controllers were trained, they were integrated into a single attitude controller as described earlier. A more environment-specific training can be done for this controller to ensure a good handling of any kind of disturbance. For this research, training was provided for indoor and outdoor conditions (with wind speeds reaching 15m/s in any direction).

When each training round was completed, the network performance was checked to determine if any changes needed to be made to the training process, the network architecture or the data sets. Figure 7-14 below shows how well the neural networks performed.
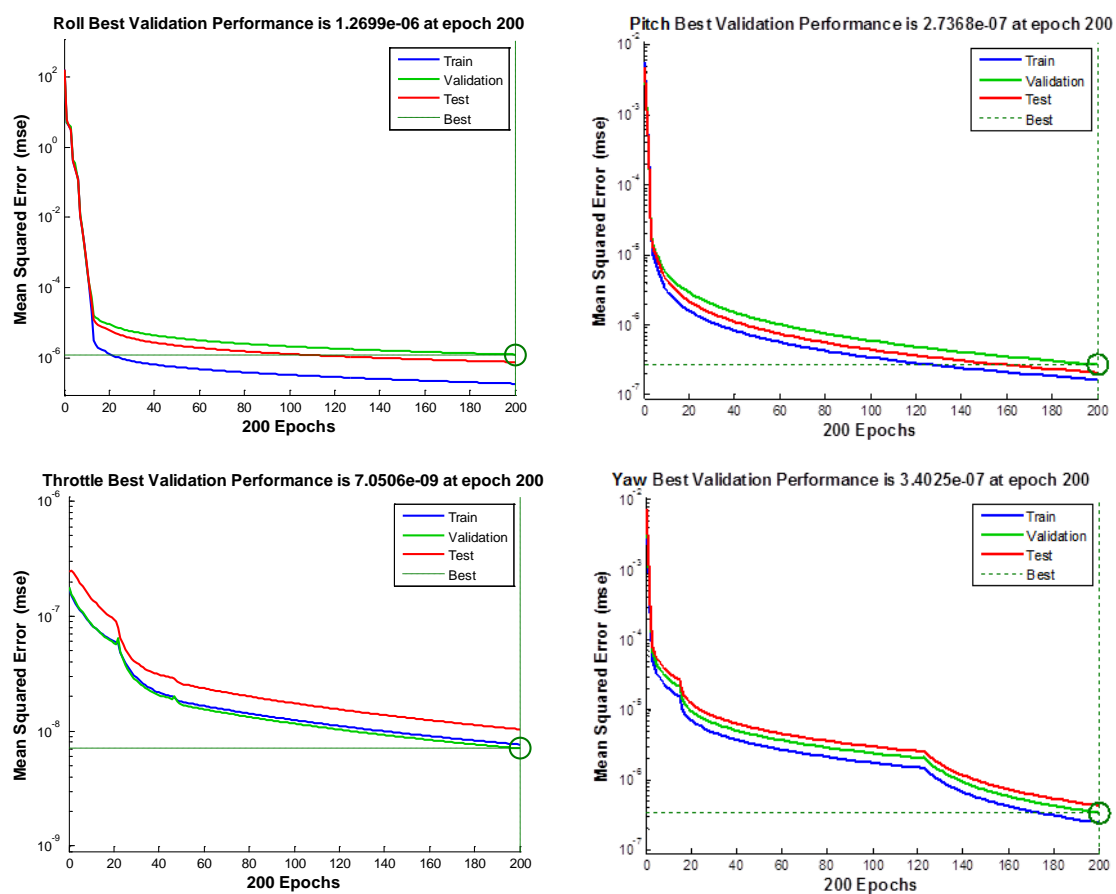
Figure 7-14: Neural network performance after training

The learning curve gives an indication as to how well the problem was learnt by the neural network. It plots the mean squared error achieved at the end of every epoch (an epoch is defined as one pass through of all training data through the network). Typically the mean squared error decreases rapidly in the beginning and flattens out at a low value. The lower the mean squared error the better the neural network has learnt the training data. The iteration at

which the validation performance reached a minimum was 200. For all the curves, the validation and test curves are very similar, suggesting a good result without over fitting.

The fuzzy-neural system provides as outputs a set of control inputs related to the operation tasks to be performed in adjusting the speeds of each of the four motors accordingly. Each node applies these control inputs to manage the speeds of the motors of the quad-rotor helicopter. Figure 7-15 shows the surface comparison between the input values of the fuzzy-neural system.
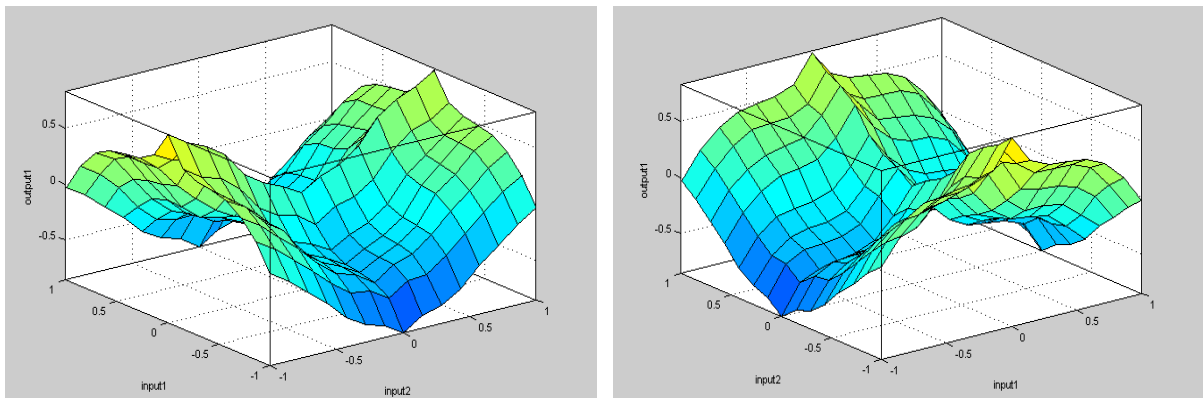
Figure 7-15: Surface comparison between the input values of the fuzzy-neural system

7.4.2 Position Controller

Attitude targets are required by the attitude controller in order to move the quad-rotor helicopter from one point to another. These targets are provided by the position controller. The position controller in this report is saddled with the task of directing the motion of the quad-rotor helicopter from one point to another, given the x, y and z coordinates as shown in figure 7-16.
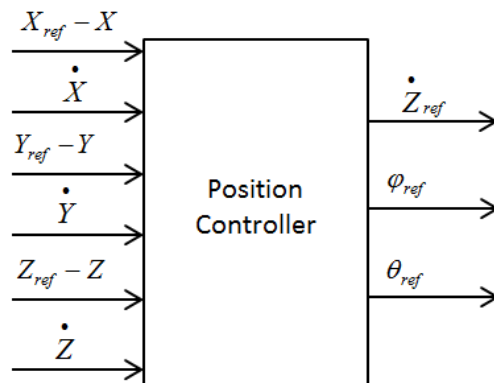
Figure 7-16: The Position controller

The position controller receives as inputs the difference between the desired and present positions in the x, y, and z directions; and also the velocity in three axes. The controller then directs the quad-rotor by sending commands about the attitude needed to move towards the desired position. Owing to the quad-rotor helicopter's tractability, only two attitude angles are required to reach any given position. Unless there is a need for a change of heading during certain missions to position the payload (e.g. camera) at a particular point, the yaw angle could always be set to 0. This allows the full motion of the quad-rotor helicopter to be controlled by only the roll and pitch angles in combination with the desired vertical velocity.

7.4.2.1 Position Controller Training

Training consisted of evaluating each potential controller based on the ability to reach a desired position as well as the total distance travelled in doing so. The training data set included a network of points covering every direction of motion from the origin. Very similar training parameters were used as in the case of the attitude controller.

7.6 Chapter Summary

This chapter detailed the development of a fuzzy-neural controller for the quad-rotor helicopter. Data obtained from the two models, which were passed through the neural network error compensation system were used to train and simulate the fuzzy-neural network behaviour in the Matlab/Simulink software environment.

Training was carried out with at least 8000 data samples for each controller. The learning curves in figures 7-14 and 7-15 show how well the problem was learnt by the fuzzy-neural network, with the mean squared error decreasing rapidly in the beginning and flattening out at a very low value suggesting good results without any over fitting.

SIMULATION RESULTS AND DISCUSSION

This chapter provides details of the simulation of the fuzzy-neural quad-rotor flight controller developed in chapter 7 of this thesis. This is intended to demonstrate the success of the developed controller in adapting to changing flight conditions. Results of the simulations are displayed and the performance of the controller is analysed for no wind and windy situations, where the quad-rotor experienced winds of different magnitudes.

8.0 Flight Controller Simulation

UAV control systems usually involve huge and complex tasks, making the design and testing of such systems time consuming and very expensive. Chapter 7 discussed the controller design for the quad-rotor helicopter, where the fuzzy-neural controller computes the control inputs for any given situation. It is theoretically possible to fly the vehicle in an open loop by sending these reference control signals to the quad-rotor helicopter. However, this will be difficult to achieve in real flight situations because when the vehicle encounters wind disturbances, noise and probably some model uncertainties, there will most certainly be speed and flight path tracking errors. Besides, the quad-rotor helicopter needs a feedback of its current states so as to ensure good stability and control [1].

In order to test the effectiveness of the developed fuzzy-neural controller, seven simulation situations have been clearly defined. In all situations, the quad-rotor starts at hover at (0, 0, 1) and consist of a short flight within less than 25 seconds to a point (66.15, 0, 1) about 66 metres north of the start point. The quad-rotor helicopter was commanded to keep up with different speeds at a time it was also allowed to experience winds speeds of different magnitudes that were either reducing or increasing its speed or pushing it off the flight path. The controller's task in simulation is to compensate the error in the roll and pitch angles, so as to stabilize the quad-rotor helicopter at an altitude of 1m and to ensure that it keeps to the desired speed and planned path. For the purpose of this simulation studies, the quad-rotor commanded yaw angle was kept at 0, since it was expected to fly northwards without any change of heading.

In consideration of the fact that during real flight situations, the quad-rotor helicopter experiences a little bit of delays and possible saturation of the actuators', owing to the wireless communications and the dynamics of the actuators; discrete-step delay blocks were built into the feedback loop and actuators models in Matlab/Simulink. Also, with the motors having a maximum angular velocity of 380 rad/sec, another saturation block was placed between the fuzzy-neural controller and the delay block to keep within the limits.

8.1 Flight Simulation in No Wind Situation

In this situation, flows around the rotor blades of the helicopter are somewhat steady and the rotors assumed to be working under the same conditions, because the wind speeds in the three directions (x, y and z) were kept at 0m/s.

The first stage of this simulation shows the quad-rotor helicopter in vertical flight, climbing to a height of 1m as shown in figure 8-1. The quad-rotor is then required to fly to (66.15, 0, 1), a position about 66m north of the start point (0, 0, 1) within 20 seconds. The desired flight path can be seen to be exactly the same with the commanded flight path, showing no errors within the x, y and z positions as there is no disturbance in the flight conditions.
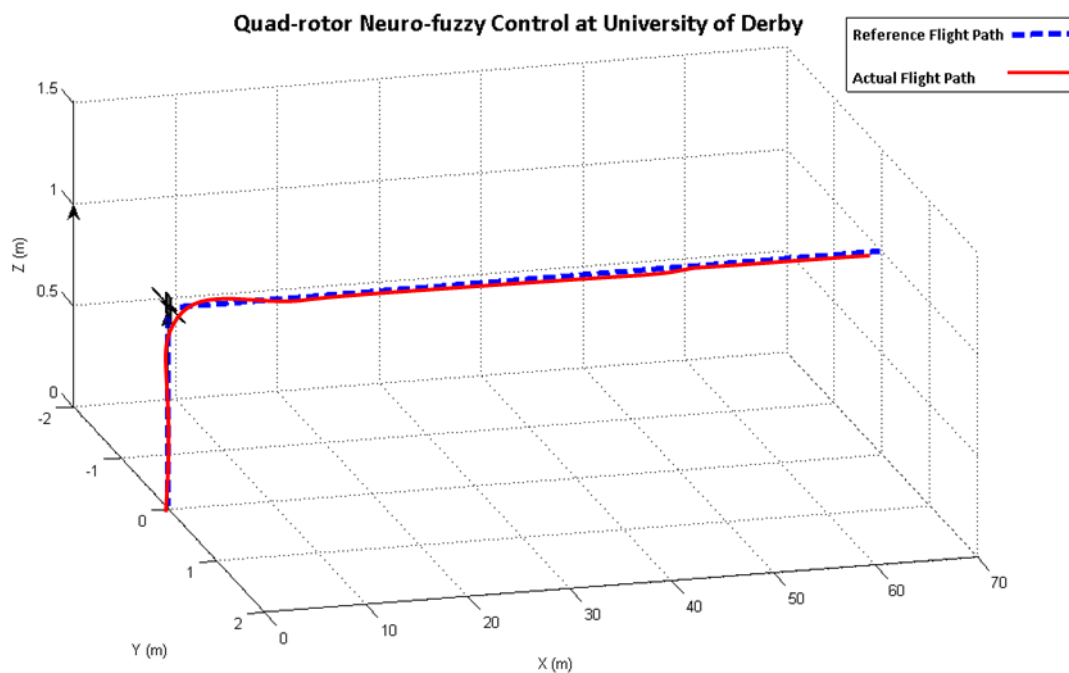
Figure 8-1: Quad-rotor flight simulation in a no wind situation

The vehicle follows the planned path, reaching the desired speed of 3.5m/s in 2 seconds. The controller is able to keep the helicopter flying at the commanded speed and path without any deviation. As can be seen in the graphs (figure 8-2), the velocity, pitch angle and height remain constant throughout the flight, after reaching their peaks.
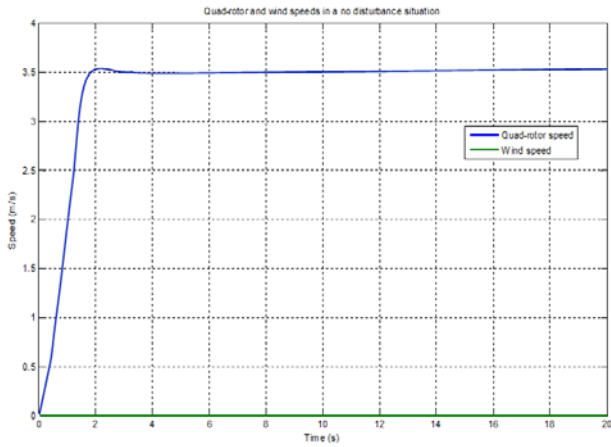
(a) Quad-rotor and wind speeds.
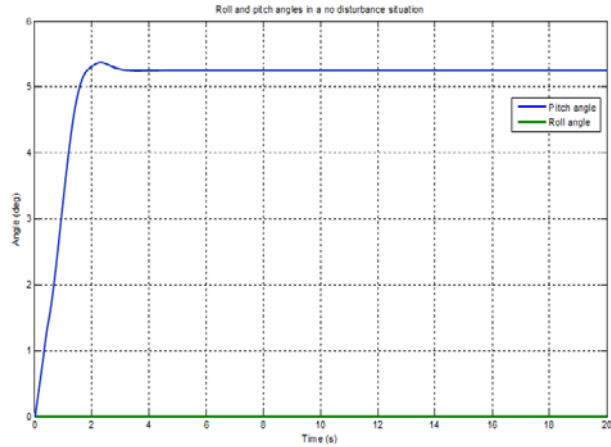
(b) Roll and pitch angles.
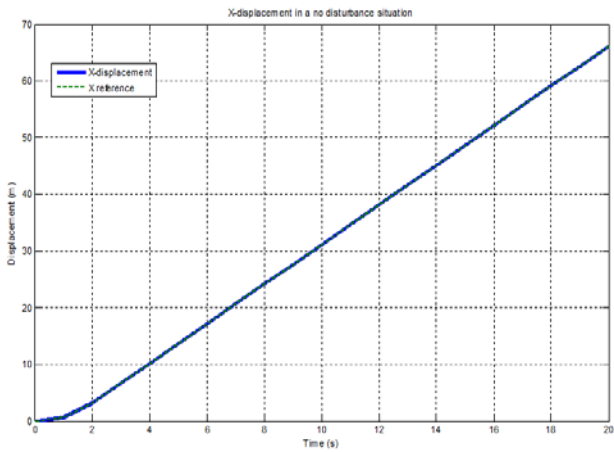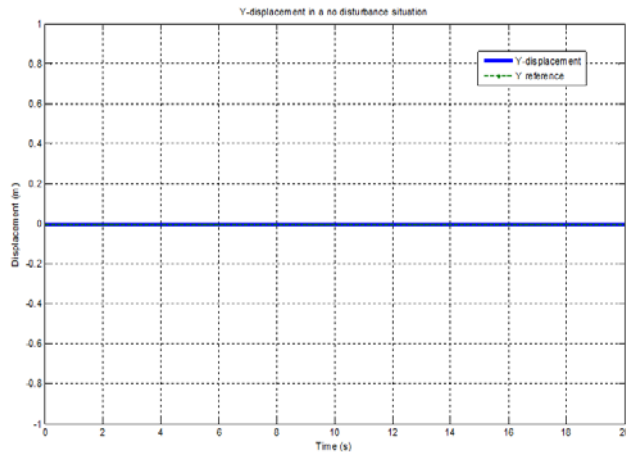
(c) X-displacement.

(d) Y-displacement.

Figure 8-2: Graphs showing the helicopter parameters in a no wind situation

The curves that describe the speeds of each motor are as shown in figure 8-3. Initially, the quad-rotor was at stable hover and all the rotors spin at the same speed, taking it to the reference height of 1 m. The controller then changes the speeds of motors 1 and 3 to create a pitch angle to move the quad-rotor forward, while keeping motors 2 and 4 at a constant speed. The quad-rotor reaches the commanded speed of 3.5m/s and experiences a stable cruise, since there is no disturbance. The speed and flight path of the helicopter are kept as commanded by keeping speeds of the motors steady, after reaching the desired speed.
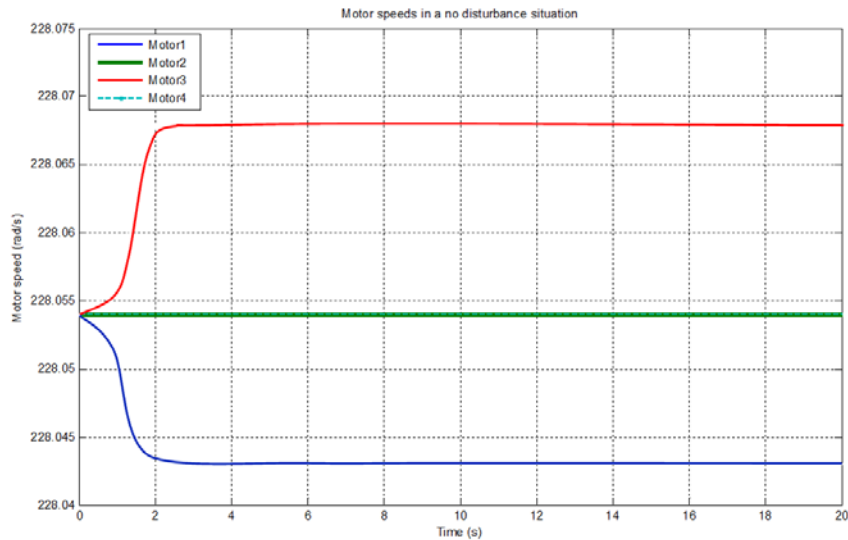
Figure 8-3: Graph showing the speeds of the four motors of the quad-rotor in a no wind situation

As explained in Chapter 4 of this thesis, creating a forward pitch effect, entails increasing the thrust in motor 3 (rear) and decreasing that of motor 1 (front), while keeping the other two unchanged. To avoid yawing, the overall reaction torque must be equal to zero during flight. This seems to impose a constraint on the amount of thrust that can be increased in one rotor relative to the other. Since the thrust and the torque are quadratic with the motor speed, this constraint does not mean that the speeds of the motor 1 and motor 3 are increased or decreased by exactly the same amount, as clearly seen in the motor 1 and motor 3 curves in figure 8-3.

In any case, maintaining a perfect balance of torques while the thrusts are being independently modified is almost impossible, because the torques also depend on other variables apart from the motor speed, such as the tangential velocities of the centres of the rotors or the pitch rate. It is clearly seen that the controller increases the thrust in motor 3 more than it decreases that of motor 1, so as to maintain the altitude that would have been lost to the thrust vector tilt as the quad-rotor pitches.

8.2. Flight Simulation in a Headwind

The horizontal wind velocity normally has a crosswind component and a headwind/tailwind component, which affect its speed relative to the ground. When the quad-rotor helicopter experiences such a flow of wind around it, there certainly will be unwanted moments in addition to other possible effects that act due to the fact that the flight conditions are much more unstable. The quad-rotor helicopter is likely to depart from equilibrium in flight, leading to a possible loss of control.

The headwind component of the horizontal wind velocity would normally reduce the speed of the quad-rotor, relative to the ground. By reducing the speed of the vehicle, the time required to reach its destination is increased. Stronger winds could even prevent the vehicle from reaching its destination, if there is no robust controller to help the vehicle recover from the effects of the disturbance. In this study, two headwind situations are considered – constant and gusty headwind situations.

8.2.1 Constant Headwind

This study describes a situation where a constant wind opposes the flight of the quad-rotor. After reaching a height of 1m (0, 0, 1) as shown in figure 8-4, the quad-rotor is then required to fly to the same position (66.15, 0, 1) from the start point within 20 seconds, similar to study 1 above. The desired flight path is maintained, but with the opposing wind flow at 1.5m/s, the controller quickly re-arranges the speeds of the motors to counter the effect of the wind and keep the helicopter in the desired speed.
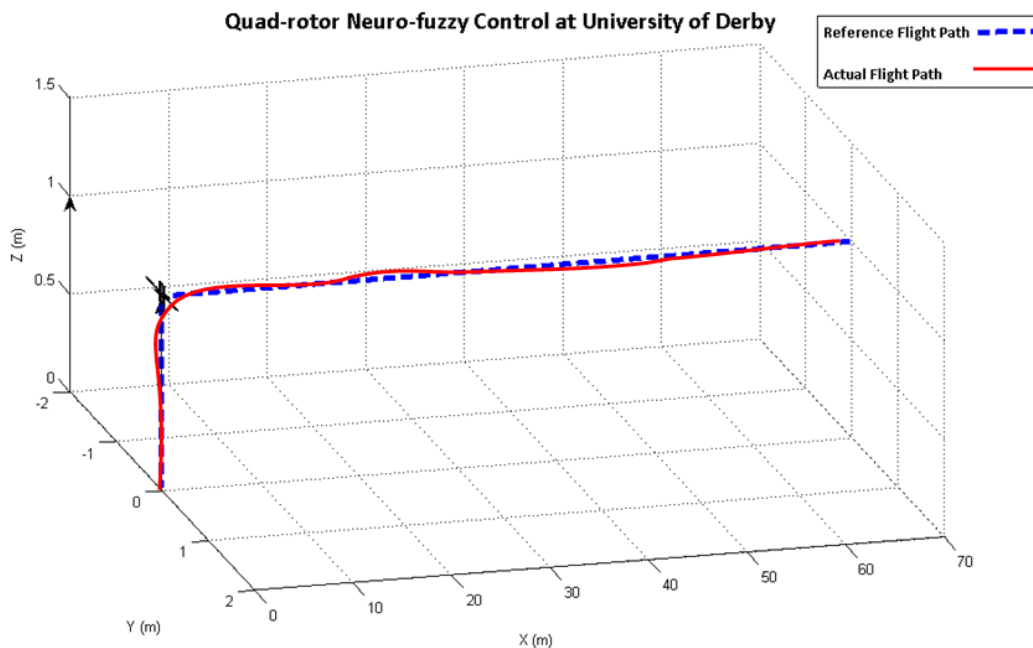
Figure 8-4: Quad-rotor flight simulation in a headwind

In a constant headwind situation, the effects of the wind slamming the front of the quad-rotor helicopter are seen from the graphs in figure 8-5. After reaching the desired speed of 3.5m/s in 2 seconds and flying steadily for another 2 seconds, a constant headwind of speed 1.5m/s was introduced to oppose the forward flight of the helicopter. The curves clearly show an initial decline in the speed of the quad-rotor to 2.09m/s. The combined effect of the headwind

and the helicopter's speed and forces always produces a resultant speed or force that is lower than the one the helicopter had before it encountered the wind, though the thrust is increased resulting in a little increase in altitude, which the controller nullifies almost immediately. Stronger winds are expected to have a greater reduction effect on the quad-rotor's speed and forces.

The curves show oscillations in the quad-rotor velocity and pitch angle between 4 and 6 seconds of flight (exactly where the wind disturbance was introduced after the quad-rotor reaches a steady cruise speed of 3.5m/s). It is clearly visible that the pitch angle is reduced, while the resultant speed is lower than the commanded speed of the helicopter, with a position error of 0.01m observed in the y-direction (east) from the plot. However, the action of the controller immediately restores the speed of the helicopter to the commanded value of 3.5m/s and eliminates the y-position error, ensuring flight stability on the planned path despite the 1.5m/s headwind effect.
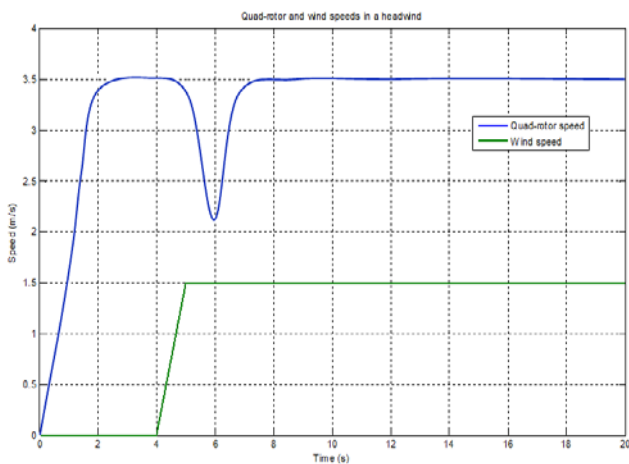
(a) Quad-rotor and wind speeds.
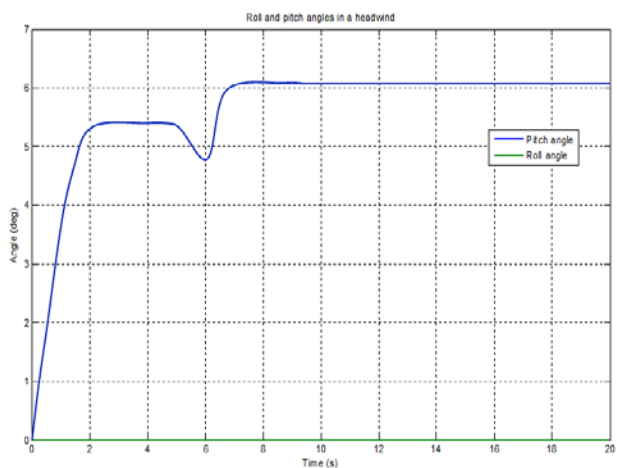
(b) Roll and pitch angles.
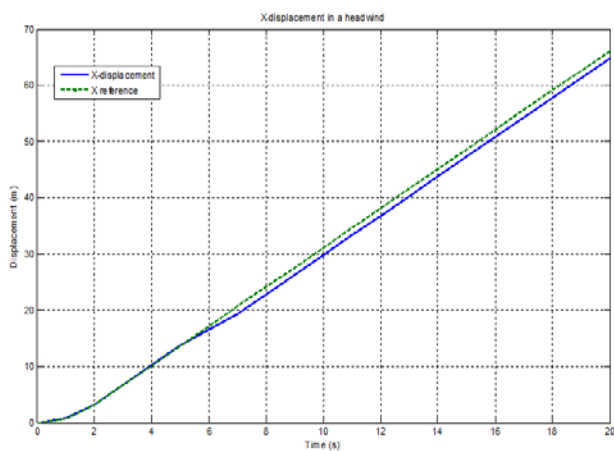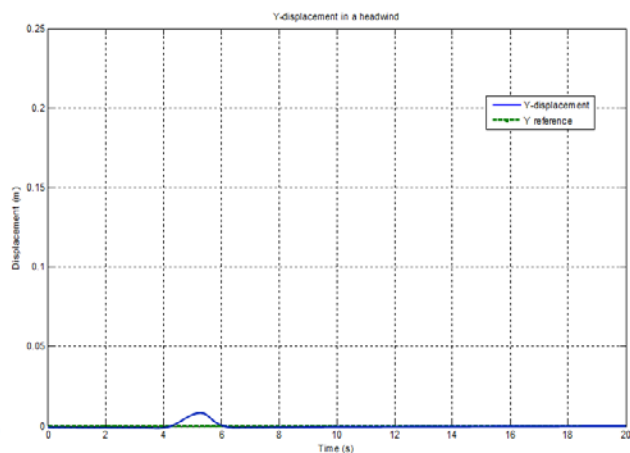
(c) X-displacement.

(d) Y-displacement.

Figure 8-5: Graphs showing the helicopter parameters in a constant headwind

Figure 8-6 shows how the controller compensates, by re-arranging the motor speeds to nullify the effect of the disturbance. The robust controller increases the thrust from the rear rotor by speeding up motor 3 and decreases that of the front rotor by slowing down motor 1 to take control of the situation.
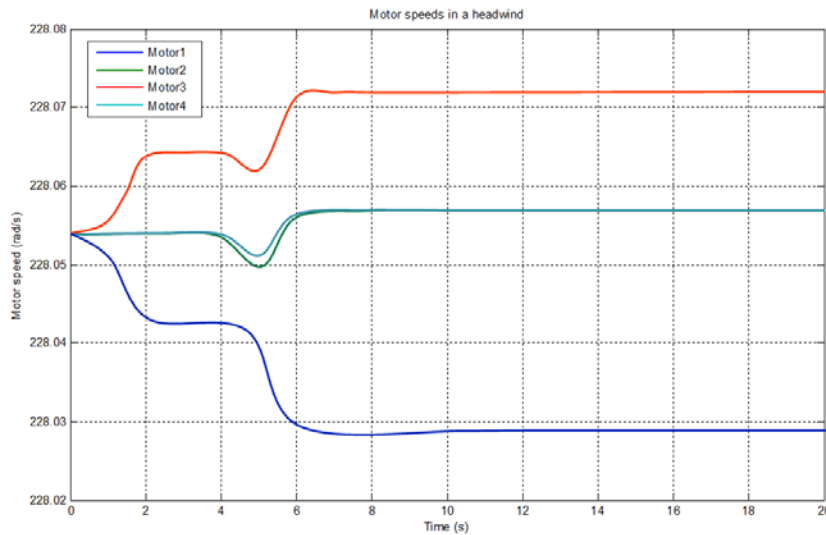
Figure 8-6: Graph showing the speeds of the four motors of the quad-rotor in a constant headwind

8.2.2 Gusty Headwind

In the case of a gusty headwind, turbulence is added in the form of a Gaussian random displacement, with a variance of 0.5m/s. The quad-rotor is expected to fly to the same position (66.15, 0, 1) from the start point. The actual flight path is maintained, but with the opposing wind flow varying between 0.5m/s and 1.5m/s, the controller quickly re-arranges the speeds of the motors at different times to counter the effect of the wind and keep the helicopter in the desired speed. The effects of the gusty headwind slamming the front of the quad-rotor helicopter are seen from the graphs in figure 8-7.

The curves show a number of crests and troughs in the quad-rotor speed and pitch angle as a result of the changing wind speeds at different times. The only crest in the quad-rotor speed is observed at the time that the wind speed drops from 1.5m/s to 0.5m/s, because the controller had earlier compensated for a greater disturbance.

A small constant error is present within the *x* and *y* position but the altitude profile is maintained despite the turbulence. The controller compensates at different times by changing the thrust, enabling the vehicle to accurately track the reference path at the required speed,

though it would take about 0.5 seconds more to arrive at the destination because of the disturbance in the flight path.

(a) Quad-rotor and wind speeds.

(b) Roll and pitch angles.

(c) X-displacement.

(d) Y-displacement.
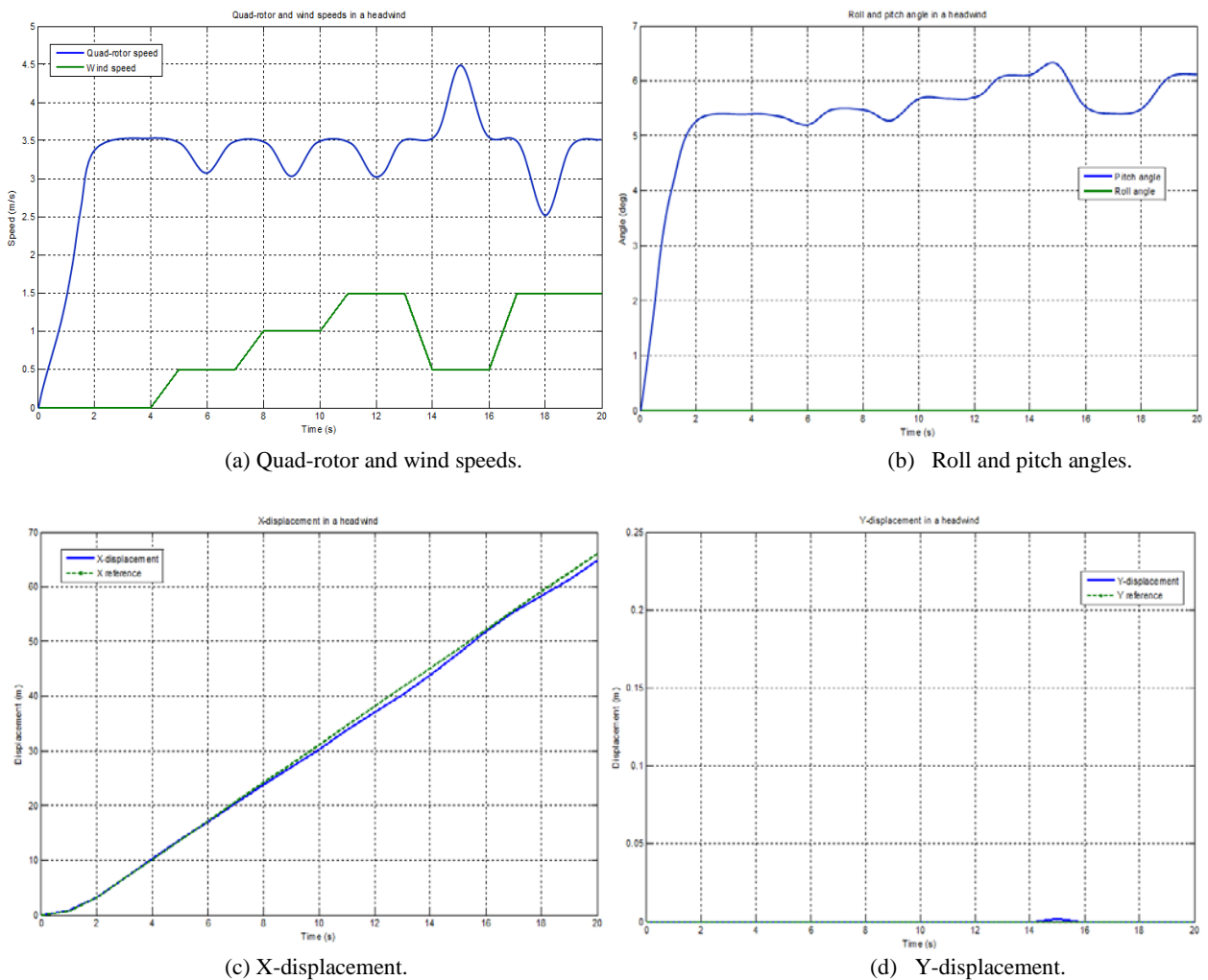
Figure 8-7: Graphs showing the helicopter parameters in a gusty headwind

Figure 8-8 shows how the controller compensates, by re-arranging the motor speeds to quash the effect of the disturbance. The curves for motors 1 and 3 are seen to be changing within very short intervals in response to the changing wind speed, which opposes the flight of the vehicle. The arrangement of the motor speeds is seen to be carefully done so as to keep the thrust and torque imbalance to the barest minimum in order to maintain the altitude and keep the commanded zero yaw angle.
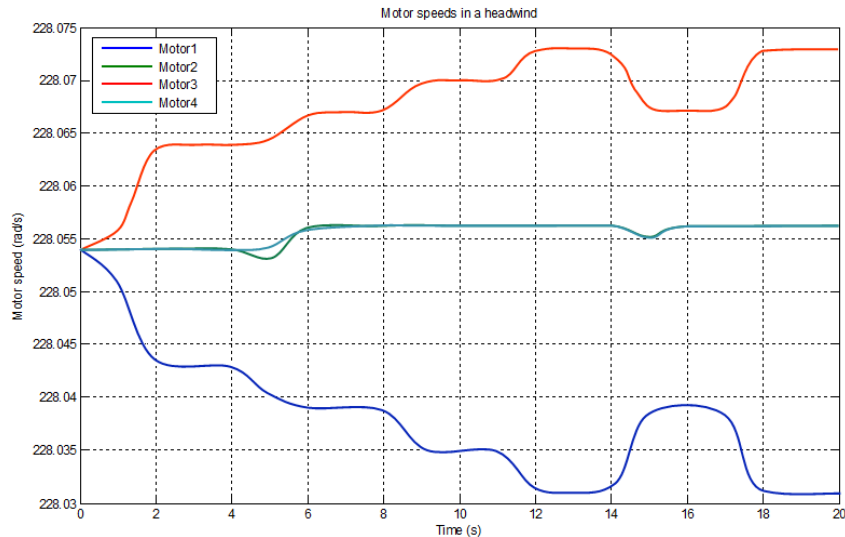
Figure 8-8: Graph showing the speeds of the four motors of the quad-rotor in a gusty headwind

8.3 Flight Simulation in a Tailwind

The tailwind component of the horizontal wind velocity would normally increase the speed of the quad-rotor, relative to the ground. By increasing the speed of the vehicle, the time required to reach its destination is reduced, which may be an advantage or disadvantage to the vehicle, depending on the mission to be accomplished. With very strong winds, the vehicle could go beyond the destination and have difficulty in returning if there is no robust controller to help the vehicle recover from the effects of the disturbance. In this study, two tailwind situations are considered – constant and gusty tailwind situations.

8.3.1 Constant Tailwind

This simulation study describes a situation where a constant wind hits the quad-rotor from the rear, increasing its speed and possibly making it deviate from the planned path. Having reached a height of 1m (0, 0, 1) as shown in figure 8-9, the quad-rotor is then commanded to fly northwards to the same position (66.15, 0, 1) from the start point. The desired flight path is maintained, but with the tailwind of 1.5m/s, the controller again has to re-adjust the motor speeds in order to reduce the resultant speed of the helicopter to the desired speed and also ensure that it keeps to the planned path.
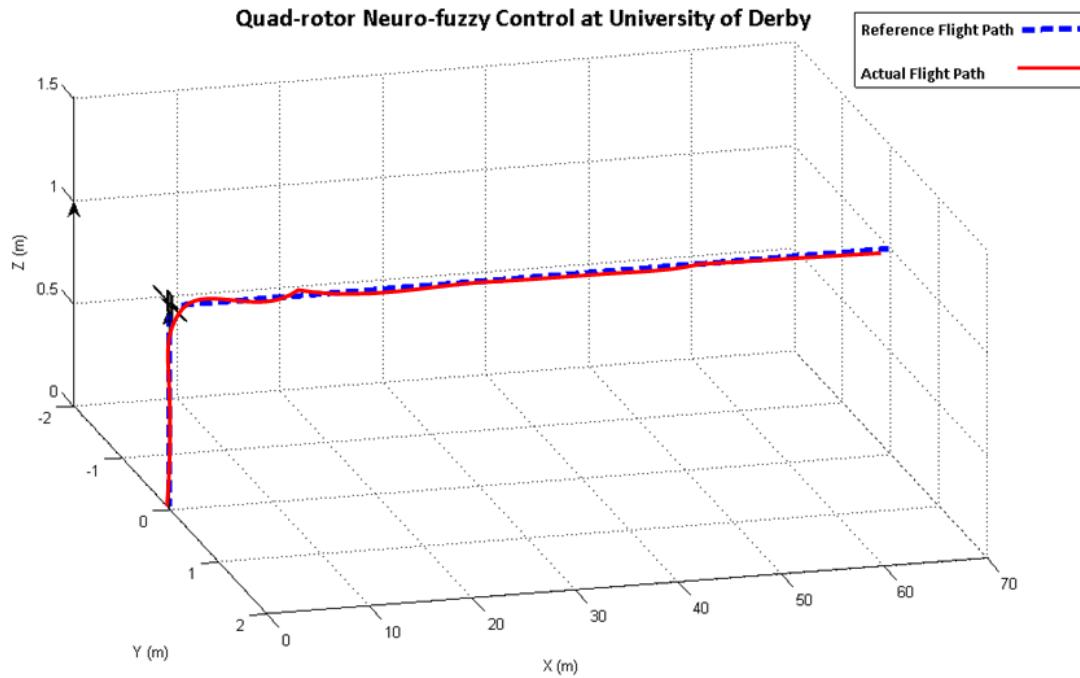
Figure 8-9: Quad-rotor flight simulation in a tailwind

As the vehicle has an induced speed due to the tail wind there is need to reduce the pitch angle, so as to slow it down and keep it on course. The graphs in figure 8-10 show oscillations in the quad-rotor speed and pitch angle after 4 seconds of flight (exactly where the wind disturbance was introduced, when the helicopter had reached a steady state). Evidently, the speed of the quad-rotor is increased to a resultant velocity of about 5m/s. It is also clear that the pitch angle of the helicopter is increased, but the swift action of the controller reduces the pitch angle and restores the speed to the commanded value of 3.5m/s, ensuring flight stability despite the tailwind effect.

(a) Quad-rotor and wind speeds.   (b) Roll and pitch angles.

(c) X-displacement.   (d) Y-displacement.
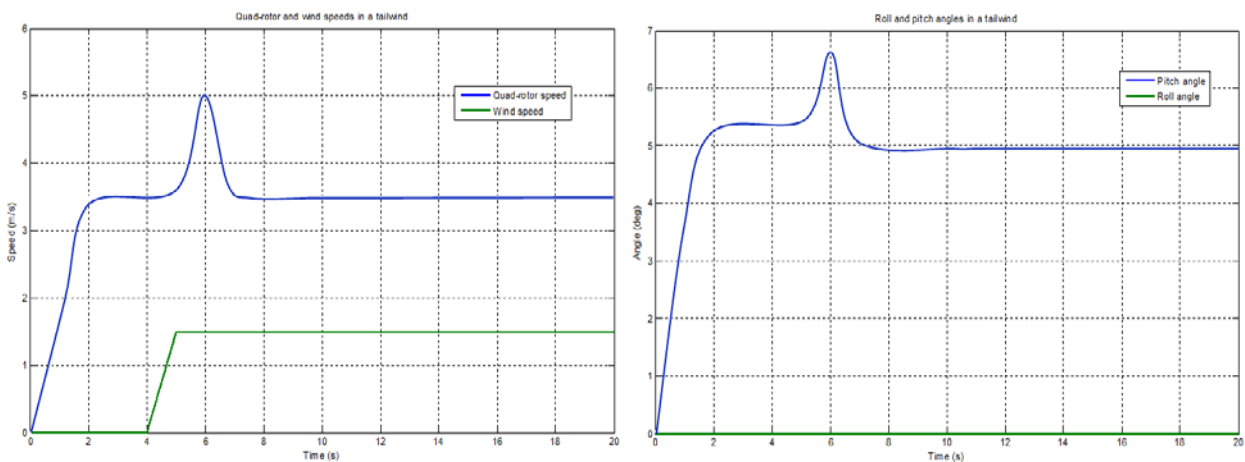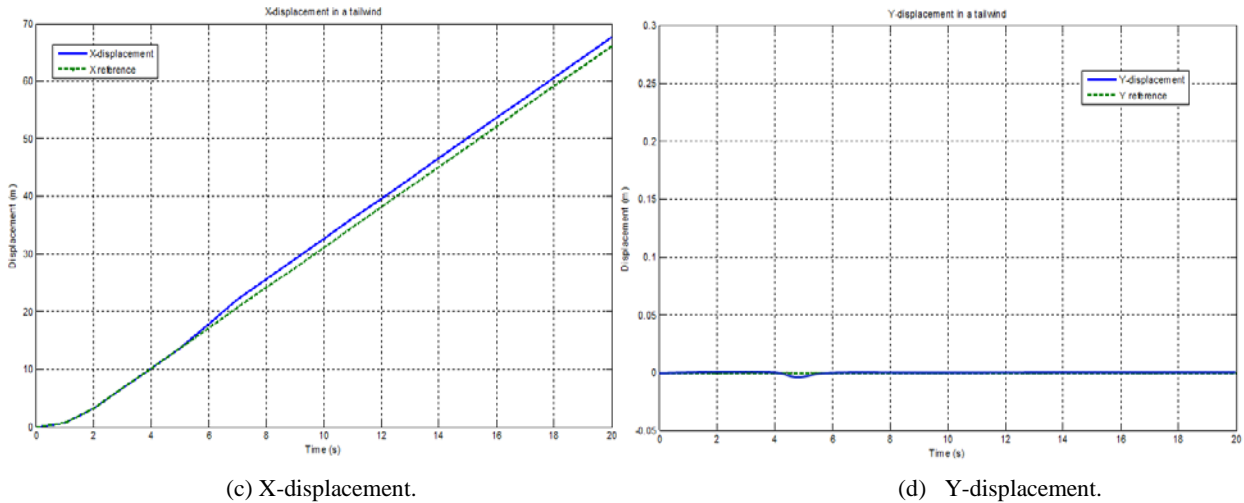
Figure 8-10: Graph showing the helicopter parameters in a constant tailwind

In compensating for the changes as a result of the tailwind, the controller re-arranges the motor speeds to counter the effect of the wind and get it back to the commanded speed of 3.5m/s. Figure 8-11 shows the motor speed curves. The robust controller decreases the thrust from the rear rotor by slowing down motor 3 and increases that of the front rotor by speeding up motor 1 to take control of the situation.
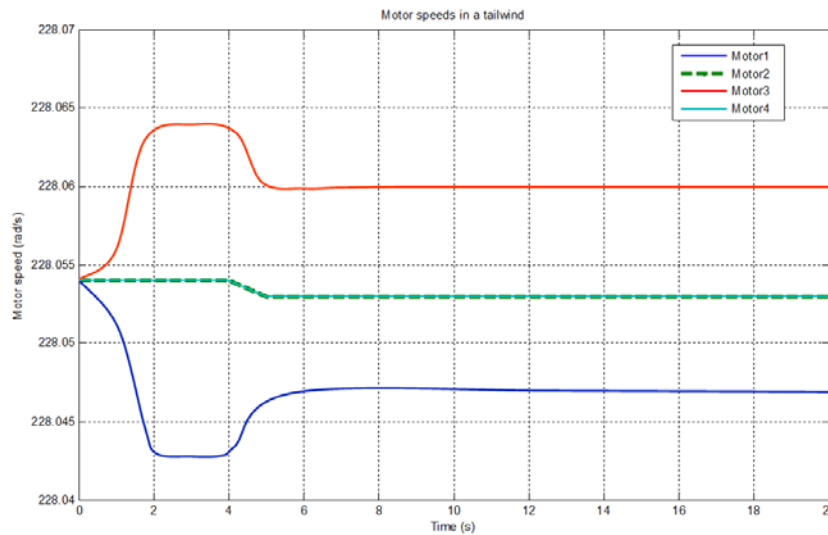
Figure 8-11: Graph showing the speeds of the four motors of the quad-rotor in a constant tailwind

8.3.2 Gusty Tailwind

Just like in the case of a gusty headwind, the gusty tailwind also has turbulence added in the form of a Gaussian random displacement, with a variance of 0.5m/s. The quad-rotor is expected to fly to the same position (66.15, 0, 1) from the start point. The wind flow varying between 0.5m/s and 1.5m/s in the direction of flight of the helicopter requires that the

175

controller quickly re-arranges the speeds of the motors at different times to reduce the quad-rotor's resultant speed to the desired speed. The effects of the gusty tailwind on the quad-rotor helicopter are seen from the graphs in figure 8-12.

Again the curves show a number of crests and troughs in the quad-rotor velocity and pitch angle owing to the changing wind speeds at different times. The controller compensates at different times by changing the thrust, enabling the vehicle to accurately track the reference path at the required speed, though it took about 0.6 seconds less to arrive at the destination because of the push of the gusty tailwind.

(a) Quad-rotor and wind speeds.

(b) Roll and pitch angles.

(c) X-displacement.

(d) Y-displacement.
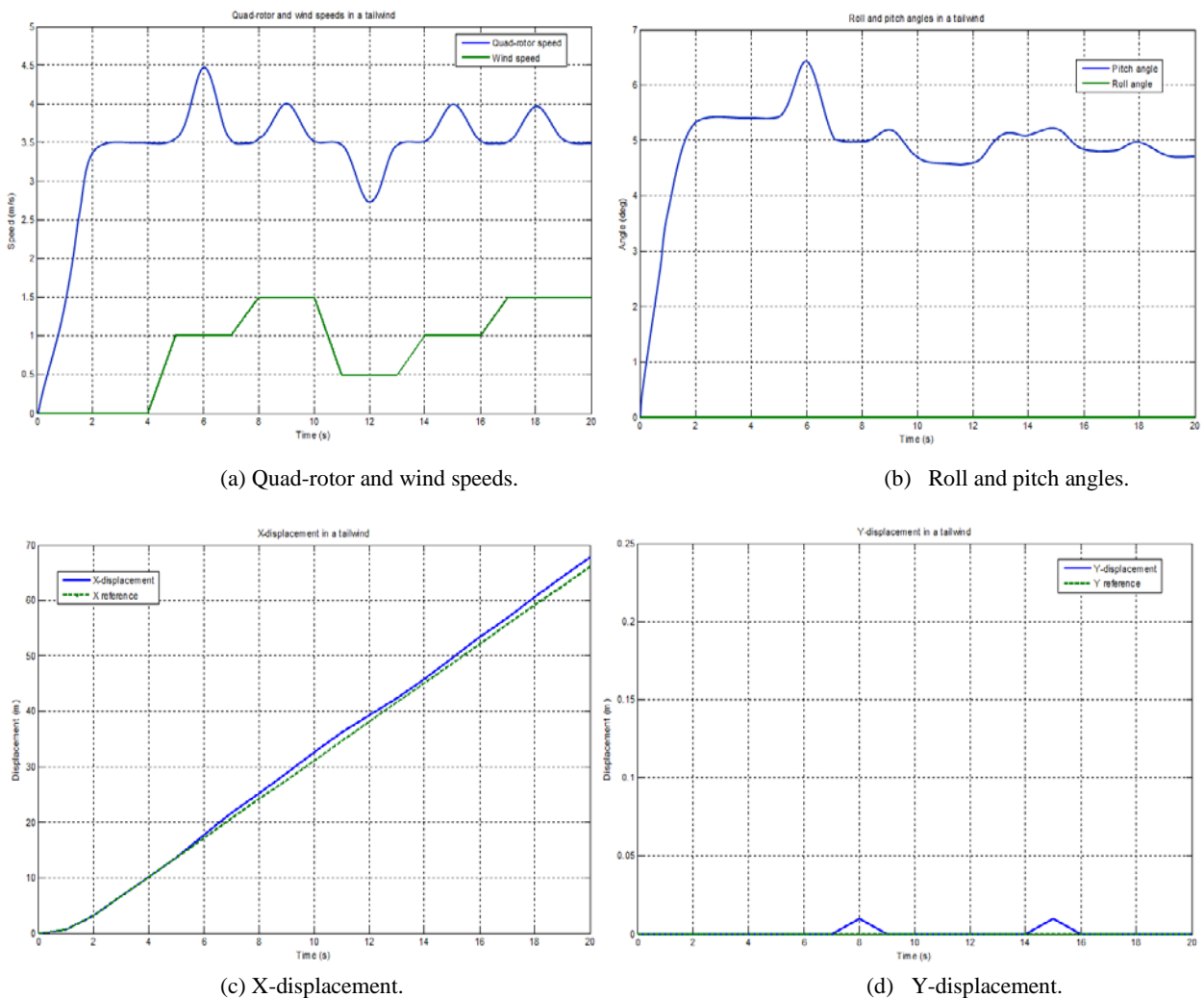
Figure 8-12: Graph showing the helicopter parameters in a gusty tailwind

Figure 8-13 shows how the controller compensates, by re-arranging the motor speeds to quash the effect of the disturbance. The curves for motors 1 and 3 are seen to be changing within very short intervals in response to the changing wind speed, which adds to the speed of the helicopter. The arrangement of the motor speeds is seen to be carefully done so as to

keep the thrust and torque imbalance to the barest minimum in order to maintain the altitude and keep the commanded zero yaw angle.
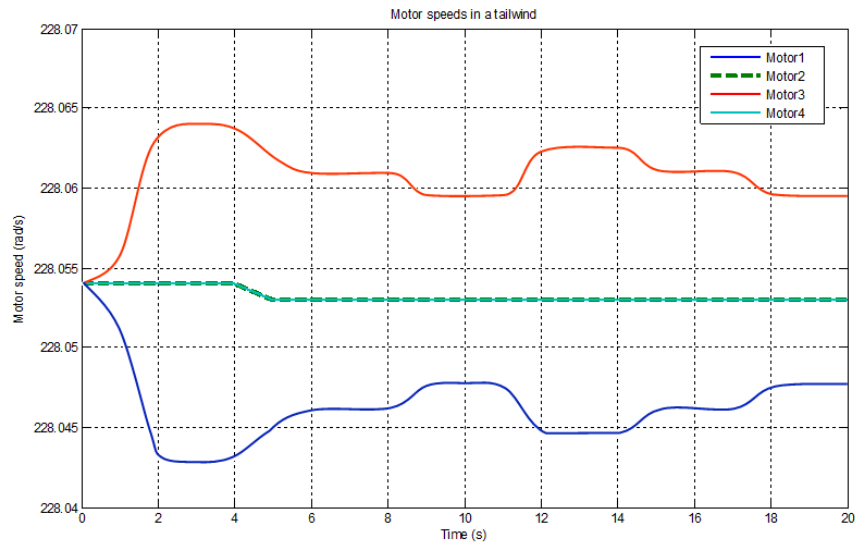
Figure 8-13: Graph showing the speeds of the four motors of the quad-rotor in a gusty tailwind

8.4 Flight Simulation in a Crosswind

A crosswind would normally create an in-plane force that acts on the vehicle and tends to create a moment that makes the quad-rotor helicopter tilt. The instant the quad-rotor starts to tilt, it accelerates in its direction of tilt. However, too much of a tilt would make the quad-rotor to start loosing equilibrium, thereby leading to a possible oscillation and loss of control of the whole vehicle. Only a timely and accurate re-arrangement of the motor speeds can maintain that equilibrium, keeping the quad-rotor in the planned path and desired speed.

8.4.1 Constant Crosswind

This simulation study describes a situation where the wind hits the quad-rotor from the side, giving it a resultant speed and trying to make it deviate from the planned path. The quad-rotor is again required to fly northwards to the same position (66.15, 0, 1) from the start point. The desired flight path is maintained from the start of the flight until a crosswind of 1.5m/s blowing towards the east is encountered. This causes a little deviation of about 0.2m to the east, before the controller is able to compensate and return the quad-rotor to the planned path and desired speed.
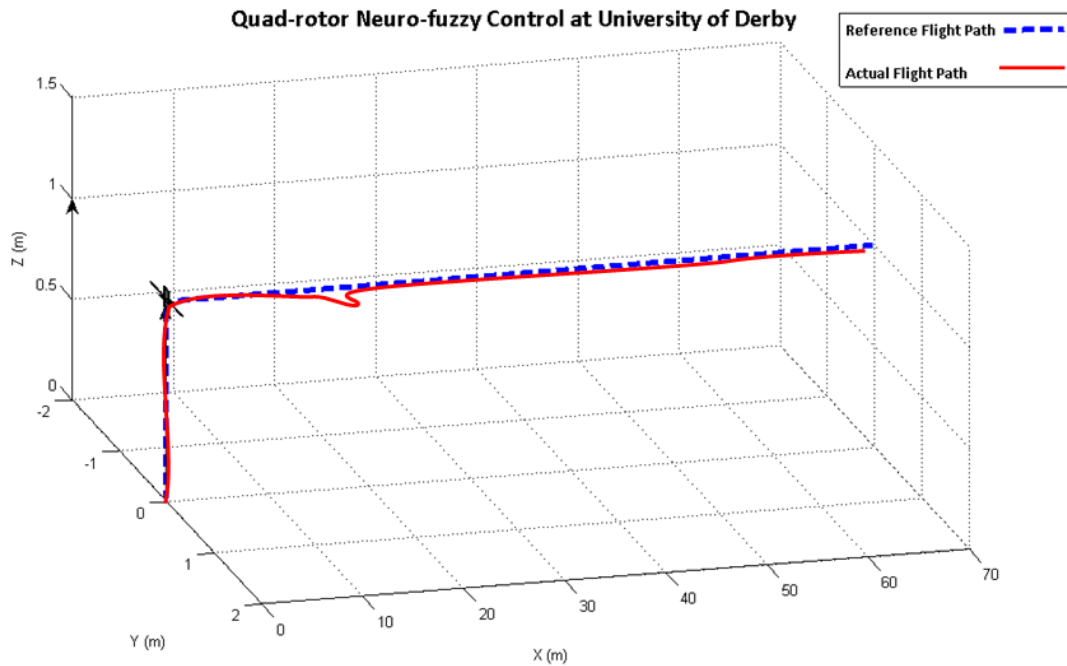
Figure 8-14: Quad-rotor flight simulation in a crosswind

As shown in graphs in figure 8-15, the wind blows from the side of the helicopter causing a disturbance, just after 4 seconds of flight. This disturbance creates a very small roll angle, tending to upset the helicopter. A resultant speed, slightly higher than the commanded speed of 3.5m/s is reached, with the pitch angle reduced and a little change in the height. The action of the controller ensures a negative roll angle and a restoration of the speed of the helicopter as commanded at the start of the flight.


(a) Quad-rotor and wind speeds.   (b) Roll and pitch angles.

178
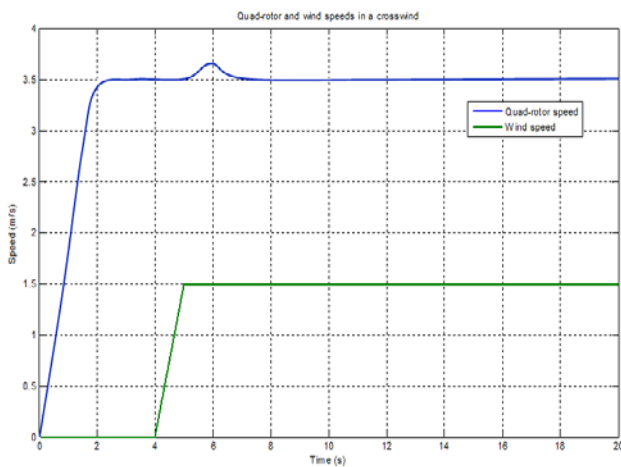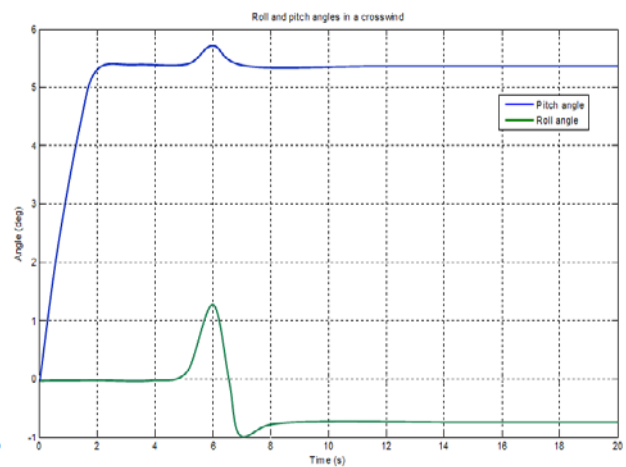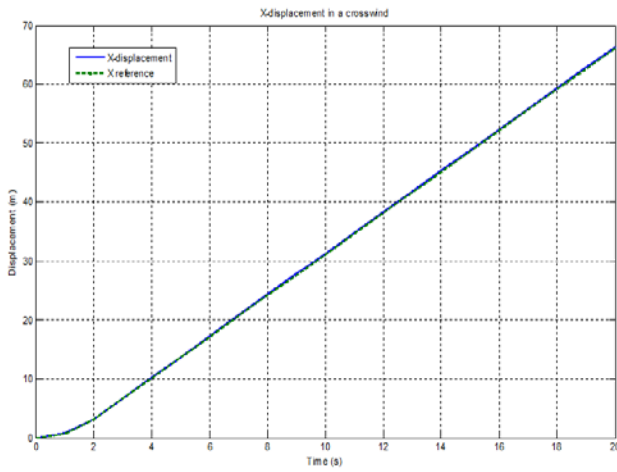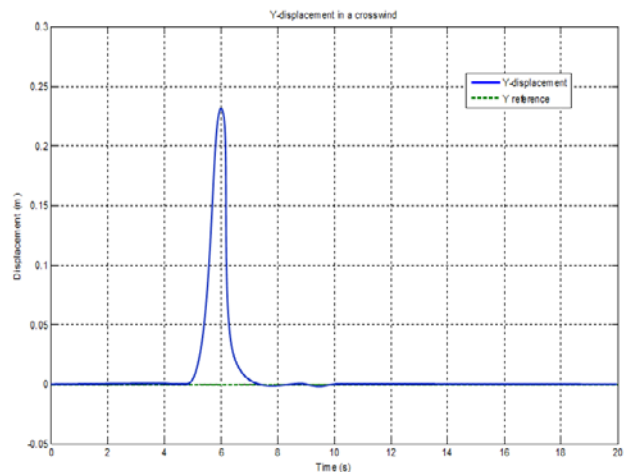
(c) X-displacement.

(d) Y-displacement.

Figure 8-15: Graph showing the helicopter parameters in a constant crosswind

The motor speed curves in figure 8-16 show the reaction of the controller when the disturbance is encountered. A constant crosswind of speed 1.5m/s in introduced after about 2 seconds of flight, blowing eastwards from the side of the helicopter to try to make it veer off course. As a result of this disturbance, the velocity of the quad-rotor is increased to a resultant velocity of 3.65 m/s in the NE direction as against the commanded speed of 3.5m/s. The change of direction from north to north-east indicates a displacement in the y-direction (east), owing to a roll angle created as a result of the disturbance. The robust controller slows down and speeds up the motors accordingly to take control of the situation. It is observed in figure 8-15 above [(c) and (d)] that the roll angle and y-displacement are reduced to a negative and zero respectively to counter the effect of the crosswind. This restores the helicopter to the commanded speed of 3.5m/s.
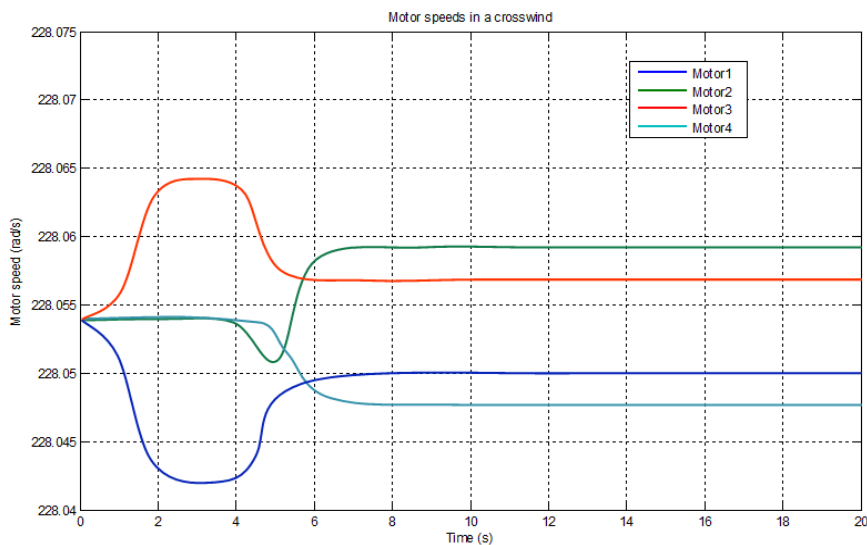
Figure 8-16: Graph showing the speeds of the four motors of the quad-rotor in a constant crosswind

179

The sideward force effect created by the crosswind, prompted the controller to increase the thrust in motor 2 and decrease that of motor 4, while keeping those of motors 1 and 3 so as to keep the desired pitch angle, yet avoiding a yaw from the reaction torque.

8.4.2 Gusty Crosswind

The gusty crosswind also has turbulence in the form of a Gaussian random displacement, with the same variance of 0.5m/s. The quad-rotor is expected to fly to the same position (66.15, 0, 1) from the start point. The side wind flow varying between 0.5m/s and 1.5m/s, tries to upset the quad-rotor, but the controller quickly re-arranges the speeds of the motors at different times to keep the helicopter on the planned path and in the desired speed. The effects of the gusty crosswind on the quad-rotor helicopter are seen from the graphs in figure 8-17.

The curves show a few crests in the quad-rotor velocity and pitch angle, but a number of crests and troughs in the roll angle as a result of the changing wind speeds at different times. This confirms the result of the constant crosswind, which shows that a crosswind mainly has an effect on the roll angle and tends to make the quad-rotor deviate from the planned path, though it adds a little to the quad-rotor speed.

A small error is present within the y position but the altitude profile is maintained despite the turbulence. The controller compensates at different times by changing the thrust and creating a roll angle in the opposite direction of flow of the crosswind to ensure that the vehicle accurately tracks the reference path at the required speed.

(a) Quad-rotor and wind speeds.   (b) Roll and pitch angles.

(c) X-displacement.

(d) Y-displacement.
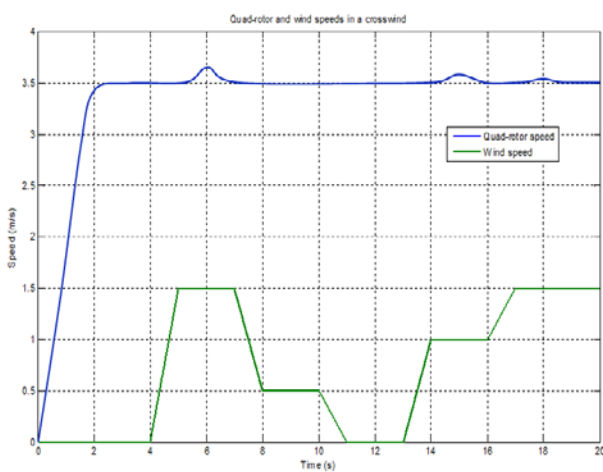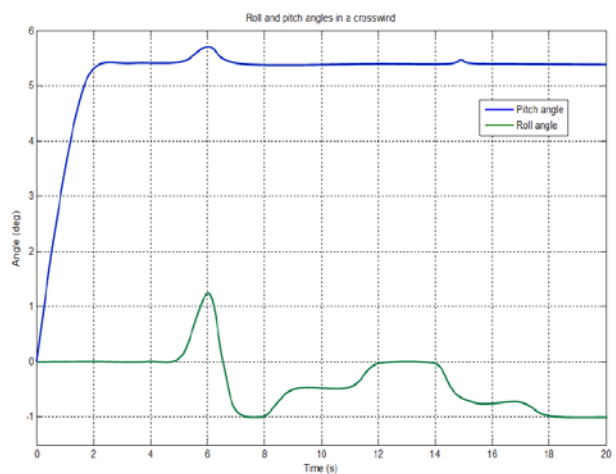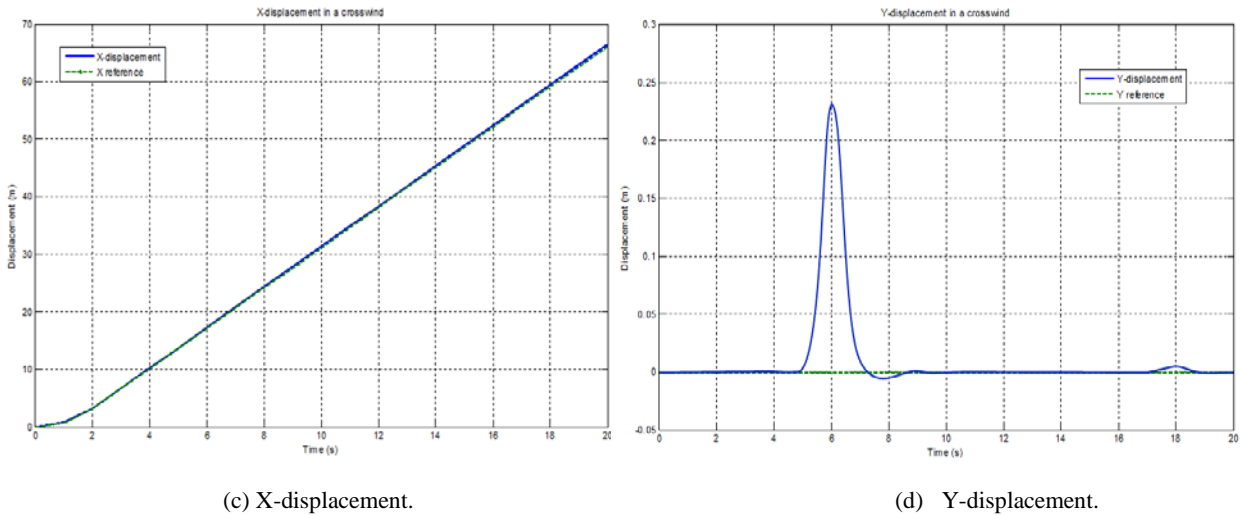
Figure 8-17: Graph showing the helicopter parameters in a gusty crosswind

The motor speed curves in figure 8-18 show the complexity of the controller action at the different points that the disturbances are encountered. The speeds of the two sets of motors are seen to be changed at different intervals to nullify the effect of the disturbance. As a result of the disturbance, the speed of the quad-rotor was increased and reduced at different times by either the disturbance or the action of the controller.
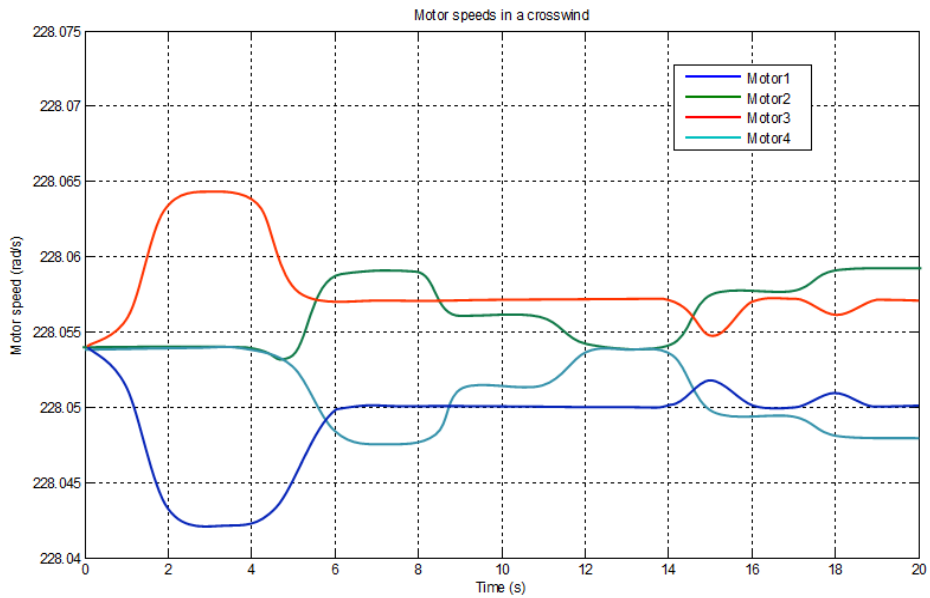
Figure 8-18: Graph showing the speeds of the four motors of the quad-rotor in a gusty crosswind

8.5 Discussion of Results

To demonstrate the robustness and effectiveness of the developed fuzzy-neural controller, a number of different situations have been considered in this chapter. At the outset, steady winds were applied along the *x* axis from the front (headwind) and from the rear (tailwind); then another steady wind was applied along the y-axis from the side (crosswind). All disturbances at this stage were kept at a constant speed of 1.5m/s.

Gusts with variance of 0.5m/s and a maximum of 1.5m/s were introduced in the simulation system in the same directions as the steady winds to test the ability of the controller to control the multi-variable flying states of the quad-rotor helicopter in complex weather conditions. The graphs in figures 8-7, 8-12 and 8-17 showing the crests and troughs at different points of increase (and decrease) of the wind speed, describe the motion of the vehicle as momentarily departing from the reference trajectory with very small tracking errors.

For all the simulation studies, the commanded flight paths and target destinations have a tolerance of 0.25m. The quad-rotor helicopter flight speed changed at different times in flight, owing to the disturbances, but the vehicle still attempted to keep up with the commanded speed and follow the planned path.

With a constant headwind opposing the flight of the vehicle, the controller had to create a larger pitch angle to keep up with the commanded speed as shown in figure 8-5 (a) and (b). A constant tailwind on the other hand created an induced velocity for the vehicle, hence the controller reduced the pitch angle to slow it down and keep it going at the required speed as shown in figure 8-10 (a) and (b). As can be seen in figures 8-7 (a) and (b) and 8-12 (a) and (b), the effects of varying speeds of the headwind and tailwind made the control problem more complex.

The lateral wind speed has a great influence on the thrust generated by the propellers, because of the aerodynamic effects. In situations where the wind speed becomes too high, the quad-rotor helicopter will find it very difficult to maintain the total vertical thrust and so the altitude control becomes difficult too. Having carried out a number of simulations, it was concluded that that the speed of the quad-rotor must not exceed 18 m/s and so a saturation block was placed on the quad-rotor speed demand to keep it in check.

This limit was set because the quad-rotor helicopter must not pitch or roll too much otherwise it would be vertically unstable. Therefore, the pitch and roll limits were set at $\theta \leq \pm28$

degrees and $\phi \leq \pm 28$ degrees, because the speed of the quad-rotor helicopter is a function of the tilt angles of pitch and roll respectively. Consequently, saturation blocks were also placed on the pitch and roll angle demands to maintain the altitude and ensure more stability in flight. This effect is also confirmed in the works of [54, 57] and also demonstrated in the figures in appendix E.

The major effect of the crosswind is to deflect the flight path in the direction of the wind by adding another vector component to the ground speed, with the aerodynamic lift force depending on the speed of the wind. The controller had to roll the quad-rotor in opposition to the wind as shown in figure 8-15 (a) and (b), so as to maintain its course. These simulation studies highlight the advantage of Fuzzy-Neural Networks over a linear tracking controller in following a reference speed and flight path, as it accounts for environmental changes such as the presence of a disturbance such as wind.

Generally, when flying forward the quad-rotor is expected to maintain a negative pitch angle, creating a horizontal component of the total thrust to overcome the drag of the airframe and the in-plane forces over the rotors. The problem of loss of altitude is always encountered when the quad-rotor starts a horizontal movement from hover and it even gets worse when there are strong winds. The total vertical thrust is supposed to be maintained, thereby keeping the helicopter at a constant height, but because of the thrust vector, this becomes difficult to achieve. However, the fuzzy-neural controller has been able to keep the altitude steady by increasing the total thrust when necessary and ensuring that if there is any loss, it is reduced to the barest minimum.

The simulation results have shown the ability of the controller to reject disturbances - as seen from the very small position and tracking errors. In situations where the disturbance is not rejected, the quad-rotor helicopter is seen to quickly return to the reference path as a result of the recovery action of the controller. The controller in re-arranging the speeds of the motors was able to compensate, enabling the quad-rotor to reach its destination – though at some times taking about 0.5 seconds longer than the required time.

8.6 Towards Implementation

The focus in this section is on the practical implementation of the control system that has been developed during the research. The test-bed for the experiments would normally consist of a complete quad-rotor helicopter, a ground station with computer, a radio base-station and remote control as shown in figure 8–19.

The control algorithms are implemented on the ground station computer and run directly in the Matlab/Simulink software environment. A special S-function block allows the Simulink model to receive sensor data from the quad-rotor and to send back the motor input commands. The block communicates via USB with the computer module in the ground station. The sample rate is limited at 50 Hz by the speed of the wireless data link. All radio communication is done in short packets with minimum latency in such a way that during the sample period of 20 ms the sensors are sampled on the quad-rotor, the data is sent over radio to the ground station and then through USB to the Simulink model, the results of the control algorithm are in turn sent back through radio to the quad-rotor to control the electric motors.

The remote control uses the same two-way communication link to send commands to either the quad-rotor or the computer (i.e. for reference inputs) and can also display important process variables to the pilot on the ground.
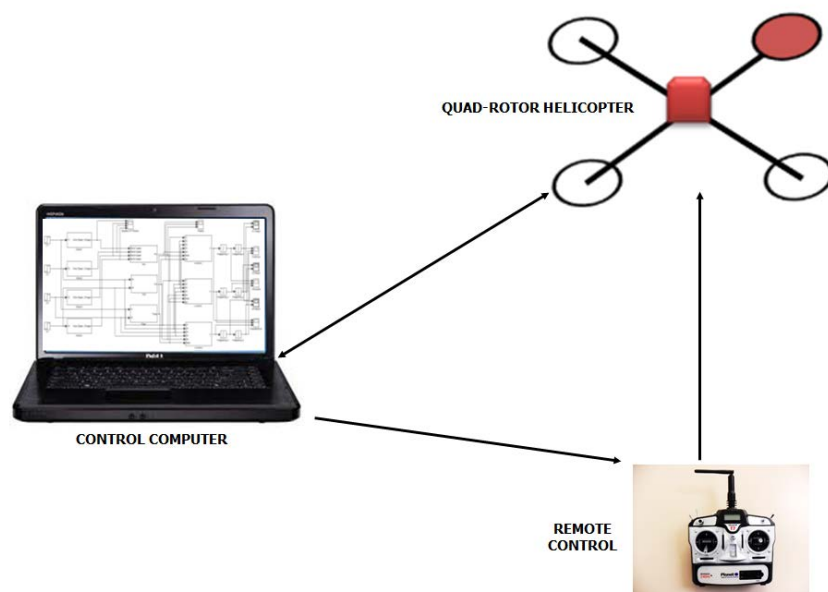
Figure 8-19: Flight experiment control system

For such small vehicles flying outdoors, the real-world task of closing the loop by providing feedback is always challenging. Larger UAVs have Inertial Navigational and Guidance Systems that provide accurate rate and acceleration information as well as a GPS for positional information. However, GPS is usually only accurate to a few meters which may not be adequate for a small UAV such as the quad-rotor helicopter.

Quad-rotor state estimation using visual feedback is a possible option, since there is a reduced dependency on GPS in areas where such signals are unavailable and since cameras are reasonably affordable and not too heavy for a payload [1, 39]. However, this is a major research component that is not within the scope of this research work.

The miniaturization of electrical components provides another alternative to these traditional systems. There are a number of commercial autopilots, offering a range of functionalities that can be fitted onto the quad-rotor helicopter. The majority include Micro-Electro-Mechanical Systems (MEMS) accelerometers, gyroscopes, magnetometers and numerous analogue-to-digital converters for connection with barometric pressure sensors and dynamic pressure sensors.
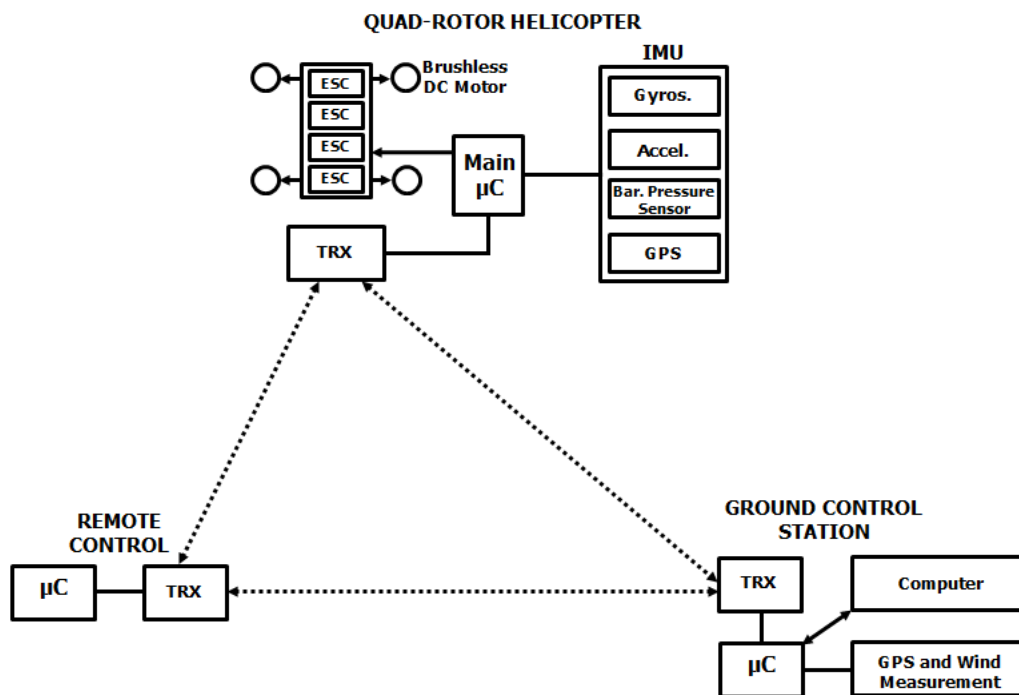
Figure 8-20: The electronic system for the quad-rotor helicopter

The variables that can be measured by the on-board sensors are:
- angular velocities in the body coordinate
- linear accelerations in the body coordinate
- the intensity of the Earth magnetic field in the body coordinates
- position and velocities in Earth coordinates (GPS)
- the altitude using the ultrasound range sensor,

- temperatures of the gyroscopes, accelerometers and magnetic field sensors for calibration,
- battery voltage and current,
- motor rotation speeds.

On-board computation of the control action is reduces time lags, however, in an experimental set up, the requirements could be different. The control law may need modification in flight or at least a quick turn-around in between flights. Furthermore, the control algorithms presented in this thesis are computationally demanding and therefore, while on-board implementation is the eventual aim, off-board computation is the initial preferred option. However, this in turn presents communication challenges with lag time being the critical factor.

It is therefore evident there is a considerable amount of work involved in the development of a suitable control system. Unfortunately, it was not possible to implement this outdoors for lack of time and the necessary equipment required for the outdoor flight experiments.

8.7 Chapter Summary

Adaptive control algorithms learn online and give controllers with guaranteed performance, even for systems whose dynamics may not be fully known. As the complexity in UAV research increases, the industry is reluctant to accept complicated theoretical solutions without a suggestion for practical implementation to prove their applicability. The previous chapters have presented the control structures, the models and some algorithms that can be used to make the quad-rotor intelligent, to allow the human pilots to provide only low-bandwidth, high-level commands without worrying about the internal dynamics of the vehicles they control, and to allow the robots to adapt to and gather knowledge about the environment.

SUMMARY, CONCLUSION AND SUGGESTED AREAS OF FUTURE RESEARCH

This chapter presents the research summary, conclusions and recommendations for quad-rotor helicopter studies in future.

9.0 Summary of the Aim and Objectives of the Research

As UAVs are reaching an exceptional level of sophistication, the interest in hovering vehicles is snowballing to meet up with the aim of missions that require the vehicle to stop mid-air and also to easily manoeuvre in small spaces. The quad-rotor helicopter is one possible solution for this with its dynamic simplicity resulting in low manufacturing costs, making it an ideal test-bed for advanced control algorithms.

The most challenging aspect of UAVs is the issue of stability and control. Accurate modelling is needed to carry out such studies on the quad-rotor helicopter.

The aim of this research as stated in chapter 2 is to demonstrate a consistent way to develop a novel robust adaptive controller for GPS-independent quad-rotor helicopters, using Fuzzy-Neural Networks; which would be used to monitor and control the non-linear, multi-variable flying states of the quad-rotor helicopter; keeping it in the planned flight path and the desired flight speed through a series of complex weather conditions.

The following objectives were set, right from the onset:

a) Development of a faithful analytical mathematical representation of the quad-rotor helicopter.

b) Investigation and evaluation of a Fuzzy-Neural network model for the quad-rotor helicopter flight controller.

c) Development of an innovative PC based controller for intelligent quad-rotor flight monitoring and control.

9.1 Research Summary and Conclusions

According to the research objectives listed above, the most exceptional features of this thesis are:

a) Analytical dynamic model of the quad-rotor

Design and analysis of control systems are usually started by carefully considering mathematical models of physical systems. The quad-rotor equations of motion were built on basic physics and aerodynamics equations, using the Newton-Euler formalism in chapter 3. An adequate dynamic system modelling of the quad-rotor helicopter involved a faithful mathematical representation of the system, normally described by differential equations. The

equations of motion of quad-rotors have been modelled and simulated using Matlab/Simulink software in chapter 4.

The model made it possible to define and predict the positions that the helicopter will reach at any point in time, by varying the speeds of the four motors. The model referred to in this contribution can be calibrated for use on any quad-rotor helicopter.

b) CFD analysis using a CAD model of the quad-rotor

A 3-D Solidworks model was developed with the same parameter values as that of the analytical dynamic model developed in Matlab/Simulink. Computational Fluid Dynamics (CFD) was then used to simulate and analyse the effects of the external environment/disturbances on the flow patterns of the quad-rotor helicopter within a given computational domain. After validation with actual flight experiment data, the model was found suitable for future analysis and prediction of the behaviour of the quad-rotor helicopter in an outdoor environment.

The use of a 3-D Solidworks model was investigated and found to significantly reduce the CFD simulation time required to create a full aerodynamics database, making it possible to model the quad-rotor static and dynamic characteristics from a limited number of time-accurate CFD simulations, preparatory to the development of a robust adaptive controller for the helicopter.

c) Verification and validation of the two quad-rotor models

Results of simulations performed with the analytical Matlab/Simulink model of the quad-rotor helicopter built in chapter 4 and those obtained using CFD on a 3-D Solidworks model of the same helicopter in chapter 5 were compared with results of real flight experiments performed at University of Essex Robot Arena. This ensured that any errors are found and fixed; it also gave a good sense of judgement on whether the simulation models and results were realistic enough to be used for the quad-rotor fuzzy-neural controller development.

d) Error compensation using artificial neural networks

A general agreement between numerical and experimental results was judged satisfactory and found to be good enough to validate the use of the CFD simulation results for future wind flow analysis and prediction of the helicopter movements, after the verification and

validation. However, in an effort to generate more reliable and accurate simulation results so as to improve the performance and control of the quad-rotor helicopter, especially in the rejection of and recovery from a disturbance; a compensation system, which adopted a post correction technique was developed to correct the error in the two models. It took inputs from the two models (Matlab/Simulink and Solidworks) developed in chapters 4 and 5 respectively. The system, having being trained with data obtained from actual flight experiments at University of Essex, computed the compensation values of the two simulation models. The output of the system was used to train the quad-rotor fuzzy-neural controller.

The use of function approximation clearly showed that a neural network is a viable technology for computing compensation values for the quad-rotor simulation errors.

e) A robust adaptive fuzzy-neural controller

A hierarchy of controllers was developed for the quad-rotor using fuzzy-neural networks, for monitoring and controlling the multi-variable flying states of the quad-rotor helicopter. At the top of the hierarchy is the position controller, which directs the movement of the quad-rotor by providing the lower level controller (the attitude controller) with the desired roll, pitch, and yaw angles in addition to the helicopter's upward velocity. The attitude controller is comprised of four lower level controllers that autonomously direct the rotor speed changes, using voltage inputs to control the four attitude variables of throttle, roll, pitch and yaw.

Many different approaches to the control and stabilization of quad-rotor helicopters have been proposed, none of which may either be completely right or wrong, because the solutions to these problems are not straight forward. Some are obviously more suited than others, depending on the situation. However, efficient control algorithms should imitate the way humans operate manned or similar vehicles as provided by fuzzy-neural control techniques.

A number of simulation studies have been considered, with some moderate wind applied in three directions at different times, causing the vehicle to momentarily depart from the reference trajectory. Obviously this is not always going to be the case with the addition of a severe wind likely to prevent the vehicle from reaching its destination, but the controller has always compensated to ensure the target is reached.

This work demonstrates a consistent way to develop a robust adaptive controller for a quad-rotor helicopter from an analytical dynamic model built in Matlab/Simulink, using Fuzzy-Neural Networks. The controller is used to monitor and control the non-linear, multi-variable

flying states of the quad-rotor helicopter; keeping it aloft in the planned path and the desired speed through a series of complex weather conditions. Results show that very stable flight can be achieved with the designed controller.

The targets of the PhD have been successfully achieved. An up to date literature review as found in chapter 2 suggests that this research is an innovative project, with a wide variety of potential applications in future, cutting across different industries.

9.2 Suggested areas for future research

Over the years, the theory of control has played a foremost role in the field of engineering and technology. The 21st century is expected to see major advancements in this field, with the swelling recognition and extensive applications of biologically-inspired concepts like neural networks and fuzzy logic.

The Quad-rotor UAV is interesting for small UAV-VTOL development, but its aerodynamics are complex and need to be accurately modelled in order to achieve precise control. Although many good works have been done, these have mostly focused on simple trajectories at low velocities with simplified models, in controlled indoor environments.

The open loop simulation with the Matlab/Simulink model provided very useful information about the indoor quad-rotor helicopter flight dynamics. For the aerodynamics of the system, the CFD simulation using a 3-D Solidworks model was used and the outdoor flight behaviour of the quad-rotor in the presence of wind disturbance was analysed. These were very useful in the design of the controller as the data generated from these models were used to train the controller.

The extension of the modelling, simulation and control methods detailed in this thesis outside of the controlled lab environment will make UAVs very useful in many practical scenarios. Quad-rotors are already in use in many military and civil applications by simply using GPS to sense the position of the vehicle, emphasizing the need for a robust adaptive controller to stabilize the vehicle. The controller developed in this thesis would make the vehicles more robust to disturbances from wind, paving way for future real time applications.

When it comes to UAV autonomy, the following categories are important aspect to be considered for further research in future:

a) Sensor fusion - combining information from different sensors for use on board the vehicle throughout the mission.

b) Communications - handling communication and coordination between multiple agents in the presence of incomplete and imperfect information to ensure that missions are successful.

c) Cooperative Tactics: Formulating an optimal sequence and spatial distribution of activities between agents in order to maximize chance of success in any given mission scenario.

d) UAV Endurance - the maximum flight duration of unmanned aerial vehicles varies widely. Solar electric UAVs hold the potential for unlimited flight.

Certainly, there are many other areas of interest with regards to UAV research and the list is endless. The potential applications of the quad-rotor helicopter are enormous, so any new study about it will be useful and of great interest.

REFERENCES

[1] I. Cowling, Towards Autonomy of a Quad-rotor UAV. PhD Thesis, Cranfield University, UK, 2008.

[2] V. Martinez, Modelling of the Flight Dynamics of a Quad-rotor Helicopter. MSc Thesis, Cranfield University, UK, 2007.

[3] M. D. Schmidt, Simulation and Control Of a Quad-rotor Unmanned Aerial Vehicle. University of Kentucky, 2011.

[4] J. G. Leishman, Principles of Helicopter Aerodynamics. New York, Cambridge University Press 2000.

[5] N. Sacco, How the Draganflyer Flies. Rotary Magazine, http://www.rctoys.com/pdf/draganyer3 rotorymagazine.pdf (accessed on 15th May 2013).

[6] P. Pounds, R. Mahony, and P. Corke, Modelling and Control of a Large Quad-rotor Robot. Control Engineering Practice, 18(7), pp. 691-699, 2010.

[7] J. Villbrandt, Quad-rotors Coming of Age. https://illumin.usc.edu/162/the-quadrotors-coming-of-age/3/ (accessed on 11th June 2013).

[8] Z. Sarris, Survey of UAV Applications in Civil Markets. STN ATLAS-3Sigma AE and Technical University of Crete DPEM, 73100 Chania, Crete, Greece, 2001.

[9] H. I. Macdonald, An Innovative Robot Aircraft for Atmospheric Monitoring. Parliament house, 1998.

[10] E. Guizzo, Aeryon Scout Quad-rotor Spies on Bad Guys from above. IEEE Spectrum Robotics blog, 2011.

[11] T. Bobbe, The Role of UAV Technology in Forest Service Natural Resource Management. USDA Forest Service Remote Sensing Applications Centre Salt Lake City, Utah, 2005.

[12] K. D. Atherton, 5 Ways Drones Could Help in a Disaster like the Boston Marathon Bombing. http://www.popsci.com/technology/article/2013-04/5-drones-help-disaster-boston-marathon-bombing5-ways-in-which-drones-help-in-a-disaster/ (accessed on 15th May 2013)

[13] R. D'Angelo and R. Levin, Design of an Autonomous Quad-rotor UAV for Urban Search and Rescue. Worcester Polytechnic Institute, 2011.

[14] S. Ahrens and D. Levine, Vision Aided Navigation in Unknown Environments. http://acl.mit.edu/projects/visionaidednav.html (accessed on 15th April 2013).

[15] P. Connie, and H. T. Liu, A Co-operative UAV/UGV Platform for Wildfire Detection and Fighting. System Simulation and Scientific Computing, Asia Simulation Conference-7th International Conference on IEEE, 2008.

[16] A. Ollero, J. R. Martinez-de-Dios and L. Merino, Unmanned Aerial Vehicles as tools for forest-fire fighting. International Conference on Forest Fire Research, 2006.

[17] ABC TV, Remote-control Helicopters with Cameras. http://www.abc.net.au/news/2012-02-21/drone-journalism-sydney/3842766 (accessed on 15th May 2012).

[18] M. Cutler, Design and control of an Autonomous Variable-Pitch Quad-rotor Helicopter. S. M Thesis, Massachusetts Institute of Technology, 2012.

[19] R. Jonsson, UPenn's GRASP Lab unleashes a swarm of Quad-rotors. http://www.gizmag.com/grasp-nano-quadrotor-robots-swarm/21302/ (accessed on 15th May 2013).

[20] W. Kazmi, M. Bisgaard, F. Garcia-Ruiz, K. D. Hansen and A. la Cour-Harbo, Adaptive Surveying and Early Treatment of Crops with a Team of Autonomous Vehicles. Aalborg University, Denmark, 2012.

[21] T. Frey, Agriculture the New Game of Drones. http://www.futuristspeaker.com/2013/08/agriculture-the-new-game-of-drones/ (accessed on 29th August 2013).

[22] Dennis, Canada's Aeryon Labs in Prime Position to help Quad-rotor Micro UAVs go Mainstream. http://novus2.com/uav360/blog/page/13/ (accessed on 15th May 2013).

[23] P. Pounds, R. Mahoney, P. Hynes and J. Roberts, Design of a four-rotor Aerial Robot. In Proceedings of Australian Conference on Robotics and Automation, Auckland, New Zealand, 2002.

[24] T. Dodd, Development of a Mini Uninhabited Air Vehicle for Urban Environments. In IET Seminar on Micro UAV's, Austin Court, Birmingham, UK, 2007.

[25] P. Castillo, R. Lozano and A. E. Dzul, Modelling and Control of Mini-Flying Machines. Springer, 2005.

[26] P. Castillo, P. Albertos, P. Garcia and R. Lozano, Simple Real-time Attitude Stabilization of a Quad-rotor Aircraft with Bounded Signals. In Proceedings of the 45th IEEE Conference on Decision and Control, San Diego, CA, USA, pp. 1533–1538, 2006.

[27] S. Bouabdallah, Design and Control of Quad-rotors with Application to Autonomous Flying. PhD thesis, Ecole Polytechnique Federale de Lausanne, 2007.

[28] A. Mokhtari, A. Benallegue and Y. Orlov, Exact Linearization and Sliding Mode Observer for a Quad-rotor Unmanned Aerial Vehicle. International Journal of Robotics and Automation 21(1), 39 – 49, 2006.

[29] T. Madani and A. Benallegue, Control of a Quad-rotor Mini Helicopter via Full State Back-stepping Technique. In Proceedings of 45th IEEE Conference on Decision Control, San Diego, CA, USA, pp. 1515–1520, 2006.

[30] A. Mokhtari and A. Benallegue, Dynamic Feedback Controller of Euler Angles and Wind Parameters Estimation for a Quad-rotor Unmanned Air Vehicle. In IEEE International Conference on Robotics and Automation, New Orleans, LA, pp. 2359–2366, 2004.

[31] A. Tayebi and S. McGilvray, Attitude Stabilization of a four-rotor Aerial Robot. In Proceedings of 43rd IEEE Conference on Decision Control, Bahamas, 2004.

[32] A. Tayebi, and S. McGilvray, Attitude Stabilization of a VTOL Quad-rotor Aircraft. IEEE Transactions on Control Systems Technology 14(3), 562–571, 2006.

[33] M. Chen and M. Huzmezan, A Simulation Model and H_∞ loop Sharing Control of a Quad-rotor Unmanned Air Vehicle. In IASTED International Conference on Modelling and Simulation, Palm Springs, California, 2003.

[34] B. J. Driessen and A. L. Robin, A Globally Convergent Tracking Controller for the X4-flyer Rotorcraft for Reference Trajectories with Positive Thrust. In Robotica, Part 4, pp. 375–388, 2004.

[35] L. Beji and A. Abichou, Streamlined Rotors Mini Rotorcraft: Trajectory Generation and Tracking. International Journal of Control, Automation and systems 3(1), 87–99, 2005.

[36] M. Valenti, B. Bethke, G. Fiore and J. P. How, Indoor Multi-vehicle Flight Test-bed for Fault Detection, Isolation, and Recovery. In Proceedings of AIAA Conference on Guidance, Navigation and Control, 2006.

[37] S. L. Waslander, G. Hoffmann, J. S. Jang and C. J. Tomlin, Multi-agent Quad-rotor Test-bed Control Design: Integral Sliding Mode vs. Reinforcement Learning. In IEEE/RSJ International Conference on Intelligent Robots and Systems. pp. 468–473, 2005.

[38] G. Hoffmann, D. G. Rajnarayan, S. L. Waslander, D. Dostal, J. S. Jang and C. J. Tomlin, The Stanford Test-bed of Autonmous Rotorcraft for Multi Agent Control (STARMAC). In Proceedings of 23rd Digital Avionics Systems Conference, Salt Lake City, Utah, 2004.

[39] E. Altug, J. P. Ostrowski and R. Mahony, Control of a Quad-rotor Helicopter using Visual Feedback. In Proceedings of IEEE Conference on Robotics and Automation, Washington DC, 2002.

[40] E. Altug and C. Taylor, Vision-based Pose Estimation and Control of a Model Helicopter. In Proceedings of IEEE Mechatronics, Istanbul, Turkey, 2004.

[41] V. K. Chitrakaran, D. M. Dawson, H. Kannan and M. Feemster, Vision Assisted Autonomous Path following for Unmanned Aerial Vehicles. In Proceedings of 45th IEEE Conference on Decision and Control, San Diego, CA, pp. 63–68, 2006.

[42] T. Hamel, R. Mahony and A. Chriette, Visual Servo Trajectory Tracking for a four rotor VTOL Aerial Vehicle. In Proceedings of IEEE International Conference on Robotics and Automation, Washington DC, pp. 2781–2786, 2002.

[43] C. Nicol, C. J. B. Macnab and A. Ramirez-Serrano, Robust Neural Network Control of a Quad-rotor Helicopter, 2008.

[44] J. Ces´Areo Raim´Undez, and A. Fern´andez Villaverde, Adaptive Tracking Control for a Quad-Rotor. In ENOC, St Petersburg, Russia, 2008.

[45] K. Miller, Path Tracking Control for Quad-rotor Helicopters, 2008.

[46] T. Bresciani, Modelling, Identification and Control of a Quad rotor Helicopter. MSc Thesis, Lund University, Sweden, 2008.

[47] Y. AI-Younes and M. A. Jarrah, Attitude Stabilization of Quad-rotor UAV using Backstepping Fuzzy Logic and Backstepping Least-Mean-Square Controllers. In Proceedings of the 5th International Symposium on Mechatronics and its Applications (ISMA08), Amman, Jordan, 2008.

[48] D. M. W. Abeywardena, L. A. K. Amaratunga, S. A. A. Shakoor and S. R. Munasinghe, A Velocity Feedback Fuzzy Logic Controller for Stable Hovering of a Quad Rotor UAV. In Proceedings of Fourth International Conference on Industrial and Information Systems, ICIIS, Sri Lanka, 2009.

[49] T. Dierks and S. Jagannathan, Neural Network Control of Quad-rotor UAV Formations. American Control Conference Hyatt Regency Riverfront, St. Louis, MO, USA, 2009.

[50] G. V. Raffo, M. G. Ortega, F. R. Rubio, An Integral Predictive/Nonlinear H_∞ Control Structure for a Quad-rotor Helicopter. Automatica, 2010.

[51] S. Theerasak, L. Pined, C. Wonlop and N. Itthisek, Path Tracking of UAV Using Self-Tuning PID Controller Based on Fuzzy Logic. SICE Annual Conference, Taipei, Taiwan, 2010.

[52] T. Dierks and S. Jagannathan, Output Feedback Control of a Quad-rotor UAV using Neural Networks. In IEEE Transactions on Neural Networks, Vol. 21, No. 1, 2010.

[53] R. He, S. Prentice, and N. Roy, Planning in Information Space for a Quad-rotor Helicopter in a GPS-denied Environment. International Conference on Robotics and Automation, 2008.

[54] C. Balas, Modelling and Linear Control of a Quad-rotor. MSc Thesis, Cranfield University, UK, 2007.

[55] T. Lee, M. Leok, and N. McClamroch, Geometric Tracking Control of a Quad-rotor UAV on SE(3). In Proceedings of the IEEE Conference on Decision and Control, 2010.

[56] M. Hehn and R. D'Andrea, Quadrocopter Trajectory Generation and Control. In IFAC World Congress, 2011.

[57] P. E. Stingu, Intelligent Control and Cooperation for Mobile Robots. PhD Thesis, University of Texas at Arlington, 2011.

[58] D. Mellinger, Trajectory Generation and Control for Quad-rotors. PhD Thesis, University of Pennsylvania, 2012.

[59] M. C. Javier, Quad-rotor UAV for Wind Profile Characterization. University of Madrid, Spain, 2012.

[60] A. Kushleyev, D. Mellinger, C. Powers, and V. Kumar, Towards a Swarm of Agile Micro Quad-rotors. Journal of Autonomous Robots, Vol. 35, Issue 4, pp. 287–300, 2013.

[61] M. Abdolhosseini, Y. M. Zhang, and C. A. Rabbath, An Efficient Model Predictive Control Scheme for an Unmanned Quad-rotor Helicopter. Journal of Intelligent and Robotic Systems, Vol. 70, Issue 1-4, pp. 27–38, 2013.

[62] K. Alexis, G. Nikolakopoulos and A. Tzes, On Trajectory Tracking Model Predictive Control of an Unmanned Quad-rotor Helicopter Subject to Aerodynamic Disturbances. Asian Journal of Control, Vol. 16, Issue 1, pp. 209–224, 2014.

[63] J. D. Anderson, Computational Fluid Dynamics: the basics with applications. New York, NY: McGraw-Hill, Inc, 1995.

[64] A. S Pawar, Computational Fluid Dynamics: An Emerging Field in Engineering. Journal of Engineering Research and Studies, 2012.

[65] Flow Science. http://www.flow3d.com/apps/microfluidics/medical-devices.html (accessed on 15th May 2013).

[66] Leap Australia, Computational Fluid Dynamics (CFD). http://www.computationalfluiddynamics.com.au/join-leap-at-the-2013-australian-international-airshow/ (accessed on 15th August 2013)

[67] R. C. Nelson and A. Pelletier, The Unsteady Aerodynamics of Slender Wings and Aircraft Undergoing Large Amplitude Manoeuvres. Progress in Aerospace Sciences, Vol. 39, No. 2, pp. 185–284, 2003.

[68] W. A. Silva, Application of Nonlinear Systems Theory to Transonic Unsteady Aerodynamics Responses. Journal of Aircrafts, Vol. 30, No. 5, pp. 660–668, 1993.

[69] M. Tobak and L. B. Schiff, On the Formulation of the Aerodynamic Characteristics in Aircraft Dynamics. NASA TRR–456, 1976.

[70] R. Liebe, Flow Phenomena in Nature: A Challenge to Engineering Design. WIT Press, Southampton, Great Britain, 2007.

[71] A. Schutte, G. Einarsson, A. Raichle, B. Schoning, W. Monnich and T. Forkert, Numerical Simulation of Manoeuvring Aircraft by Aerodynamic, Flight Mechanics, and Structural Mechanics Coupling. Journal of Aircrafts , Vol. 46, No. 1, pp. 53–64, 2009.

[72] M. Ghoreyshi, D. Vallespin, A. Da Ronch, K. J. Badcock, J. Vos and S. Hitzel, Simulation of Aircraft Manoeuvres based on Computational Fluid Dynamics. AIAA Paper, 2010.

[73] M. Ghoreyshi, A. Jir´asek and R. M. Cummings, CFD Modeling for Trajectory Predictions of a Generic Fighter Configuration. AIAA Paper, 2011.

[74] P. Lisandrin, G. Carpentieri and M. van Tooren, Investigation over CFD-based Models for the Identification of Nonlinear Unsteady Aerodyanmics Responses. AIAA Journal, Vol. 44, No. 9, pp. 2043–2050, 2006.

[75] D. R. McDaniel, R. M. Cummings, K. Bergeron, S. A. Morton, and J. P. Dean, Comparisons of CFD Solutions of Static and Maneuvering Fighter Aircraft with Flight Test Data. Journal of Aerospace Engineering, Vol. 223, No. 4, pp. 323–340, 2009.

[76] J. Juang, System Identification of a Vortex Lattice Aerodynamic Model. NASA TM-2001-211229, 2001.

[77] M. Ghoreyshi, M. L. Post, R. M. Cummings, A. D. Ronch and K. J. Badcock, Transonic Aerodynamic Loads Modelling of X-31 Aircraft Pitching Motions. AIAA Journal, Vol 51, No 10, pp. 2447-2464, 2013.

[78] M. Hayati and Y. Shirvany, Artificial Neural Network Approach for Short Term Load Forecasting for Illam Region. International Journal of Electrical, Computer, and System Engineering, 2007.

[79] L. N. Long and A. Gupta, Scalable Massively Parallel Artificial Neural Networks, AIAA Journal, 2005.

[80] L. C. Jain and N.M. Martin, Fusion of Neural Networks, Fuzzy Systems and Genetic Algorithms: Industrial Applications, CRC Press LLC, 1998.

[81] J. Bur ken, P. S. Williams-Hayes, J. Kaneshige, and S. Stachowiak, Reconfigurable Control with Neural Network Augmentation for a Modified F-15 Aircraft. Technical Report TR-2006-213678, NASA, 2006.

[82] P. Melin and O. C. Castillo, Adaptive Intelligent Control of Aircraft Systems with a Hybrid Approach Combining Neural Networks, Fuzzy logic and Fractal Theory. Applied Soft Computing, vol. 3, pp. 353-362, 2003.

[83] B. S. Kim and A. J. Calise, A Nonlinear flight control using neural networks. Journal of Guidance, Control and Dynamics, vol. 20, pp. 26- 33, 1997.

[84] B. R. Valluru, C++ Neural Networks and Fuzzy Logic, M&T Books, IDG Books Worldwide, Inc, 1995.

[85] S. F. Wu, C. J. H. Engelen, R. Babuska, Q. P. Chu and J. A. Mulder, Fuzzy Logic based Full-envelope Autonomous Flight Control for an Atmospheric re-entry Spacecraft. Control Engineering Practice, vol 11, no 1, pp 11-25, 2003.

[86] L. I. Larkin, A Fuzzy Logic Controller for Aircraft Flight Control. In Sugeno M. Ed Industrial Applications of Fuzzy Control, North Holland. Amsterdam, pp 87-103, 1985.

[87] M. Livchitz, A. Abershitz, U. Soudak and A. Kandel, Development of an Automated Fuzzy Logic based Expert System for Unmanned Landing. Fuzzy Sets and Systems, vol 93, pp 145-159, 1998.

[88] D. Atherton, Control Engineering: An Introduction with the use of Matlab. Ventus Publishing, 2009.

[89] A. Bousbaine, M. H. Wu and G. T. Poyi, Modelling and Simulation of a Quad-rotor Helicopter. 6th IET International Conference on Power Electronics, Machines and Drives (PEMD), Bristol, UK, 2012.

[90] G. Milionis, A Framework for Collaborative Quad-rotor – Ground Robot Missions. Naval Postgraduate School, Monterey, Carlifornia, USA, 2011.

[91] B. L. Stevens and F. L. Lewis, Aircraft Control and Simulation. John Willey & Sons, Inc, 2003.

[92] Y. A. Khan, Modeling and Neural Control of Quad-rotor Helicopter. Saarbrücken: LAP, 2010.

[93] D. Halidey, R. Resnik and J. Walker, Fundamentals of Physics. John Willey & Sons, Inc, 2008.

[94] Matlab, The Language of Technical Computing. www.mathworks.co.uk/products/matlab (accessed on 15th July 2013).

[95] G. H. Saunders, Dynamics of Helicopter Flight. Wiley-Interscience, 1975.

[96] E. Altug, J. P. Ostrowski and R. Mahony, Control of a Quad-rotor Helicopter using Visual Feedback. International Conference on Robotics and Automation, 2002.

[97] D. Hunt, Computational Fluid Dynamics. Tessella Support Services PLC, 2005.

[98] G. T. Poyi, M. H. Wu, A. Bousbaine, and B. Wiggins, Validation of a Quad-rotor Helicopter Matlab/Simulink and Solidworks Models. IET International Conference on Control and Automation, Birmingham, UK, 2013.

[99] J. E. Matsson, An Introduction to Solidworks Flow Simulation 2012. SDC Publications, 2012.

[100] T. Petrila and D. Trif, Basics of Fluid Mechanics and Introduction to Computational Fluid Dynamics, vol 3, Springer, 2005.

[101] M. Ragheb, Aerodynamics of Rotor Blades, 2012.

[102] J. Oyekan, Towards Autonomous Patrol Behaviour on a Military Unmanned Aerial Vehicle, MSc Thesis, University of Essex, 2008.

[103] G. T. Poyi, M. H. Wu, A. Bousbaine and D. Harmanto, Quad-rotor CFD Simulation and Analysis with Artificial Neural Networks Error Compensation. Applied Mechanics and Materials (AMM) Journal, 2013.

[104] A. R. S. Bramwell, Helicopter Dynamics. Edward Arnold Ltd, 1976.

[105] Fuzzy Logic Controller in Simulink. http://www.mathworks.co.uk (accessed on 15th August 2013).

[106] E. Abbasi, M. J. Mahjoob and R. Yazdanpanah, Control of Quad-rotor UAV using a Fuzzy System for Tuning the PID Gains in Hovering Mode, University of Tehran, Iran, 2010.

[107] J. F. Shepherd III and K. Tumer, Robust Neuro-Control for a Micro Quad-rotor. Oregon State University, Corvallis, OR, USA, 2010.

APPENDIX A: MATLAB/SIMULINK MODEL

The analytical dynamic model simulates the flight dynamics of the quad-rotor helicopter. It is essential for many reasons, including the fact that it enables realistic constraints to be included in the control algorithm. The model as shown in Figure A-1 has a total of 10 subsystems, with four of them simulating the actuator dynamics (the actuator subsystem – being that the quad-rotor has four electric motors), three of them simulating the angular accelerations (pitch, roll and yaw subsystems) and the last three simulating the linear accelerations (x-motion, y-motion and z-motion subsystems).

The dynamics represent the physics of the quad-rotor and provide the position, velocity and acceleration of both linear and angular quantities. The inputs, labelled V_1, V_2, V_3 and V_4 are the voltages, which serve as motor control inputs for the brushless DC motors. Outputs of the actuator subsystems are the angular velocities of the propellers (rad/s). These serve as inputs to the yaw subsystem, which computes the yaw angular acceleration. The other subsystems labelled roll, pitch, x-motion, y-motion and z-motion are also fed with the same motor speed control inputs. The outputs can be selected at will from the variables available, some of which are $x, y, z, u, v, w, \varphi, \theta, \psi, p, q, r$.
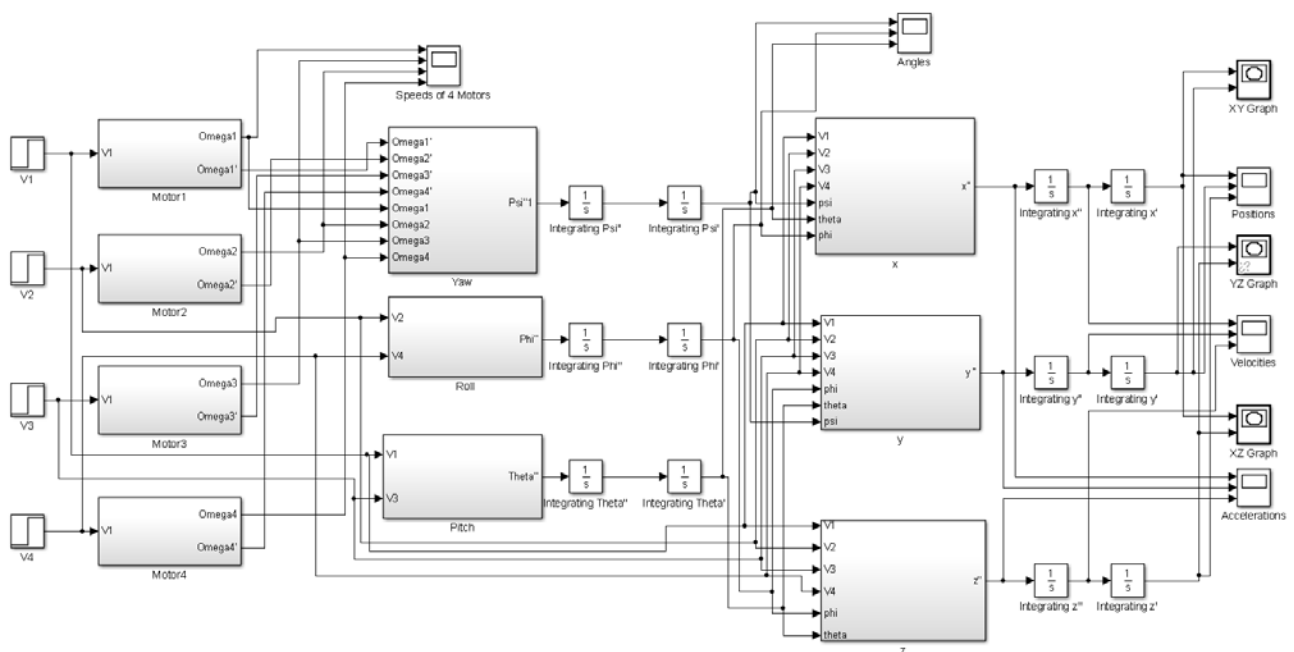
Figure A-1: Quad-rotor Non-linear Simulink Model

In order to evaluate the model's response to changes in voltage inputs, a 3-D visualization system was included in the simulation system as shown in figure A-2. This allows for the analysis of the position and the orientation of the quad-rotor, hence verifies its performance.
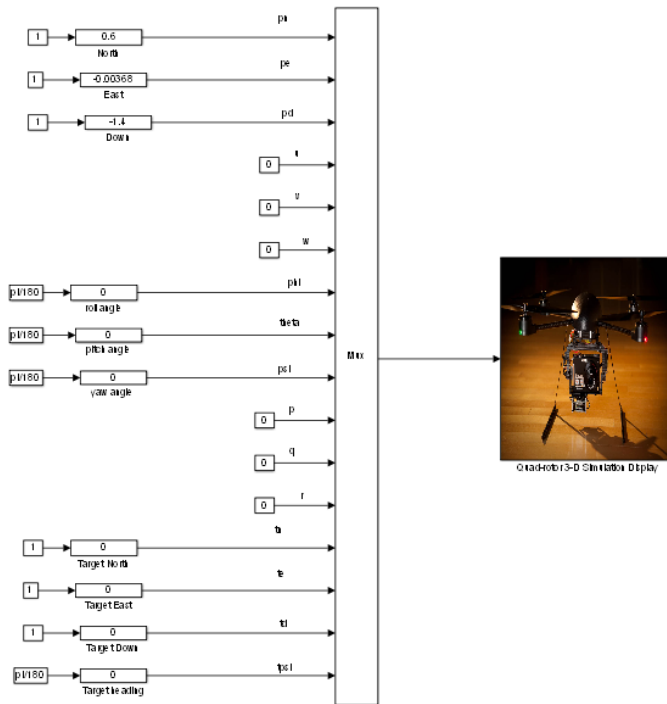
Figure A-2: 3-D simulation display

The figures A-1 and A-2 were used for all simulations within this thesis.

APPENDIX B: QUAD-ROTOR SOLIDWORKS 3-D CAD MODEL

Computer-aided design (CAD) is the use of computer systems to create, modify, analyse, or optimize a design. CAD software is used to increase the productivity of the designer, improve the quality of design, improve communications through documentation, and to create a database for manufacturing. CAD output is often in the form of electronic files for print, machining, or other manufacturing operations.

Building a CAD model of the quad-rotor helicopter commonly begins with a 2-D draft of the helicopter parts. The draft comprises of geometry such as points, lines, arcs, conics and etc. Measurements are then added to the draft to outline the size and positions of the geometry. The relationships between the parts such as their intersections at tangents, their being perpendicular or parallel or concentric are normally used to define attributes. With its parametric nature, SolidWorks allows the measurements and relations to drive the geometry. The measurements in the draft can be organized individually, or by relationships to other parameters inside or outside of the draft.

Motor

The quad-rotor's actuation mechanisms are designed as shown in figure B-1. Once one is designed, it can be replicated to make up all the four motors required for the assembly.
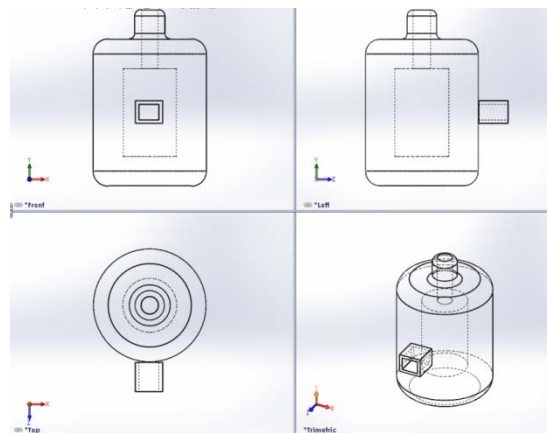
Figure B-1: CAD electric motor design

Arm

The quad-rotor arm shown in figure B-2 forms a major part of the cross-frame, explained in chapter 1 of this thesis. There are four of them for this assembly. At the end of each arm is a fixed motor mount to which the electric motor is attached.
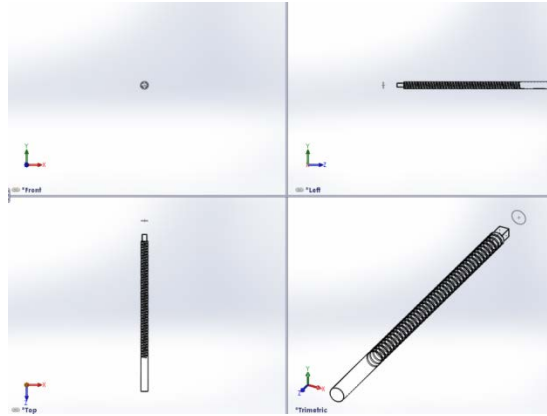
Figure B-2: CAD quad-rotor arm design

Propeller

The propeller blades are used to generate the aerodynamic thrust for lifting and maneuvering the quad-rotor. They have to be designed as airfoils with high aspect ratio in a shape that minimizes drag from tip vortices as shown in figure B-3. Each propeller is directly attached to a motor.
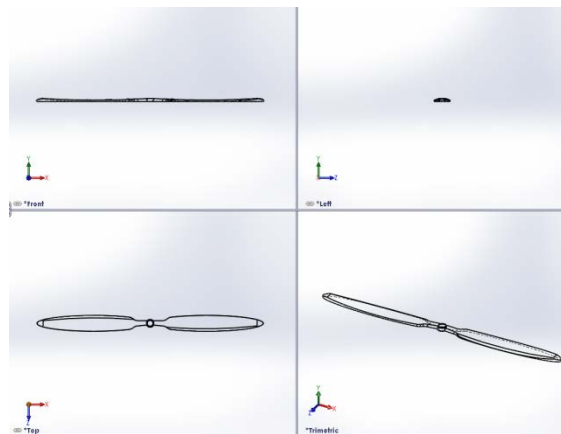
Figure B-3: CAD quad-rotor propeller design

Central Hub

The cross-frame (the four arms) passes through the center of the central hub, which houses the electronics in a flat bay area as shown in figure B-4. Provisions can be made underneath the central hub for a payload such as camera or robotic arm, depending on the mission for which the quad-rotor is designed.
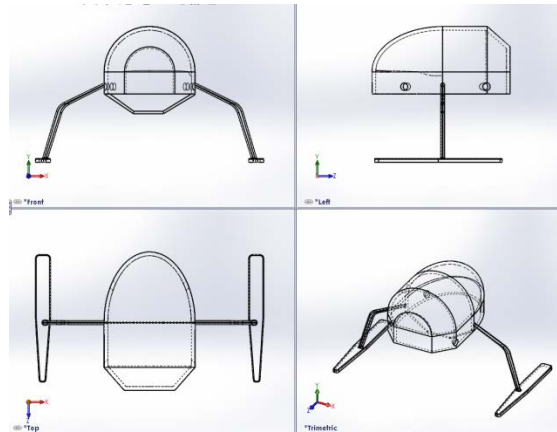
Figure B-4: CAD quad-rotor central hub design

Landing Gear

Quad-rotors could have different types of landing gears. However, it should be as light as possible, but strong enough to withstand any forceful landing as shown in figure B-5.
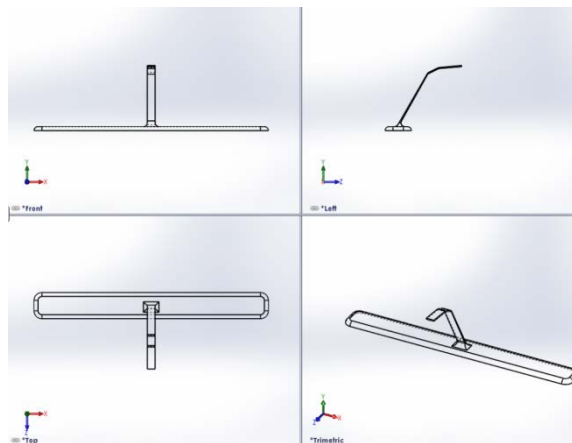
Figure B-5: CAD quad-rotor landing gear design

Payload

The camera payload is normally attached to the cross-frame, directly under the central hub. With it, the quad-rotor can do amazing stuff, when it comes to photography as it flies around. A very light weight camera as shown in figure B-6 has been included in this assembly.
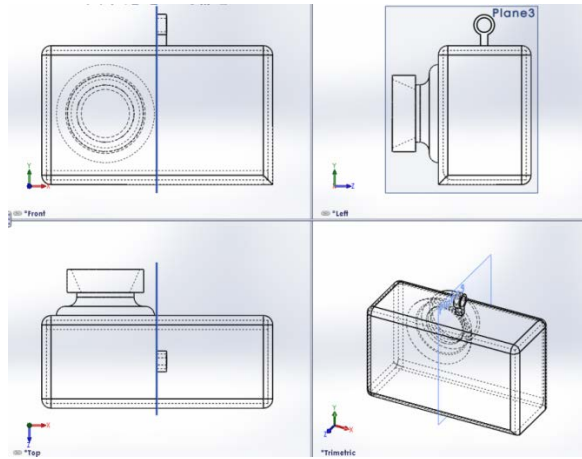
Figure B-6: CAD quad-rotor camera payload design

Once all the necessary parts of the assembly are designed, they are fit together to finish the assembly as shown in figure B-7. This assembly can then be used for any type of CFD simulation.

Figure B-7: CAD quad-rotor assembly

APPENDIX C: SAMPLE OF MODEL SIMULATION RESULTS

Throttle Command

MATLAB/ SIMULINK (outputs - motor speeds, angles and accelerations)													SOLIDWORKS (output – forces)					
Motor Speeds (rad/s)	Angles (deg)						Accelerations (m/s²) / Forces (N) [F = ma]						Forces (N) / Accelerations (m/s²) $[a = \frac{F}{m}]$					
Ω_1	Ω_2	Ω_3	Ω_4	θ (Pitch)	φ (Roll)	ψ (Yaw)	X		Y		Z		X		Y		Z	
							a	F	a	F	a	F	F	a	F	a	F	a
226.2251				0	0	0	0	0	0	0	-0.0006	-0.0004	0	0	0	0	0	0
	226.2251																	
		226.2251																
			226.2251															
226.2808				0	0	0	0	0	0	0	0.0055	0.0036	0	0	0	0	0	0
	226.2808																	
		226.2808																
			226.2808															
230.4342				0	0	0	0	0	0	0	0.4697	0.3053	0	0	0	0	0.2200	0.3385
	230.4342																	
		230.4342																
			230.4342															
241.2847				0	0	0	0	0	0	0	1.7597	1.1438	0	0	0	0	1.0563	1.6251
	241.2847																	
		241.2847																
			241.2847															
251.8294				0	0	0	0	0	0	0	4.0486	2.6316	0	0	0	0	2.2247	3.4226
	251.8294																	
		251.8294																
			251.8294															
262.0927				0	0	0	0	0	0	0	6.0851	3.9553	0	0	0	0	3.7024	5.696
	262.0927																	
		262.0927																
			262.0927															
272.0961				0	0	0	0	0	0	0	9.3481	6.0763	0	0	0	0	5.7965	8.9177
	272.0961																	
		272.0961																
			272.0961															
281.8584				0	0	0	0	0	0	0	11.0934	7.2107	0	0	0	0	6.8333	10.5128
	281.8584																	
		281.8584																
			281.8584															
291.3961				0	0	0	0	0	0	0	15.502	10.0763	0	0	0	0	9.2430	14.2200
	291.3961																	
		291.3961																
			291.3961															
300.7242				0	0	0	0	0	0	0	18.7938	12.2160	0	0	0	0	11.9826	18.4347
	300.7242																	
		300.7242																
			300.7242															

Roll Command

	MATLAB/ SIMULINK (outputs - motor speeds, angles and accelerations)												SOLIDWORKS (output – forces)					
Motor Speeds (rad/s)				Angles (deg)			Accelerations (m/s²) / Forces (N) [F = ma]						Forces (N) / Accelerations (m/s²) $[a = \frac{F}{m}]$					
Ω_1	Ω_2	Ω_3	Ω_4	θ (Pitch)	Φ (Roll)	ψ (Yaw)	X		Y		Z		X		Y		Z	
							a	F	a	F	a	F	F	a	F	a	F	a
227.6706	227.6666	227.6706	227.6745	0	-2	0	0	0	0.3496	0.2272	0.1529	0.0994	0	0	0.1050	0.1615	0.0500	0.0769
227.6706	227.6627	227.6706	227.6785	0	-4	0	0	0	0.6988	0.4542	0.1346	0.0875	0	0	0.3902	0.6003	0.0460	0.0708
227.6706	227.6588	227.6706	227.6824	0	-6	0	0	0	1.0472	0.6807	0.1041	0.0677	0	0	0.5903	0.9082	0.0410	0.0631
227.6706	227.6548	227.6706	227.6863	0	-8	0	0	0	1.3943	0.9063	0.0615	0.0400	0	0	0.8307	1.2780	0.0386	0.0594
227.6706	227.6509	227.6706	227.6903	0	-10	0	0	0	1.7396	1.1307	0.0068	0.0044	0	0	0.9984	1.5360	0.0320	0.0492
227.6706	227.6469	227.6706	227.6943	0	-12	0	0	0	2.0877	1.3570	-0.0609	-0.0396	0	0	1.1092	1.7065	0.0294	0.0452
227.6706	227.6429	227.6706	227.6983	0	-14	0	0	0	2.4332	1.5816	-0.1409	-0.0916	0	0	1.4033	2.1590	0.0221	0.0340
227.6706	227.6389	227.6706	227.7023	0	-16	0	0	0	2.7756	1.8041	-0.2331	-0.1515	0	0	1.6542	2.5450	0.0183	0.0282
227.6706	227.6349	227.6706	227.7063	0	-18	0	0	0	3.1145	2.0244	-0.3374	-0.2193	0	0	1.8906	2.9086	0.0106	0.0163
227.6706	227.6309	227.6706	227.7103	0	-20	0	0	0	3.4496	2.2242	-0.4536	-0.2948	0	0	2.0973	3.2266	0.0050	0.0077

Pitch Command

	MATLAB/ SIMULINK (outputs - motor speeds, angles and accelerations)												SOLIDWORKS (output – forces)					
Motor Speeds (rad/s)				Angles (deg)			Accelerations (m/s²) / Forces (N) [F = ma]						Forces (N) / Accelerations (m/s²) $[a = \frac{F}{m}]$					
Ω_1	Ω_2	Ω_3	Ω_4	θ (Pitch)	Φ (Roll)	ψ (Yaw)	X		Y		Z		X		Y		Z	
							a	F	a	F	a	F	F	a	F	a	F	a
227.6666				2	0	0	0.3496	0.2272	0	0	0.1529	0.0994	0.1101	0.1694	0	0	0.0505	0.0777
	227.6706																	
		227.6745																
			227.6706															
227.6627				4	0	0	0.6988	0.4542	0	0	0.1346	0.0875	0.4008	0.6166	0	0	0.0468	0.0720
	227.6706																	
		227.6785																
			227.6706															
227.6588				6	0	0	1.0472	0.6807	0	0	0.1041	0.0677	0.5861	0.9017	0	0	0.0419	0.0645
	227.6706																	
		227.6824																
			227.6706															
227.6548				8	0	0	1.3943	0.9063	0	0	0.0615	0.0400	0.8811	1.3555	0	0	0.0394	0.0606
	227.6706																	
		227.6863																
			227.6706															
227.6509				10	0	0	1.7396	1.1307	0	0	0.0068	0.0044	0.9993	1.5374	0	0	0.0322	0.0495
	227.6706																	
		227.6903																
			227.6706															
227.6469				12	0	0	2.0877	1.3570	0	0	-0.0609	-0.0396	1.1955	1.8392	0	0	0.0290	0.0446
	227.6706																	
		227.6943																
			227.6706															
227.6429				14	0	0	2.4332	1.5816	0	0	-0.1409	-0.0916	1.4028	2.1582	0	0	0.0217	0.0334
	227.6706																	
		227.6983																
			227.6706															
227.6389				16	0	0	2.7756	1.8041	0	0	-0.2331	-0.1515	1.6401	2.5232	0	0	0.0179	0.0275
	227.6706																	
		227.7023																
			227.6706															
227.6349				18	0	0	3.1145	2.0244	0	0	-0.3374	-0.2193	1.8719	2.8798	0	0	0.0101	0.0155
	227.6706																	
		227.7063																
			227.6706															
227.6309				20	0	0	3.4496	2.2422	0	0	-0.4536	-0.2948	2.1755	3.3469	0	0	0.0061	0.0094
	227.6706																	
		227.7103																
			227.6706															

Yaw Command

	MATLAB/ SIMULINK (outputs - motor speeds, angles and accelerations)													SOLIDWORKS (output – forces)					
Motor Speeds (rad/s)	Angles (deg)						Accelerations (m/s²) / Forces (N) [F = ma]						Forces (N) / Accelerations (m/s²) [$a = \frac{F}{m}$]					
Ω_1	Ω_2	Ω_3	Ω_4	θ (Pitch)	φ (Roll)	Ψ (Yaw)	X		Y		Z		X		Y		Z	
							a	F	a	F	a	F	F	a	F	a	F	a
227.6761	227.6706	227.6761	227.6706	0	0	2	0	0	0	0	0.1593	0.1035	0	0	0	0	0.2141	0.3294
227.6817	227.6706	227.6817	227.6706	0	0	4	0	0	0	0	0.1596	0.1037	0	0	0	0	0.2203	0.3389
227.6872	227.6706	227.6872	227.6706	0	0	6	0	0	0	0	0.1599	0.1039	0	0	0	0	0.2262	0.3480
227.6928	227.6706	227.6928	227.6706	0	0	8	0	0	0	0	0.1602	0.1041	0	0	0	0	0.2307	0.3549
227.6983	227.6706	227.6983	227.6706	0	0	10	0	0	0	0	0.1606	0.1044	0	0	0	0	0.2365	0.3638
227.7039	227.6706	227.7039	227.6706	0	0	13	0	0	0	0	0.1609	0.1046	0	0	0	0	0.2397	0.3688
227.7094	227.6706	227.7094	227.6706	0	0	15	0	0	0	0	0.1612	0.1048	0	0	0	0	0.2432	0.3742
227.7150	227.6706	227.7150	227.6706	0	0	17	0	0	0	0	0.1615	0.1050	0	0	0	0	0.2477	0.3811
227.7205	227.6706	227.7205	227.6706	0	0	19	0	0	0	0	0.1618	0.1052	0	0	0	0	0.2501	0.3848
227.7261	227.6706	227.7261	227.6706	0	0	21	0	0	0	0	0.1621	0.1054	0	0	0	0	0.2587	0.3980

APPENDIX D: SAMPLE OF FLIGHT EXPERIMENT DATA

Time	Height (mm)	Desired Output	Throttle value	Present X Position (mm)	Desired X Position (mm)	Present Y Position (mm)	Desired Y Position (mm)
2585031	219.1174	0	0	515.5879	500	1580.662	1600
2585265	219.0924	0	1	515.6742	500	1580.592	1600
2585281	219.0919	0	1	515.62	500	1580.614	1600
2585281	219.1135	0	1	515.6428	500	1580.645	1600
2585296	219.0887	0	1	515.6744	500	1580.665	1600
2585312	219.0981	0	1	515.5722	500	1580.62	1600
2585312	219.0916	0	1	515.6461	500	1580.588	1600
2585328	219.1592	0	1	515.528	500	1580.553	1600
2585343	219.1215	0	1	515.6463	500	1580.591	1600
2585343	219.0924	0	1	515.6204	500	1580.624	1600
2585359	219.1132	0	1	515.65	500	1580.608	1600
2585375	219.1233	0	1	515.6182	500	1580.613	1600
2585375	219.1382	0	1	515.6416	500	1580.623	1600
2585390	219.1029	0	1	515.6322	500	1580.611	1600
2585390	219.1822	0	1	515.4797	500	1580.528	1600
2585406	219.0802	0	1	515.6396	500	1580.665	1600
2585406	219.1087	0	1	515.5698	500	1580.675	1600
2585421	219.105	0	1	515.657	500	1580.675	1600
2585437	219.0765	0	1	515.5884	500	1580.695	1600
2585437	219.1335	0	1	515.6006	500	1580.604	1600
2585453	219.0795	0	1	515.6195	500	1580.579	1600
2585453	219.1057	0	1	515.5947	500	1580.635	1600
2585468	219.116	0	1	515.6479	500	1580.63	1600
2585468	219.1209	0	1	515.5812	500	1580.623	1600
2585484	219.1326	0	1	515.5894	500	1580.659	1600
2585500	219.123	0	1	515.6052	500	1580.66	1600
2585515	219.0897	0	1	515.6481	500	1580.617	1600
2585546	219.1044	0	1	515.5405	500	1580.621	1600
2585562	219.1317	0	1	515.5137	500	1580.59	1600
2585578	219.0905	0	1	515.5781	500	1580.63	1600
2585609	219.0806	0	1	515.6712	500	1580.673	1600
2585625	219.0942	0	1	515.6267	500	1580.619	1600
2585640	219.1425	0	1	515.5991	500	1580.627	1600
2585656	219.1053	0	1	515.612	500	1580.572	1600
2585687	219.1007	0	1	515.6479	500	1580.588	1600
2585703	219.1322	0	1	515.5644	500	1580.546	1600
2585718	219.0935	0	1	515.6012	500	1580.627	1600
2585750	219.0842	0	1	515.6346	500	1580.65	1600
2585765	219.1148	0	1	515.6503	500	1580.603	1600
2585781	219.1302	0	1	515.6143	500	1580.661	1600
2585796	219.1039	0	1	515.6277	500	1580.595	1600

| Time	Height (mm)	Desired Output	Throttle value	Present X Position (mm)	Desired X Position (mm)	Present Y Position (mm)	Desired Y Position (mm)
2585828	219.0995	0	1	515.6162	500	1580.624	1600
2585843	219.1138	0	1	515.6106	500	1580.614	1600
2585859	219.0795	0	1	515.6521	500	1580.639	1600
2585890	219.1305	0	1	515.6695	500	1580.621	1600
2585906	219.1292	0	1	515.4652	500	1580.529	1600
2585921	219.105	0	1	515.5855	500	1580.65	1600
2585937	219.1133	0	1	515.6595	500	1580.646	1600
2585968	219.0318	0	1	515.5965	500	1580.704	1600
2585984	219.1322	0	1	515.5838	500	1580.617	1600
2586000	219.1443	0	1	515.6219	500	1580.663	1600
2586015	219.089	0	1	515.6021	500	1580.633	1600
2586046	219.0828	0	1	515.6451	500	1580.692	1600
2586062	219.0954	0	1	515.6476	500	1580.596	1600
2586093	219.1045	0	1	515.6026	500	1580.607	1600
2586109	219.1447	0	1	515.6112	500	1580.662	1600
2586125	219.0796	0	1	515.5681	500	1580.646	1600
2586140	219.126	0	1	515.6712	500	1580.589	1600
2586171	219.1075	0	1	515.5401	500	1580.638	1600
2586187	219.0887	0	1	515.5599	500	1580.583	1600
2586203	219.1071	0	1	515.6609	500	1580.699	1600
2586218	219.1234	0	1	515.6172	500	1580.631	1600
2586250	219.1455	0	1	515.5348	500	1580.56	1600
2586265	219.1215	0	1	515.6514	500	1580.57	1600
2586281	219.1678	0	1	515.5909	500	1580.567	1600
2586296	219.0992	0	1	515.6171	500	1580.66	1600
2586328	219.0724	0	1	515.5973	500	1580.67	1600
2586343	219.0947	0	1	515.5735	500	1580.61	1600
2586359	219.1184	0	1	515.5482	500	1580.614	1600
2586375	219.0874	0	1	515.642	500	1580.653	1600
2586406	219.0767	0	1	515.634	500	1580.659	1600
2586421	219.1213	0	1	515.6464	500	1580.61	1600
2586437	219.1294	0	1	515.5466	500	1580.647	1600
2586468	219.1288	0	1	515.6613	500	1580.644	1600
2586484	219.1143	0	1	515.677	500	1580.614	1600
2586500	219.0761	0	1	515.5826	500	1580.68	1600
2586515	219.0996	0	1	515.6128	500	1580.571	1600
2586546	219.0961	0	1	515.6142	500	1580.677	1600
2586562	219.1018	0	1	515.6105	500	1580.653	1600
2586578	219.1165	0	1	515.6464	500	1580.637	1600
2586609	219.1085	0	1	515.6709	500	1580.627	1600
2586625	219.0863	0	1	515.6895	500	1580.635	1600
2586640	219.0981	0	1	515.6568	500	1580.59	1600
2586656	219.1136	0	1	515.6312	500	1580.618	1600

Time	Height (mm)	Desired Output	Throttle value	Present X Position (mm)	Desired X Position (mm)	Present Y Position (mm)	Desired Y Position (mm)
2586687	219.1086	0	1	515.6532	500	1580.616	1600
2586703	219.0875	0	1	515.6154	500	1580.681	1600
2586718	219.1084	0	1	515.6049	500	1580.661	1600
2586734	219.0935	0	1	515.5886	500	1580.682	1600
2586765	219.0933	0	1	515.6729	500	1580.58	1600
2586781	219.1109	0	1	515.6059	500	1580.596	1600
2586796	219.1007	0	1	515.6382	500	1580.64	1600
2586828	219.1085	0	1	515.6739	500	1580.543	1600
2586843	219.0546	0	1	515.5886	500	1580.621	1600
2586859	219.0723	0	1	515.6282	500	1580.651	1600
2586890	219.0666	0	1	515.6189	500	1580.606	1600
2586906	219.0975	0	1	515.7095	500	1580.612	1600
2586921	219.1243	0	1	515.6832	500	1580.637	1600
2586937	219.0677	0	1	515.5527	500	1580.632	1600
2586968	219.1334	0	1	515.6182	500	1580.546	1600
2586984	219.092	0	1	515.5962	500	1580.656	1600
2587000	219.0903	0	1	515.6216	500	1580.632	1600
2587031	219.0795	0	1	515.7178	500	1580.611	1600
2587046	219.1007	0	1	515.585	500	1580.639	1600
2587062	219.091	0	1	515.6195	500	1580.649	1600
2587078	219.1591	0	1	515.6031	500	1580.55	1600
2587109	219.1247	0	1	515.614	500	1580.589	1600
2587125	219.0909	0	1	515.6566	500	1580.605	1600
2587140	219.0526	0	1	515.561	500	1580.686	1600
2587156	219.1267	0	1	515.5947	500	1580.619	1600
2587187	219.0918	0	1	515.6287	500	1580.674	1600
2587203	219.1063	0	1	515.6747	500	1580.626	1600
2587218	219.1441	0	1	515.4996	500	1580.584	1600
2587250	219.1066	0	1	515.6153	500	1580.701	1600
2587265	219.0988	0	1	515.6313	500	1580.606	1600
2587281	219.0624	0	1	515.6332	500	1580.656	1600
2587296	219.0825	0	1	515.5574	500	1580.715	1600
2587328	219.1308	0	1	515.5934	500	1580.634	1600
2587343	219.0741	0	1	515.551	500	1580.623	1600
2587359	219.1788	0	1	515.6138	500	1580.557	1600
2587390	219.1156	0	1	515.6061	500	1580.608	1600
2587406	219.08	0	1	515.6871	500	1580.617	1600
2587421	219.1246	0	1	515.6132	500	1580.663	1600
2587437	219.0819	0	1	515.589	500	1580.677	1600
2587468	219.0656	0	1	515.5996	500	1580.689	1600
2587484	219.1014	0	1	515.6455	500	1580.639	1600
2587500	219.1325	0	1	515.5158	500	1580.548	1600
2587515	219.124	0	1	515.6379	500	1580.625	1600

APPENDIX E: ADDITIONAL CONTROL SIMULATION RESULTS

No Wind Situation

In this situation, flows around the rotor blades of the helicopter are somewhat steady and the rotors assumed to be working under the same conditions, because the wind speeds in the three directions (x, y and z) were kept at 0m/s.

The vehicle follows the planned path, reaching the desired speed of 15m/s, having pitched about 23 degrees. The controller is able to keep the helicopter flying at the commanded speed and path without any deviation. As can be seen in the graphs in figure E-1, the velocity and pitch angle remain constant throughout the 20 seconds flight, after reaching their commanded values.
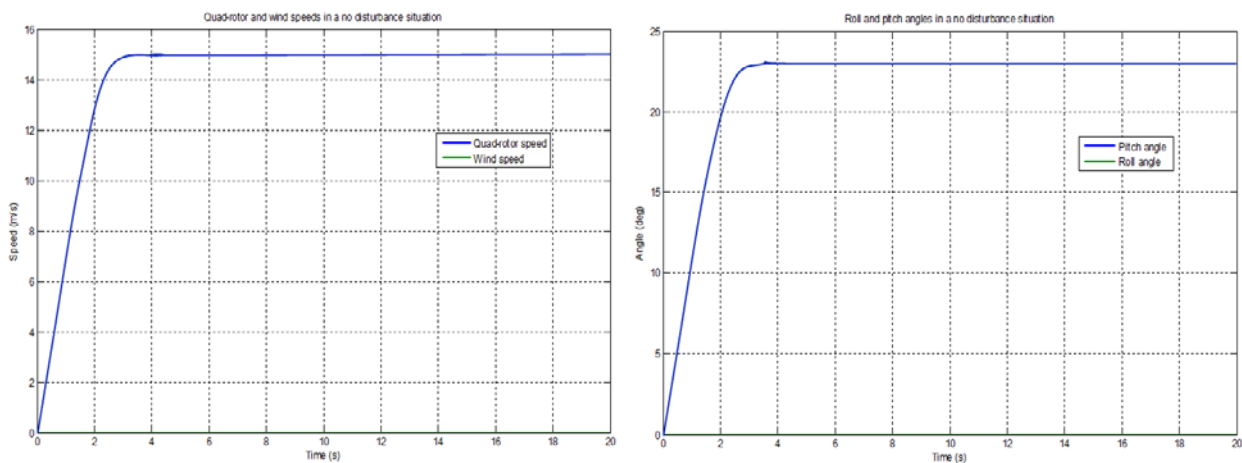
(a) Quad-rotor and wind speeds.   (b)   Roll and pitch angles.

Figure E-1: Graphs showing the helicopter parameters in a no wind situation

The curves that describe the speeds of each motor are as shown in figure E-2. Initially, the quad-rotor was at stable hover and all the rotors spin at the same speed, taking it to the reference height of 1 m. The controller then changes the speeds of motors 1 and 3 to create a pitch angle to move the quad-rotor forward, while keeping motors 2 and 4 at a constant speed. The quad-rotor reaches the commanded speed of 15m/s and experiences a stable cruise with no disturbance. The speed and flight path of the helicopter are kept as commanded by keeping speeds of the motors steady, after reaching the desired speed.

Figure E-2: Graph showing the speeds of the four motors of the quad-rotor in a no wind situation

Headwind

This study describes a situation where a constant wind opposes the flight of the quad-rotor. In a constant headwind situation, the effects of the wind slamming the front of the quad-rotor helicopter are seen from the graphs in figure E-3. After reaching the desired speed of 15m/s, a constant headwind of speed 5m/s was introduced to oppose the forward flight of the helicopter. The curves show an initial decline in the speed of the quad-rotor to 10m/s.

However, the action of the controller immediately tries to restore the speed of the helicopter to the commanded value of 15m/s without success. The curve shows clearly that the saturation block placed on the pitch angle, limits the quad-rotor to a maximum of 28 degrees (as discussed in section 8.5 of chapter 8). Therefore it keeps to that restriction in the pitch angle and only achieves a speed of 13.7 m/s. To make the quad-rotor regain its commanded speed of 15 m/s, it needs to tilt more than 28 degrees, in which case the quad-rotor becomes very unstable and difficult to control.

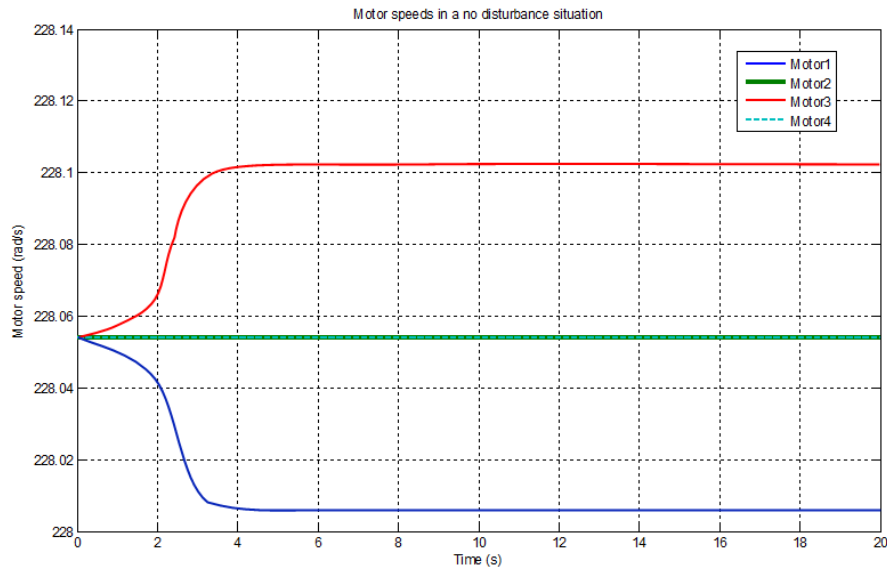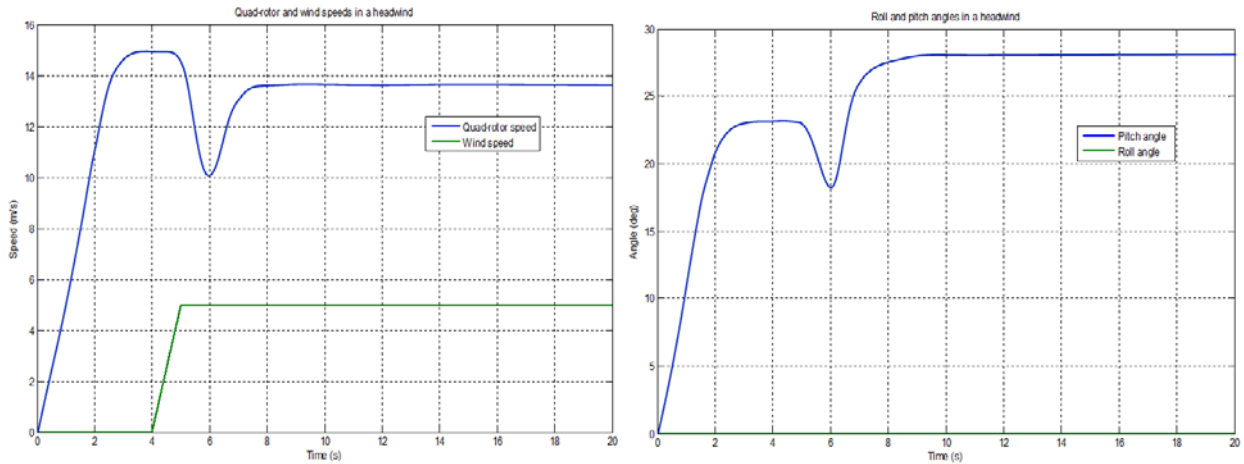(a) Quad-rotor and wind speeds.

(b) Roll and pitch angles.

Figure E-3: Graphs showing the helicopter parameters in a constant headwind

Figure E-4 shows how the controller compensates, by re-arranging the motor speeds to try to nullify the effect of the disturbance. The robust controller increases the thrust from the rear rotor by speeding up motor 3 and decreases that of the front rotor by slowing down motor 1 to take control of the situation, but because of the saturation limit, the speed of the quad-rotor falls short by about 1.3 m/s.
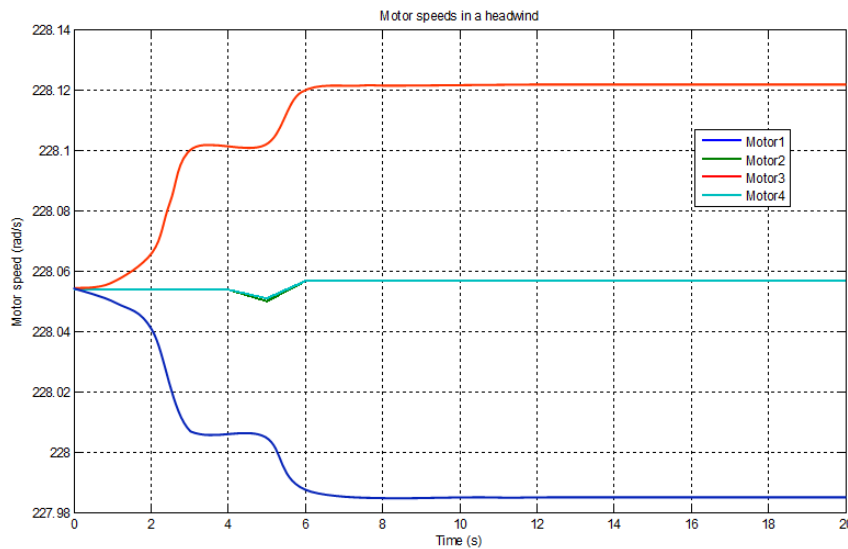
Figure E-4: Graph showing the speeds of the four motors of the quad-rotor in a constant headwind

Tailwind

This simulation study describes a situation where a constant wind hits the quad-rotor from the rear, increasing its speed and possibly making it deviate from the planned path. As the vehicle has an induced speed due to the tail wind there is need to reduce the pitch angle, so as to slow it down and keep it on course. The graphs in figure E-5 show oscillations in the quad-

216

rotor speed and pitch angle. Evidently, the speed of the quad-rotor is increased to a resultant velocity of about 20 m/s. It is also clear that the pitch angle of the helicopter is slightly increased, but the swift action of the controller reduces the pitch angle and restores the speed to the commanded value of 15m/s, ensuring flight stability despite the tailwind effect.


(a) Quad-rotor and wind speeds. (b) Roll and pitch angles.

Figure E-5: Graphs showing the helicopter parameters in a constant tailwind

In compensating for the changes as a result of the tailwind, the controller re-arranges the motor speeds to counter the effect of the wind and get it back to the commanded speed of 15m/s. Figure E-6 shows the motor speed curves. The robust controller decreases the thrust from the rear rotor by slowing down motor 3 and increases that of the front rotor by speeding up motor 1 to take control of the situation.
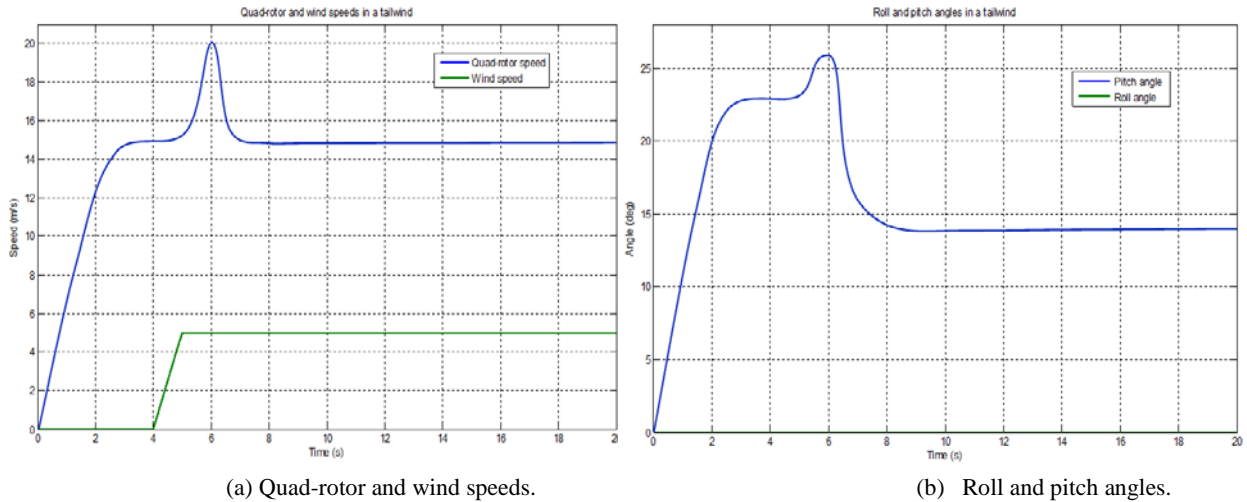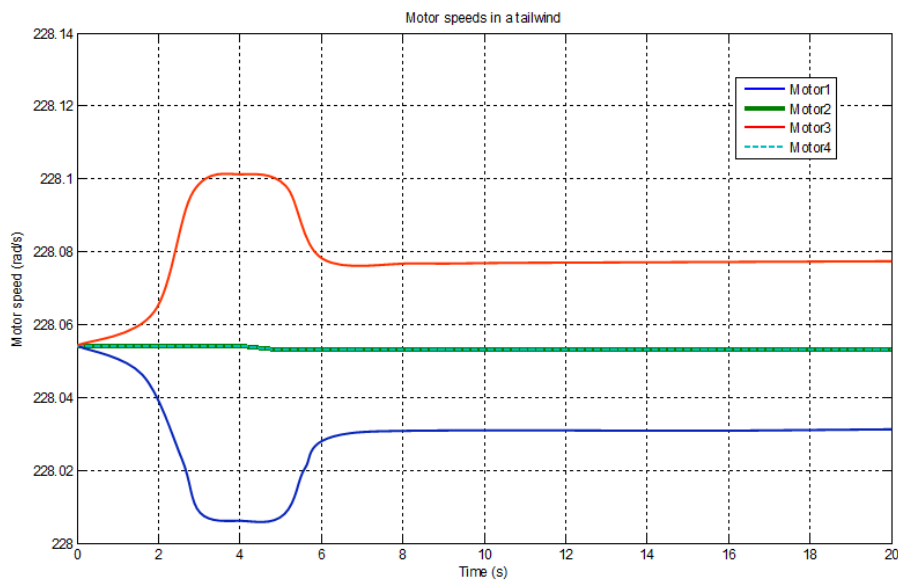

Figure E-6: Graph showing the speeds of the four motors of the quad-rotor in a constant tailwind

Crosswind

This simulation study describes a situation where the wind hits the quad-rotor from the side, giving it a resultant speed and trying to make it deviate from the planned path. As shown in graphs in figure E-7, the wind blows from the side of the helicopter causing a disturbance. This disturbance creates a small roll angle, which tends to upset the helicopter. A resultant speed, slightly higher than the commanded speed of 15m/s is reached. The action of the controller creates a negative roll angle and a restoration of the speed of the helicopter as commanded at the start of the flight.

| (a) Quad-rotor and wind speeds. | (b) Roll and pitch angles. |
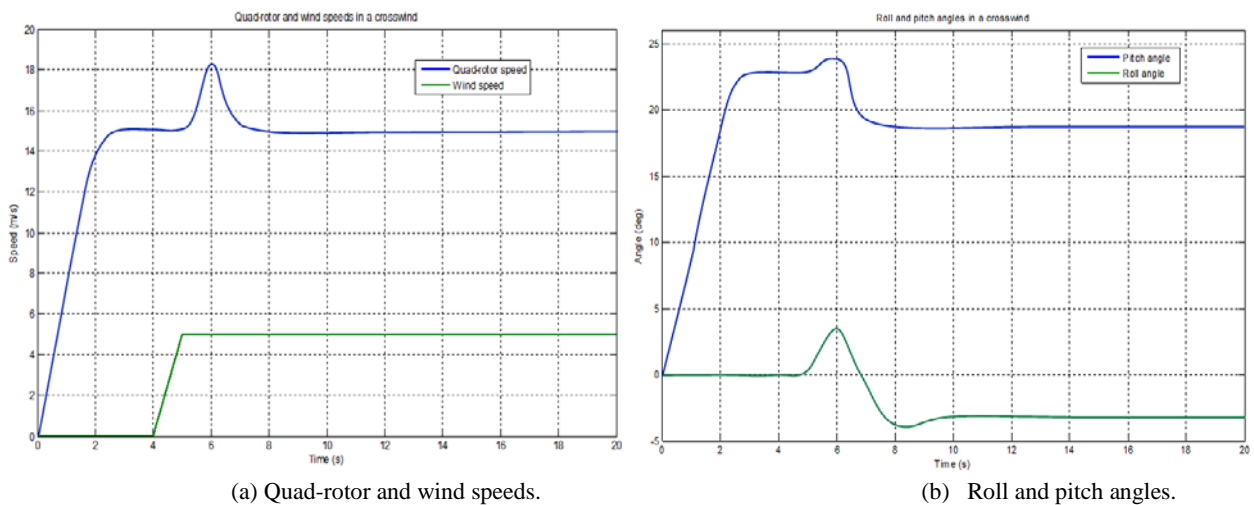
Figure E-7: Graphs showing the helicopter parameters in a constant crosswind

The motor speed curves in figure E-8 show the reaction of the controller when the disturbance is encountered. A constant crosswind of speed 5m/s in introduced, blowing eastwards from the side of the helicopter to try to make it veer off course. As a result of this disturbance, the velocity of the quad-rotor is increased to a resultant velocity of 18.3m/s in the NE direction as against the commanded speed of 15m/s. The robust controller is seen to slow down and speed up the motors accordingly to take control of the situation.

Figure E-8: Graph showing the speeds of the four motors of the quad-rotor in a constant crosswind

APPENDIX F: LINEARIZATION OF QUAD-ROTOR MODEL

Taylor series approximation

The method used in the process of linearizing the quad-rotor non-linear dynamic system of equations is Taylor series approximat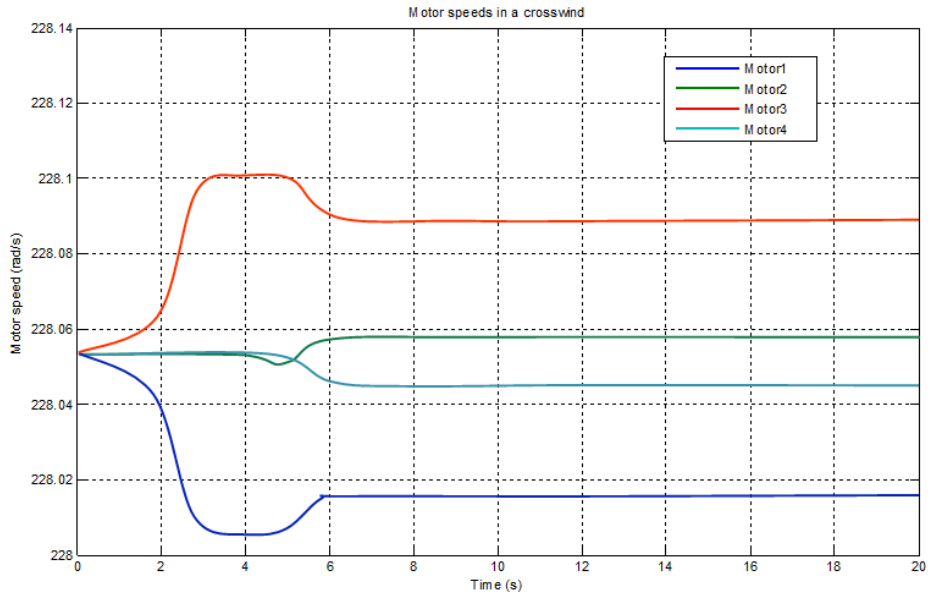ion. The approximation is done by representing a given function with a series of terms calculated from the function's derivatives at a single point known as the operating point.

$$f(x) \approx f(\bar{x}) + \frac{f'(\bar{x})}{1!}(x-\bar{x})^1 + \frac{f''(\bar{x})}{2!}(x-\bar{x})^2 + \frac{f'''(\bar{x})}{3!}(x-\bar{x})^3 + ... + \frac{f^n(\bar{x})}{n!}(x-\bar{x})^n$$

In linearizing the system equations, the first order Taylor approximation is used, written as

$$f(x) \approx f(\bar{x}) + f'(\bar{x})(x-\bar{x})\Big|_{n=1}$$

In the case of the quad-rotor the normal behaviour is when it is in stable hover. This implies that the vehicle's x-y body plane is parallel to the x-y earth plane, equivalent to a situation when the vehicle's roll, pitch and yaw angles are all equal to or close to zero. The operating input voltage that corresponds to achieving the above conditions can be calculated from the quad-rotor system equations. Here, all operating points are represented with subscript 'h'.

$$\ddot{z} = \frac{2\rho A}{m}\left[\frac{f\eta k_t}{k_q}\right]^2 \left(V_1^2 + V_2^2 + V_3^2 + V_4^2\right)(\cos\theta\cos\varphi) - g$$

With

$$\left|\begin{cases} \theta = \varphi = \psi = \dot{\theta} = \dot{\varphi} = \dot{\psi} = \ddot{\theta} = \ddot{\varphi} = \ddot{\psi} = 0 \\ \Omega = \Omega_h \\ \dot{\Omega} = \ddot{\Omega} = 0 \\ \dot{x} = \ddot{x} = \dot{y} = \ddot{y} = \dot{z} = \ddot{z} = 0 \end{cases}\right.$$

Substituting the values of all the constants from the calibration table 4-1 (chapter 4) and the conditions listed above, the following is obtained

$$0 = \left(\frac{2 \times 1.1 \times 0.08042}{0.65}\right)\left(\frac{0.5 \times 0.75 \times 0.01}{0.0056}\right)^2 \left(V_1^2 + V_2^2 + V_3^2 + V_4^2\right)(\cos 0 \cos 0) - 9.81$$

$$0 = (0.27219)(0.44842)\left(V_1^2 + V_2^2 + V_3^2 + V_4^2\right) - 9.81$$

$$0 = 0.12206 \times \left(V_1^2 + V_2^2 + V_3^2 + V_4^2 \right) - 9.81$$

Here, it is assumed that all the motors behave in exactly the same way and the design of the helicopter is symmetric; hence their voltage inputs at operating point are thought to be equal.

$$V_h = V_1 = V_2 = V_3 = V_4$$

$$0 = 0.12206 \times \left(4V_h^2 \right) - 9.81$$

$$V_h = \sqrt{20.09333}$$

$$V_h = 4.48 Volts$$

For this voltage, the speed with which the motors spin can be found at the operating point by substituting using the equation 4-1, which describes the relationship between the motor speed and voltage input.

$$V = \frac{JR\dot{\Omega}}{k_q} + k_e\Omega + \frac{RD\Omega^2}{k_q}$$

At the operating point voltage V_h, let the motor speed be Ω_h

$$V_h = \left(\frac{0.00006 \times 0.6}{0.0056} \right)\dot{\Omega} + 0.0015\Omega + \left(\frac{0.60 \times 0.00000075}{0.0056} \right)\Omega^2$$

$$4.48 = 0.00643\dot{\Omega} + 0.0015\Omega + 0.0000804\Omega^2$$

$$\dot{\Omega} = 696.73406 - 0.23328\Omega - 0.01250\Omega^2$$

Since the motor speeds remain constant at hover, $\dot{\Omega}=0$ and on substituting, the following quadratic equation is obtained

$$696.73406 - 0.23328\Omega - 0.01250\Omega^2 = 0$$

Using the almighty formula for solving quadratic equations,

$$x = \frac{-b \pm \sqrt{b^2 - 4ac}}{2a}$$

$$\Omega_h = \frac{-(-0.23328) \pm \sqrt{(-0.23328)^2 - [4 \times (-0.01250) \times 696.73406]}}{2 \times (-0.01250)}$$

$$\Omega_h = \frac{0.23328 \pm \sqrt{34.89112}}{-0.025}$$

$$\Omega_h = \frac{0.23328 + \sqrt{34.89112}}{-0.025} \text{ Or } \Omega_h = \frac{0.23328 - \sqrt{34.89112}}{-0.025}$$

$$\Omega_h = -245.61 rad/s \text{ Or } \Omega_h = 226.94 rad/s$$

By discarding the negative root of the quadratic equation, the speed at operating voltage is

$$\Omega_h = 226.94 rad/s$$

Linearization of Quad-rotor Equations

From the equation $V_h = V = 0.00643\dot{\Omega} + 0.0015\Omega + 0.0000804\Omega^2$

Let A=0.00643, B=0.0015 and C=0.0000804

This leads to

$$V = A\dot{\Omega} + B\Omega + C\Omega^2$$

Making $\dot{\Omega}$ the subject of the formula gives

$$\dot{\Omega} = \frac{V}{A} - \frac{B}{A}\Omega - \frac{C}{A}\Omega^2 = f(\Omega, V)$$

First, the coefficients of the first order Taylor series have to be found.

$$\tilde{L} = \left.\frac{\partial f}{\partial \Omega}\right|_h = -\frac{B}{A} - \frac{2C\Omega_h}{A} = \frac{-B - 2C\Omega_h}{A}$$

$$\tilde{M} = \left.\frac{\partial f}{\partial V}\right|_h = \frac{1}{A}$$

$$\frac{d}{dt}(\Delta\Omega) = \tilde{L}\Delta\Omega + \tilde{M}\Delta V$$

$$\frac{d}{dt}(\Delta\Omega) = \frac{-B - 2C\Omega_h}{A}\Delta\Omega + \frac{1}{A}\Delta V$$

$$\frac{d}{dt}(\Delta\Omega) = -5.909\Delta\Omega + 155.521\Delta V = 155.521\Delta V - 5.909\Delta\Omega$$

Where $\Delta\Omega = \Omega(t) - \Omega_h; \Delta V = V(t) - V_h$

For the roll angular acceleration,

$$\ddot{\varphi} = 4.52245\left(V_2{}^2 - V_4{}^2\right)$$

Let A= 4.52245 , then

$$\ddot{\varphi} = A\left(V_2{}^2 - V_4{}^2\right) = f(V_2, V_4)$$

At the operating point, $\varphi = \dot{\varphi} = \ddot{\varphi} = 0$

$$\tilde{L} = \left.\frac{\partial f}{\partial \varphi}\right|_h = 0$$

$$\tilde{M} = \left.\frac{\partial f}{\partial V_2}\right|_h = 2AV_2 = 2AV_h$$

$$\tilde{N} = \left.\frac{\partial f}{\partial V_4}\right|_h = -2AV_4 = -2AV_h$$

$$\frac{d}{dt}(\Delta\dot{\varphi}) = \tilde{L}\Delta\varphi + \tilde{M}\,\Delta V_2 + \tilde{N}\,\Delta V_4$$

$$\frac{d}{dt}(\Delta\dot{\varphi}) = 0 + 2AV_h\Delta V_2 - 2AV_h\Delta V_4 = 2AV_h(\Delta V_2 - \Delta V_4)$$

$$\frac{d}{dt}(\Delta\dot{\varphi}) = 2052.6496(\Delta V_2 - \Delta V_4)$$

Similarly, for the pitch angular acceleration,

$$\ddot{\theta} = 4.52245\left(V_3{}^2 - V_1{}^2\right)$$

This results in

$$\frac{d}{dt}(\Delta\dot{\theta}) = 2AV_h\Delta V_3 - 2AV_h\Delta V_1 = 2AV_h(\Delta V_3 - \Delta V_1)$$

$$\frac{d}{dt}(\Delta\dot{\theta}) = 2052.6496(\Delta V_3 - \Delta V_1)$$

For the yaw angular acceleration,

$$\ddot{\psi} = 0.004615[\dot{\Omega}_1 - \dot{\Omega}_2 + \dot{\Omega}_3 - \dot{\Omega}_4] + 0.0000577[\Omega_1{}^2 - \Omega_2{}^2 + \Omega_3{}^2 - \Omega_4{}^2]$$

Let A=0.04615 and B=0.0000577. At the operating point, $\psi = \dot{\psi} = \ddot{\psi} = 0$, since all the motors are rotating at the same speed. The Taylor series coefficients are,

$$\tilde{L} = \left.\frac{\partial f}{\partial\psi}\right|_h = 0; \qquad \tilde{M} = \left.\frac{\partial f}{\partial\Omega_1}\right|_h = 2B\Omega_1 = 2B\Omega_h; \qquad \tilde{N} = \left.\frac{\partial f}{\partial\Omega_2}\right|_h = -2B\Omega_2 = -2B\Omega_h;$$

$$\tilde{O} = \left.\frac{\partial f}{\partial\Omega_3}\right|_h = 2B\Omega_3 = 2B\Omega_h; \qquad \tilde{P} = \left.\frac{\partial f}{\partial\Omega_4}\right|_h = -2B\Omega_4 = -2B\Omega_h; \qquad \tilde{Q} = \left.\frac{\partial f}{\partial\dot{\Omega}_1}\right|_h = A;$$

$$\tilde{R} = \left.\frac{\partial f}{\partial\dot{\Omega}_2}\right|_h = -A; \qquad \tilde{S} = \left.\frac{\partial f}{\partial\dot{\Omega}_3}\right|_h = A; \qquad \tilde{T} = \left.\frac{\partial f}{\partial\dot{\Omega}_4}\right|_h = -A$$

Therefore,

$$\frac{d}{dt}(\Delta\dot{\psi}) = \tilde{L}\Delta\psi + \tilde{M}\Delta\Omega_1 + \tilde{N}\Delta\Omega_2 + \tilde{O}\Delta\Omega_3 + \tilde{P}\Delta\Omega_4 + \tilde{Q}\Delta\dot{\Omega}_1 + \tilde{R}\Delta\dot{\Omega}_2 + \tilde{S}\Delta\dot{\Omega}_3 + \tilde{T}\Delta\dot{\Omega}_4$$

$$\frac{d}{dt}(\Delta\dot{\psi}) = 2B\Omega_h(\Delta\Omega_1 - \Delta\Omega_2 + \Delta\Omega_3 - \Delta\Omega_4) + A(\Delta\dot{\Omega}_1 - \Delta\dot{\Omega}_2 + \Delta\dot{\Omega}_3 - \Delta\dot{\Omega}_4)$$

$$\frac{d}{dt}(\Delta\dot{\psi}) = 0.004615(\Delta\dot{\Omega}_1 - \Delta\dot{\Omega}_2 + \Delta\dot{\Omega}_3 - \Delta\dot{\Omega}_4) + 0.02619(\Delta\Omega_1 - \Delta\Omega_2 + \Delta\Omega_3 - \Delta\Omega_4)$$

For the vertical acceleration,

$$\ddot{Z} = 0.12206(V_1{}^2 + V_2{}^2 + V_3{}^2 + V_4{}^2)(\cos\theta\cos\varphi) - g$$

At operating point, it is assumed that all the angles are small or very close to 0 and so their cosines are approximately 1. Also, the vertical acceleration and velocity are 0, since the altitude of the vehicle is not changing.

Let A=0.12206

$$\ddot{Z} = A\left(V_1^2 + V_2^2 + V_3^2 + V_4^2\right)(\cos\theta\cos\varphi) - g = f(V_1, V_2, V_3, V_4)$$

The coefficients are

$$\tilde{L} = \left.\frac{\partial f}{\partial Z}\right|_h = 0; \qquad \tilde{M} = \left.\frac{\partial f}{\partial V_1}\right|_h = 2AV_1 = 2BV_h; \qquad \tilde{N} = \left.\frac{\partial f}{\partial V_2}\right|_h = 2AV_2 = 2AV_h;$$

$$\tilde{O} = \left.\frac{\partial f}{\partial V_3}\right|_h = 2AV_3 = 2AV_h; \qquad \tilde{P} = \left.\frac{\partial f}{\partial V_4}\right|_h = 2AV_4 = 2AV_h$$

$$\frac{d}{dt}(\Delta\dot{Z}) = \tilde{L}\Delta Z + \tilde{M}\,\Delta V_1 + \tilde{N}\,\Delta V_2 + \tilde{O}\,\Delta V_3 + \tilde{P}\,\Delta V_4$$

$$\frac{d}{dt}(\Delta\dot{Z}) = 2AV_h(\Delta V_1 + \Delta V_2 + \Delta V_3 + \Delta V_4)$$

$$\frac{d}{dt}(\Delta\dot{Z}) = 1.0937(\Delta V_1 + \Delta V_2 + \Delta V_3 + \Delta V_4)$$

Linearized Quad-rotor Model

The Simulink model of the linearized quad-rotor system is based on the equations below. The inputs of this model are the voltage control input of the motors whereas the output signals are the roll, pitch and yaw angular acceleration and the vertical acceleration.

$$\frac{d}{dt}(\Delta\Omega) = 155.521\Delta V - 5.909\Delta\Omega$$

$$\frac{d}{dt}(\Delta\dot{\varphi}) = 2052.6496(\Delta V_2 - \Delta V_4)$$

$$\frac{d}{dt}(\Delta\dot{\theta}) = 2052.6496(\Delta V_3 - \Delta V_1)$$

$$\frac{d}{dt}(\Delta\dot{\psi}) = 0.004615(\Delta\dot{\Omega}_1 - \Delta\dot{\Omega}_2 + \Delta\dot{\Omega}_3 - \Delta\dot{\Omega}_4) + 0.02619(\Delta\Omega_1 - \Delta\Omega_2 + \Delta\Omega_3 - \Delta\Omega_4)$$

$$\frac{d}{dt}(\Delta\dot{Z}) = 1.0937(\Delta V_1 + \Delta V_2 + \Delta V_3 + \Delta V_4)$$

Transfer Functions of Linear Model

When the equations of motion are linearized the transfer function of quad-rotor plant can be easily obtained by using the Laplace transform.

The Transfer function of the system, which presents the ratio of the output (angular velocity) to the input (motor voltage).

$$\dot{\Omega} = 155.521\Delta V - 5.909\Delta\Omega$$

Using the Laplace transform gives

$$s\Omega(s) + 5.909\Omega(s) = 155.521V(s)$$

$$\frac{\Omega(s)}{V(s)} = \frac{155.521}{(s + 5.909)}$$

Similarly the rest of the transfer functions of the linearized Quad-rotor model can be obtained

$$\ddot{\varphi} = 2052.6496(\Delta V_2 - \Delta V_4)$$

$$s^2\varphi(s) = 2052.6496[V_2(s) - V_4(s)]$$

$$\frac{\varphi(s)}{V_2(s) - V_4(s)} = \frac{2052.6496}{s^2}$$

The same for the linearized pitch motion equation

$$\frac{\theta(s)}{V_3(s) - V_1(s)} = \frac{2052.6496}{s^2}$$

For the yaw angular acceleration,

$$\ddot{\psi} = 0.004615(\Delta\dot{\Omega}_1 - \Delta\dot{\Omega}_2 + \Delta\dot{\Omega}_3 - \Delta\dot{\Omega}_4) + 0.02619(\Delta\Omega_1 - \Delta\Omega_2 + \Delta\Omega_3 - \Delta\Omega_4)$$

$$s^2\psi(s) = 0.004615[s\Omega_1(s) - s\Omega_2(s) + s\Omega_3(s) - s\Omega_4(s)] + 0.02619[\Omega_1(s) - \Omega_2(s) + \Omega_3(s) - \Omega_4(s)]$$

$$s^2\psi(s) = 0.004615s[\Omega_1(s) - \Omega_2(s) + \Omega_3(s) - \Omega_4(s)] + 0.02619[\Omega_1(s) - \Omega_2(s) + \Omega_3(s) - \Omega_4(s)]$$

$$s^2\psi(s) = (0.004615s + 0.02619)[\Omega_1(s) - \Omega_2(s) + \Omega_3(s) - \Omega_4(s)]$$

$$\frac{\psi(s)}{[\Omega_1(s) - \Omega_2(s) + \Omega_3(s) - \Omega_4(s)]} = \frac{(0.004615s + 0.02619)}{s^2}$$

Since $\qquad \Omega(s) = \dfrac{155.521}{(s + 5.909)}V(s),$ $\qquad$ then

$$\psi(s) = \frac{(0.718s + 4.073)}{s^2(s + 5.909)}V_1(s) - \frac{(0.718s + 4.073)}{s^2(s + 5.909)}V_2(s) + \frac{(0.718s + 4.073)}{s^2(s + 5.909)}V_3(s) - \frac{(0.718s + 4.073)}{s^2(s + 5.909)}V_4(s)$$

$$\ddot{Z} = 1.0937(\Delta V_1 + \Delta V_2 + \Delta V_3 + \Delta V_4)$$

$$s^2 Z(s) = 1.0937[V_1(s) + V_2(s) + V_3(s) + V_4(s)]$$

$$Z(s) = \frac{1.0937}{s^2}V_1(s) + \frac{1.0937}{s^2}V_2(s) + \frac{1.0937}{s^2}V_3(s) + \frac{1.0937}{s^2}V_4(s)$$

The transfer functions obtained can be implemented in Simulink and used to formulate any type of controller for any quad-rotor helicopter.

APPENDIX G: FLIGHT SIMULATION DISPLAY PROGRAM

```matlab
function quadrotorsimulationdisplay(uu,V_quad,F_quad,colors_quad,targetPts)


    posx      = uu(1);
    posy      = uu(2);
    posz      = uu(3);
    u         = uu(4);
    v         = uu(5);
    w         = uu(6);
    phi       = uu(7);
    theta     = uu(8);
    psi       = uu(9);
    p         = uu(10);
    q         = uu(11);
    r         = uu(12);
    tx        = uu(13);
    ty        = uu(14);
    tz        = uu(15);
    tpsi      = uu(16);
    t         = uu(17);


    persistent quadrotor_handle;
    persistent target_handle;


    if t<0.1,
        figure(1), clf
        quadrotor_handle = drawQuadrotorBody(V_quad,F_quad,colors_quad,...

posx,posy,posz,phi,theta,psi,...
                                          [], 'normal');
        hold on
        target_handle    = drawTarget(targetPts,tx,ty,tz,tpsi,[],'normal');
        title('Quad-rotor Neuro-fuzzy Control at University of Derby')
        xlabel('Y (m)')
        ylabel('X (m)')
        zlabel('Z (m)')
        view(75,35)
        axis([-2,2,0,30,0,1.5]);
        grid on


    else
        drawQuadrotorBody(V_quad,F_quad,colors_quad,...
                          posx,posy,posz,phi,theta,psi,...
                          quadrotor_handle);
        drawTarget(targetPts,tx,ty,tz,tpsi,target_handle);
    end
end

function handle = drawQuadrotorBody(V_quad,F_quad,colors_quad,...
                                    posx, posy, posz, phi, theta, psi,...
                                    handle, mode);
  V_quad = rotate(V_quad', phi, theta, psi)';
  V_quad = translate(V_quad', posx, posy, posz)';

  [V_fov, F_fov, colors_fov] = fovVertFace(posx,posy,posz,phi,theta,psi);
```

```matlab
    V = [...
        V_quad;...
        V_fov;...
        ];
    F = [...
        F_quad;...
        size(V_quad,1) + F_fov;...
        ];
    patchcolors = [...
        colors_quad;...
        colors_fov;...
        ];

    R = [...
        0, 1, 0;...
        1, 0, 0;...
        0, 0, -1;...
        ];
    V = V*R;

    if isempty(handle),
    handle = patch('Vertices', V, 'Faces', F,...
                   'FaceVertexCData',patchcolors,...
                   'FaceColor','flat',...
                   'EraseMode', mode);
    else
      set(handle,'Vertices',V,'Faces',F);
      drawnow
    end
end


function [V_fov, F_fov, colors_fov] =
fovVertFace(posx,posy,posz,phi,theta,psi,P)
  cam_fov = 0*pi/180;

  V_fov = posz*[...
    0, 0, 0;...
     tan(-theta + cam_fov/2), tan(phi + cam_fov/2), 0;...
     tan(-theta + cam_fov/2), tan(phi - cam_fov/2), 0;...
    -tan( theta + cam_fov/2), tan(phi + cam_fov/2), 0;...
    -tan( theta + cam_fov/2), tan(phi - cam_fov/2), 0;...
    ];
  V_fov = rotate(V_fov',0,0,psi)';
  V_fov = translate(V_fov',posx, posy, posz)';

  F_fov = [...
        1, 1, 2, 2;...
        1, 1, 3, 3;...
        1, 1, 4, 4;...
        1, 1, 5, 5;...
        2, 3, 5, 4;...
    ];

  brown   = [0, 0, 1];
  red = [1, 1, 0];
  colors_fov = [brown; brown; brown; brown; red];

end
```

```matlab
function handle = drawTarget(NED,tx,ty,tz,tpsi,handle,mode)

  NED = rotate(NED,0,0,tpsi);
  NED = translate(NED,tx,ty,tz);

   R = [...
       0, 1, 0;...
       1, 0, 0;...
       0, 0, -1;...
       ];
   XYZ = R*NED;

  if isempty(handle),
    handle = patch(XYZ(1,:), XYZ(2,:), XYZ(3,:), 'r', 'EraseMode', mode);
  else
    set(handle,'XData',XYZ(1,:),'YData',XYZ(2,:),'ZData',XYZ(3,:));
    drawnow
  end

end


function XYZ=rotate(XYZ,phi,theta,psi);
  R_roll = [...
          1, 0, 0;...
          0, cos(phi), -sin(phi);...
          0, sin(phi), cos(phi)];
  R_pitch = [...
          cos(theta), 0, sin(theta);...
          0, 1, 0;...
          -sin(theta), 0, cos(theta)];
  R_yaw = [...
          cos(psi), -sin(psi), 0;...
          sin(psi), cos(psi), 0;...
          0, 0, 1];
  R = R_roll*R_pitch*R_yaw;

  XYZ = R*XYZ;
end

function XYZ = translate(XYZ,posx,posy,posz)
  XYZ = XYZ + repmat([posx;posy;posz],1,size(XYZ,2));
end
```

APPENDIX H: LIST OF PUBLICATIONS

The following journal paper was published during the course of the research work:

1. G. T. Poyi, M. H. Wu and A. Bousbaine. "Quad-rotor CFD Simulation and Analysis with Artificial Neural Networks Error Compensation", Applied Mechanics and Materials (AMM) Journal (www.scientific.net), 2013.

The following journal papers have been completed and are in the process of publication:

1. G. T. Poyi, M. H. Wu, A. Bousbaine and H. Hu. "A Novel Approach to the Design of a Robust Adaptive Controller for Quad-rotor Helicopters".

2. G. T. Poyi, A. Bousbaine and M. H. Wu. "Design of an Intelligent Non-linear Fuzzy-Neural Networks Controller for Quad-rotor Helicopters".

3. G. T. Poyi, M. H. Wu and A. Bousbaine. "Artificial Neural Network Based Validation for Quad-rotor Helicopter Simulink and SolidWorks Models".

4. G. T. Poyi, M. H. Wu, A. Bousbaine and S. Sugiono. "CFD Model of a Quad-rotor Helicopter for Dynamic Analysis".

The following conference papers were written during the course of the research work:

1. G. T. Poyi, M. H. Wu and A. Bousbaine. "Quad-rotor Flight Simulation Error Compensation using Artificial Neural Networks", UPEC, Cluj-Napoca, Romania, 2014.

2. G. T. Poyi, M. H. Wu, A. Bousbaine, and B. Wiggins. "Validation of a Quad-rotor Helicopter Matlab/Simulink and Solidworks Models", IET Control and Automation Conference, Birmingham 2013.

3. G. T. Poyi, M. H. Wu and A. Bousbaine. "Neuro-Fuzzy Control of the X4-flyer", Research snapshot presented at the East Midlands Universities conference, Derby 2013.

4. A. Bousbaine, M. H. Wu and G. T. Poyi. "Modelling and Simulation of a Quad-rotor Helicopter", 6th IET International Conference on Power Electronics, Machines and Drives (PEMD), Bristol 2012.

5. G. T. Poyi, M. H. Wu and A. Bousbaine. "Modelling and CFD Simulation of a Quad-rotor Helicopter", Derby Electrical and Electronics Research Showcase 2012.

6. G. T. Poyi, M. H. Wu and A. Bousbaine. "Modelling and Control Simulation of a Quad-rotor Helicopter", University of Derby New horizons Post-graduate Research conference 2012.

7. G. T. Poyi, M. H. Wu and A. Bousbaine. "Neuro-Fuzzy Control of the X4-flyer", University of Derby New horizons Post-graduate Research conference 2012 (poster).

8. G. T. Poyi, M. H. Wu and A. Bousbaine. "A Novel Approach to the Control of the X-4 Flyer", University of Derby New horizons Post-graduate Research conference 2011.

9. G. T. Poyi, M. H. Wu and A. Bousbaine. "A Novel Approach to the Control of the X-4 Flyer using Fuzzy-Neural Networks", University of Derby Faculty of Arts Design and Technology Research Conference 2011.